REGULATION OF PHOSPHATIDYLCHOLINE SYNTHESIS BY CELLULAR METABOLITES AND ENZYME LOCALIZATION

by

Thomas Alfred Lagace

Submitted in partial fulfillment of the requirements

for the degree of Doctor of Philosophy

at

Dalhousie University

Halifax, Nova Scotia

June 2004

Your file Votre référence
ISBN: 0-612-94030-6
Our file Notre référence
ISBN: 0-612-94030-6

DALHOUSIE UNIVERSITY

To comply with the Canadian Privacy Act the National Library of Canada has requested that the following pages be removed from this copy of the thesis:

Preliminary Pages
- Examiners Signature Page (pii)
- Dalhousie Library Copyright Agreement (piii)

Appendices
- Copyright Releases (if applicable)

This thesis is dedicated in memory of my parents
Alma and Alfred

and to Diane

Table of Contents

List of Tables

List of Figures

Abstract

CTP:phosphocholine cytidylyltransferase (CCT)α is a ubiquitously expressed nuclear-localized enzyme in mammalian cells that catalyzes the rate-limiting and regulated reaction in the CDP-choline pathway for the synthesis of the major membrane phospholipid phosphatidylcholine (PtdCho). Soluble CCTα is activated upon binding to membranes via an amphipathic α-helical domain. To better understand the regulation of PtdCho synthesis and its integration with other cellular processes we examined the control of CCTα activity by membrane translocation and resultant effects on PtdCho synthesis and cell viability. In Chinese hamster ovary (CHO) cells with increased activity of sterol regulatory element binding proteins (SREBPs), PtdCho synthesis was upregulated coordinately with cholesterol synthesis due to CCTα translocation to the nuclear envelope (NE) and activation. This process was dependent on SREBP-mediated fatty acid synthesis. The cholesterol intermediate farnesol also induced CCTα activation in CHO cells. Farnesol-stimulated PtdCho synthesis was transient followed by profound inhibition. This coincided with CCTα nuclear export and apoptosis, which was prevented by supplementation of cells with CDP-choline pathway substrate (fatty acids or DAG). During apoptosis, CCTα was proteolyzed by caspase activity resulting in removal of its nuclear localization signal, implying an essential role of CCTα nuclear localization. Sites of intranuclear CCTα membrane binding in response to the fatty acid activator oleate were examined. Under these conditions, CCTα associated with and caused an increase in tubules of the nucleoplasmic reticulum (NR) continuous with the NE and containing cytoplasm and endoplasmic reticulum components. Electron microscopy analysis identified membrane arrays associated with oleate-induced tubules suggesting the NR could be a site of PtdCho synthesis. Membrane binding ability of CCTα was necessary for oleate-induced nuclear tubule formation and CCTα directly tubulated liposomes *in vitro*. These results support that regulation of CCTα by membrane binding and nuclear localization coordinates PtdCho and cholesterol synthesis and affects the cellular processes of apoptosis and NR formation.

List of Abbreviations and Symbols Used

3-D	three-dimensional
ACAT	acyl-CoA:cholesterol acyltransferase
Ap1	Activator protein 1
ARF	ADP-ribosylation factor
ATP	adenosine triphosphate
BAR	Bin/Amphiphysin/Rvs
BEL	bromoenol lactone
BSA	bovine serum albumin
C/EPT	choline/ethanolamine phosphotransferase
CCT	CTP:phosphocholine cytidylyltransferase
cDNA	complementary DNA
CDP	cytosine di-phosphate
CHO	Chinese hamster ovary
ChoK/EtnK	choline/ethanolamine kinase
CMP	cytosine monophosphate
Con A	concanavalin A
$cPLA_2$	Ca^{2+}-dependent phospholipase A_2
CPT	CDP-choline:1, 2-diacylglycerol cholinephosphotransferase
CTP	cytosine triphosphate
DAG	1,2 dioleoyl-sn-glycerol
diC8	1,2-dioctanoyl-sn-glycerol
DMEM	Dulbecco's modified Eagle's medium

DNA	deoxyribonucleic acid
domain M	membrane binding domain
domain P	phosphorylation domain
DTT	dithiothreitol
E2F	elongation factor 2
ECT	CTP:phosphoethanolamine cytidylyltransferase
EDTA	ethylenediaminetetraacetic acid
EGTA	ethyleneglycolaminoethylethertetraacetic acid
ER	endoplasmic reticulum
Ets-1	epithelium-specific transcription factor 1
FAS	fatty acid synthase
FCS	fetal calf serum
FITC	fluorescein isothiocyanate
FOH	farnesol
FXR	farnesoid X-receptor
G418	geneticin
GAM	goat anti-mouse
GAR	goat anti-rabbit
GCT	CTP:phosphoglycerol cytidylyltransferase
GFP	green fluorescent protein
GPC	glycerophosphocholine
GST	glutathione S-transferase
h	hours

Ha-Ras	Harvey retrovirus-associated Ras
HMGR	HMG-CoA reductase
HRP	horseradish peroxidase
INM	inner nuclear membrane
$iPLA_2$	Ca^{2+}-independent phospholipase A_2
Km	Michaelis-Menten constant
LDLR	low density lipoprotein receptor
LPDS	lipoprotein-deficient serum
LSCM	laser scanning confocal microscope
LXR	liver X-receptor
mRNA	messanger ribonucleic acid
NE	nuclear envelope
NFκB	Nuclear Factor kappa B
NLS	nuclear localization signal
NMR	nuclear magnetic resonance
NPC	nuclear pore complex
NTE	neuropathy target esterase
OAG	1-oleyl, 2-acetyl-sn-glycerol
OLOH	oleyl alcohol
OSER	organized smooth ER
PA	phosphatidic acid
PARP	poly (ADP-ribose) polymerase
PBS	phosphate-buffered saline

PBS-IF	PBS immunofluorescence buffer
PDI	protein disulfide isomerase
PEMT	PtdEtn-N-methyltransferase
PH	pleckstrin homology
PIP_2	phosphatidylinositol 4,5-bisphosphate
PLA	phospholipase A
PLB	phospholipase B
PLC	phospholipase C
PLD	phospholipase D
PMSF	phenylmethylsulfonyl fluoride
PPAR	peroxisome proliferator receptor
PtdCho	phosphatidylcholine
PtdEtn	phosphatidylethanolamine
PtdIns	phosphatidylinositol
PtdIns-4-P	phosphatidylinositol 4-phosphate
PtdSer	phosphatidylserine
SCAP	SREBP-cleavage activating protein
Sp1	specificity protein 1
Sp2	specificity protein 2
Sp3	specificity protein 3
SRD	sterol regulatory defective
SRE	sterol regulator element
SREBP	sterol regulatory element binding protein

TBS-T	tris-buffered saline with tween-20
TEM	transmission electron microscopy
TLC	thin layer chromatography
TMCs	tubular membrane clusters
TPA	12-O-tetradecanoyl-phorbol 13-acetate
tRNA	transfer ribonucleic acid
UPR	unfolded protein response

Acknowledgments

This thesis is the culmination of a long and perhaps unorthodox path to this significant stage in my life. Many people have kept me on that path, even when it may have seemed out of my reach. First of all, my parents instilled in me a desire to become as educated and productive as possible. They were the guiding lights in the early stages of my education, when I could have easily made the wrong decision to choose another career based on a whim of youth. I was very proud of my mother and father, and wanted them to be proud of me in return – even following their deaths they remained a strong driving force in my resolve to get my PhD. My brothers and sisters and nieces and nephews continue to support and encourage me in my life and I love them all.

Neale Ridgway has been a great friend and mentor throughout the 12 years that I worked in his lab. In hindsight, not getting accepted into graduate school the first times I applied before meeting Neale was probably the best thing that could have happened to me (...surely nothing else could be as exciting as working on lipids!). I leave with regret that the Cats never did defeat the hated Panthers for the field hockey title.

The Atlantic Research Centre was a second home to me in Halifax. I worked with so many great people there. I especially want to thank Bob Zwicker for all his help with my experiments and the various gadgets he fixed or rigged up. I'd like to say I learned something about that from him, but I'm still all thumbs when it comes to fixing things. Thanks to everyone for their patience and understanding with my "last-minute" style (Debbie, Bob, Allyson, etc., etc.).

I have many great friends in Halifax, and it will be very sad to leave. I'll especially miss the great Canadian sport of curling!! I can't believe I won't be bonspieling in Lunenburg next year. And sorry to tell you Bob and Pete, my thesis was not really about giant radioactive crickets – I made that up.

Most of all, my beautiful Diane has been the best part of my life and the main reason I have reached this important milestone. She always gave me the gentle push I needed when the doubts crept in and took the heat off of Neale by giving me a sounding board for all my crazy ideas. I know we'll keep being there for each other the rest of the way...

Chapter 1: General Introduction

1.1 The CDP-choline pathway for phosphatidylcholine synthesis

The structure and organization of biological membranes is dependent on lipids containing a polar head group that orients towards the aqueous environment and a non-polar region that is sequestered from water. This amphipathic character of lipid constituents results in formation of a membrane bilayer that serves as a permeability barrier to the passage of large molecules and of small ions into cells. Cellular membranes also compartmentalize organelles and metabolic pathways and provide a matrix for the association of proteins (31, 273). Cells contain an immense variety of membrane lipids with different physical and functional properties (275). Phospholipids are major molecular components of membranes and impart unique characteristics to membranes and participate in diverse cellular processes beyond structural roles (41). Phosphatidylcholine (PtdCho) is the most abundant phospholipid in eukaryotic membranes, comprising ~50% of total phospholipid in cells and tissues (152, 330). PtdCho consists of a glycerol phosphate backbone, a choline head group attached at the *sn*-3 position, and two fatty acid moieties at positions *sn*-1 and *sn*-2. PtdCho species found in biological membranes form lamellar (bilayer) phases when dispersed in excess water (182). This property in conjunction with non-lamellar lipids, such as unsaturated phosphatidylethanolamine (PtdEtn) (251), and lipid modifying enzymes serves to modulate the physical structure of the bilayer, thereby affecting the function of membrane associated proteins and membrane remodeling events involved in lipid and protein transport (37, 70, 88, 94).

PtdCho reflects of the functional and physical diversity of lipids in cells by virtue of the variety of fatty acids with different chain lengths and double bonds esterified to the *sn*-1 and *sn*-2 positions. In addition to its role as an essential structural component of eukaryotic membranes, PtdCho also has other important functions. PtdCho is the main component of a layer of phospholipids surrounding lipid storage droplets in eukaryotic cells, and is required for the synthesis of pulmonary surfactant, bile and serum lipoproteins (275). Degradation of highly unsaturated PtdCho through agonist stimulation of phospholipases results in the release of numerous biologically active molecules (reviewed in refs. 85, 283). These include arachidonic acid used in the formation of the inflammatory mediators prostaglandins and leukotrienes (165, 299), and diacylglycerol (DAG) which is involved in membrane recruitment and activation of a myriad of proteins involved in essential cell signalling pathways (34), including members of the protein kinase C family (201). Reflective of its importance in mammalian cell physiology, disruption of PtdCho synthesis by genetic (61, 81) or pharmacological means (27-29) results in cell death by apoptosis.

The CDP-choline pathway for PtdCho synthesis was first described by Kennedy and co-workers in the 1950s, following their seminal discovery of the use of cytosine nucleotides in the synthesis of phospholipids (150, 298). The CDP-choline pathway is present in all nucleated eukaryotic cells, including plants (69), yeast (41) and nematodes (97). *Streptococcus pneumoniae* is a member of a small group of bacteria that display phosphocholine on the cell surface, covalently attached to the sugar groups of teichoic acid and lipoteichoic acid. This pathway could represent a predecessor to the CDP-choline pathway since its first two enzymatic reactions are similar (39). In mammals, the

CDP-choline pathway is responsible for *de novo* PtdCho production in all cells and tissues, although the methylation of phosphatidylethanolamine also has a major role in liver (276). Further metabolism of *de novo* synthesized PtdCho involves fatty acid-chain remodeling controlled by the coordinated action of acyltransferases, transacylases and lipases (316). The CDP-choline pathway is non-essential in yeast cells, which have the capacity to synthesize all PtdCho via PtdEtn-methylation with the relative contributions of the two pathways to production of PtdCho dependent on the supply of exogenous choline (41, 122).

The enzymatic reaction and substrates involved in the CDP-choline pathway are depicted in Figure 1.1. The CDP-choline pathway consists of three enzyme reactions for the conversion of choline to PtdCho, with associated consumption of ATP, CTP and DAG: (i) phosphorylation of choline by choline kinase using ATP to produce phosphocholine, (ii) the CCT-catalyzed transfer of a CMP moiety from CTP to phosphocholine to form CDP-choline, and (iii) the transfer of phosphocholine from CDP-choline to DAG by CDP-choline:1,2-diacylglycerol cholinephosphotransferase (CPT). CMP formed in this reaction can be reconverted into CTP by cellular salvage pathways (153). It is well-established that CCT is the rate-limiting and regulated enzyme in the CDP-choline pathway (151, 295), although regulation of PtdCho synthesis at other enzymatic steps is described (4, 136, 156, 291).

1.1.1 Choline kinase

Several isoforms of a dual specificity choline/ethanolamine kinase (ChoK/EtnK) have been cloned from mammalian tissues (130). The specificity of the ChoK/EtnK

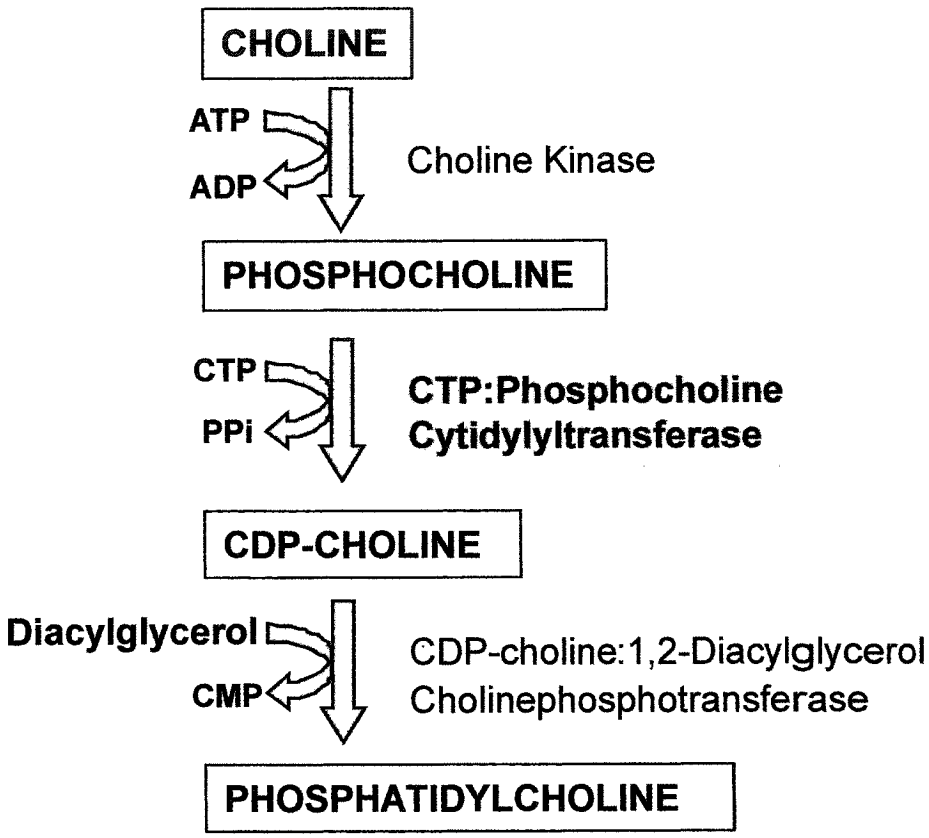

Figure 1.1 - The CDP-choline pathway for phosphatidylcholine synthesis. Schematic representation of the CDP-choline pathway showing enzymes, choline intermediates and other substrate molecules.

enzymes for choline, together with the recent cloning of a ethanolamine-specific kinase from a human cDNA library (172), suggests that choline and ethanolamine can be phosphorylated by separate enzymes *in vivo*. ChoK/EtnK is a cytosolic enzyme in yeast, plants and mammals, and the active form exists as combinations of isoforms (α1, α2, and β) that generate dimers or oligomers (3). Choline kinase activity *in vivo* is primarily regulated by substrate availability dependent on the rate of choline uptake. Evidence of mitogen stimulation of ChoK activity implies a regulatory role in elevating PtdCho synthesis during rapid cell growth (156, 217, 291).

1.1.2 CDP-choline:1,2-diacylglycerol cholinephosphotransferase

Two human genes encode what is presumed to be the entire complement of CPT activities (113, 114). CPT1 is localized to the Golgi apparatus and displays tissue specific expression, whereas a dual specificity choline/ethanolamine phosphotransferase (C/EPT) is localized in the endoplasmic reticulum (ER) and nuclear envelope (NE) and is ubiquitously expressed (114, 115). Certain conditions can cause the CPT-catalyzed reaction to become rate-limiting for PtdCho synthesis, leading to accumulation of CDP-choline. These include conditions of decreased availability of DAG substrate (4, 136, 166) and apoptosis (2, 279, 304).

1.2 CTP:phosphocholine cytidylyltransferase-α

1.2.1 CCT isoforms and domain structure

In mammals there are two genes, *Pcyt1a* and *Pcyt1b* that encode the CCTα and CCTβ enzymes, respectively. CCTα is ubiquitously expressed, whereas CCT β_1, β_2 and β_3 are splice variants that display restricted tissue distribution and may play a specialized

role in regulation of PtdCho synthesis at these sites (42, 147, 169). The murine genes for CCTα and CCTβ have been cloned and characterized (147, 257). The intron-exon arrangement of the genes correspond to the functional domain structure in the respective CCT isoforms. CCT α and β display extensive sequence identity in the catalytic and membrane binding domains but not in the N- and C-terminal regions (Figure 1.2).

CCTα cDNAs have been cloned from rat (145), hamster (254), mouse (227) and human (146) with only minor amino acid sequence differences between these mammalian proteins. CCTα from rat liver has a molecular mass of 41.7 kDa (145) and is found as a homo-dimer in soluble cell extracts. Beginning at the N-terminus, the first functional domain in CCTα is a region containing a cluster of positively charged amino acids followed by an acidic tract (amino acids 8-28) that serves as a nuclear localization signal (NLS) (290). The CCTβ isoforms lack a NLS and are localized in the cytoplasm/ER (169) (Figure 1.2). The main catalytic core of CCTα is highly conserved among all cytidylyltransferases, such as CTP:phosphoethanolamine cytidylyltransferase (ECT) and CTP:phosphoglycerol cytidylyltransferase (GCT) (203, 294). The murine cDNAs for CCTα and the CCT β-isoforms share almost complete amino acid identity in the catalytic region (147). Next to the catalytic domain is a membrane-binding region (M) in CCTα that contains three 11-residue repeats that form an amphipathic α-helix and regulates CCTα activity through reversible membrane association (58) (Figure 1.2). The CCTβ isoforms also contain three α-helical repeats and enzyme activity is similarly enhanced by lipids (171). The C-terminus of rat CCTα contains a phosphorylation domain (P) with 16 serine residues that accounts for all the phosphorylation sites within the enzyme (Figure 1.2). Phosphorylation of CCTα appears to modulate enzyme activity by partially

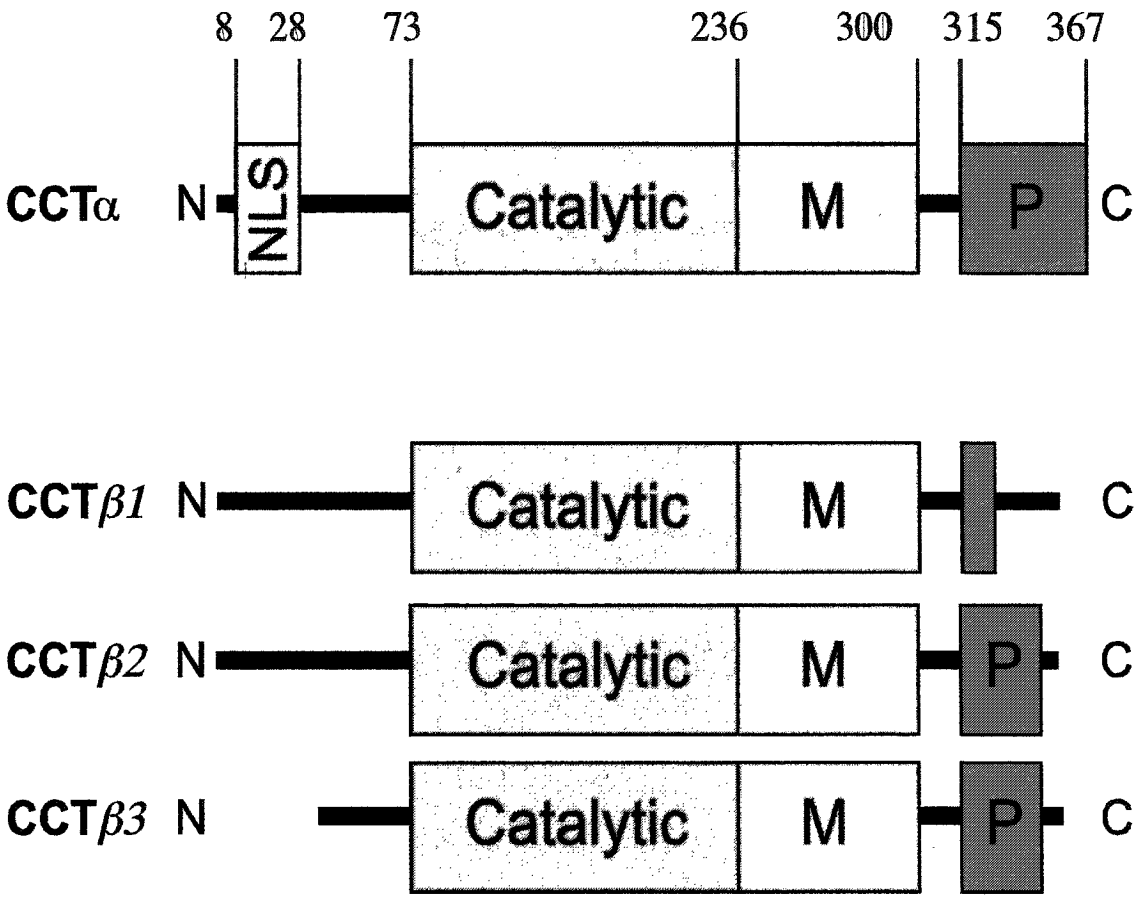

Figure 1.2 - Domain structure of CCTα and CCTβ isoforms - Schematic representation of α and β CCT and their functional domains. Amino acids numbers in CCTα correspond to the rat sequence. CCTβ isoforms consist of three splice variants (β1-β3). The main differences between the α and β isoforms is the lack of the nuclear localization signal (NSL) and shorter phosphorylation (P) domain in CCTβ isoforms. These four isoforms have highly similiar sequence aligment within their catalytic core (nearly identical) and membrane binding helical domains (M) (88% identity - human CCTα and CCTβ1).

interfering with membrane binding (286). The C-terminal phosphorylation domain of CCTα is distinct from the CCTβ isoforms. CCTβ2 and CCTβ3 both have potential C-terminal serine phosphorylation sites, but whether these sites are phosphorylated or control enzyme activity has not been investigated (147, 169). CCTβ1 is missing most of the C-terminal phosphorylation domain due to alternative splicing and contains only three potential serine phosphorylation sites (171). An alternative cDNA transcript for CCTα has recently been identified from a murine EST database that is highly transcribed in testis. This transcript contains a unique 5' untranslated region, but otherwise encodes a protein identical to full-length CCTα (147). Much of the work characterizing CCT regulation in mammalian cells and tissues predates the discovery of the CCT β-isoforms. In cases where there is ambiguity with regards to CCT isoforms within a particular study, the enzyme will be referred to simply as CCT.

1.2.1.1 Catalytic domain

The catalytic domain encompasses amino acids 73 to 236 in rat CCTα. The catalytic region is highly conserved throughout the cytidylyltransferase superfamily, which includes ECT and GCT. The tertiary structure of the eukaryotic CCTα catalytic region remains unknown. However, the crystal structure has been solved for bacterial GCT, which contains the catalytic region but lacks the N- or C-terminal regulatory domains found in CCTα (203, 294). The structure of GCT contains a characteristic fold also found in class I aminoacyl-tRNA synthases, suggesting a common mechanism relying on transition-state stabilization for catalysis (202, 294). Using GCT as a predictive model, several critical residues in the CCTα active site have been identified by site-directed mutagenesis. These include H89 and H92 within a HXGH motif required

for CTP binding (277, 294), and K122 (112), which has an analogous lysine residue in GCT that contacts the product CDP-glycerol in the active site (203).

Like CCTα, GCT also forms homo-dimers (203). Interestingly, a high degree of negative cooperativity was demonstrated for the binding of substrate to the respective active sites in GCT dimers, and products were formed only when both sites were occupied (203). Precise dimerization determinants have yet to be identified in CCTα. However, limited proteolysis has narrowed the minimal dimerization region to amino acids 1 to 236 (59). A more recent study showed evidence for dimerization determinants in both the N-terminal region (amino acids 1 to 72) and the catalytic domain (311). Early studies demonstrated the existence of CCT in both dimeric light (L)-form and multimeric heavy (H)-forms following density centrifugation analysis of soluble CCT from various tissue sources (296, 297). Further analysis determined that the L-form of CCT converted to the more active H-form with the addition of lipid (296).

1.2.1.2 Membrane binding domain

Between amino acids 237 and 299 is a membrane binding domain (domain M) composed of an extended α-helix that mediates transient association of CCTα with biological and artificial membranes in response to lipid activators and/or membrane structure (11, 52, 59). Membrane-association is critical for CCTα enzyme activity, causing a >30 fold decrease in the K_m for CTP (320). Truncation of CCTα following the catalytic region results in a soluble, constitutively-active enzyme, indicating that domain M has an auto-inhibitory activity in the soluble enzyme (287). Other studies have suggested that domain M acts as a co-activator when lipid-bound (320).

The membrane binding region in CCTα has been delineated by chymotrypsin proteolysis (59), deletion mutagenesis (57, 287, 317, 320) and lipid photoaffinity labelling (139). The structure of a synthetic peptide corresponding to this region has been solved by two-dimensional NMR (73). It consists of an N-terminal bend, proposed to act as a hinge region between domain M and the catalytic domain, followed by a continuous helix of at least 50 residues with strong amphipathic properties. An 11-mer motif (amino acids 267 to 277) repeated three times within domain M conferred lipid binding capability when fused to glutathione S-transferase (GST) and was defined as a minimal binding region (317). Lipid binding to domain M has been shown to result in a conformational switch from a mixed structure dominated by random coil conformations to an ordered α-helix (256). This finding has led to the proposal that the lipid-induced conformational switch creates a hydrophobic face for membrane insertion. A similar mechanism for membrane insertion of a lipid-ordered amphipathic helix has recently been proposed for the amphitropic protein epsin (93).

Both electrostatic and hydrophobic interactions promote binding of CCTα to membranes (58). Studies *in vitro* and *in vivo* have identified two distinct classes of membrane lipid activators of CCT (52, 55, 56, 244, 272). Class I activators include anionic lipids and fatty acids. These lipids presumably interact favourably with numerous positively charged lysine residues near the interfacial region in domain M (58, 73). Class II activators, including DAG and unsaturated PtdEtn, promote non-bilayer phases in membranes (10, 11, 135). These activating lipids are proposed to induce lateral packing stress, introducing gaps in the regular packing of polar head groups within the bilayer and favouring insertion of the hydrophobic face of the domain M amphipathic

helix (63). Since PtdCho is a bilayer-forming lipid (182), its relative abundance in membranes could affect lateral packing stress. This suggests a mechanism whereby domain M 'senses' decreased lipid packing in PtdCho-deficient membranes, resulting in increased CCTα activity and restoration of PtdCho levels (54). A synergistic effect of Class I and Class II activators on CCTα membrane binding and activity has been demonstrated *in vitro* (5, 6) supportive of a model for separate modes of CCTα activation by these lipids. Several lipids also act as negative regulators of CCTα membrane binding, including lysophosphatidylcholine (28), sphingosine (247) and C2-ceramide (216).

CCT activity *in vivo* is responsive to increased intracellular levels of lipid activators (52, 151, 244). In the case of fatty acids and DAG, this provides a homeostatic response to PtdCho degradation by phospholipases (58). In addition, since fatty acids and DAG act as indirect and direct substrates, respectively, for CPT, membrane activation of CCTα serves to coordinate PtdCho synthesis with substrate supply. This is an important consideration given the alternative role of DAG as a lipid-signalling molecule (34, 282). Interestingly, CHO cells expressing a constitutively-active CCTα mutant lacking the membrane binding domain were dependent on exogenous unsaturated fatty acids for growth, suggesting that lipid activation of CCTα played a role in maintenance of fatty acid homeostasis (96).

1.2.3.2 Phosphorylation domain

CCTα is a highly phosphorylated protein *in vivo* (289). Characterization of baculovirus-expressed rat CCTα showed that phosphorylation occurred exclusively within a C-terminal region (amino acids 315-367) containing 16 serines residues (174).

In vitro and *in vivo* studies demonstrated that phosphorylation partially interfered with membrane association and lipid activation of CCTα (6, 286). Many of the lipid activators that promote CCTα membrane translocation also induce dephosphorylation (289, 293). However, dephosphorylation of CCTα was not required for, and occurred subsequent to, membrane binding (120). Mutation of sixteen serine phosphorylation sites to either alanine (16SA) or glutamic acid (16SE) had no effect on the capacity of the mutant enzymes to restore PtdCho synthesis and cell growth in MT58 cells (a CHO cell line harboring a temperature-sensitive inactivating mutation in a single functional allele of CCTα (82)), but did shift the distribution of enzyme between soluble and membrane bound forms (286).

The physiological role of CCTα phosphorylation remains enigmatic. It has been suggested to be a mechanism for coordinating PtdCho synthesis with cell cycle progression (133). Alternatively, it could serve to increase the half-life of CCTα based on the observation that the CCTα 16SE mutant displayed increased levels of expression in MT58 cells compared to CCT 16SA and wild-type CCTα (286). Numerous kinases have been demonstrated to phosphorylate CCTα *in vitro* (57, 302, 303). However, the relevant kinases and phosphatases that regulate CCTα phosphorylation *in vivo* are unknown. Phosphorylation is increased in Ha-Ras-transformed HaCaT cells (303), by growth factor stimulation of HeLa cells (302) and during the G1→S transition (133), suggesting CCTα phosphorylation is affected by signal transduction pathways involved in cell cycle progression. In addition to containing numerous phosphorylation sites, the C-terminal region of CCTα contains sequences that impart regulation of enzyme activity by anionic lipids (170).

1.2.3.3 Nuclear localization domain

A unique feature of CCTα not found in the CCTβ isoforms is an N-terminal motif (Figure 1.2) containing a cluster of positively charged amino acids followed by an acidic tract that serves as a NLS (288). The development of specific antibodies in the early 1990s led to the first identification of CCTα nuclear localization in CHO cells by indirect immunofluorescence techniques (292). Nuclear localization of CCTα was subsequently demonstrated by immunofluorescence analysis in several cell types and primary rat liver slices, and was confirmed biochemically by enucleation studies (289, 290). Although predominantly nuclear-localized, overexpressed CCTα was also shown to be associated with the ER in CHO, HeLa, and mouse macrophage cells (169). A recent study showed that nuclear localization of CCTα is not universal among all cell types (223). In lung-derived cells and tissues, CCTα is a cytoplasmic protein based on various immunolocalization techniques and direct visualization of green fluorescent protein (GFP)-tagged CCTα, perhaps reflecting an increased requirement for PtdCho in surfactant synthesis (223). A subsequent study showed that cytoplasmic localization of CCTα in mouse lung epithelial cells was cell cycle independent (269).

The physiological significance of CCTα nuclear localization remains speculative. Expression of a mutant CCTα protein lacking the NLS restored PtdCho synthesis and growth in MT58 cells cultured at the non-permissive temperature, suggesting that nuclear localization was non-essential for cell-growth (288). However, this mutant CCTα was not completely excluded from the nucleus, thus casting doubt on the conclusions of this study. Nuclear localized CCTα could (1) allow for the coordination of PtdCho synthesis with cell cycle regulated events in the nucleus (132), (2) be required for the synthesis of

an endonuclear pool of PtdCho involved in aspects of chromatin function (126) or (3) act as a reservoir for inactive CCTα (58). The latter proposal arose from a study which showed transient export of CCTα from the nucleus in conjunction with increased PtdCho synthesis following serum-stimulation of quiescent IIC9 cells (196). In opposition to this result, CCTα-GFP was exclusively nuclear under different cell cycle conditions and in various cell lines (67). However, the GFP tag may have affected nuclear export in this cell model.

Despite extensive efforts to definitively localize CCTα within various cell types under both basal and activating conditions, the fundamental question still remains: where is the site of CDP-choline synthesis? Two alternative models have been proposed. In the first model (Figure 1.3, A), CDP-choline synthesis occurs at the ER following nuclear export of CCTα in response to activating signals. In this model, the nucleus acting as a 'holding bin' for inactive CCTα (58). Several aspects of this model are attractive. For instance, localization to the cytoplasm and ER would put CCTα in an ideal position to respond to changes in the lipid environment and affect PtdCho synthesis accordingly (169). As well, the ER is the main location of CPT activity, which catalyzes the subsequent reaction in the CDP-choline pathway. In Figure 1.3, B, CDP-choline, made in the nucleus by CCTα associated with the inner nuclear membrane (INM), moves through nuclear pores to be utilized by CPT in the ER. This model is supported by indirect immunofluorescence data showing exclusive localization of CCTα to the NE under conditions of increased PtdCho synthesis and in several cell-types (289, 292). The potential drawback of this model is that nuclear localization of active CCTα would physically separate CDP-choline synthesis from CPT in the ER and Golgi (115).

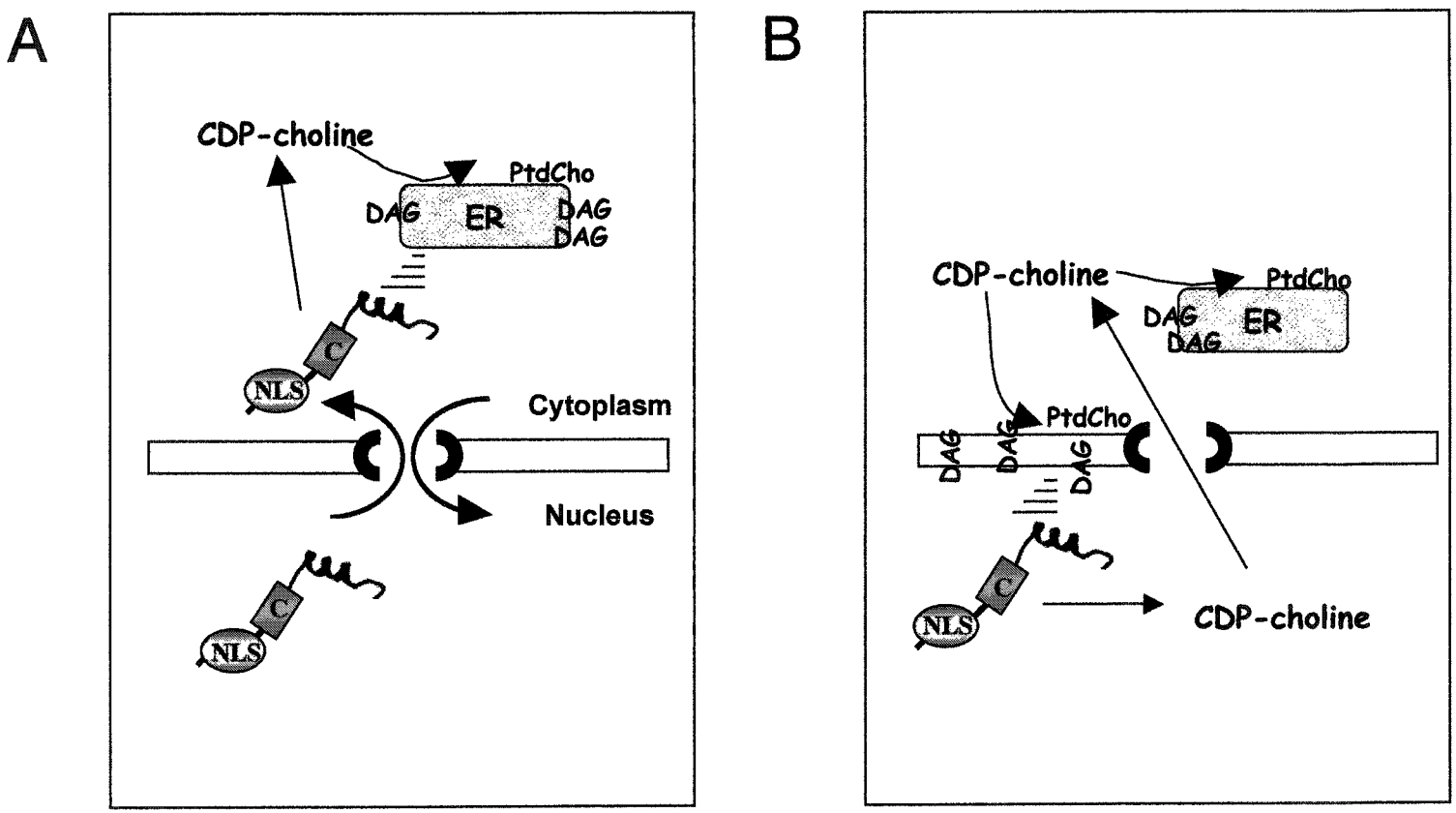

Figure 1.3 - Opposing models for the cellular site of CDP-choline synthesis by CCTα. Current models depicting CDP-choline synthesis in the ER (**A**) or nucleus (**B**). Abbreviations: NLS, nuclear localization signal; C, catalytic domain; ER, endoplasmic reticulum; PtdCho, phosphatidylcholine.

Regardless of this apparent physical separation of the enzymatic reactions, substrate channelling has been demonstrated to occur within the CDP-choline pathway (26, 100, 219), indicating a functional compartmentalization of pathway enzymes and intermediates. Substrate channelling is a common feature in numerous metabolic pathways, with the transfer of intermediates within multi-subunit or multi-enzyme complexes considered to be the universal mechanism (185, 249). Substrate channelling has been proposed to increase the efficiency of metabolic pathways by (1) decreasing transit time of intermediates, (2) decreasing loss of intermediates due to diffusion, (3) protecting labile intermediates from solvent and (4) preventing entrance of intermediates into competing metabolic pathways (200). It is unclear how nuclear localization of CCTα can be reconciled with observations of substrate channelling in the CDP-choline pathway because this would presumably preclude the formation of a multi-enzyme complex. A recent study has shown a small fraction of overexpressed epitope-tagged C/EPT was associated with an isolated nuclear fraction in CHO cells, leading to the proposal that substrate channelling and PtdCho synthesis occurs at the INM (115). This seems unlikely given the primary localization of CPT and C/EPT to the ER/Golgi compartments. Definitive localization of C/EPT to the INM awaits the development of antibodies that can detect the endogenous protein. Given the current data, the location of nuclear CDP-choline synthesis suggests a novel mechanism for metabolite coupling with the subsequent step in the pathway.

1.2.2 Transcriptional regulation of CCTα

CCTα mRNA levels increased following growth factor stimulation (260), in proliferating liver following partial hepatectomy (121) and during S phase of the cell

cycle (19, 106). CCTα mRNA levels were suppressed in response to sphingosine (228) and in transformed hepatocytes overexpressing PtdEtn-N-methyltransferase (PEMT), which catalyzes PtdCho synthesis by PtdEtn methylation (62). The cloning of the murine CCTα gene (257) has led to detailed analysis of the proximal promoter region. This region contains several potential positive and negative *cis* elements. These include potential binding sites for Ap1, NFκB and E2F, as well as three sites for binding Sp1 and related factors (14). Sp1 sites have basal, activating and suppressing functions, with the overall level of CCTα expression dependent on competing activities of the Sp1, Sp2 and Sp3 transcription factors (16). The transcription factor Ets-1 is important for basal CCTα mRNA transcription (253) and is enhanced in combination with the binding of transcription enhancer factor 4 to an upstream regulatory sequence (252). Reporter gene assays have demonstrated that CCTα transcription is increased following expression of oncogenic Ha-Ras (15). This and previous observations of increased CCTα transcriptional rates during the S phase of the cell cycle (19, 106) suggest that CCTα transcription is positively regulated by signalling pathways involved in cell proliferation. Since CCTα activity is also dependent on post-translational regulatory mechanisms such as membrane binding and phosphorylation, it remains unclear to what extent transcriptional regulation affects the overall rate of PtdCho synthesis. Increased expression of CCTα could serve to augment post-translational modes of activation or provide sufficient enzyme for partitioning into daughter cells during mitotic division (106).

1.3 The cellular context of CDP-choline pathway regulation

The regulation of the CDP-choline pathway and PtdCho synthesis is ultimately dependent on membrane binding and activation of CCTα in response to appropriate cellular cues. The response of CCTα to regulatory signals can be further modulated by transcription, phosphorylation and subcellular localization. These regulatory mechanisms must allow the rapid response of CCTα to membrane perturbations, such as altered levels of other membrane lipids. In rapidly proliferating cells, CCTα activity must be coordinated with increased PtdCho required for new membrane synthesis and production of bioactive signalling molecules. Studies of CCTα regulation are continuing to illuminate some of these mechanisms.

1.3.1 Regulation of CCTα activity by cholesterol

The proper ratios of phospholipids, sphingolipids, and cholesterol in eukaryotic membranes is essential for maintaining permeability, fluidity and microdomain structure and the activity of membrane-associated proteins. Therefore, there are numerous mechanisms for co-regulation of lipid metabolic pathways in order to maintain membrane lipid homeostasis (reviewed in ref. 221). It is well established from various experimental and pathological models that ratios of the major membrane lipids PtdCho and cholesterol are maintained within a narrow range in cell membranes, although the mechanisms that underlie this co-regulation remain poorly defined (46, 245).

One important pathway for the co-regulation of PtdCho and cholesterol within mammalian cells is the sterol regulatory element binding protein (SREBP) pathway. SREBPs are a family of three transcription factors that bind as dimers to consensus sterol regulatory elements (SREs) in the promoter regions of numerous genes involved in

cholesterol and fatty acid synthesis, lipoprotein internalization and production of NADPH (reviewed in ref. 78). The SREBP isoforms have separable but overlapping gene targets; SREBP-1a activates both cholesterol and fatty acid synthesis, while SREBP-1c and SREBP-2 are relatively specific for fatty acid and cholesterol synthesis, respectively. While partially redundant in their transcriptional targets, mouse transgenic studies have indicated distinct roles of individual SREBPs in maintenance of lipid homeostasis, especially in the liver and adipose (reviewed in ref. 118).

SREBPs are initially synthesized as inactive membrane-bound precursors localized in the ER. Vesicle-mediated transport to the Golgi apparatus results in the sequential cleavage of SREBP by two Golgi-resident proteases, releasing a cytosolic mature form that translocates to the nucleus to activate target genes (78, 195). Processing of SREBPs is mainly regulated by cholesterol, but is also affected by insulin signalling and unsaturated fatty acids (110, 313). The cholesterol 'sensor' is SREBP-cleavage activating protein (SCAP) that binds to and escorts SREBP from the ER to the Golgi (35, 231). When cholesterol is in excess, the SCAP/SREBP complex is retained in the ER by a cholesterol-dependent interaction between SCAP and the ER-resident protein Insig-1 (319). Sterol-mediated suppression of SREBP processing can be subverted by saturation of the SCAP/Insig-1 interaction through overexpression of SCAP (312, 319) or by expression of a mutant version of SCAP (SCAP D443N) that is defective in its interaction with Insig-1 (314).

The discovery of a putative SRE within the proximal promoter region of the murine CCTα gene (14, 149) raised the possibility that CCTα mRNA levels could be coordinately regulated with genes involved in cholesterol and fatty acid metabolism.

Indeed, lipoprotein deprivation, which is known to cause an increase in SREBP processing, resulted in increased CCTα mRNA levels and reporter gene activities in THP-1 macrophages, HepG2 cells and CHO cells (149). However, changes in CCTα activity and PtdCho synthesis were not explored in this study. Also, in a direct comparison in HepG2 cells, expression of a reporter gene driven by the CCTα promoter region was only increased 1.7-fold in HepG2 cells following incubation in lipoprotein-deficient serum compared to an 8.8-fold increase for a reporter gene under control of the low density lipoprotein receptor (LDLR) promoter, a well characterized SREBP-target gene. Therefore, transcriptional activation of the CCTα gene by SREBPs could be minor compared to that of other SREBP-regulated genes involved in cholesterol and fatty acid metabolism. Mice fed a lipid-deprived diet display increased expression of CCTα and a corresponding increase in alveolar surfactant PtdCho synthesis (176). In murine type II alveolar cells, lipoprotein deprivation caused a 2-fold increase in CCTα mRNA and protein (229). Paradoxically, this was accompanied by significantly decreased PtdCho synthesis and mass. This suggests that transcriptional regulation is unlikely to be the primary mechanism for co-regulation of PtdCho and cholesterol levels in the lung, but may serve to augment regulation by other mechanisms.

A useful model for studying co-regulation of PtdCho and cholesterol are sterol regulatory defective (SRD) CHO cells developed in the Goldstein and Brown laboratory (reviewed in ref. 105). These cell lines have been instrumental in the identification by complementation analysis of numerous proteins involved in the regulation of SREBP processing, including SCAP (124) and the proteases that cleave SREBP (218, 232). SRD-6 cells have reduced rates of cholesterol and fatty acid synthesis due to defective

processing of SREBPs resulting from a mutation in the site-2 protease that cleaves SREBPs (84, 218). These cells also have decreased CCTα activity and PtdCho synthesis (250). Suppression of CCTα activity in SRD-6 cells was overcome by culturing cells with exogenous fatty acids but not cholesterol, suggesting that suppression of CCTα activity was the result of decreased fatty acid synthesis or decreased levels of a fatty acid-derived CCTα activator.

A well-characterized example of post-translational CCTα activation in response to elevated cellular cholesterol levels occurs in macrophage foam cells, which accumulate large amounts of cholesterol and eventually undergo cell death by necrotic and apoptotic mechanisms (reviewed in ref. 255). Tabas and co-workers have shown that elevated CCTα activity results in the formation of membrane whorls that may act as 'sinks' for the excess cholesterol in these cells, thereby reducing toxic levels in membranes. Consistent with this interpretation, macrophages deficient in CCTα are especially susceptible to cholesterol-induced cell death (326). Cholesterol has been shown to be a poor-activator of CCTα *in vitro* (63), so associated cholesterol metabolites or other activating signals must be involved. CCTα activation in this model was correlated with enzyme dephosphorylation, and was blunted by the phosphatase inhibitor calyculin, indicating involvement of a cholesterol-sensitive phosphatase activity (240). In this same study, CHO cells loaded with cholesterol did not upregulate PtdCho synthesis, suggesting that this response is macrophage-specific. This could also reflect differences between CHO cells and macrophages in cholesterol trafficking to specific membrane sites. Recently, the ER has been identified as the site of toxic accumulation of cholesterol in macrophage foam cells (89). This results in depletion of ER Ca^{2+}-stores, initiating an ER-stress

signalling pathway known as the unfolded protein response (UPR), the end result of which is expression of the cell death effector CCAAT/enhancer-binding protein-homologous protein (CHOP) and apoptosis. Whether CCTα activation in macrophage foam cells is linked to elevated ER cholesterol levels and ER-stress signalling pathways remains to be investigated. Although increased phospholipid synthesis is a feature of the UPR in *Saccharomyces cerevisae* (267), the potential role of PtdCho synthesis in the mammalian UPR remains unclear. However, CCT is activated by Ca^{2+} ionophores (236), and loss of CCTα function and PtdCho synthesis in MT58 cells grown at the non-permissive temperature resulted in CHOP-induced apoptosis (274). Thus, ER stress-related signalling events may be responsive to CCT regulation and PtdCho synthesis.

In addition to SREBPs, numerous fatty acid-regulated transcription factors contribute to lipid homeostasis within mammalian cells. Several members of the steroid/thyroid superfamily of nuclear receptors have been reported to bind to fatty acids or their metabolites, including peroxisome proliferator receptors (PPARs), liver X-receptor (LXR) and retinoid X-receptor (RXR) (reviewed in ref. 144). Interestingly, transcription of SREBP-1 isoforms is suppressed in cells treated with polyunsaturated fatty acids, in part due to antagonism of oxysterol-mediated activation of LXR, a positive regulator of SREBP-1 transcription (66, 199). Fatty acid treatment of cells also can affect gene transcription by mechanisms not involving direct binding to transcription factors (74). For instance, palmitate and oleate induce the immediate-early response genes c-*fos* and *nur*-77 in pancreatic β-cells to an extent similar to that seen with tumor-promoting phorbol esters (225). Since CCT is potently activated by fatty acids, PtdCho synthesis

could play a role in mediating fatty acid effects on gene transcription in lipid homeostatic and cell-signalling mechanisms.

1.3.2 Cellular responses to excess phosphatidylcholine

Maintenance of PtdCho levels in cellular membranes also depends on mechanisms for the degradation of excess PtdCho and inhibition of CCTα activity under these conditions. Increased PtdCho synthesis due to overexpression of CCTα leads to increased levels of the degradation product glycerophosphocholine (GPC), indicating involvement of phospholipase A_2 (PLA_2) followed by a lysophospholipase activity (13, 20, 284, 285).

PLA_2 enzymes compose a large and diverse family. These enzymes primarily catalyze the hydrolysis of fatty acids from the sn-2 position of phospholipids, generating a lysophospholipid and a free fatty acid (reviewed in ref. 68). Dennis and colleagues have assigned PLA_2 enzymes to 14 separate Groups (I-XIV) containing 20 subgroups (eg. Group IVA). These include both secretory ($sPLA_2$) and cellular PLA_2, and calcium-dependent ($cPLA_2$) and calcium-independent ($iPLA_2$) forms. The ubiquitous occurrence of $iPLA_2$ and its lack of regulation by Ca^{2+} or other agonist stimulation suggest a general housekeeping role within the cell involved in PtdCho remodeling (17). In this process, highly saturated PtdCho from the CDP-choline pathway is deacylated by $iPLA_2$ and subsequently reacylated by lyso-PtdCho acyltransferase, resulting in the exchange on the PtdCho molecule of a saturated fatty acid for a polyunsaturated fatty acid such as arachidonic acid (316). Phospholipase-mediated degradation of remodeled PtdCho can result in the release of bioactive unsaturated DAG molecules or, through the action of

$cPLA_2$, arachidonic acid for the production of inflammatory mediators such as leukotrienes and prostaglandins (165, 299, 300)

Bromoenol lactone (BEL), a PLA_2-inhibitor that preferentially affects $iPLA_2$, partially inhibited degradation of excess PtdCho caused by overexpression of CCTα, suggesting involvement of more than one activity (13). Recently, the mammalian ER-localized protein neuropathy target esterase (NTE) has been shown to possess PLB activity that liberated fatty acids from both the *sn*-1 and *sn*-2 positions of PtdCho (325). NTE has been identified as a target of organophosphates that cause nerve axon degeneration (305). In yeast, GPC production is correlated with increased PtdCho synthesis by the CDP-choline pathway, but not the PtdEtn-methylation pathway, indicating that CDP-choline pathway activity is also coordinated with PtdCho degradation by PLA_2 and/or PLB in this organism (71).

1.3.3 Phosphatidylcholine degradation in cell proliferation and survival signalling

Several lines of evidence indicate that PtdCho degradation plays an essential role in cell cycle progression. For instance, PtdCho has been shown to be a major source of the mitogenic signalling lipid DAG in growth factor-stimulated and *ras*-transformed cells (158, 207, 215). DAG acts as a membrane activator for proteins involved in cell growth and survival pathways, including classical PKC isoforms (α, β, γ) (192, 201) and Ras-activating proteins (76). The acute phase of mitogenic signalling involves phospholipase C (PLC)-mediated degradation of phosphatidylinositol 4,5-bisphosphate (PIP_2) at the plasma membrane (220). This results in a transient rise in two signalling components: inositol 1,4,5-trisphosphate (IP_3), which binds to intracellular receptors to initiate the release of calcium from intracellular stores, and DAG, which allosterically activates

PKC. PtdCho-derived DAG appears to be involved in an extended phase of PKC activation that augments the acute signalling phase (85, 208). Phorbol esters are DAG analogues that are slowly metabolized, leading to a prolonged state of PKC activation and cell transformation. Similarly, NIH-3T3 cells overproducing PtdCho-derived DAG due to expression of a bacterial PtdCho-phospholipase C (PLC) displayed a malignant phenotype (138), indicating that prolonged PtdCho hydrolysis can mimic the tumor promoting ability of phorbol esters.

DAG production from PtdCho in agonist-stimulated mammalian cells results from the coupled actions of phospholipase D (PLD) and phosphatidic acid (PA)-phosphatase (reviewed in refs. 47, 181). Two PtdCho-PLD isoforms have been cloned from mammalian sources; PLD1 and PLD2 (48, 49). Both isoforms are highly dependent on PIP_2 for activity and PLD1 is also dependent on the small G protein ADP-ribosylation factor (ARF). PLD2 is constitutively active, suggesting that it is responsible for basal PLD activity, whereas agonist-stimulated PLD activity is attributable to PLD1. Phorbol esters and calcium are considered universal activators of PLD1 (181).

Numerous reports ascribe agonist-stimulated biological effects in mammalian cells to a putative PtdCho-specific phospholipase C (PLC), although no such mammalian enzymatic activity has been purified. PtdCho-PLC is often implicated based on attenuation of signalling pathways by the drug D609, a potent inhibitor of prokaryotic PtdCho-PLC. However, the specificity of D609 in mammalian cells remains dubious (184, 206).

1.3.3.1 The phosphatidylcholine cycle

In addition to activating PLD1, phorbol esters and growth factors also stimulate CCT activity and PtdCho synthesis (189, 204, 260). Within the cell cycle, increased CCTα activity and PtdCho synthetic rates during G1 phase coincides with rapid PtdCho turnover (133). Therefore, increased PtdCho synthesis in G1 could be necessary to supply PtdCho-derived lipid signalling molecules and/or to maintain cellular PtdCho levels for entry into S phase (132, 258). Since CCTα membrane-binding and activity is responsive to the lipid products of PtdCho degradation (135, 244), this suggests a PtdCho cycle (268) wherein CCTα has a central role in the coordination of PtdCho catabolism and anabolism (Figure 1.4). The PtdCho cycle provides a theoretical framework for the regulation of lipid signalling and membrane biogenesis during the cell cycle. In growth factor stimulated quiescent cells, or cycling cells reentering G1 following mitosis, PtdCho turnover rates are elevated due to mitogen-stimulated PtdCho degradation by phospholipases. In this model, various lipid products of PtdCho degradation such as arachidonic acid, phosphatidic acid (PA) and DAG stimulate CCTα activity and PtdCho synthesis, thereby maintaining membrane homeostasis (58, 268). A predictive outcome of this cycle would be that PtdCho resynthesis would consume lipid products of PtdCho degradation and attenuate agonist-stimulated lipid signalling events. However, this does not appear to be the case under most cellular conditions. For instance, signalling pools of DAG are primarily metabolized by conversion to PA by DAG kinases (117). Importantly, the activity of various DAG kinase isoforms appears finely coordinated with signalling events such as PKC activation, thereby appropriately modulating the strength and duration of the signal (264, 265).

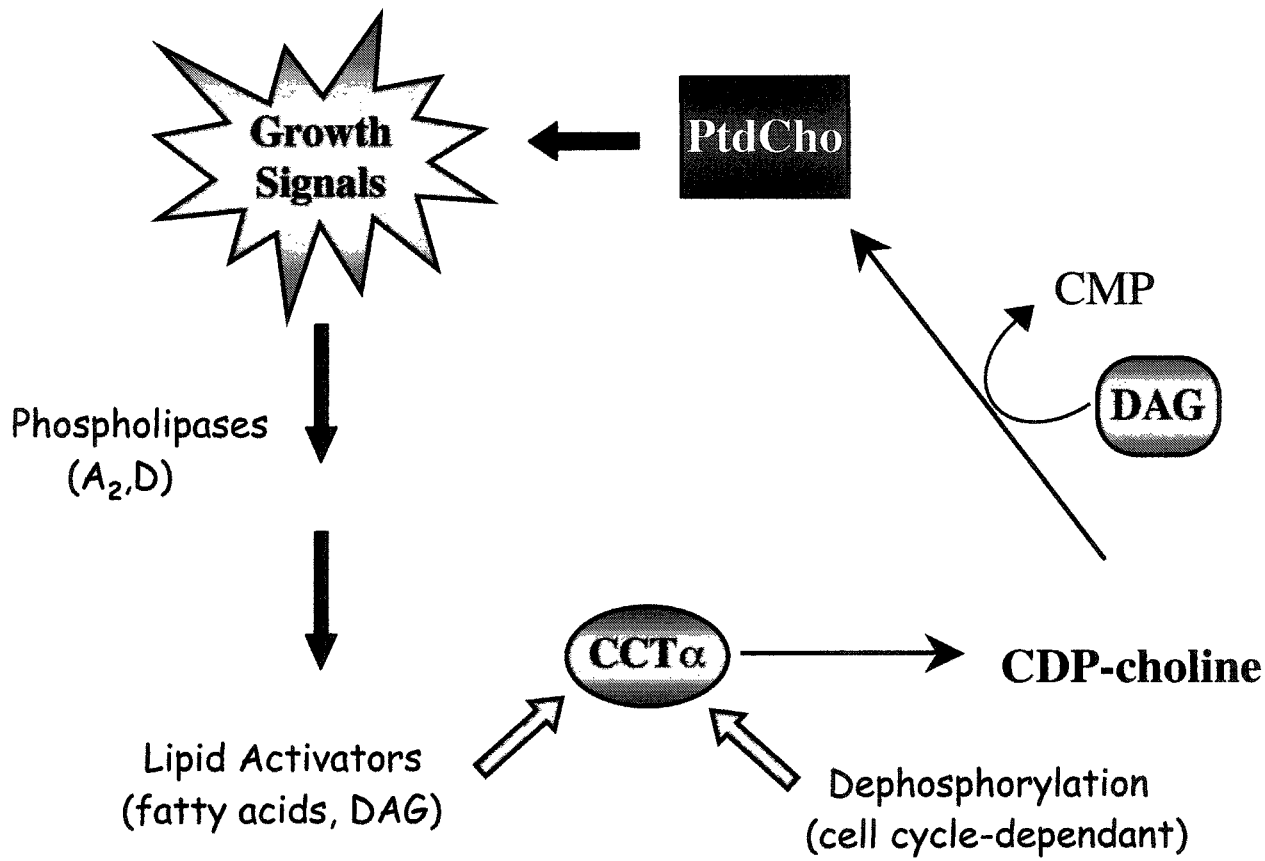

Figure 1.4 - The phosphatidylcholine cycle. Schematic model of the coordination of agonist-stimulated PtdCho degradation with PtdCho resynthesis mediated by membrane-binding and phosphorylation modes of CCTα regulation. See text for details.

A steady supply of fatty acid for *de novo* DAG and PtdCho synthesis could be critical to prevent the CDP-choline pathway from negatively impacting on lipid signalling events and support new membrane synthesis during the cell cycle. In this context, it is interesting to note that fatty acid synthase (FAS) is a target for anti-cancer drug development. FAS is highly expressed in a variety of human malignancies (157), and FAS inhibitors, such as cerulenin and derivatives, have been shown to selectively induce apoptosis in tumor-derived and oncogene-transformed cell lines (116, 210).

The FAS gene is transcriptionally regulated by the SREBP pathway (78, 118), and in several experimental models increased SREBP processing has been correlated with elevated FAS expression during cell transformation (321, 322). In a recent report, inhibition of phospholipid synthesis was shown to be the mechanism by which the FAS inhibitor C75 induced apoptosis in a human breast cancer cell model (328), indicating that transformed cells are highly dependent on *de novo* phospholipid synthesis.

1.3.3 Disruption of the CDP-choline pathway and apoptotic cell death

Given the importance of PtdCho, not only for the synthesis of new membranes, but also as a source of bioactive signalling molecules involved in cell proliferation and signalling pathways, it is perhaps not surprising that disruption of the CDP-choline pathway has been shown to be involved in the induction of apoptosis in both genetic and pharmacological models. In a recent survey of metabolic markers of apoptosis, CDP-choline was elevated in response to all apoptotic agents tested (304) indicating that the CDP-choline pathway is disrupted during the apoptotic program.

1.3.3.1 The caspase cascade: execution of the apoptotic program

Apoptosis, or "cell suicide", is an essential process in multicellular organisms resulting in the orderly disposal of unneeded or damaged cells. Apoptosis is a stringently controlled process that can be induced by various stimuli such as DNA and mitochondrial damage, ER-stress and signalling events at the cell surface. The initial stimulus results in the activation of a family of specialized proteases, known as caspases (reviewed in refs. 107, 108, 306). Autocatalytic removal of an inhibitory prodomain results in activation of initiator caspases that then cleave and activate downstream executionor caspases in what is known as the 'caspase cascade' (306). Individual executioner caspases play non-redundant roles in the demolition phase of apoptosis, resulting in the alteration or inactivation of substrate protein function and the eventual breakdown and packaging of cellular components (243). This process is very efficient, as evidenced by the select number of proteins that are proteolyzed, often at only one site (261). A recent survey has categorized 480 caspase substrates reported in the literature (90). Substrate proteins are involved in essential cell functions such as DNA repair, cytoskeletal arrangements, metabolism and anti- and pro-apoptotic mechanisms (75, 90). Several changes in lipid organization and metabolism have been shown to play important roles in apoptosis. The phospholipid phosphatidylserine (PtdSer) is exchanged from the inner leaflet of the plasma membrane to the outer surface of the cell where it acts as an 'eat-me' signal by binding to receptor molecules on macrophages that subsequently engulf the apoptotic cell remnants (86, 237). A recent report has identified lyso-PtdCho as a chemo-attractant signal secreted from dying apoptotic cells to attract macrophages (161). The production of this lyso-PtdCho signal requires caspase-3 cleavage and activation of Type VI $iPLA_2$. Interestingly, Type IVA cPLA2 is also a caspase target, resulting in its inactivation (8).

Caspase cleavage and activation of $iPLA_2$ also plays a role in increased arachidonic acid release that is a component of Fas-ligand induced apoptosis (9). Elevated arachidonic acid has been implicated as a second messenger in the initiation of apoptosis (40), and enzymes that metabolize arachidonic acid, such as cyclooxygenase-2, are often upregulated in various types of cancers (212, 271).

Apoptosis can be triggered by inappropriate growth signals, allowing for the removal of rapidly proliferating cells that could potentially pose a threat to the organism (109). Cells harboring single oncogenic mutations in genes associated with cell growth, such as *ras* and *myc*, are acutely sensitive to many apoptotic stimuli (143, 233). Due to the close coupling between the antagonistic processes of cell proliferation and apoptosis, it is apparent that apoptosis inhibition through mutation must accompany tumorigenesis (83). In spite of these inactivating mutations, the mode of cell death induced by most chemotherapeutic agents is apoptosis, indicating that cells are programmed with several redundant apoptotic pathways (109). This potential 'Achilles heel' of the cancer cell has led to intense research to understand the molecular links between cell proliferation and apoptosis in order to better design drug therapies and overcome drug resistance in cancer treatment (142).

1.3.3.2 Inhibition of CCTα and apoptosis

Inhibition of the CDP-choline pathway at the CCTα-catalyzed reaction has been implicated in several genetic and pharmacological models of apoptosis (reviewed in ref. 60). An unambiguous role of CCTα inhibition in apoptotic cell death occurs in MT58 cells that express a single CCTα allele containing a point mutation that renders the resultant enzyme temperature-sensitive (82, 254). Incubation at the non-permissive

temperature resulted in detection of apoptotic markers after 14 hours (61). Cells could be rescued by supplementation of the media with lyso-PtdCho (61), which can be utilized for PtdCho synthesis by the remodeling pathway, or PtdCho (81). This indicates that the CDP-choline pathway can be substituted with alternative PtdCho sources. Expression of PEMT and establishment of the PtdEtn-methylation pathway for PtdCho synthesis also rescued the MT58 cells at the non-permissive temperature, but only under high serum conditions (281).

Inhibition of CCT has also been proposed as a mechanism of apoptosis induction by the anti-tumor agent edelfosine (1-*O*-Octadecyl-2-*O*-methyl-rac-glycero-3-phosphocholine) and related ether-linked lyso-PtdCho analogues that inhibit CCT membrane binding and activity (12, 27-29, 137). Supplementation with lyso-PtdCho prevents edelfosine-induced apoptosis, similar to MT58 cells grown at the non-permissive temperature. Overexpression of CCTα inhibited the cytotoxic but not cytostatic effects of edelfosine (12). However, this study did not measure PtdCho synthesis rates under the various conditions. It remains unclear if CCTα is the relevant target of these lyso-PtdCho analogues since numerous other mechanisms have been implicated in cytotoxicity (reviewed in ref. 7). These include elevated levels of the pro-apoptotic lipid ceramide (301), disruption of cellular Ca^{2+} homeostasis (24) and inhibition of Ras activity (235).

1.3.3.3 Induction of apoptosis by farnesol

Farnesol (FOH) is a naturally occurring isoprenoid compound derived from the cholesterol biosynthetic pathway that preferentially induces apoptosis in transformed cells when administered at non-physiological concentrations (1, 224). FOH and related

isoprenoids are potent inhibitors of the CDP-choline pathway, imposing a metabolic block at the terminal reaction catalyzed by CPT, as indicated by accumulation of CDP-choline (2, 186, 279). In contrast to previous reports (2, 186), a recent study has shown that FOH does not act as a direct inhibitor of CPT *in vitro* (307). FOH effects on the CDP-choline pathway *in vivo* remain ambiguous. CDP-choline accumulation in cells could result from limiting levels of the CPT substrate DAG (4, 136), cellular acidification that occurs during apoptosis (2) or a disruption in the functional coupling of the CCT and CPT reactions (26). Since inhibition of PtdCho synthesis by genetic inactivation of CCTα (61) or the use of CCTα inhibitors (12, 27, 28) results in apoptotic cell-death due to PtdCho depletion, it has therefore been proposed that FOH similarly induces apoptosis by reducing PtdCho levels (2, 186). The addition of PtdCho to FOH-treated cells can prevent the initiation of apoptosis (2, 186), although it is unclear if this protection is due to intact PtdCho or its degradation products. Similar protection against FOH-induced apoptosis was also conferred by DAG (280), and phorbol esters delayed the induction of apoptosis in response to the FOH-related isoprenoid geranylgeraniol in a PKC-dependent manner (180). These results suggest that FOH and related isoprenoids disrupt DAG-signalling events, perhaps by limiting the amount of PtdCho available for DAG generation by PLD and/or a putative PtdCho-specific PLC (280). Interestingly, one study showed evidence of CCTα activation by FOH, with an increase in CCTα association with the membrane fractions of cells, indicating CCTα activation by FOH. This could have contributed to the observed increase in CDP-choline in FOH-treated cells in addition to CPT inhibition.

1.4 Rationale and objective of the study

The primary objective of my thesis research is the regulation of CCTα in mammalian cells. Specifically, I have focused on how CCTα senses and responds to cellular requirements for PtdCho leading to altered activity and cellular localization. Previous work in our laboratory identified coordination of cholesterol and PtdCho synthesis in CHO SRD cell lines with defective regulation of SREBP processing. The underlying mechanisms remained uncharacterized. The initial aim of this work was to test the hypothesis that the SREBP regulatory pathway exerted control of PtdCho synthesis at the level of substrate supply and also through transcriptional and/or post-translational affects on the rate-limiting enzyme in the CDP-choline pathway, CCT. Specifically we wanted to test whether CCT activity was responsive to cellular levels of cholesterol and/or fatty acid metabolites controlled by SREBP activity.

The work presented in Section 3 examined the regulation of CCT in cell lines with increased cholesterol and fatty acid synthesis due to deregulation of SCAP function. In Section 4, experiments were designed to examine the effect of the apoptotic agent FOH, a cholesterol biosynthetic pathway metabolite, on CCT activity and PtdCho synthesis. Since the results from this section suggested an important role for nuclear localization of CCT in cellular PtdCho metabolism, the nuclear sites of CCT membrane localization were examined in detail as presented in Section 5.

Chapter 2

Materials and Methods

2.1 Materials

1,2 dioleoyl-*sn*-glycerol (DAG), fraction V and essentially fatty acid-free bovine serum albumin (BSA), cardiolipin, choline, CDP-choline, farnesol (FOH, prepared in ethanol), octyl-β-D-glucoside, oleyl alcohol (OLOH, prepared in ethanol), 1,4-diazabicyclo-[2.2.2]-octane and phosphocholine were purchased from Sigma-Aldrich. Arachidonic acid and oleic acid were purchased from Matreya Inc. Phorbol 12-myristate 13 acetate (TPA), 1-oleyl, 2-acetyl-sn-glycerol (OAG) and 1,2-dioctanoyl-sn-glycerol (diC8) were from BioMol. 25-hydroxycholesterol was purchased from Steraloids Inc., Wilton, NH. PtdEtn (egg), PtdCho (egg), phosphatidylserine (PtdSer, brain) and phosphatidylinositol 4-phosphate (PtdIns-4-P, brain) were obtained from Avanti Polar Lipids. Cerulenin was from Sigma-Aldrich and was prepared as a 10 mg/ml stock in DMSO. Triacsin C was from BioMol and supplied as a 4.9 mM stock in DMSO. [Methyl-^{3}H]choline, CDP-[methyl-^{14}C]choline, phospho[methyl-^{14}C]choline, and [γ-^{32}P]ATP, [α-^{32}P]dATP, [^{32}P]phosphate and [1-^{14}C]acetate were from Mendel-New England Nuclear. SI nuclease (from *Aspergillus olyzae*) was from Gibco-BRL. *Escherichia coli* DAG kinase was from CalBiochem. z-VAD-FMK and z-DEVD-FMK were from Calbiochem (prepared as 25 mM stocks in DMSO and stored at –20°C). Silica gel 60 TLC plates were from EM Science and Silica gel G plates from Fisher Scientific. Acetyl-DEVD-*p*-nitroanilide and acetyl-VEID-*p*-nitroanilide were from BioMol. Recombinant rat CCTα expressed in the baculovirus system was provided by Rosemary Cornell, Simon Fraser University, Vancouver. Gene Editor ™ site-directed mutagenesis kits were from Promega. Cell Death ELISA™ kits was purchased from Roche. Cell culture medium was from Life Technologies, Inc. Complete™ protease

inhibitor cocktail (used at 50-fold dilution), which inhibits a broad spectrum of serine, cysteine and metalloproteases as well as calpain, was from Boehringer Mannheim. G418 was from Life Technologies, Inc. Lipoprotein-deficient serum was prepared from fetal calf serum by centrifugation at 150,000 x *g* for 26 hours, followed by extensive dialysis against 10 mM phosphate (pH 7.4) and 150 mM NaCl (104). Triton X-100 was from Pierce. Hoechst 33258 was from Riedel-De Haen, Seelze, Germany. Lysine-fixable, Oregon Green-488-conjugated 70 kDa dextran, Alexafluor-conjugated concanavalin A were from Molecular Probes. All other reagents were of the highest quality commercially available.

2.1.1 Preparation of albumin-bound fatty acids

A 10 mM stock solution of each fatty acid was prepared by diluting the free fatty acid in ethanol and converted to the sodium salt by the addition of NaOH (final concentration 0.25 M). The ethanol was then evaporated under N_2, and the dried sodium salt of free fatty acids was dissolved in 150 mM NaCl and stirred at room temperature for 10 min with essentially fatty acid-free BSA (final concentration of 10% (w/v) in 150 mM NaCl). Solutions were adjusted to pH 7.4 with NaOH and stored in multiple aliquots at -20°C protected from light under N_2.

2.1.2 Antibodies

A rabbit polyclonal antibody raised against 45 amino acids of the C-terminal phosphorylation domain of rat CCTα was kindly provided by Martin Post, Hospital for Sick Children, Toronto, Canada (317). This antibody does not cross-react with the CCTβ isoforms because of sequence divergence in the C-terminal phosphorylation domain (169,

171). Dephosphorylation of CCTα by treatment with λ protein phosphatase did not affect recognition of CCTα with this antibody (results not shown). A rabbit anti-rat CCTα antibody raised against the full-length protein was kindly provided by Suzanne Jackowski, St. Jude Children's Research Hospital, Memphis, TN. Antibody against the membrane binding region of CCTα was kindly provided by Rosemary Cornell, Simon Fraser University, Vancouver (139). Monoclonal antibody 131C3 detecting a common epitope in lamin A and C and was kindly supplied by Dr. Yves Raymond, Université de Montreal, Montreal. A monoclonal antibody to protein disulfide isomerase (PDI) was from Stressgen. A rabbit polyclonal antibody against poly (ADP-ribose) polymerase (PARP) was from Santa Cruz Biotechnology, Inc. (Santa Cruz, CA). Monoclonal antibody 414 directed against a common epitope found in Nup62 and related components of the nuclear pore complex was from Berkeley Antibody Co. (Richmond, CA). Secondary horseradish peroxidase-coupled antibodies were from Bio-Rad. Alexafluor-conjugated secondary antibodies for immunofluorescence were from Molecular Probes.

2.2 Cell culture and transfections

2.2.1 Routine maintenance of mammalian cells

CHO cells (ATCC CCL61) were cultured in Dulbecco's modified Eagle's medium (DMEM) with 5% fetal calf serum (FCS) and proline (34 μg/ml) (medium A) in an atmosphere of 5% CO_2 at 37°C. For experiments, cells were seeded at a density of 100,000 - 150,000 cells per 60 mm dish in 3 ml of medium A. On day 2, cells received 2 ml of DMEM with 5% lipoprotein-deficient serum (LPDS) and proline (34 μg/ml) (medium B). Experiments were started 18 to 24 h after this medium change when cells were ~70% confluent.

SRD-4 cells were cultured in medium B supplemented with 0.5% FCS and 25-hydroxycholesterol (0.3 μg/ml) at 37 °C in 5% CO_2. CHO7 cells were maintained in medium B supplemented with 0.5% FCS. For experiments, cells were seeded at a density of 200,000 cells per 60-mm dish in 3 ml of medium B supplemented with 0.5% FCS. On day 2, cells received 2 ml of medium B. Experiments were started 18 to 24 h after this medium change when cells were 70% confluent. NIH 3T3, HEK 293, and F8 cells were cultured in DMEM with 10% FCS. Twenty-four h before the start of experiments, cells received DMEM with 10% LPDS.

CHO MT58 cells with a temperature sensitive CCTα allele (82) were provided by Dennis Vance, U. of Alberta, Edmonton. For experiments, CHO MT58 cells were seeded at 500,000 cells per 60 mM dish in medium A in an atmosphere of 5% CO_2 at 33°C.

2.2.2 Stable Cell Lines

CHO cells overexpressing SCAP (CHO-SCAP) and SCAP D443N (CHO-SCAP D443N) were prepared by calcium phosphate transfection with pTK-HSV-SCAP-T7, pTK-HSV-SCAP-T7 (D443N) or empty vector (124). Cells were grown in medium B with G418 (600 μg/ml) until individual colonies were evident at 12-14 days. SCAP transfected cells were trypsinized and cultured in medium B containing geneticin (G418) (600 μg/ml) and 25-hydroxycholesterol (0.5 μg/ml). After 10 days, thirty G418 and 25-hydroxycholesterol resistant colonies were harvested, expanded in culture for 10-14 days and screened for expression of SCAP and SCAP D443N by immunoblotting of total cell extracts with monoclonal antibodies specific for T7 or HSV epitope tags. Mock transfected cells were selected after growth in G418. Four transfected cell lines expressing epitope-tagged SCAP, SCAP D443N or empty vector were selected for

further characterization. Stock cultures of SCAP transfected cells were maintained in medium B supplemented with 0.5% FCS and with G418 (300 μg/ml) and 25-hydroxycholesterol (0.3 μg/ml). For experiments, cells were seeded at a density of 200,000 cells per 60-mm dish in 3 ml of medium A supplemented with 0.5% FCS on day 0. On day 2, cells received 2 ml of medium B. Experiments were started 18 to 24 h after this medium change when cells were 70% confluent.

CHO MT58 cells overexpressing CCTα and CCTα mutants were prepared by calcium phosphate transfection in 60 mm dishes with pcDNA3.1/V5His-CCT, pcDNA3.1/V5His-CCT H89G, pcDNA3.1/V5His-CCT K122A or pcDNA3.1/V5His-CCTΔ236. Cells were grown in DMEM with 10% FCS and proline (34 μg/ml) (medium C) with G418 (800 μg/ml) until individual colonies were evident after 12-14 days. Clones from each dish (>100) were collected by trypsinization and cultured in medium C containing G418 (800 μg/ml). Following expansion, cells were split and seeded onto coverslips for screening of expression by immunofluorescence detection with the anti-V5-monoclonal antibody. Optimally expressing pools were maintained in medium C containing G418 (400 μg/ml). As a control, cells were transfected with empty vector and selected as described above.

CHO-MT58 cells overexpressing CCTα and CCT D28E were prepared by the calcium phosphate method in 60 mm dishes with pCMV5-CCT and pCMV5-CCT D28E. Cells were grown in medium C with G418 (800 μg/ml) until individual colonies were evident at 12-14 days. Individual clones were picked and expanded in 60 mm dishes. Clones were screened for expression of CCT or CCT D28E by immunofluorescence analysis using a polyclonal antibody against a C-terminal epitope in CCTα. These cells

are used in experiments shown in Figure 4.7 and are called MT58-CCT and MT58-CCT D28E to distinguish them from the cells described below which also overexpress wild-type rat CCT.

CHO MT58 cells homogenously overexpressing CCTα (CHO58–CCT) and vector transfected controls cells (CHO58-Vec) were provided by Dennis Vance, University of Alberta, Edmonton. These cells are used in experiments presented in Section 5 as indicated in figure legends.

2.3 Site-directed mutagenesis

Site-directed mutagenesis of the rat CCTα cDNA in pCMV5 (pCMV5-CCT) (173) was performed using the Gene Editor System (Promega) and confirmed by sequencing. The following oligonucleotides were used: CCT D28E; ACAGAGGAAGAAGGAATTCCTTCC, and CCT D54E; ATTGAAGTT-GAATTTAGTAAGCCC.

V5-epitope tagged CCTα constructs were prepared as follows. To create the wild-type plasmid (pcDNA3.1/V5His-CCT), the HindIII/XbaI fragment of pCMV5-CCT was ligated into pcDNA3.1/V5 His TOPO TA (Invitrogen) that had been digested with HindIII/XbaI. The stop codon of CCT was changed to a tyrosine residue and a single nucleotide was removed to bring the V5-epitope tag into frame using the mutagenic oligonucleotide ATCAAGAGGACTATAATCTAGAGGCG. To create pcDNA3.1/ V5His-CCT H89G and pcDNA3.1/V5His-CCT K122A, the HindIII/XbaI fragment of pcDNA3.1/V5His-CCT was subcloned back into pcDNA3.1/V5HisTOPO TA since the pcDNA3.1-V5His-CCT had gained resistance to the Gene Editor antibiotic mix during prior mutagenesis. Mutagenesis reactions were performed on the resultant plasmid using

the following oligonucleotides; H89G; TTGACTTATTTGGCTCTAGTCACGC, and K122A; CGCACAACTTCGCGGGCTTCACTGT. To create pcDNA3.1/V5His-CCTΔ236, an XbaI site was introduced into pCMV5-CCT after amino acid 236 using the oligonucleotide TCAGCTTTATCAATCTAGAGAAATAACACT. The HindIII/Xba1 fragment from the resulting plasmid was excised and cloned into HindIII/Xba1 digested pcDNA3.1/V5His-CCT.

2.4 Transient Transfections

On day 2, cells were transiently transfected by the Lipofectamine method as per manufacturer's instructions (Life Technologies Inc) using 0.5 μg DNA and 3 μl Lipofectamine reagent in 1.5 ml DMEM per 60 mm dish. After 6 hours an equal volume of DMEM plus 10% fetal calf serum and proline (68 μg/ml) was added to the cells. On day 3, medium was replaced with 3 ml medium A and cells were cultured for another day before start of experiments.

2.5 Analysis of labeled phospholipids, choline metabolites, fatty acids and sterols

2.5.1 Extraction and analysis of phosphatidylcholine and choline metabolites

After labelling with [^{3}H]choline (see figure legends for specific conditions), cells were rinsed once with cold phosphate-buffered saline (PBS) and scraped in 1 ml of methanol-water (5:4, v/v). The culture dish was rinsed with 1 ml of methanol-water, the extracts were combined in a glass screw cap tube and sonicated with a needle-tip sonicator at maximum power for 30 s. After an aliquot was taken for protein determination, 4 ml of chloroform was added to each tube, the phases were separated by centrifugation at 2,000 x g for 5 min and 1.5 ml of the aqueous phase was removed to a glass test tube for separation of water soluble [^{3}H]choline metabolites. The organic phase

was extracted twice with 2 ml methanol/0.58% NaCl/chloroform (45:47:3, v/v), evaporated under N_2 and redissolved in 1 ml of chloroform. [^{3}H]PtdCho was measured by liquid scintillation counting of an aliquot of the chloroform phase (>98% of radioactivity was in PtdCho). Aqueous choline metabolites were separated by thin layer chromatography (TLC) on silica G plates in ethanol-water-ammonia (48:95:6, v/v). [^{3}H]Choline, [^{3}H]phosphocholine, [^{3}H]glycerophosphocholine and [^{3}H]CDP-choline were identified by co-migration with authentic standards stained with 1% phosphomolybdic acid in chloroform-ethanol (1:1, v/v) and 1% stannous chloride in 3 N HCL. Zones were scraped into vials with 0.5 ml water for quantification of radioactivity by liquid scintillation counting.

2.5.2 Measurement of oleate incorporation into triglycerides and phospholipids

The incorporation of [1-^{3}H]oleate into triglycerides and phospholipids in cultured CHO cells was measured by incubating cells with 0.1 mM [1-^{3}H]oleate-BSA complex (6000-7000 dpm/nmol) for 1 h at 37°C. Cells were extracted on the dishes with 2 ml hexane/isopropanol (1:1, v/v) for 30 min at room temperature. Lipid extracts were transferred to a glass screwcap test tube, dishes were rinsed with 1 ml hexane/isopropanol and combined. Protein remaining on the culture dish was dissolved in 1 ml 0.5 N NaOH and protein determination was carried out on an aliquot (168). Lipid extracts were dried under N_2, redissolved in 50 μl hexane, applied to TLC Silica gel 60 plates and separated in a solvent system of hexane/diethyl ether/acetic acid (90:30:1, v/v). Triacylglycerides were identified by co-migration with authentic standards visualized by brief exposure to iodine. Identified zones on the TLC plate were scraped into vials and radioactivity quantified by liquid scintillation counting.

2.6 Measurement of diacylglycerol mass

DAG was quantified in chloroform extracts of cells (as described in 2.5.1) by the DAG kinase assay (211). Briefly, aliquots (corresponding to 80-100 μg cell protein) of the chloroform phase were evaporated under N_2 in a glass test tube. The dried lipid was solubilized in 20 μl of an octyl-β-D glucoside/cardiolipin solution (7.5% octyl-β-D-glucoside, 5 mM cardiolipin in 1 mM diethylenetriaminepenta-acetic acid (DETAPAC)) using a bath sonicator for 15 s followed by incubation at room temperature for 15 min. The reaction buffer was prepared as a 2 X solution containing 100 mM imidazole HCl (pH 6.6), 100 mM NaCl, 25 mM $MgCl_2$ and 2 mM ethyleneglycolaminoethylethertetra acetic acid (EGTA). To the solubilized lipid/octylglucoside solution was added 50 μl of 2X reaction buffer, 10 μl of freshly prepared 100 mM dithiothreitol (DTT), 10 μl of diluted membranes (5 μg of protein) and water to a total volume of 90 μl. The reaction was started by the addition of 10 μl of 10 mM [γ-^{32}P]ATP prepared in 100 mM imidazole and 1 mM DETAPAC (pH 6.6). After mixing, the reaction proceeded at 25°C for 45 min and was terminated by the addition of 1 ml chloroform and 1 ml 0.7% perchloric acid ($HClO_4$). The lower chloroform phase was washed 2 times with distilled water and dried under N_2. Dried extracts were dissolved in 50 μl of 5% methanol in chloroform and 20 μl of the sample was resolved on a Silica Gel 60 TLC plate in chloroform:methanol:acetic acid (65:15:5, v/v). Plates were air-dried, subjected to radioautography, the radioactive spot corresponding to phosphatidic acid was scraped into a vial and radioactivity measured by a scintillation counter. The amount of sn-1,2-DAG present in the original sample was calculated based on the specific activity of ATP employed and a DAG standard curve generated using dioleoylglycerol (Sigma).

2.7 Protein quantification

Proteins from samples that contained TX-100, which interferes with the μLowry assay, were precipitated prior to assay (168). Briefly, samples were diluted to 1 ml in dH_20, mixed with 100 μl of 0.15% sodium deoxycholate for 10 min at 20°C, 100 μl 72% tricholoroacetic acid was added and samples were subjected to centrifugation at 20°C for 15 min. The supernatant was removed and precipitated proteins or samples that did not contain TX-100 were diluted in 400 μl dH_20, mixed with 400 μl Solution A (equal volumes of 10% SDS, 0.8 M NaOH, dH_20 and CTC (10% sodium carbonate, 0.1% copper sulfate, 0.2% potassium tartarate)) and incubated at 20°C. After 10 min, 200 μl of Solution B (5 X dilution of Folin-Ciocalteu reagent in dH_20) was added and the samples were incubated at 20°C for a further 30 min. The absorbance at 660 nm was determined and used to calculate protein concentrations by comparison to BSA standard curve (2 to 20 μg).

2.8 Preparation of cell extracts

2.8.1 Isolation of soluble and particulate CCTα by digitonin permeabilization

This protocol was employed for immunoblot analysis of CCTα presented in Figure 3.6 and for CCTα enzyme activity and immunoblot analyses presented in Section 4. Digitonin permeabilization was carried out at room temperature as previously described (308) with minor modifications. Briefly, 60-mm dishes were rinsed once with cold PBS and incubated for 1 min without agitation in 0.5 ml of permeabilization buffer (10 mM Tris-HCl (pH 7.4), digitonin (0.05 mg/ml), 0.25 M sucrose, 2.5 mM ethylenediaminetetraacetic acid (EDTA), 1 mM DTT, 0.1 mM phenylmethylsulfonyl fluoride (PMSF) and Complete protease inhibitor). The permeabilization buffer was

removed from cells and subjected to centrifugation for 15 min at 20,000 x *g* at 4°C to remove debris (designated the soluble fraction). Cell ghosts were scraped in 0.5 ml of permeabilization buffer without digitonin and homogenized by 10 passages through a 23-gauge needle (designated the membrane fraction). This protocol extracted >95% of lactate dehydrogenase activity into the soluble fraction.

2.8.2 Cellular fractionation by high-speed centrifugation

This protocol was employed in experiments in Section 3 for the separation of CCTα into soluble and particulate fractions prior to CCT enzyme assays and for the immunoprecipitation of ^{32}P-labeled CCTα, and also to prepare particulate fractions for immunoblot analysis of SCAP expression and CPT enzyme assays. Cells were harvested in cold PBS and sedimented for 5 min at 2,000 x *g*. Cell pellets were homogenized in buffer A (20 mM Tris-HCl (pH 7.4), 0.1 mM PMSF, 10 mM sodium fluoride (NaF), 1mM EDTA and 5 mM DTT) by 15 passages through a 23-gauge needle. Homogenates were centrifuged for 5 min at 2,000 x *g* to sediment unbroken cells. The resulting supernatent was centrifuged for 15 min at 400,000 x *g*, the supernatant (soluble fraction) was collected and the pellet (particulate) was resuspended with a 23-gauge needle in buffer A containing 0.25 M sucrose (50 µl/100 ml dish). To extract SCAP, the particulate fraction was treated in buffer A containing 1% (v/v) Nonidet NP-40 and the soluble fraction was collected by centrifugation for 15 min at 15,000 x g.

2.8.3 Preparation of total cell extracts

CCTα and the precursor and caspase-cleaved forms of PARP were extracted as follows for immunoblot analyses presented in Section 4. Cells in 60 mm dishes were rinsed once with cold PBS, scraped into 1 ml cold PBS and collected by centrifugation

for 1 min at 15,000 x g. Cell pellets were resuspended in 150 µl high-salt Triton X-100 solubilization buffer (10 mM Tris-HCl (pH 7.4), 1% (w/v) Triton X-100, 500 mM NaCl, 2 mM EDTA, 1mM DTT, 0.1 mM PMSF and Complete protease inhibitors), incubated at 0°C for 15 minutes, and subjected to centrifugation at 4°C for 15 min at 21,000 x *g* to remove Triton X-100 insoluble material.

2.9 Immunoblotting and immunoprecipitation

Equivalent amounts of protein from soluble, particulate or total cell extracts were resolved by SDS-PAGE on 8% - 10% gels and electroblotted to nitrocellulose. The nitrocellulose filter was incubated with Tris-buffered saline with Tween-20 (TBS-T) (20 mM Tris-HCl, 150 mM NaCl, pH 7.4 0.1%, (v/v) Tween-20) containing 5% (w/v) skim milk powder. The filter was subsequently incubated with a primary antibody for 1-2 h at 25°C and then with secondary antibody (1:10,000) conjugated to horseradish peroxidase (HRP) for 45 min. Following primary and secondary incubation, blots were washed for three times each with TBS-T containing 5% (w/v) skim milk powder and developed by the chemiluminescence method according to manufacturer's instructions (Amersham Pharmacia Biotech).

CHO7, SRD-4, CHO-Mock, CHO-SCAP and CHO-SCAP D443N cells were labeled for 12 h in phosphate-free medium A containing [^{32}P]phosphate (25 µCi/ml). Soluble and particulate fractions were isolated as described (see 2.8.2) in buffer A. Triton X-100 was added to particulate and soluble fractions to a final concentration of 0.3% (w/v) and samples were subjected to centrifugation for 15 min at 10,000 x g. The soluble fractions were recovered and incubated for 1 h at 4°C with a 1:200 dilution of the rabbit anti-rat CCTα antibody directed against the membrane-binding domain, followed

by incubation with protein A-Sepharose for 45 min. Sepharose beads were washed 6-7 times with PBS containing 1% (w/v) Triton X-100, boiled in SDS-PAGE sample buffer and ^{32}P-labeled CCTα was resolved by SDS-10%PAGE. Dried gels were exposed to film at –70°C.

2.10 *In vitro* enzyme assays

2.10.1 CCT activity

CCT activity in soluble and membrane fractions (see 2.8.1 and 2.8.2 for specific details) was assayed in the presence of PtdCho-oleate vesicles by monitoring the conversion of phospho[^{3}H]choline to CDP-[^{3}H]choline as previously described (50). Briefly, the reaction mixture contained 50 μM Tris-HCl (pH 7.4), 0.1 M NaCl, 10 mM $MgCl_2$, 3 mM CTP, 1.5 mM [^{3}H]phosphocholine, PC/oleic acid vesicles (0.1 mM/0.1 mM) and 30 μl of enzyme source in a volume of 50 μl. PC/oleate vesicles were prepared by dissolving lipids in chloroform, evaporating the solvent under reduced pressure and hydrating at room temperature for at least 1 h. Vesicles were formed by sonication for 3 min at 4°C. The assay was initiated by the addition of [^{3}H]phosphocholine. After 25 min at 37°C, the reaction was terminated by the addition of 50 μl of methanol/ammonia hydroxide (9:1, v/v) and [^{3}H]CDP-choline was isolated by TLC and quantified by liquid scintillation counting.

Recombinant CCTα activity with FOH- and oleate-supplemented PtdCho vesicles was also assayed by this method. PtdCho-FOH and PtdCho-oleate vesicles were prepared by sonication of lipids suspensions at 4°C in 10 mM Tris-HCl (pH 7.4) and1 mM EDTA.

2.10.2 CPT Activity

CPT activity was assayed in the membrane/particulate fraction (see 2.8.2) (53). The particulate fractions were suspended in 40 mM Tris (pH 8.0), 10 mM $MgCl_2$, 1 mM EGTA, 0.2 mM [^{14}C]CDPcholine and 1 mM 1,2,-dioleoylglycerol (prepared as an emulsion in 0.015% (w/v) Tween 20) in a final volume of 100 µl. The assays were incubated for 15 min at 37°C and terminated by the addition of 3 ml of cholorform:methanol (2:1, v/v), 1.5 ml of water was added, the organic phase washed twice with 40% methanol in water and dried under N_2. The residue was dissolved in chloroform and [^{14}C]PtdCho quantified by liquid scintillation counting.

2.10.3 Caspase 3 and 6 Activity

CHO cells on 4 x 100 mm dishes were harvested in PBS and sedimented for 5 min at 3,000 x g. Homogenates were made using a "B" type 1 ml pestle in 200 µl buffer (25 mM HEPES (pH 7.0), 5 mM $MgCl_2$, 1 mM EGTA, 5 mM EDTA, 1 mM DTT, Complete protease inhibitor cocktail, 0.1 mM PMSF, 0.1% (w/v) Triton X-100). Samples were subjected to centrifugation for 15 min at 400,000 x g using a TLA 120.2 rotor and supernatant was collected. Caspase 3 and 6 activity was measured in 100 μg of supernatant for 1 h at 30°C using 200 μM acetyl-DEVD-*p*-nitroanilide or acetyl-VEID-*p*-nitroanilide. Activity was based on the release of nitroanilide measured at A_{420}.

2.11 mRNA quantification

Total RNA was isolated by the guanidinium thiocyanate/phenol/chloroform extraction method (44). CCTα mRNA was quantified using a single strand antisense probe prepared from M13 mp19 containing a 86 bp Hind III-Eco RI fragment of the rat cDNA (250, 320). The CCTα S1 probe hybridized to the 5' end of the mRNA and did not

hybridize to CCTβ mRNA because of lack of sequence similarity in that region (169, 171). The glyceraldehyde-3-phosphate dehydrogenase (GAPDH) S1 probe contains nucleotides 467-562 of the human GAPDH cDNA and recognizes the hamster sequence (250, 270).

^{32}P-labeled probes for quantitative S1 nuclease protection assays were prepared from M13 templates and purified by 7 M urea-6% polyacrylamide gel electrophoresis (43). Total RNA for CCTα (30 μg) and GAPDH (10 μg) were hybridized in 90% formamide buffer with an excess of single-stranded DNA probe at 90°C followed by slow cooling to 37°C and incubation at that temperature for 16 h. Hybridization reactions were digested with S1 nuclease, separated on 7 M urea-6% polyacrylamide gels and exposed to Kodak XAR film at -70 °C for 3–18 h. S1-partial products were quantitated by scanning of films and analyzed using the NIH Image software package (Version 1.6.2)

2.12 Immunofluorescence microscopy

2.12.1 Fixation and permeabilization of cells, and incubation with antibodies

Cells were cultured on glass coverslips to 50% confluence, fixed in 3% formaldehyde-PBS immunofluorescence buffer (PBS-IF; 10 mM Na_2HPO_4 (pH 7.4), 225 mM NaCl and 2 mM $MgCl_2$) for 15 min, washed twice in PBS-IF containing 5 mM ammonium chloride and permeabilized in PBS-IF containing 0.05% (w/v) Triton X-100 for 10 min at -20°C. In experiments investigating localization of lamin A/C, cells were fixed and permeabilized on glass coverslips in cold methanol/acetone (1:1, v/v) for 15 min at -20°C. Coverslips were air-dried for 1 min and washed three times in PBS. For all experiments, coverslips were blocked with 1% (w/v) BSA (Fraction V) in PBS-IF for 30 min prior to incubation with antibodies. Primary antibody incubations were in 1%

(w/v) BSA in PBS-IF (0.5 ml) for 12 to 18 h at 4°C or 1 h at 25°C. Primary antibody incubations were followed by three washes for 15 min each in 1% (w/v) BSA in PBS-IF, and incubated with cross-absorbed fluorophore-conjugated secondary goat anti-mouse (GAM) or goat anti-rabbit (GAR) antibodies in 1% (w/v) BSA in PBS-IF (1 ml) for 1 h at 25°C. Next, coverslips were washed three times for 15 min each in 1% (w/v) BSA in PBS-IF and rinsed once in dH_2O. For dual-labelling experiments, all incubations and washing steps were carried out separately. Following final washes, the coverslips were rinsed in dH_2O, mounted in 50 mM Tris-HCl (pH 9.0), 2.5% (w/v) 1,4-diazabicyclo-[2.2.2]-octane and 90% (v/v) glycerol and sealed with clear nail polish. Images were collected using a Zeiss Laser Scanning Confocal Microscope (LSCM) model LSM510 or LSM 510 Meta equipped with a 100X oil immersion objective. 3-D images were reconstructed from 18-20 serial Z-axis scans of 0.5-0.6 μM thickness using LSM510 Meta and Adobe Photoshop software. Images using Hoechst staining were obtained using an Axioplan 2 fluorescence microscope with a Planapo 100x oil immersion objective and equipped with a Spot CCD camera. Single images were merged using Adobe Photoshop software.

2.12.2 Direct fluorophore labelling

For labelling with Alexa 488-conjugated Con A, coverslips were incubated for 15 min in Con A (2 μg/ml) in 1% (w/v) BSA in PBS-IF followed by three washes for 15 min each in 1% (w/v) BSA in PBS-IF. In dual- and triple-labelling experiments, Con A incubations were carried out prior to antibody incubations. Hoechst 33258-staining was carried out following the final wash step. Coverslips were washed once with PBS-IF,

incubated for 10 min at 4°C in Hoechst 33258 (10 μg/ml) in PBS-IF and washed three times for 10 min each in PBS-IF.

2.12.3 Scrape-loading of CHO cells with fluorescent dextran

Lysine-fixable, Oregon green 488-labeled dextran (70 kDa) was introduced into CHO cells by scrape-loading (238). CHO cells cultured on 60 mm dishes in medium A were grown to >90% confluence. Dishes were placed on ice, medium was removed and cells were washed once with 3 ml cold PBS. Cells were gently scraped from dishes with a rubber policeman in 0.5 ml of ice-cold PBS containing fluorescent tagged dextran (1 mg/ml). Cells were allowed to take up dextran for 5 min on ice, diluted with 8 ml of medium A and collected by centrifugation for 5 min at 300 x *g*. Cells were reseeded onto glass coverslips in 6-well plates in medium A for 8 h and then switched to medium B for 18 h prior to treatment. Coverslips were fixed and permeabilized in 3% formaldehyde and 0.05% TX-100 and processed for immunofluorescence as described in 2.12.1.

2.13 Quantification of nuclear tubules in the NR network

Images for quantification of nuclear tubules were obtained using confocal laser scanning microscopy. Pinhole settings were maintained at 0.5 μm, while gain settings were manually selected to optimize visualization of intranuclear structures and standardized to assess all samples within an experimental set. Datasets were collected from cell images obtained from randomly selected fields within the cell population and were scored by direct count by blinded and unblinded observers.

2.13.1 Identification of nuclear tubules using Lamin A/C

To identify nuclear tubules, lamin A/C immunostaining was examined in 3-D reconstructions of serial optical Z-sections (18-20 sections, 0.5-0.6 μm thickness) spanning the nucleus. Projections were performed using LSM 510 software. Filamentous lamin A/C-positive structures continuous with the peripheral nuclear envelope (NE) and spanning >50% of the nuclear volume (characteristic of nuclear tubules) were scored.

2.13.2 Identification of nuclear tubules using fluorescent Con A

3-D reconstructions of entire nuclei stained with Alexa488-conjugated Con A verified that Con A-positive intranuclear structures in single optical sections represented tubular extensions of the NE (Figure 5.1, C). Single optical Z-sections (0.5 μm) of the mid-nuclear region of cells were collected for quantification of intranuclear Con A-positive structures corresponding to nuclear tubules.

2.14 Preparation of liposomes and tubulation by CCTα

Liposomes (1 mg/ml) containing total brain lipid extract or a synthetic formulation (50, 25, 17.5, 5, and 2.5 mol% of PtdCho, PtdEtn, PtdSer, oleic acid and PtdIns-4-P, respectively) were prepared by extrusion. Briefly, lipids were dried under vacuum in 50 ml round bottom flasks, sealed under N_2 and left overnight at –20°C. Lipids were resuspended in 2 ml liposome buffer (25 mM HEPES (pH 7.4), 100 mM potassium chloride (KCl), 2.5 mM $MgCl_2$) with gentle shaking for 1 h at 25°C. Lipid suspensions were extruded 20 times through a polycarbonate membrane with 0.4 μm pores as per manufacturer's instructions (LiposoFast™ Basic, Cat # LF-1, Avestin Inc).

For sedimentation assays, liposomes (250 μM) were incubated with recombinant

CCTα or a GST-fusion protein containing the PH domain of oxysterol binding protein (GST-PH) (310) (2.5 μM) for 15 min at 37°C in 50 μl of liposome buffer and placed on ice. To assess protein binding to liposomes, reactions were subjected to centrifugation at 125,000 x *g* for 20 min in a Beckman TLA-45 rotor. Following centrifugation, supernatants were removed immediately and pellets were resuspended in an equal volume of buffer. Proteins associated with supernatent and pellet fractions were resolved on SDS-10%PAGE, visualized by Coomassie stain and photographed with a Bio-Rad VersaDoc Model 3000 imaging system.

To visualize changes in liposome morphology, liposomes were incubated with proteins as above, spread on Formvar and copper-coated grids (200 mesh), negatively stained with 2% uranyl acetate and observed using a Philips EM300 transmission electron microscope (TEM).

2.15 Thin section transmission electron microscopy of CHO cells

CHO cells were cultured to 70% confluence on 60 mm dishes and fixed on the dish in 2.5% (w/v) glutaraldehyde in 0.1 M sodium cacodylate buffer (pH 7.2) for 1 h at room temperature. Cells were collected by gentle scraping with a rubber policeman, sedimented by centrifugation at 1000 x g for 2 min and preserved in fresh fixative overnight. Thin sections were then prepared by Mary Ann Trevors at the TEM Facility at Dalhousie University, Halifax. Briefly, samples were post-fixed in 2% (w/v) osmium tetroxide in cacodylate buffer to stabilize phospholipids and enhance membrane contrast, and embedded in epoxy resin TAAB 812 (Marivac Ltd.). Ultrathin sections (80 to 100 nm) were post-stained with 2% (w/v) uranyl acetate and lead citrate and were picked up on 300-mesh copper coated grids for subsequent examination. Grids were examined in a

Philips EM300 TEM at an accelerating voltage of 80 kV. Micrographs and prints were made at a defined magnification.

Chapter 3

Mechanisms of co-regulation of phosphatidylcholine and cholesterol synthesis

Portions of the results in this chapter appear in the following publication:

Lagace TA, Storey MK, Ridgway ND. Regulation of phosphatidylcholine metabolism in Chinese hamster ovary cells by the sterol regulatory element-binding protein (SREBP)/SREBP cleavage-activating protein pathway. *J Biol Chem.* 2000 May 12;275(19):14367-74.

3.1 Results

3.1.1 Increased phosphatidylcholine synthesis in SCAP-overexpressing CHO cells

Previous results from our lab showed evidence of coordinate regulation of cholesterol and PtdCho synthesis by the SCAP/SREBP pathway. Specifically, it was demonstrated that low levels of cholesterol synthesis was accompanied by decreased PtdCho synthesis and mass in cholesterol auxotrophic SRD-6 cells, which are defective in the processing of SREBPs and fail to upregulate genes involved in cholesterol and fatty acid synthesis in response to growth in lipoprotein-deficient medium (250). Conversely, elevated cholesterol synthesis was associated with increased PtdCho synthesis and turnover in SRD-4 cells, which constitutively process SREBPs due to expression of a sterol-resistant SCAP protein (SCAP D443N) (160). The results in SRD-4 cells suggested that the SCAP mutation resulted in increased PtdCho synthesis. In addition to the SCAP D443N mutation, SRD-4 cells also harbor an inactivating mutation in the single active allele for acyl-CoA:cholesterol acyltransferase (ACAT), the enzyme that converts cholesterol to cholesterol-ester storage form. Therefore, it was possible that the ACAT defect or another mutation contributed to altered PtdCho metabolism in SRD-4 cells.

To assess the role of SCAP in the regulation of PtdCho synthesis independent of other alterations in cholesterol metabolism we examined parameters of PtdCho metabolism in CHO cell lines stably overexpressing epitope-tagged wild-type SCAP or constitutively active SCAP D443N. These cells were resistant to down-regulation of cholesterol synthesis and killing by 25-hydroxycholesterol, thus mimicking the SCAP defect in SRD-4 cells (160). The expression of HSV-epitope tagged and endogenous SCAP and SCAP D443N in two chosen cell lines (CHO-SCAP and CHO-SCAP D443N)

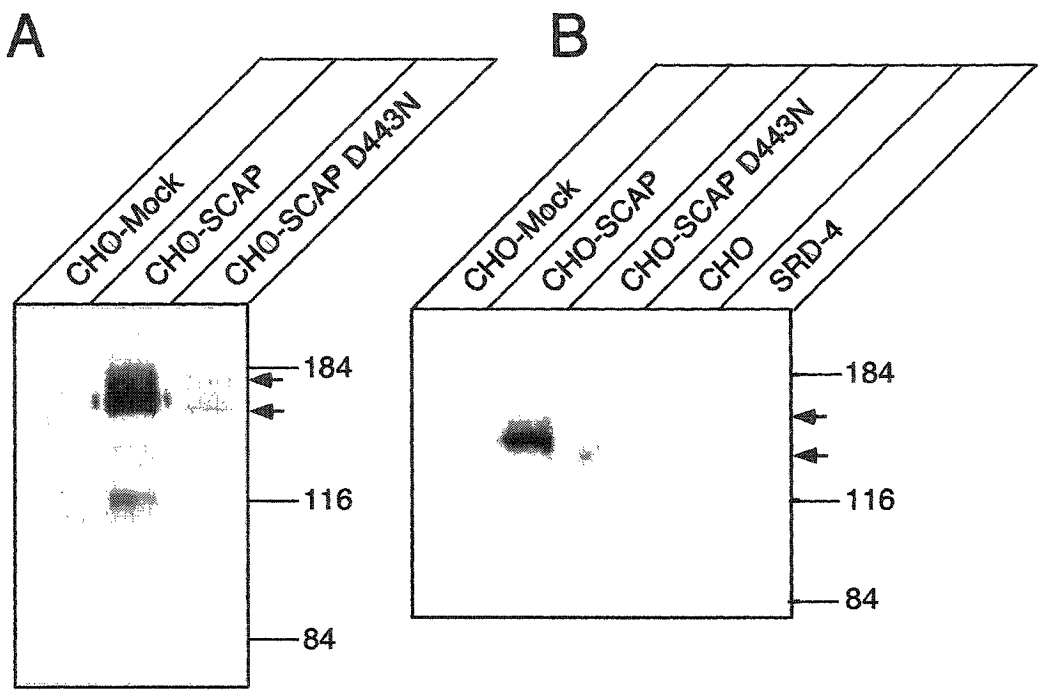

Figure 3.1 - Expression of epitope-tagged SCAP and SCAP D443N in CHO cells. Differentially glycosylated SCAP proteins migrate between ~140-150 kDa (arrows). **(A)** Total membrane fraction was isolated from the indicated cell lines as described in "Material and Methods." NP40-soluble supernatant (40 μg) was resolved by SDS-6 %PAGE. Overexpressed, epitope-tagged SCAP was detected using a 1:500 dilution of HSV monoclonal. **(B)** Endogenous and overexpressed SCAP and SCAP D443N was detected using polyclonal antibody R-139 (5 μg/ml). Differentially glycosylated SCAP proteins migrate between ~140-150 kDa (arrows).

compared to mock-transfected control cells is shown in Figure 3.1. SDS-PAGE and immunoblotting analysis using an anti-HSV monoclonal antibody detected a protein doublet, corresponding to differentially glycosylated forms of SCAP (193), of approximately 140-150 kDa in NP-40 extracts of CHO-SCAP and CHO-SCAP D443N cell membranes (Figure 3.1, A). In this and several other clones, it appeared that the expression wild-type SCAP was higher than that of the D443N mutant. The cell extracts from Figure 3.1, A, as well as those from CHO7 and SRD-4, were also probed with antibody R139 to detect both endogenous and overexpressed SCAP (231). This antibody also detected a 140-150 kDa doublet in all cells. As expected, expression was highest in the CHO-SCAP and CHO-SCAP D443N cells relative to mock, CHO7 and SRD-4 cells (Figure 3.1, B).

Previous results from our laboratory demonstrated that both cholesterol and fatty acid synthesis were increased (3-fold) in SRD-4 cells compared to parental CHO7 cells (160). Similarly, cholesterol and fatty acid synthesis was measured in SCAP overexpressing cells by pulse-labelling with [^{14}C]acetate. Both CHO-SCAP and CHO-SCAP D443N cells displayed a 2-fold increase in [^{14}C]acetate incorporation into cholesterol relative to mock transfected controls (Figure 3.2). [^{14}C]acetate incorporation into fatty acids in the SCAP overexpressing cell lines was increased, but not significantly.

PtdCho synthesis was examined in SCAP overexpressing cells by pulse-labelling with [^{3}H]choline for 1 h followed by a 4 h chase period (Figure 3.3). At the end of the pulse (0 h) and throughout the 4 h chase, PtdCho synthesis was increased 1.5- to 2.5-fold in CHO-SCAP and CHO-SCAP D443N cells compared to mock transfected controls. Increased PtdCho synthesis in these cells was accompanied by a 2-fold reduction in

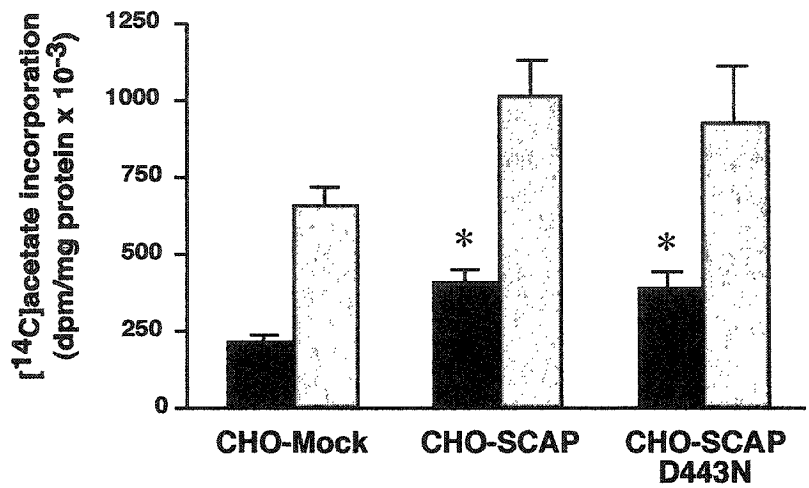

Figure 3.2 - Cholesterol and fatty acid synthesis in SCAP transfected CHO cells. On day 1, cells were subcultured at 150,000-200,000 cells/60 mm dish in 3 ml medium B supplemented with 0.25% FCS. On day 3, cells were cultured in 2 ml medium B for 24 hours prior to start of experiments. After pulse-labeling cells with [^{14}C]acetate (7.5 μCi/ml) for 2 h, incorporation of radiolabel into cholesterol (solid bars) and fatty acids (grey bars) was determined as described in "Material and Methods." Results are the mean and standard deviation of three separate experiment. *$p < 0.025$ *versus* mock transfected cells.

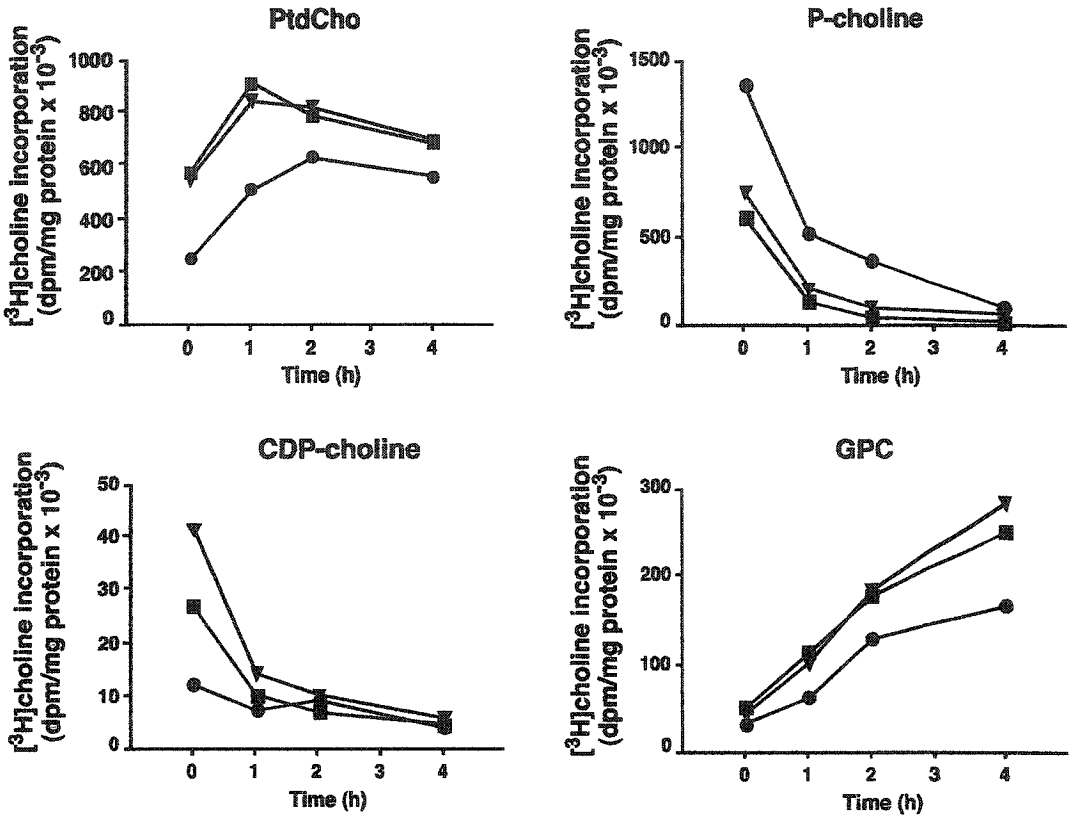

Figure 3.3 - Pulse/chase analysis of PtdCho metabolism in SCAP transfected CHO cells. Mock transfected (●), CHO-SCAP (■) and CHO-SCAP D443N (▲) cells cultured as described in the legend to Figure 3.2 received choline-free medium containing [^{3}H]choline (2 μCi/ml) for 1 h. Medium was then removed, cells were rinsed once with PBS, and fresh medium B containing choline (25 μM) was added. After 0, 1, 2 and 4 h at 37°C, cells were harvested and [^{3}H]choline incorportion into PtdCho and choline metabolites was measured as described in "Material and Methods." Results are the mean of duplicate determinations from a representative experiment repeated two other times with similar results.

[^{3}H]phosphocholine levels and a 2-to 3-fold increase in [^{3}H]CDP-choline, indicative of CCTα activation. There was also a 2-fold elevation in [^{3}H]GPC production, indicating increased rates of PtdCho turnover. The finding that SCAP overexpression partially recapitulated the SRD-4 cells (D443N) phenotype of increased PtdCho synthesis and turnover supported the conclusion that constitutive SREBP processing, and not other mutations in SRD-4 cells, was causative.

3.1.2 Inhibition of cholesterol synthesis does not downregulate PtdCho synthesis in SRD-4 and SCAP overexpressing cells

SREBPs regulate cellular programs for both cholesterol and fatty acid synthesis (36). To determine if elevated PtdCho synthesis in SRD-4 and SCAP overexpressing cells was in response to increased levels of one or both of these lipids, the relationship between cholesterol synthesis and PtdCho metabolism was examined in SRD-4 and SCAP transfected cells by measuring rates of [^{3}H]choline incorporation into PtdCho in the presence of lovastatin, a potent inhibitor of HMG-CoA reductase activity and cholesterol synthesis (80) (Table 3.1). As expected, [^{3}H]choline incorporation into [^{3}H]PtdCho was significantly elevated in SRD-4, CHO-SCAP and CHO-SCAP D443N cells compared to CHO7 and mock transfected cells. Treatment with lovastatin did not affect [^{3}H]choline incorporation into PtdCho in control, SRD-4, CHO-SCAP or CHO-SCAP D443N cells. Under these conditions, [^{14}C]acetate incorporation into cholesterol was reduced by >90%, while incorporation into fatty acids was unaffected (results not shown).

	PtdCho synthesis *dpm/mg protein x 10-3*	
Cell Line	NA	Lovastatin
CHO	641±72	544±134
SRD-4	2461±262	2441±117
Mock	462±203[a]	393±92
CHO-SCAP	1016±233[b]	1097±240
CHO-SCAP D443N	1086±337[c]	986±377

Table 3.1 - Inhibition of cholesterol synthesis by lovastatin does not influence PtdCho synthesis in SRD-4, CHO-SCAP and CHO-SCAP D443N cells.
Cells were treated lovastatin (10 μM) in medium A for 8 or 10 h, and labelled with [^{3}H]choline (2 μCi/ml) for the final 1 h. [^{3}H]Choline incorporation into PtdCho was measured as described in "Materials and Methods." Results are the mean and standard deviation of 3-5 experiments. [a]$p<0.001$ *versus* CHO7 cells, [b]$p<0.01$, [c]$p<0.05$ *versus* mock transfected cells. NA, no addition.

3.1.3 Increased PtdCho synthesis in SRD-4 cells is correlated with increased fatty acid synthesis

Next, the relationship between elevated fatty acid and PtdCho synthesis was examined by selectively reducing fatty acid synthesis in SRD-4 cells to the level of control CHO7 and examining [^{3}H]choline incorporation into PtdCho and choline metabolites (Figure 3.4). SRD-4 cells were treated with cerulenin, a potent irreversible inhibitor of mammalian/bacterial fatty acid synthase (213), for up to 4 h combined with pulse-labelling with [^{3}H]choline to measure PtdCho and choline metabolite levels. To monitor effectiveness of cerulenin inhibition of fatty acid synthesis, [^{14}C]acetate incorporation into fatty acid was measured at the same time points. Treatment of SRD-4 cells with cerulenin for >2 h was sufficient to reduce [^{14}C]acetate incorporation into fatty acids to the level in untreated CHO7 cells. Treatment of SRD-4 cells with cerulenin for 4 h did not significantly influence radiolabelling of cholesterol (172±8 *versus* 182±29 dpm [^{14}C]acetate incorporation/mg protein x 10^3 in untreated and cerulenin-treated SRD-4 cells, respectively). Cerulenin caused a time-dependent suppression of [^{3}H]choline incorporation into PtdCho and the PtdCho degradation product GPC that mirrored its inhibitory effects on fatty acid synthesis. [^{3}H]PtdCho and [^{3}H]GPC were decreased by 70% and 85% relative to untreated controls, respectively, following cerulenin treatment for 4 h. Cerulenin also dramatically increased [^{3}H]phosphocholine (9-fold) in SRD-4 cells at 4 h, indicating decreased CCT activity.

3.1.4 CCTα mRNA levels in SRD-4 and CHO-SCAP cells

Since [^{3}H]choline labelling experiments implicated CCT activity in increased PtdCho synthesis in SRD-4 (159) and SCAP overexpressing cells (Figure 3.3), various

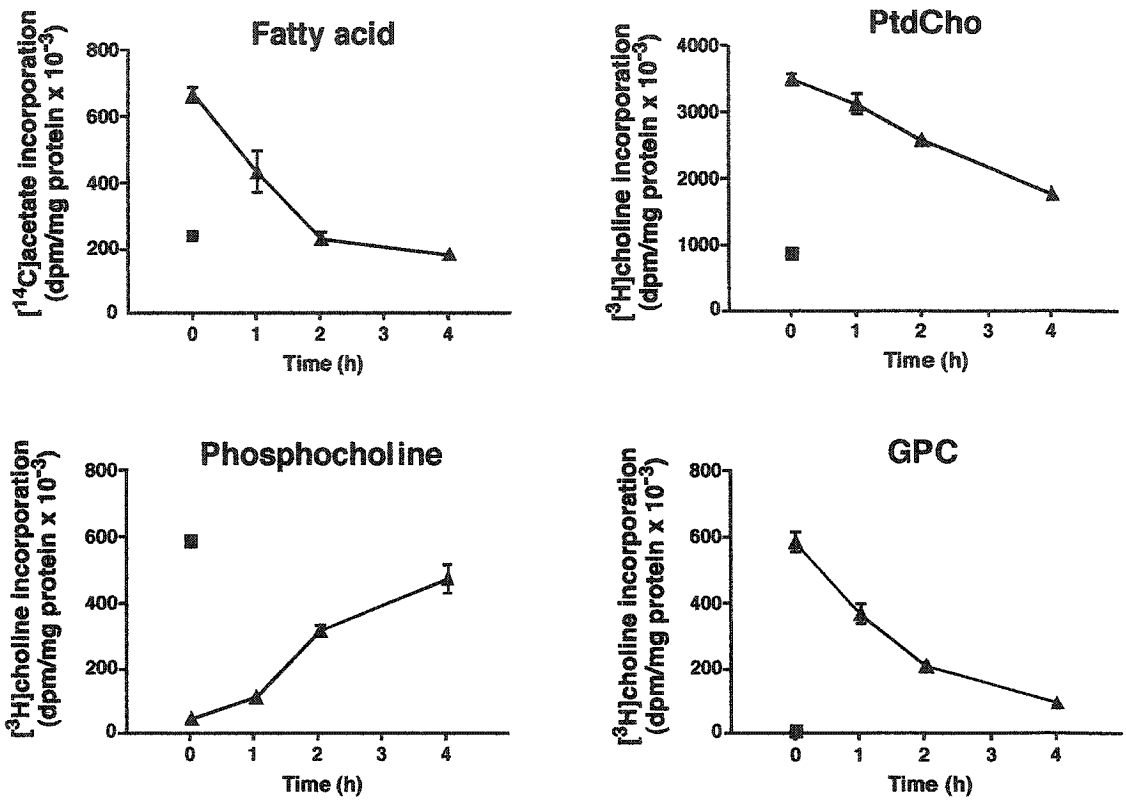

Figure 3.4 - Down-regulation of PtdCho synthesis in cerulenin-treated SRD-4 cells. CHO and SRD-4 cells were cultured as described in the legend to Figure 3.3. SRD-4 cells (▲) were treated with cerulenin (10 μg/ml) for up to 4 h. The 0 h controls for CHO (■) and SRD-4 cells received solvent alone (DMSO). Cells were labeled with [^{14}C]acetate (2.5 μCi /ml) or [^{3}H]choline (2 μCi/ml) for the final 1 h of each treatment. Cells were harvested and isotope incorporation into fatty acids, phosphocholine, PtdCho, and the PtdCho degradation product GPC was measured as described in "Materials and Methods." Results are the mean and standard deviation of triplicate determinations from a representative experiment repeated two other times with similar results.

aspects of CCTα regulation in these cells were examined in more detail. CHO cells express only CCTα since CHO MT58 cells with a temperature sensitive mutation in CCTα fail to grow and undergo apoptosis at the non-permissive temperature (61, 81). As well, we have not detected expression of CCTβ in CHO cells using a CCTβ-specific antibody (data not shown). Previous results from our laboratory have demonstrated that CCTα mRNA levels were reduced by 30% in SRD-4 cells relative to CHO7 controls (159). However, CCTα mRNA levels in CHO-SCAP and CHO-SCAP D443N cells were unchanged relative to mock transfected controls (Figure 3.5).

3.1.5 CCT and CPT activity in SRD-4 and CHO-SCAP cells

The primary mechanism for CCTα regulation is via post-transcriptional mechanisms involving phosphorylation and translocation to membranes (151). To assess whether *in vivo* activation of CCTα was caused by changes in enzyme distribution, enzyme activity associated with the soluble and total particulate (membrane) fraction of cells was measured *in vitro* either in the presence or absence of PtdCho:oleate vesicles (Table 3.2). *In vitro* CCTα activity in SRD-4 cells was reduced 3- and 2-fold in the soluble and particulate fractions, respectively, relative to controls. Residual CCTα activity in soluble and particulate fractions from SRD-4 cells was activated by PtdCho:oleate vesicles to a similar extent as controls. CPT activity in SRD-4 and CHO7 cells was not significantly different. The relative amount of protein in soluble and particulate fractions was similar between SRD-4 and CHO7 cells (data not shown).

In vitro CCTα activity associated with soluble and particulate fractions was also measured in CHO-SCAP and CHO-SCAP D443N cells (Table 3.3). CCTα activity,

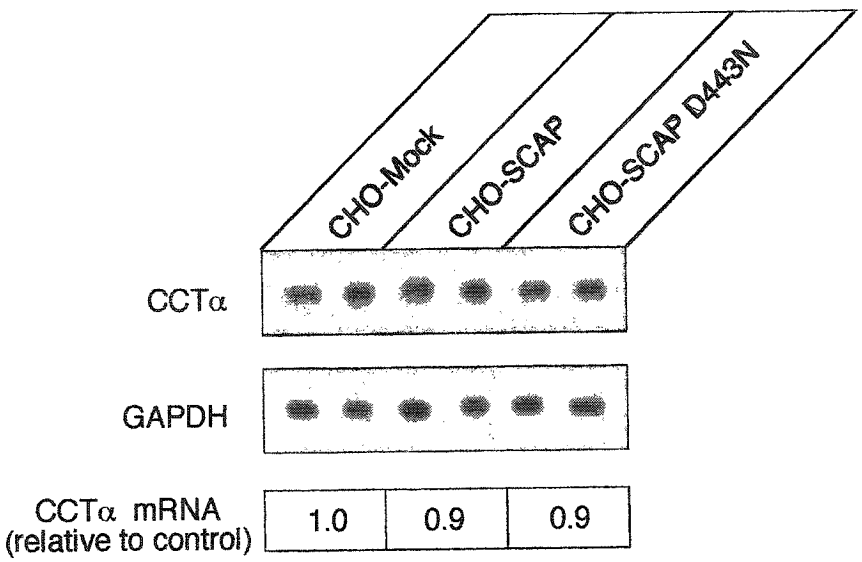

Figure 3.5 - CCTα mRNA levels in SCAP transfected CHO cells. Cells were cultured as described in the legend to Figure 3.2. CCTα and glyceraldehyde-3-phosphate dehydrogenase (GAPDH) mRNA levels were assayed in mock transfected, CHO-SCAP and CHO-SCAP D443N cells as described in "Materials and Methods." CCTα mRNA levels were normalized to GAPDH mRNA and expressed relative to control cells. Results are the mean of three separate experiments.

	Choline Phosphotransferase	CTP:Phosphocholine Cytidylyltransferase			
		Soluble		Particulate	
		NA	+PtdCho/Oleate	NA	+PtdCho/Oleate
CHO	1.53±0.49	2.64±0.46	12.43±2.55	4.58±1.48	9.41±3.53
SRD-4	1.10±0.18	0.72±0.19[b]	3.75±0.91[a]	1.96±0.76[a]	3.16±0.96[a]

Table 3.2 - *In vitro* activity of CTP:phosphocholine cytidylyltransferase and choline phosphotransferase in the soluble and total particulate fraction of CHO and SRD-4 cells. CCT activity was assayed in the soluble and particulate fraction of cells as described in "Materials and Methods." CPT activity was assayed in total membranes. Results are expressed as nmol/min/mg protein and represent the mean and standard deviation of 3 or 4 experiments. [a]$p<0.01$, [b]$p<0.005$ *versus* CHO cells. NA, no addition.

	Choline Phosphotransferase	CTP:Phosphocholine Cytidylyltransferase			
		Soluble		Particulate	
		NA	+PtdCho/Oleate	NA	+PtdCho/Oleate
Mock	1.52±0.33	1.75±0.28	7.38±1.16	3.92±1.23	5.66±1.40
CHO-SCAP	1.72±0.24	1.81±0.70	4.72±1.95	5.60±2.30	6.20±3.10
CHO-SCAP D443N	1.47±0.38	2.86±0.18[a]	7.79±0.56	3.91±0.36	5.80±0.65

Table 3.3 - *In vitro* activity of CTP:phosphocholine cytidylyltransferase and cholinephosphotransferase in soluble and total particulate fractions of CHO-SCAP, CHO-SCAP D443N and mock transfected cells. CCT activity in the soluble and particulate fractions wasassayed as described in "Materials and Methods." CPT activity was assayed in total membranes only. Results are expressed as nmol product formed/min/mg protein, and are the mean and standard deviation of 3 to 6 experiments. [a]$p<0.005$ *versus* mock transfected cells. NA, no addition.

measured in the absence or presence of PtdCho:oleate vesicles, was not significantly different between controls and the two SCAP overexpressing cell lines. The exception was a significant increase (60%) in soluble CCTα activity measured in the absence of PtdCho/oleate vesicles in CHO-SCAP D443N cells. CPT activity in CHO-SCAP D443N cells was also not significantly different from controls.

3.1.6 CCTα protein expression, phosphorylation and intracellular localization in SRD-4 and SCAP transfected CHO cells

The levels of CCTα protein in soluble, particulate, and total homogenates of SRD-4 and SCAP overexpressing cells was measured by SDS-PAGE and immunoblotting analysis using a polyclonal antibody against the C-terminal phosphorylation domain of CCTα (317). In agreement with *in vitro* enzyme activities (Table 3.2), CCTα protein levels were reduced in total homogenates as well as in soluble and particulate fractions of SRD-4 cells relative to controls (Figure 3.6). In CHO-SCAP and CHO-SCAP D443N cells, CCTα protein expression was similar to mock transfected cells in all fractions, in agreement with enzyme activity measurements in Table 3.3.

The phosphorylation status of CCTα was determined in SRD-4 and SCAP overexpressing cells by [^{32}P]phosphate labelling *in vivo* followed by immunoprecipitation from soluble and particulate fractions and resolution by SDS-PAGE (Figure 3.7). Phosphorylation of soluble and particulate CCTα from SRD-4 cells was reduced relative to CHO controls, consistent with reduced protein expression (Figure 3.6) and enzyme activity (Table 3.2) in both these fractions. There were no apparent changes in the phosphorylation of CCTα in the particulate or soluble fractions from CHO-SCAP or CHO-SCAP D443N cells compared to mock transfected cells.

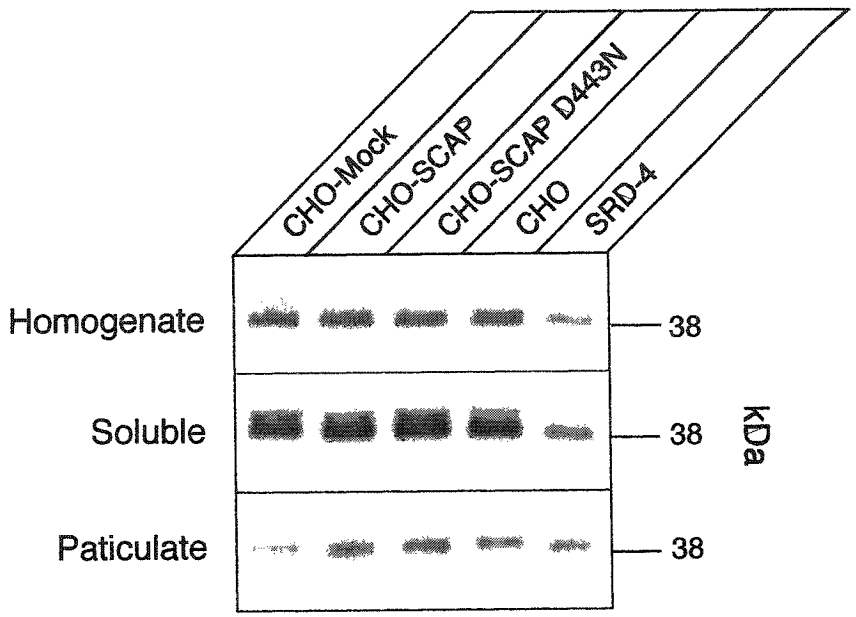

Figure 3.6 - Expression of CCTα protein in SRD-4 and SCAP-transfected CHO cells. Cell homogenate, 100,000 x *g* paticulate and soluble fractions were prepared as described in "Materials and Methods." Proteins (25 μg) were separated by SDS-10%PAGE and transferred to nitrocellulose. CCTα was localized by immunoblotting with a rabbit polyclonal antibody against the C-terminal phosphorylation domain of CCTα. Similar results were obtained in three other experiments.

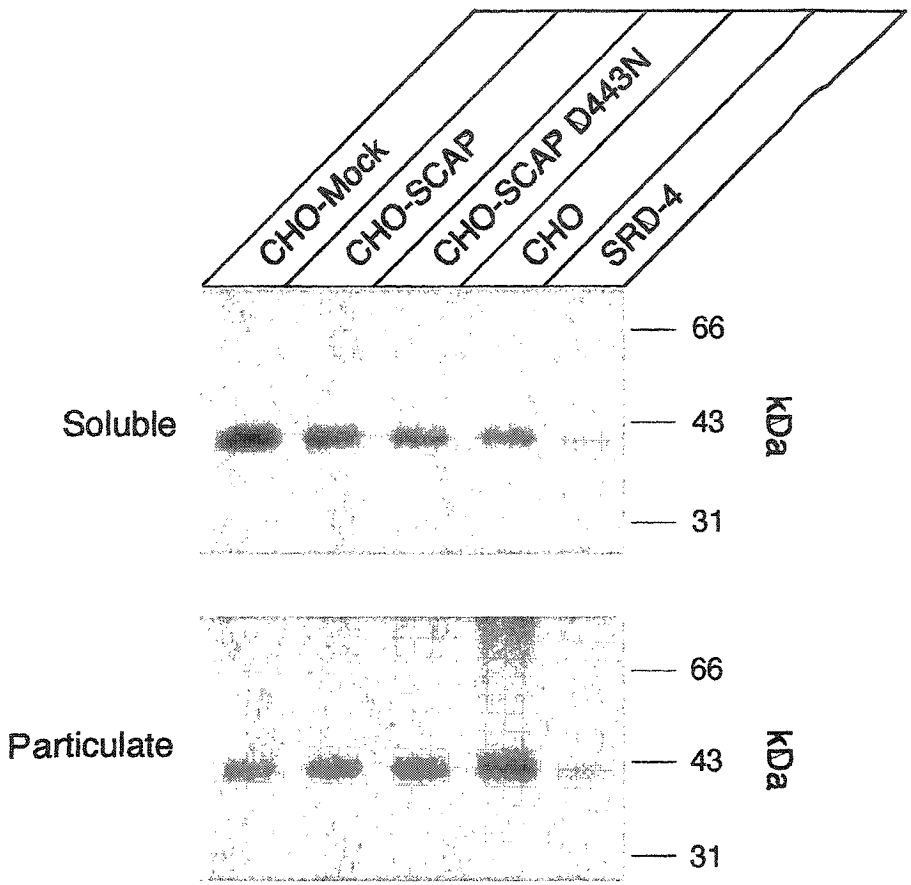

Figure 3.7 - Phosphorylation of CCTα was not influenced by SCAP or SCAP D443N expression. CCTα phosphorylation was assayed by [^{32}P]phosphate labeling and immunoprecipitation with a rabbit polyclonal antibody against the membrane binding region of CCTα as described in "Materials and Methods." [^{32}P]CCTα was resolved by SDS-10%PAGE and the dried gel was exposed to film for 2 days at –70°C. Similar results were obtained from two other experiments.

3.1.7 Localization of CCTα in SRD 4 and SCAP transfected CHO cells

CCTα activation in CHO and HeLa cells in response to PtdCho degradation by PLC or by addition of exogenous oleate has been shown to result in translocation of the enzyme from the nucleoplasm to the NE (289, 290, 292). This raised the possibility that CCTα activities shown in Tables 3.2 and 3.3 did not accurately reflect the distribution of CCTα in intact cells due to trapping in the nucleus or disruption of CCTα membrane association during cell fractionation. Therefore, to overcome these potential problems we analyzed the intracellular distribution of CCTα by indirect immunofluorescence and confocal microscopy (Figure 3.8). Localization of CCTα in SRD-4 and CHO-SCAP D443N cells was assessed and compared to control CHO and mock transfected cells. Similar to CHO-K1 cells (292), CCTα in CHO cells was exclusively localized within the nucleoplasm with no evidence of nuclear envelope (NE) staining (Figure 3.8A). In contrast, SRD-4 cells displayed reduced CCTα immunofluorescence in the interior of the nucleus and a prominent fluorescent ring around the periphery corresponding to the NE (Figure 3.8B). This staining pattern was reproduced in CHO7 cells treated with oleate (100 μM) for 1 h (Figure 3.8C). CCTα also localized to structures within the nucleus of SRD-4 and oleate-treated CHO cells that did not appear to be associated with the NE. CCTαin CHO-SCAP cells was primarily in the interior of the nucleus and was not localized to the NE (Figure 3.8E). CCTα was partially associated with the NE and also with unidentified intranuclear structures in a subset of CHO SCAP D443N cells (Figure 3.8F).

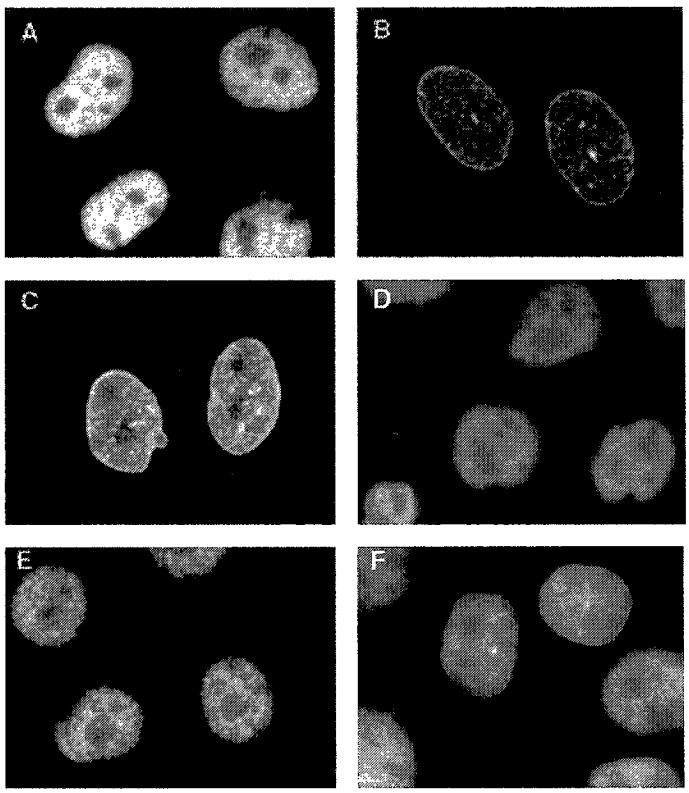

Figure 3.8 - Immunofluorescence localization of CCTα in SRD-4 and CHO-SCAP D443N cells. Cells were cultured in medium A on glass coverslips for 3 days prior to the start of experiments. CHO7 cells (**A**), SRD-4 cells (**B**), CHO7 cells treated with 100 μM oleate for 1 h (**C**), CHO mock transfected cells (**D**), CHO-SCAP cells (**E**) and CHO-SCAP D443N cells (**F**) were fixed in 3% formaldehyde/0.05% Triton X-100 as described in "Material and Methods." Coverslips were incubated with a 1:4000 dilution of a rabbit polyclonal antibody followed by a FITC-conjugated secondary antibody. Images were obtained with a laser scanning confocal microscopy (Zeiss LSM 510) and images were processed using Adobe Photoshop software.

3.2 Discussion

SREBPs are positive transcription factors that regulate the synthesis of sterols as well as the synthesis and desaturation of fatty acids (36). Regulation of SREBP processing is dependent on the molecular chaperone SCAP, an ER-resident transmembrane protein that "senses" sterol levels in this compartment (124, 194). The results in this section demonstrate that uncoupling this regulatory loop by overexpression of SCAP or a sterol insensitive SCAP mutant (D443N) results not only in increased synthesis of cholesterol and fatty acids, but also increased PtdCho synthesis. These findings provide further evidence that the SCAP/SREBP pathway is involved in the coordinate regulation of sterol, fatty acid and PtdCho synthesis. Unlike SCAP/SREBP-mediated regulation of cholesterol and fatty acid synthesis, PtdCho synthesis was not affected at the transcriptional level, but was instead controlled by the availability of fatty acids or a fatty acid-derived activator of CCTα, the rate-limiting enzyme in the CDP-choline pathway.

PtdCho metabolism was examined in three cell lines that had increased sterol and fatty acid synthesis due to altered SCAP function. It is now established that SCAP binds to the ER-resident integral membrane protein Insig-1 in a cholesterol-dependent manner, which serves to retain the SCAP/SREBP complex in the ER when sterol levels are high (319). This prevents transport of the SCAP/SREBP complex to the Golgi apparatus where SREBPs are proteolytically processed to their active soluble forms. The D443N mutation interferes with the interaction of SCAP with Insig-1 (314), whereas overexpression of SCAP saturates this interaction (312, 319). The end result in either instance is constitutive processing of SREBPs that is non-responsive to sterols. As

expected, SRD-4 cells (which harbor the SCAP D443N mutation) and CHO cells stably transfected with epitope-tagged versions of SCAP and SCAP D443N had significantly elevated cholesterol synthesis. However, SRD-4 cells also had a 3-fold increase in fatty acid synthesis (160), compared with only a 25-30% increase in CHO-SCAP and CHO-SCAP D443N cells. The reasons for this difference are unclear, but could be related to the high-level of SCAP expression or differences in SCAP D443N function in a wild-type background. Nevertheless, this is a significant variation in phenotype between SRD-4 cells and SCAP transfected cells that may explain differences in PtdCho metabolism and CCTα activity and localization. All three cell lines displayed alterations in PtdCho synthesis and choline metabolite profiles, as determined by [^{3}H]choline pulse/chase analysis. However, the changes in SRD-4 cells were much greater compared with CHO-SCAP and CHO-SCAP D443N cells. In SRD-4 cells, there was rapid flux of [^{3}H]choline through the biosynthetic pathway such that virtually no phosphocholine accumulated and PtdCho was the major biosynthetic product at the end of a 1 h pulse (160). Taking into account the high level of GPC in SRD-4 cells at the end of the pulse period, it was apparent that as much as 30% of newly made PtdCho was degraded during this time. Factoring for loss of radiolabeled PtdCho due to degradation, PtdCho synthesis in SRD-4 cells was elevated by approximately 6-fold relative to controls at the end of a 1 h pulse (160). In comparison, the majority of the [^{3}H]choline incorporated into control and SCAP-transfected cells was confined to phosphocholine at the end of the 1 h pulse (Figure 3.3). [^{3}H]phosphocholine levels in SCAP-overexpressing cells were decreased 2-fold with a corresponding 2-fold increase in radiolabeled PtdCho at the end of the 1 h pulse. This indicates that CCTα was activated by overexpression of SCAP or SCAP

D443N, supporting the conclusion that deregulated SCAP function in SRD-4 cell contributes to the altered PtdCho metabolism phenotype in these cells. The decreased activation of PtdCho synthesis in SCAP overexpressing cells compared to SRD-4 cells is consistent with their lower rate of fatty acid synthesis.

Also consistent with a role for fatty acids in elevated CCTα activity was the localization of CCTα to the NE in SRD-4 cells. CCTα translocation to the NE and membrane/particulate cell fractions was previously observed in response to exogenous fatty acids in numerous cell models (52, 289, 292). Exogenous oleate addition to CHO cells also stimulated CCTα translocation to the NE, suggesting that elevated fatty acid synthesis in SRD-4 cells is responsible for CCTα activation, membrane localization, and increased PtdCho synthesis. In addition to localization to the peripheral NE, CCTα in SRD-4 cells and oleate-treated CHO7 cells was localized to intranuclear structures. Using three-dimensional confocal microscopy techniques we have determined that these structures correspond to tubular invaginations of the NE in CHO cells (Section 5). CCTα in CHO-SCAP was not localized to the NE, consistent with reduced stimulation of fatty acid synthesis in these cells relative to SRD-4 cells. However, several experiments showed that a minority of CHO-SCAP D443N cells (~20%) displayed weak translocation to the NE and prominent immunostaining of NE invaginations (Figure 3.8F). CCTα translocation was often observed in closely paired cells, perhaps products of the same cell division synchronized in a particular stage of the cell cycle. Incomplete NE translocation of CCTα in CHO-SCAP D443N cells is consistent with lower stimulation of PtdCho synthesis and decreased fatty acid synthesis compared to SRD-4 cells.

Contrary to the immunofluorescence localization of CCTα to the NE in SRD-4 cells, CCTα activity and/or mass was not increased in the particulate/membrane fraction of these cells. Instead CCTα activity was significantly decreased in both the soluble and particulate fractions compared to CHO7 cells. A previous study has shown a correlation between CCTα phosphorylation, decreased membrane binding and increased protein levels (286). This suggests that active membrane-bound CCTα may be more readily degraded than the soluble inactive enzyme, thus providing a mechanism to prevent over-activity of the CDP-choline pathway that could perhaps explain the decreased protein levels in SRD-4 cells. The possibility that one or more of the CCTβ isoforms (169, 171) interfered with activity measurements seems unlikely since the total CCT activity in cytosol and membranes closely paralleled decreased CCTα protein mass in these fractions. CCTα mRNA levels were decreased by 30% in SRD-4 cells compared to control cells. This is in contrast to reports from others demonstrating that lipoprotein deprivation increased the rate of CCTα transcription (176, 228). It is interesting to note that in cholesterol and fatty acid auxotrophic SRD-6 cells, decreased CCTα activity and membrane association was accompanied by increased protein expression (250), the opposite situation to that observed in SRD-4 cells which have increased cholesterol and fatty acid synthesis. In SRD-4 cells the decrease in mRNA and protein could represent an adaptive response to increased CCT activity and PtdCho turnover, suggesting multiple mechanisms of the cell to prevent excess CCT activity.

Although numerous studies have demonstrated that exogenous fatty acids induce membrane association and activation of CCT in intact cells, resulting in elevated PtdCho synthesis (52, 151, 205, 289), the effect of endogenous fatty acid levels on CCT activity

remains undefined. Our finding that inhibition of fatty acid synthesis by cerulenin in SRD-4 cells decreased radiolabelling of PtdCho is compelling evidence of a role for *in vivo* fatty acid synthesis in regulating CCTα activity. Reduction of fatty acid synthesis by cerulenin appeared to down-regulate CCTα activity based on a 9-fold increase in [^{3}H]phosphocholine levels in treated SRD-4 cells. This relationship between fatty acid and PtdCho synthesis is supported by previous results with SRD-6 cells, which have a 60-80% reduction in both fatty acid and PtdCho synthesis (36, 250) due to defective SREBP processing (230). Addition of exogenous oleate to SRD-6 cells restored PtdCho synthesis to control levels through activation of CCTα. Cholesterol supplementation had no effect on PtdCho synthesis in SRD-6 cells (250) indicating that cholesterol did not have a direct role in regulating CCTα activity in this cell model. Similarly, inhibition of cholesterol synthesis by lovastatin had no effect on PtdCho synthesis in SRD-4, SCAP-transfected, or control cells in the current study.

A subsequent study from our laboratory has further supported a role for SREBPs in regulating PtdCho synthesis via control of cellular levels of a fatty acid-derived activator of CCTα (222). Inducible expression of mature soluble forms of either SREBP-1a or SREBP-2 in cholesterol- and fatty acid-auxotrophic CHO M19 cells resulted in elevated fatty acid and cholesterol synthesis (10- and 50-fold, respectively), and an accompanying 2-fold increase in PtdCho synthesis. The PtdCho synthetic rate in these cells was decreased by inhibition of fatty acid synthesis by cerulenin, and by inhibition of their fatty acly-CoA ester synthesis by the fatty acyl CoA synthase inhibitor triacsin C, implicating a fatty acid derived activator of CCT in the observed increase in PtdCho synthesis in response to enforced expression of mature SREBPs (222). In these cells,

CCTα mRNA was increased 2-fold by enforced expression of either mature SREBP-1a or SREBP-2. However, this was minor compared to increases in other SREBP-regulated genes involved in cholesterol and fatty acid synthesis. The difference between these result and those presented in this section regarding the effect of SREBPs on CCTα transcription could reflect differences in SREBP levels between cell models and/or long-term adaptations to altered SCAP function in SRD-4 and SCAP transfected cell lines. Inducible overexpression of mature SREBPs in CHO M19 cells also resulted in increased CCTα protein levels. However, this was mainly confined to the inactive soluble fraction, and as a result no *in vivo* increase in CCTα activity was detected. It was concluded from these studies that SREBPs regulated PtdCho synthesis in CHO cells by both transcriptional and posttranscriptional mechanisms, with the primary mode of regulation being through control of cellular levels of a fatty-acid derived activator of CCTα. The blunted response of SREBPs on CCTα transcription compared to other genes may serve to prevent overstimulation of the CDP-choline pathway thereby preventing the diversion of fatty acid and DAG supplies to PtdCho synthesis at the expense of other essential cellular functions that rely on these lipids. This is supported by other studies that demonstrated the elevation of CCTα mRNA transcription in cells cultured under lipoprotein deficient conditions to be minor compared to the gene for LDLR, a main cholesterol regulatory gene (149).

An interesting feature of PtdCho metabolism in SRD-4 cells (160) and to a lesser extent in SCAP transfected cells (Section 3) was the coordinate increase in the synthesis and degradation of radiolabeled PtdCho. As a result of this balance, there was no significant change in PtdCho mass in SRD-4 cells (160). PtdCho degradation has also

been shown to increase in concordance with increased PtdCho synthesis in several cell models where CCTα activity was increased through overexpression (13, 20, 284). Because of the large accumulation of GPC that accompanied PtdCho degradation in these cell models, PLA activity was implicated in PtdCho catabolism. Recently, a calcium-independent phospholipase A_2 ($iPLA_2$) (18) was implicated in turnover of excess PtdCho generated by overexpression of CCTα in HeLa cells (13) and CHO cells (20). Since GPC production is also elevated in SRD-4 cells, $iPLA_2$ is also likely involved in PtdCho degradation in SRD-4 cells. However, a novel PLB has recently been identified that could play an important role in PtdCho turnover (325).

One possible explanation for the increased rate of PtdCho synthesis in SRD-4 cells is that CCTα is continually activated by fatty acids released through PtdCho degradation by phospholipase A and/or B activities. As in the case of CCTα overexpression studies (13, 20, 284), CCTα in SRD-4 cells may be non-responsive to negative-feedback mechanisms that down-regulate its activity when PtdCho is in excess. This could be related to an independent effect of SREBP/SCAP on PtdCho metabolism in SRD-4 cells, or possibly to an additional unknown mutation that conferred a growth advantage during selection for resistance to killing by 25-hydroxycholesterol. In this regard, the CCTα gene is not mutated in SRD-4 cells (A. Poranek and N. Ridgway, unpublished results). Future studies will be aimed at examining the futile cycle of PtdCho synthesis and degradation in SRD-4 cells and determining the enzymes involved in GPC production in this cell line.

The results presented in this section support the concept that PtdCho, fatty acid, and cholesterol synthesis are co-regulated by the SCAP/SREBP regulatory pathway to

maintain cellular membrane homeostasis. The finding that PtdCho synthesis is primarily controlled post-transcriptionally suggests that the influence of SREBPs goes beyond the transcriptional level, and could involve regulation of other lipid metabolic pathways through control of cellular levels of regulatory and substrate lipid molecules.

Chapter 4

Regulation of phosphatidylcholine synthesis during farnesol-induced apoptosis

Portions of the results in this chapter appear in the following publication:

Lagace TA, Miller JR, Ridgway ND. Caspase processing and nuclear export of CTP:phosphocholine cytidylyltransferase alpha during farnesol-induced apoptosis. *Mol Cell Biol.* 2002 Jul;22(13):4851-62.

4.1 Results

4.1.1 Regulation of PtdCho synthesis by FOH

To examine the effect of FOH on PtdCho synthesis, CHO cells were treated with FOH (20 or 60 μM) for up to 6 h, pulse-labeled with [^{3}H]choline for the final 30 min of treatment, and incorporation into PtdCho and the CDP-choline pathway intermediates choline, phosphocholine and CDP-choline was measured. Relative incorporation of [^{3}H]choline into PtdCho and its precursors provides an indication of the activities in the CDP-choline pathway enzymes (top of Figure 4.1). In order to reduce the influence of exogenous phospholipids and DAG on FOH-induced apoptosis, cells were cultured in medium containing lipoprotein-deficient serum (LPDS) for 18-24 h prior to FOH addition. The addition of 20 μM FOH increased [^{3}H]PtdCho at all time points (Figure 4.1, A). This appeared to be a result of increased CCTα activity, as indicated by a decrease in [^{3}H]phosphocholine levels. Increased [^{3}H]CDP-choline levels indicated partial inhibition of CPT activity that was maximal by 1 h of FOH addition.

In contrast to the increase in [^{3}H]PtdCho synthesis observed with 20 μM FOH, we and others found that treatment with 60 μM FOH greatly decreased [^{3}H]PtdCho synthesis (Figure 4.1, B) (2, 186, 279). A >2-fold decrease in [^{3}H]phosphocholine levels after FOH treatment for 30 min indicated stimulation of CCTα activity, but this did not result in increased [^{3}H]PtdCho synthesis. Instead, decreased [^{3}H]phosphocholine levels was accompanied by drastically elevated [^{3}H]CDP-choline levels. Choline kinase activity did not appear to be inhibited by FOH treatment, as this would have resulted in decreased [^{3}H]choline incorporation into all subsequent CDP-choline pathway metabolites and

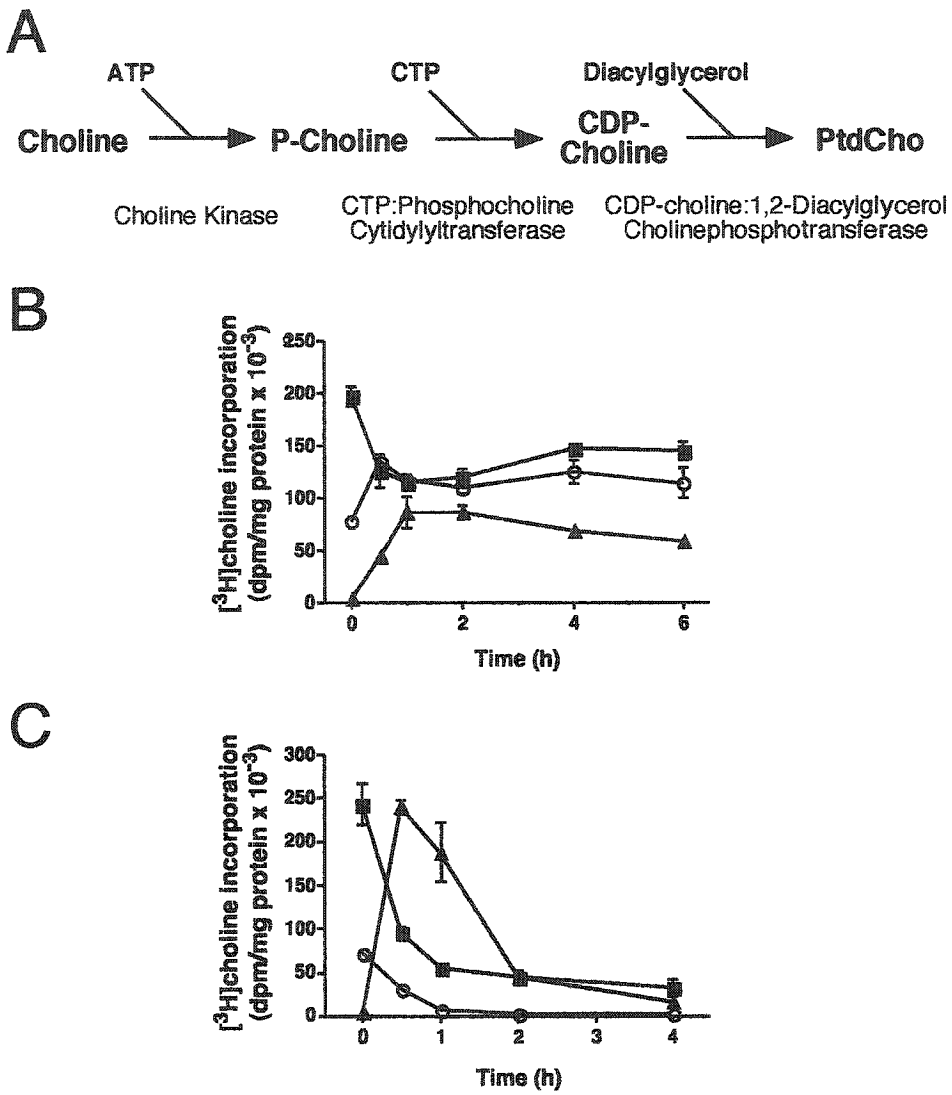

Figure 4.1 - [^{3}H]Choline-pulse analysis in CHO cells following high- and low-dose FOH treatment. (A) Schematic of the CDP-choline pathway showing enzymes and metabolic intermediates involved in PtdCho synthesis. On day 1, CHO cells were seeded at 150,000-200,000 cells/60 mm dish in 3 ml of medium A. On day 3, cells were cultured in medium B for 24 h prior to the addition of 20 μM (B) or 60 μM (C) FOH for the indicated times. Cells received choline-free medium containing of [^{3}H]choline (2 μCi/ml) for the final 30 min of FOH treatment. Cells were harvested and [^{3}H]choline incorportion into PtdCho (○), phosphocholine (■) and CDP-choline (▲) was measured. Results are the mean and standard deviation of triplicate determinations from representative experiments repeated two other times with similar results.

PtdCho. This did not occur until after >2 h treatment with 60 μM FOH, when there was global suppression of PtdCho synthesis.

4.1.2 Activation, membrane translocation and caspase cleavage of CCTα in response to FOH

Since [^{3}H]choline labelling experiments indicated that CCT activity was stimulated by FOH, the *in vivo* effects of FOH on CCTα localization and activity were measured. CCTα is localized primarily in the nucleoplasm in CHO cells and associates with the NE in response to lipid activators such as fatty acids and DAG (52, 58, 244). To examine whether FOH activated CCTα, CHO-K1 cells were treated with 60 μM FOH for up to 8 h, permeabilized with digitonin, and CCT activity and protein was measured in isolated soluble and particulate fractions (Figure 4.2). In untreated cells, CCTα activity was equally distributed between the fractions, with 54% and 40% in the soluble and particulate fraction, respectively. Following FOH treatment for 30 min, the bulk of CCTα activity was associated with the particulate fraction and this distribution persisted for the entire 8 h time course (Figure 4.2, A).

Translocation of soluble CCTα to membranes also occurred after FOH treatment for 30 min, as assessed by immunoblotting of isolated soluble and particulate fractions of FOH-treated cells with an antibody against a C-terminal epitope in CCTα (Figure 4.2, B). Soluble CCTα has been shown to migrate as a diffuse series of bands on SDS-PAGE due to phosphorylation of multiple serine residues in the C-terminal phosphorylation domain. After membrane translocation and activation, CCTα shifts to a single faster migrating band (120, 174, 289). Compared to untreated cell extracts, CCTα migrated as a species of 38- to 39-kDa on SDS-PAGE following a 30-minute FOH treatment (Figure 4.2, B),

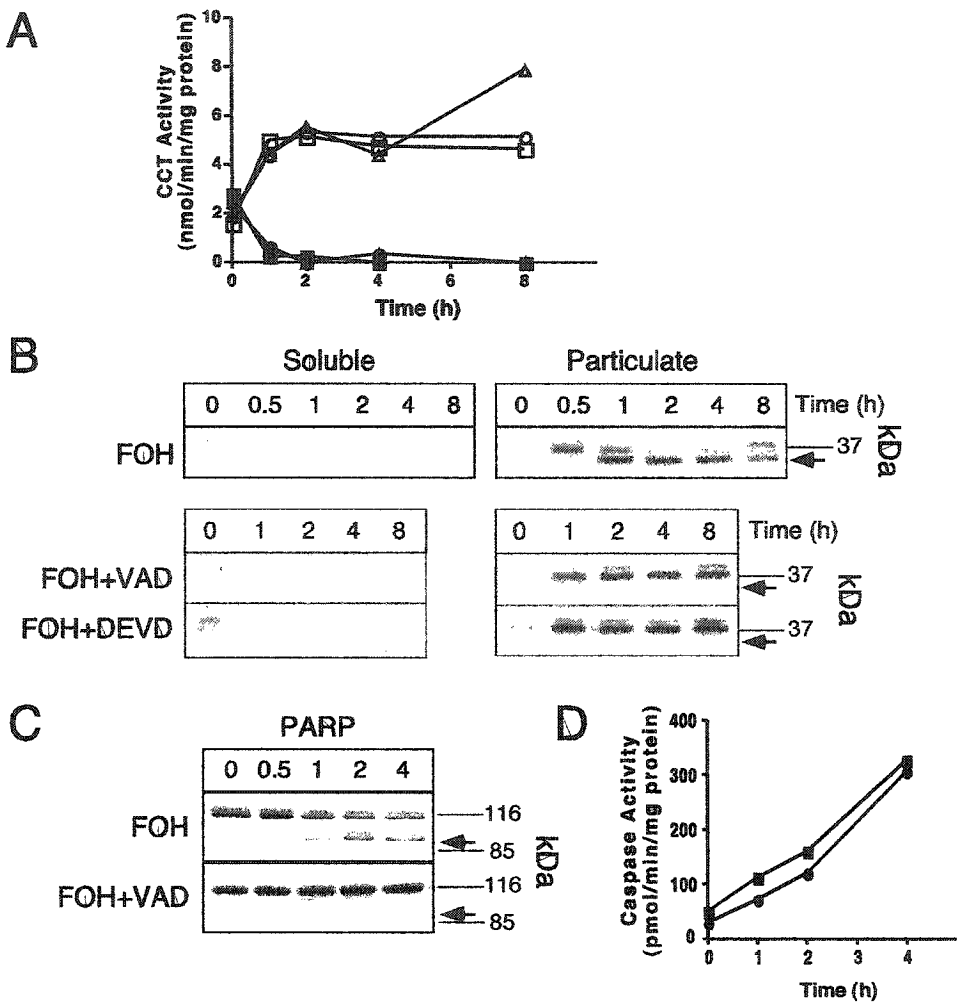

Figure 4.2 - FOH causes membrane translocation and caspase-mediated cleavage of CCTα. CHO cells were cultured as described in Figure 4.1 and were treated with z-VAD-fmk (VAD -75 μM), z-DEVD-fmk (DEVD - 75 μM), or DMSO control (0.3% vol/vol) for 15 min, followed by addition of FOH (60 μM) for the indicated times. At each time point, soluble and particulate fractions were isolated from digitonin-permeabilized cells as described in "Material and Methods." (**A**) Soluble (solid symbols) and particulate (open symbols) fractions (10 to 15 μg protein) from cells treated with FOH (□ and ■), FOH plus VAD (△and ▲), or FOH plus DEVD (○ and ●) were assayed for CCT activity. (**B**) Soluble and particulate fractions (7.5 μg protein) were resolved by SDS-10%PAGE and immunoblotted with an antibody against a C-terminal epitope in CCTα. The position of proteolyzed CCTα is indicated by an arrow. (**C**) PARP was detected by immunoblotting of total cell protein (15 μg) from cells treated with FOH or FOH plus VAD for the indicated times. The position of proteolyzed PARP is indicated by an arrow. (**D**) Caspase-3 (■) and -6 (●) activity was assayed in 100 μg of the 100,000 x *g* soluble fraction of FOH-treated CHO cells with acetyl-DEVD-*p*-nitroanilide or acetyl-VEID-*p*-nitroanilide, respectively. Results are from single experiments repeated two other times with similar results.

indicating dephosphorylation of the protein.

In addition to inducing alterations in CCTα localization and phosphorylation, FOH (60 μM) induced an apparent proteolysis of CCTα after treatment for 1 h (arrow in Figure 4.2, B). The truncated protein was reduced in mass by 3-5 kDa, indicating proteolysis near the N- or C-terminus of CCTα. Since FOH and related isoprenoids induce apoptosis, leading to activation of caspase-mediated proteolytic cascades (190), we tested whether this proteolytic cleavage could be prevented by the addition of the broad-range caspase inhibitor z-VAD-fmk or the caspase-3 inhibitor z-DEVD-fmk. Pretreatment of cells for 15 minutes with caspase inhibitors (75 μM) completely prevented CCTα proteolysis associated with FOH treatment (Figure 4.2, B). However, treatment with caspase inhibitors did not affect CCTα membrane translocation and dephosphorylation (Figure 4.2, B) or *in vitro* enzyme activity (Figure 4.2, A).

Cleavage of poly(ADP-ribose) polymerase (PARP) by caspase 3 is commonly used to monitor the occurrence of apoptosis (242). Since FOH treatment was associated with proteolytic cleavage of CCTα, the effect of FOH treatment on cleavage of PARP and activation of caspase 3 and 6 was assessed. In FOH-treated CHO cells, proteolysis of PARP occurred within the same time frame as CCTα proteolysis and was completely blocked by z-VAD-fmk (Figure 4.2, C). Concurrent with the cleavage of PARP and CCTα, caspase-3 and -6 activity in cell extracts from FOH-treated cells increased linearly over 4 h (Figure 4.2, D). These results show that FOH induced translocation of CCTα to membranes within 30 min and subsequently activated an apoptotic program resulting in cleavage of CCTα by caspases after 1 h.

The dose-dependency of FOH-mediated membrane translocation, phosphorylation and caspase-cleavage of CCTα were further characterized (Figure 4.3). In digitonin-permeabilized control cells, CCTα was equally distributed between soluble and particulate fractions. This distribution shifted increasingly to the particulate fraction with increasing FOH concentration, with complete translocation to membranes occurring at 60 and 80 μM FOH. CCTα and PARP cleavage was absent at 20 μM FOH, yet was apparent at 60 μM FOH, which was the same concentration that caused dramatic inhibition of PtdCho synthesis (Figure 4.1, B). Interestingly, CCTα and PARP proteolytic processing was not complete in FOH-treated cells.

Results from [^{3}H]choline labelling and cell fractionation studies indicated that FOH caused membrane translocation and activation of CCTα. To determine if FOH is a direct activator of CCTα, recombinant rat CCTα was assayed in the presence of PtdCho vesicles containing increasing mol% of FOH (Figure 4.4). For comparison purposes, parallel incubations were carried out using PtdCho vesicles containing the CCTα activator oleate. CCTα activity was enhanced 2-fold by 2 mol% FOH in PtdCho vesicles, and was maximally enhanced (4-fold) by 10-20 mol% FOH. CCTα activity was also maximally enhanced by 7-fold at 10-20 mol% of oleate in PtdCho vesicles. Thus, FOH acts as a direct activator of CCTα activity *in vitro*.

4.1.3 Identification of the caspase cleavage site in CCTα

Caspases recognize loosely conserved four amino acid consensus sequences with cleavage occurring on the carboxyl side of an absolutely conserved aspartate residue at the fourth position (306). The antibody that was used to detect CCTα in FOH treated cells recognized a C-terminal epitope (Figure 4.2, B), which would have been completely

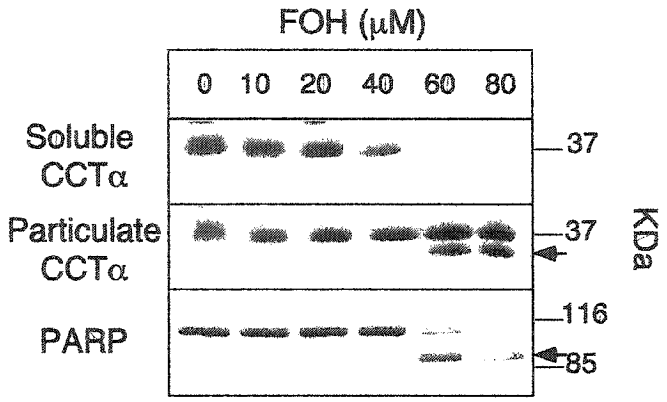

Figure 4.3 - Dose dependence of FOH-mediated membrane translocation and proteolysis of CCTα. CHO cells were cultured in medium B for 24 h prior to the addition of the indicated concentrations FOH for 1 h. Soluble and particulate fractions were isolated from digitonin-permeabilized cells. Proteolysed CCTα and PARP are indicated by arrows and were resolved and detected as described in Figure 4.2. This representative experiment was repeated two other times with similar results.

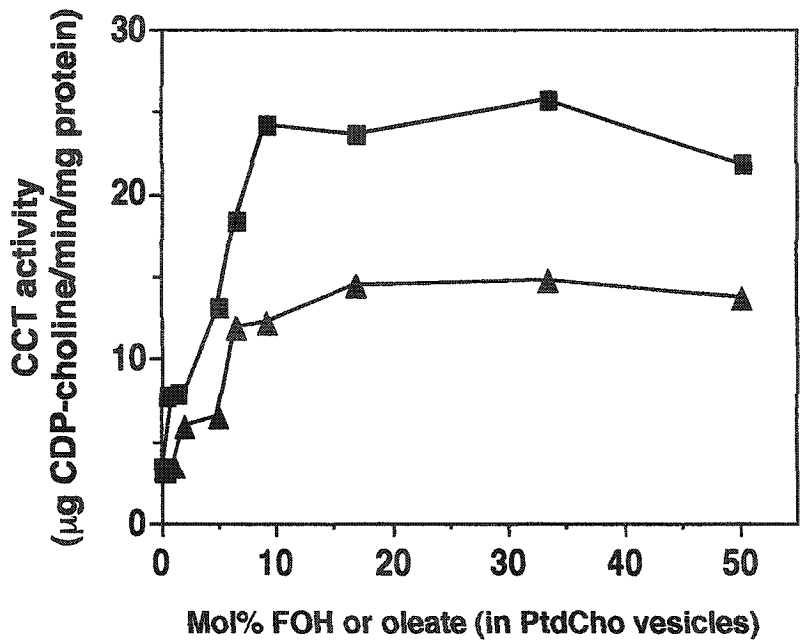

Figure 4.4 - Activation of CCTα by FOH *in vitro*. Purified recombinant rat CCTα (70 ng) was assayed for 15 min in the presence of PtdCho vesicles containing increasing mol% of oleate (■) or FOH (▲). CCTα activity was measured as described in "Material and Methods." Total lipid in the assays was 100 μg. Results are the mean of duplicate determinations from a representative experiment repeated two other times with similar results.

or partially lost by caspase proteolysis of 3-5 kDa. Therefore, the caspase-cleavage site had to be in the N-terminal region of CCTα. Inspection of the rat CCTα protein sequence indicated two candidate caspase cleavage sites within this N-terminal region; $TEED^{28}G$, $IEVD^{54}F$ (Figure 4.5, A). In order to determine if caspase cleavage of CCTα occurred at one or both of these sites, essential aspartate residues were changed to glutamate by site-directed mutagenesis and the corresponding cDNAs were expressed in CHO MT58 cells. These cells were chosen for transfection because they express low levels of a temperature-sensitive allele of CCTα (82), thereby negating interference by endogenous CCTα. In mock-transfected cells, endogenous CCTα was virtually undetectable by immunoblotting at both the permissive (33°C) and non-permissive (40°C) temperatures (Figure 4.5, B). Following FOH treatment (60 μM) for 2 h at 40°C, a major CCTα cleavage product was readily detected in cells expressing wild-type CCTα and CCT D54E, indicating that this was not a caspase-cleavage site. In contrast, CCT D28E was resistant to FOH-induced proteolysis, indicating that the sequence $TEED^{28}$ is the caspase-recognition site in CCTα. Interestingly, D28 is also the final amino acid in the CCTα nuclear localization signal (287), and cleavage at this site would result in a protein unable to enter the nucleus.

We also tested whether caspase-cleavage of CCTα occurred in response to other apoptotic stimuli and in other cells. Exposure of CHO MT58 cells to the apoptotic agents chelerythrine (a non-specific protein kinase inhibitor) and UV light resulted in cleavage of transfected wild-type CCTα, but not CCT D28E (Figure 4.5, C). SDS-PAGE and immunoblotting analysis was also used to monitor PARP and CCTα cleavage in NIH-3T3 and HEK-293 cells treated with FOH (60 μM) for up to 4 h. Similar to CHO cells

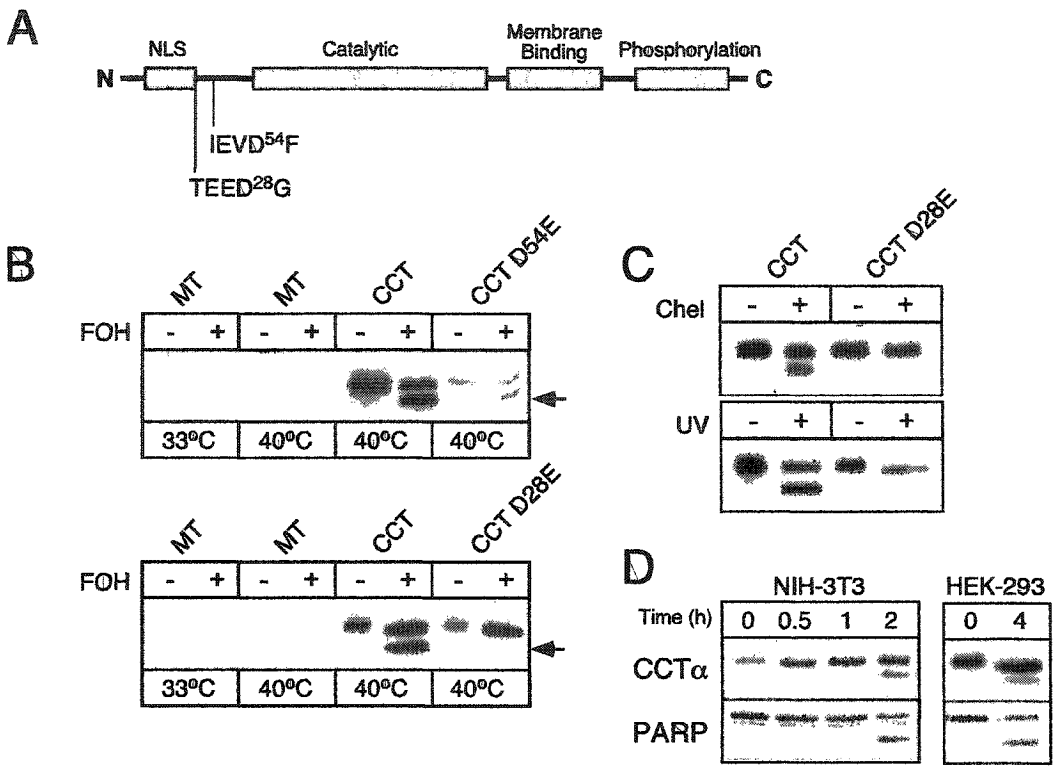

Figure 4.5 - Identification of the caspase cleavage site in CCTα. **(A)** Schematic of CCTα showing position of domains and putative caspase cleavage sites near the N-terminus (NLS - nuclear localization signal). **(B)** cDNAs encoding wild-type CCTα, CCTD54E, CCTD28E, or empty vector (MT, mock transfected) were transiently transfected into CHO MT58 cells cultured at 33°C in medium A. After 24 h, cells received 3 ml of medium B. Following an additional 24 h incubation at 33°C, MT58 cells were either kept at 33°C or switched to 40°C and treated with FOH (60 μM) or ethanol vehicle for 2 h. Cells were harvested and total homogenates (10 μg protein) were resolved on SDS-10% PAGE and immunoblotted for CCTα. The position of proteolyzed CCTα is indicated by arrows. **(C)** cDNAs were transfected into MT58 cells as described in (B), treated with chelerytherine (20 μM) for 2 h or exposed to UV light (254 nm) for 10 min and cultured for an additional 12 h. Cells were shifted to 40°C for 60 min prior to harvest to reduce expression of endogenous CCTα. **(D)** NIH-3T3 and HEK 293 cells were cultured in DMEM with 10% LPDS for 24 h prior to addition of FOH (60 μM) for the indicated times. CCTα and PARP were immunoblotted (15 μg total cell extract) as described in the legend to Figure 4.2.

(Figures 4.2 and 4.3), FOH treatment resulted in the partial cleavage of CCTα and PARP in both cell lines (Figure 4.5, D).

4.1.4 Nuclear envelope translocation and nuclear export of CCTα in FOH-treated cells

To determine the intracellular site of FOH-induced CCTα membrane translocation, CHO cells were treated with FOH (60 μM) for up to 2 h and CCTα localization was assessed by indirect immunofluorescence analysis using an antibody against a C-terminal epitope in CCTα (Figure 4.6). The DNA-binding dye Hoechst 33258 was employed as a counterstain to visualize the nucleus and monitor changes in chromatin structure during FOH treatment. As reported previously (119), untreated CHO cells displayed diffuse nucleoplasmic CCTα immunostaining. Following FOH treatment for 30 min, CCTα was prominently localized to the NE, providing further evidence for *in vivo* CCTα activation by FOH. Addition of FOH to cells for 1 h resulted in partial localization of CCTα to a perinuclear region that did not overlap with Hoechst staining, indicating nuclear export of CCTα. NE localization was still evident in these cells; however, the immunostaining was more fragmented and localized to discreet regions of the NE. Also evident in some cells with extranuclear CCTα immunostaining was chromatin condensation, a characteristic of apoptotic cells (327). Similar results were obtained following 2 h FOH treatment, but with an increased proportion of cells displaying extranuclear CCTα immunostaining (30-40%) and chromatin condensation (10-20%). No appreciable fluorescence signal was obtained in CHO MT58 cells under the same experimental conditions, indicating that the anti-CCTα antibody did not cross-react with other proteins in CHO cells (data not shown).

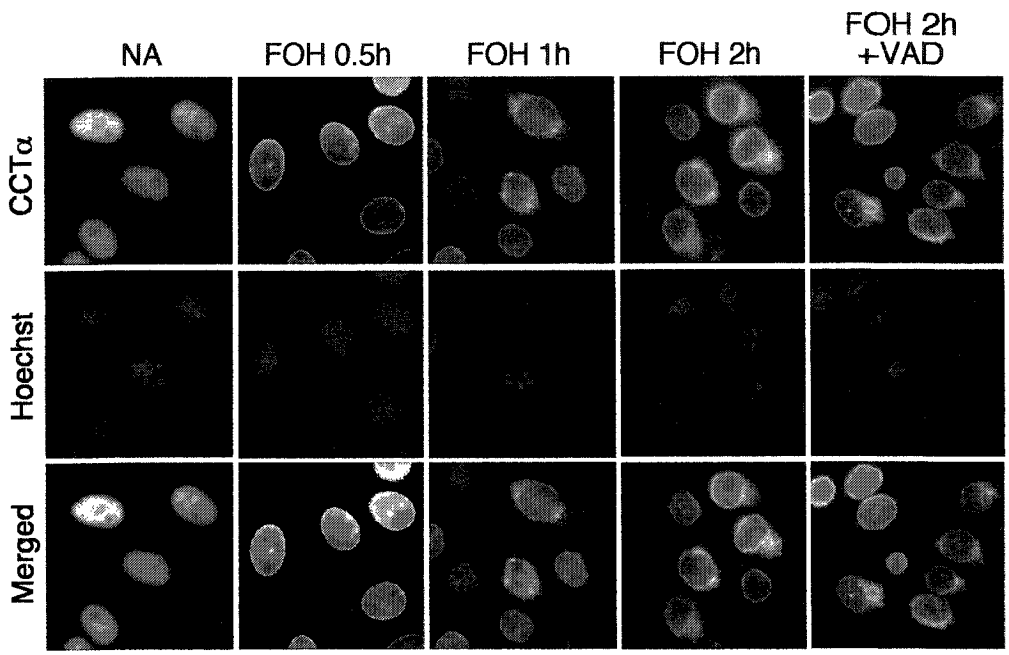

Figure 4.6 - FOH promotes nuclear envelope localization and nuclear export of CCTα. On day 1, CHO cells were seeded at 75,000-100,000 cells/60 mm dish on glass coverslips in 3 ml medium A. On day 3, cells were cultured in 2 ml medium B for 24 h prior to the addition of FOH (60 μM). One set of cells were treated with z-VAD-fmk (VAD - 75 μM) 15 min prior to addition of FOH. At the indicated times, cells were fixed and permeabilized in 3% formaldehyde/0.05% Trition X-100 and processed for immunofluorescence localization of CCTα and stained with Hoechst 33258 as described in "Material and Methods." CCTα was visualized using an FITC-conjugated secondary antibody. Images were obtained using an Axioplan 2 fluorescence microscope with a Planapo 100x oil immersion objective and equipped with a Spot CCD camera.

The appearance of CCTα outside the nucleus corresponded to the time frame of caspase-mediated removal of its N-terminal nuclear localization domain (Figure 4.2, B). We therefore investigated the involvement of caspase-mediated proteolysis in CCTα nuclear export. CHO cells were pretreated with z-VAD-fmk (75 μM) prior to the addition of FOH (60 μM) for 2 h and CCTα localization was assessed by immunofluorescence analysis (Figure 4.6). In cells treated with FOH and z-VAD-fmk, CCTα was localized outside the nucleus in a pattern similar to the cells treated with FOH alone. These results indicate that caspase-mediated removal of the nuclear localization signal from CCTα is not involved in its translocation to membranes or export from the nucleus.

To more precisely assess the involvement of caspase cleavage in release of CCTα from the nucleus, CHO MT58 cells stably transfected with wild-type CCTα or caspase-resistant CCT D28E were treated with FOH (60 μM) for 1 h and CCTα was localized by immunofluorescence analysis (Figure 4.7). As seen with endogenous CCTα in CHO cells, ectopically expressed CCTα and CCT D28E were diffusely localized within the nucleus in untreated CHO MT58 cells, indicating that the D28E mutation does not affect CCTα nuclear localization. Upon addition of FOH, both wild-type CCTα and CCT D28E were robustly exported from the nucleus. Similar to results seen with endogenous CCTα in CHO cells, over-expressed wild-type CCTα remained partially associated with the NE, whereas CCT D28E was excluded from the nucleus and NE and diffusely localized throughout the cytoplasm.

Rather than active export, a trivial explanation for release of CCTα from the nucleus during FOH-induced apoptosis could be the loss of NE integrity. To test this

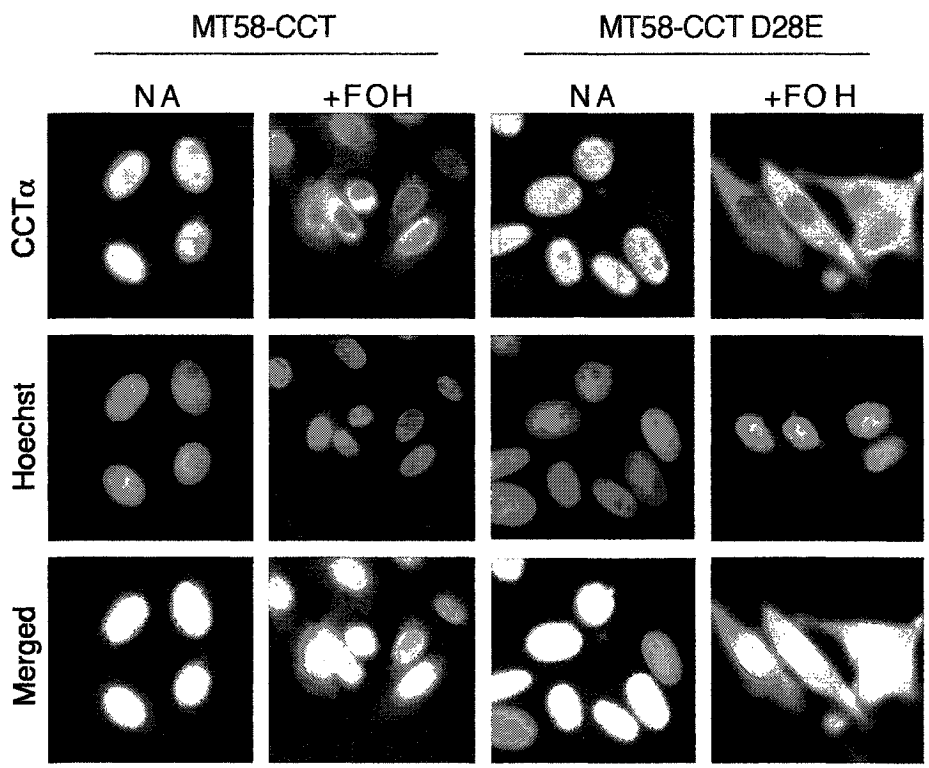

Figure 4.7 - Nuclear export of caspase-resistant CCT D28E in response to FOH. On day 1, CHO MT58 cells stably transfected with cDNAs encoding wild-type CCTα or CCT D28E were seeded at 150,000-200,000/60 mm dish on glass coverslips in 3 ml medium A at 33°C. On day 3, cells were cultured in 2 ml medium B 24 h prior to addition of FOH (60 μM) or ethanol vehicle (no addition, NA) for 2 h at 40°C. Cells were processed for immunofluorescence localization of CCTα and Hoechst 33258 as described in Figure 4.6. CCTα was visualized using an Alexa-488 conjugated secondary antibody. Images were obtained using an Axioplan 2 fluorescence microscope with a Planapo 100x oil immersion objective and equipped with a Spot CCD camera.

possibility, CHO cells were scrape-loaded with Oregon green 488-labeled 70 kDa dextran, a soluble inert marker of nuclear integrity (238), prior to FOH treatment. Due to the size exclusion properties of the nuclear pore complex, dextran with a molecular mass > 50 kDa distributes throughout the cytoplasm and only enters the nucleus if NE integrity has been compromised (87). In addition, 70 kDa dextran closely approximates the molecular mass of CCTα, which exists as a dimer of 42 kDa subunits *in vivo* (50), thereby providing an index of passive diffusion of CCTα across the NE. Scrape-loaded cells were treated with FOH (60 μM) for up to 2 h, and CCTα and 70 kDa dextran distribution in cells was assessed (Figure 4.8, A). In untreated cells, CCTα immunostaining displayed a diffuse nucleoplasmic pattern, whereas dextran was cytoplasmic and excluded from the nucleus. CCTα translocated to the NE within 30 min following FOH addition, and was detected in a perinuclear region following FOH treatment for 1 and 2 h. Importantly, in cells in which CCTα immunostaining was clearly evident outside the nucleus, dextran remained cytoplasmic and excluded from the nucleus. As seen in merged images, CCTα immunostaining outside the nucleus did not significantly overlap with the soluble cytoplasmic marker dextran, indicating that extranuclear CCTα predominantly associated with membranes in FOH-treated cells.

To confirm that nuclear pore complexes (NPCs) were intact in CHO cells excluding dextran and permeable to dextran in cells with diminished NPC integrity, scrape-loaded CHO cells were treated with FOH (60 μM) and immunostained with an antibody directed against a subunit of the NPC, Nup62 (Figure 4.8, B). In untreated cells, NPC immunostaining was prominent within the NE while dextran was excluded from the nuclear region. Following 2 h treatment with FOH, NPC immunostaining was greatly

Figure 4.8 - Nuclear integrity and nuclear export of CCTα in FOH-treated CHO cells. (A) CHO cells were scrape-loaded with lysine-fixable, Oregon green 488-labeled 70kDa dextran and reseeded on glass coverslips in medium A as described in "Material and Methods". After 8 h, culture medium was exchanged for medium B and cells were incubated for 18 h prior to the addition of FOH (60 μM). At the indicated times, cells were processed for immunofluorescence localization of CCTα as described in Figure 4.6. (B) Oregon green 488-dextran loaded cells cultured as described in (A) were treated with FOH (60 μM) for 1 h and the nuclear pore complex (NPC) was visualized by immunofluorescence analysis using an Alexa-555 conjugated secondary antibody. (C) Oregon green 488-dextran loaded CHO MT58 cells stably overexpressing wild type rat CCTα were exposed to chelerytherine (20 μM) for 1 h or UV light (254 nm for 10 min followed by 10 h of incubation) and processed for immunofluorescence localization of CCTα using an Alexa-555 conjugated secondary antibody. Cells were shifted to 40°C 60 min prior to harvest to reduce expression of endogenous CCTα. Images in A-C are single optical sections (0.5 - 0.7 μm) obtained using a Zeiss LSM510 confocal microscope with a 100X oil immersion objective lens.

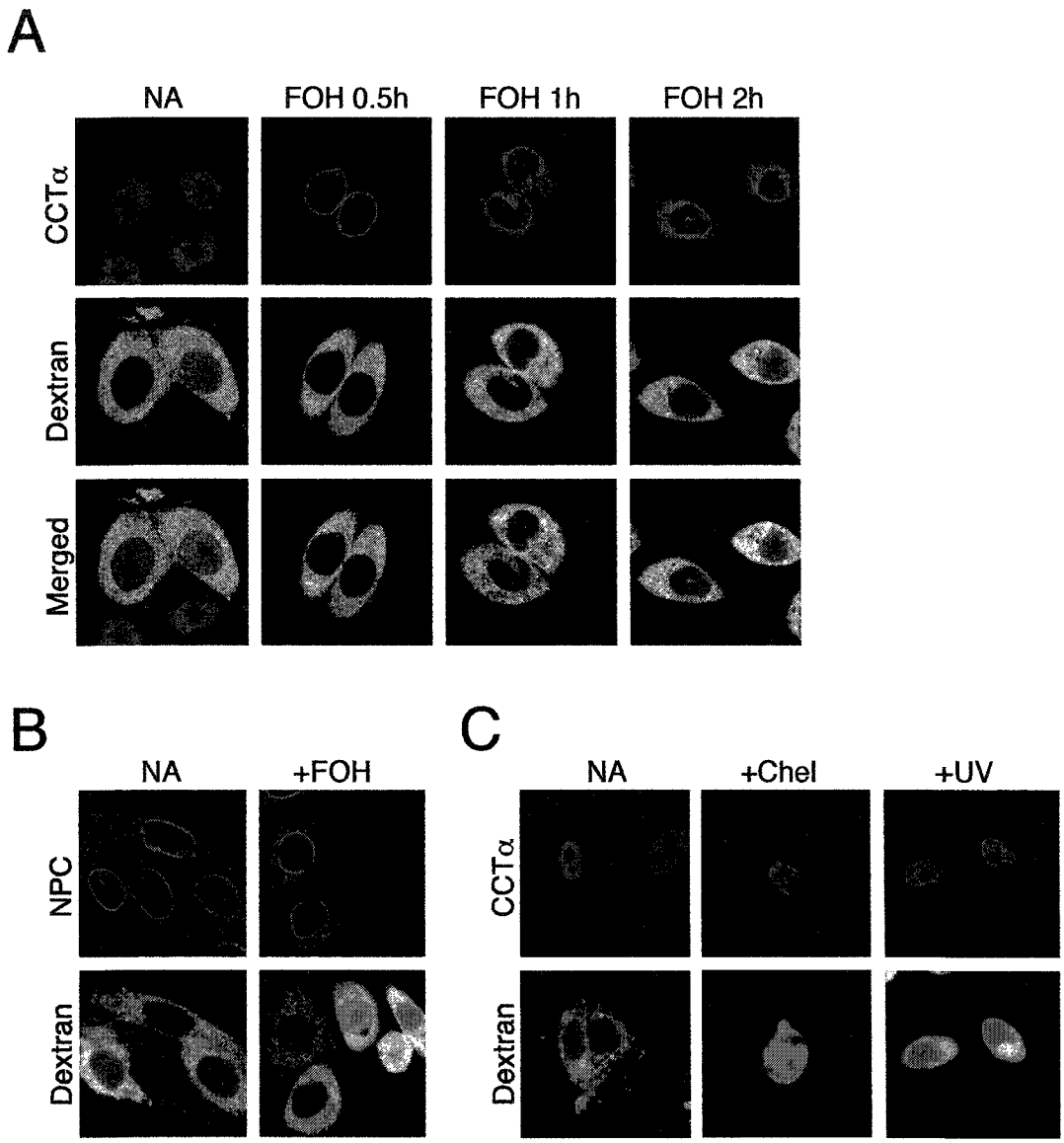
A
NA
FOH 0.5h
FOH 1h
FOH 2h
CCTα
Dextran
Merged
B
NA
+FOH
NPC
Dextran
C
NA
+Chel
+UV
CCTα
Dextran

Figure 4.8

diminished in numerous cells, indicating breakdown of nuclear pore components, resulting in loss of antigenicity towards the NPC antibody. In scrape-loaded cells, diminished NPC immunostaining was invariably accompanied by dextran fluorescence within the nucleus. Thus loss of NE integrity, based on permeability to 70 kDA dextran, is not the cause of CCTα nuclear export in FOH-treated cells.

To test whether CCTα NE localization and nuclear export occurred in response to other apoptotic stimuli, CHO MT58 cells stably overexpressing CCTα were exposed to UV irradiation or chelerythrine (20 μM) and localization of CCTα and maintenance of NE integrity were monitored (Figure 4.8, C). In cells treated with UV light, CCTα did not associate with the NE and remained within the nucleus. NE integrity was rapidly lost in chelerythrine-treated cells, leading to uptake of Oregon green 488-dextran into the nucleus, but CCTα remained associated with the nucleus, even in cells in which the nuclear region had become fragmented. This shows that caspase cleavage of CCTα can occur within the nucleus, and CCTα NE translocation and nuclear export are not features of all apoptotic programs.

4.1.5 Rapid induction of PtdCho synthesis and DAG depletion in FOH-treated cells

FOH caused activation, NE localization, and nuclear export of CCTα in CHO-K1 cells. However, it remained unclear what influence these FOH-mediated effects had on PtdCho synthesis. Metabolic labelling results indicated that PtdCho synthesis was transiently stimulated by 20 μM FOH, but inhibited by the higher dose of 60 μM FOH despite enhanced CCTα activation and membrane association (Figures 4.1 and 4.3). In agreement with previous reports (2, 186, 279), a dramatic elevation in CDP-choline levels suggested profound inhibition of CPT by 60 μM FOH, which correlated with

FOH-induced caspase activation (Figure 4.3). Previous studies have shown that indirect inhibition of CPT activity and CDP-choline accumulation can result from diminished availability of DAG, effectively shifting the rate limiting reaction in the CDP-choline pathway from CCT to CPT (4, 136, 166). We therefore explored the relationship between cellular DAG mass and synthesis of CDP-choline pathway intermediates and PtdCho in cells treated with increasing concentrations of FOH. Previous metabolic labelling experiments employed a protocol in which cells were pulse-labeled with [^{3}H]choline for the final 30 min of FOH treatment (Figure 4.1). We reasoned that activation of PtdCho synthesis could be masked using this protocol due to insufficient labelling of metabolic intermediates prior to FOH-mediated CPT inhibition. Therefore, we used a continuous radiolabelling protocol, in which cells were labeled with [^{3}H]choline for 30 min prior to and during FOH treatment (Figure 4.9, A). FOH (5 - 20 μM) treatment for 30 min caused a dose-dependent increase in [^{3}H]PtdCho synthesis, concurrent with a dose-dependent decrease in cellular DAG mass (Figure 4.9, B) that reached a maximum reduction of 50% at 40 μM FOH. [^{3}H]Choline incorporation into PtdCho reached a maximal >2-fold increase in response to 20 μM FOH. The dose-dependent increase in [^{3}H]PtdCho synthesis was accompanied by a steady decrease in [^{3}H]phosphocholine levels, indicating increasing CCTα activation, and increasing [^{3}H]CDP-choline accumulation, indicating CPT inhibition. At higher FOH doses of 40 and 60 μM, no increase in PtdCho synthesis was observed, likely due to a metabolic block at the CPT-catalyzed reaction.

To assess the effect of chronic FOH treatment, DAG mass in CHO cells was measured in response to 20 and 60 μM for up to 6 h following FOH addition (Figure 4.9,

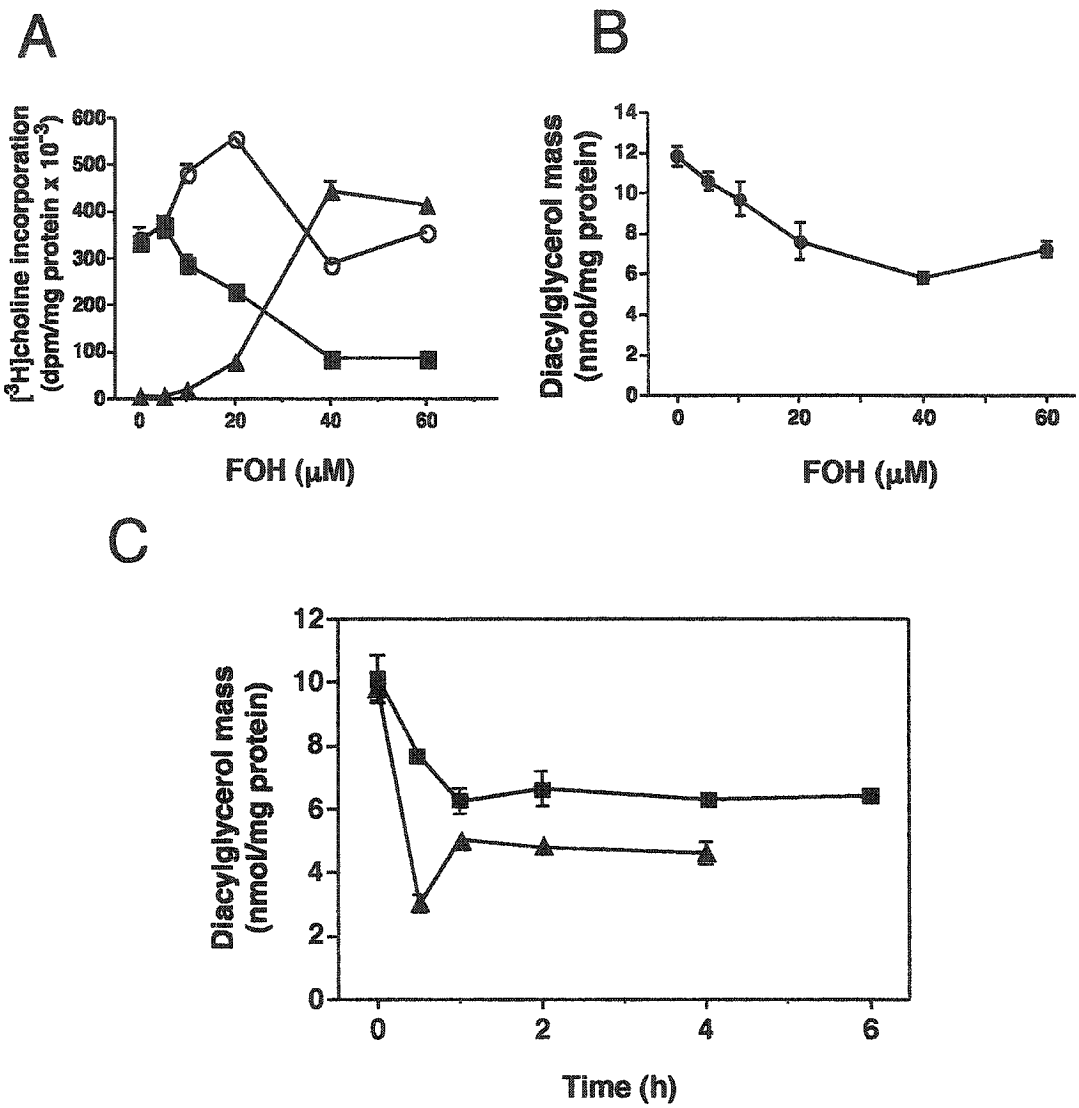

Figure 4.9 - Dose-dependent increase in PtdCho synthesis is accompanied by DAG depletion in FOH-treated CHO cells. CHO-K1 cells were cultured in medium B for 24 h prior to the addition of choline-free medium containing [^{3}H]choline (2μCi/ml) prior to the addition of FOH (5 - 20 μM) for 30 min. (A) Cells were harvested and [^{3}H]choline incorportion into PtdCho (○), phosphocholine (■) and CDP-choline (▲) was measured. (B) Diacylglycerol mass was determined in the same lipid extracts as described in "Material and Methods." (C) Diacyglycerol mass was determined in cells treated with 60 μM FOH (▲) or 20 μM FOH (■) for the indicated times. Results are the mean and standard deviation of triplicate determinations from representative experiments repeated two other times with similar results.

C). DAG mass was decreased by >40% within 1 h in cells treated with 20 μM FOH compared to untreated controls, and remained low during the 6 h time course. DAG levels were even more dramatically affected by 60 μM FOH, decreasing by >60% following 30 min FOH treatment and recovering slightly at later time points. Cells treated with 60 μM FOH for 6 h were apoptotic and detaching from culture dishes, confounding attempts to measure DAG mass.

Increased PtdCho synthesis at lower doses of FOH but not at higher doses, suggested that DAG depletion became a limiting factor and CCTα activation could not outweigh CPT inhibition due to decreased substrate availability. Therefore, it was likely that 60 μM FOH was activating PtdCho synthesis, but in a rapid and transient manner. To test this hypothesis, the effect of acute (5 - 30 min) FOH exposure on the synthesis of PtdCho and its precursors phosphocholine and CDP-choline was determined in cells prelabeled with [^{3}H]choline for 30 min (Figure 4.10). Treatment of cells with 60 μM FOH for 15 min caused a significant 30% increase in PtdCho synthesis compared to controls. This observed increase in [^{3}H]PtdCho synthesis was transient, as levels normalized to that of control cells by 30 min. A decrease in [^{3}H]phosphocholine (indicating activation of CCTα) and accumulation of [^{3}H]CDP-choline (indicating CPT inhibition) was observed as early as 5 min following FOH addition. The effect of FOH on cellular DAG mass was also swift, with a decrease of >40% detected as early as 10 min following FOH addition. Thus, initially FOH stimulated PtdCho synthesis in CHO cells via activation of CCTα. Eventual FOH-induced inhibition of CPT activity and PtdCho synthesis occurred concurrently with decreased cellular DAG mass.

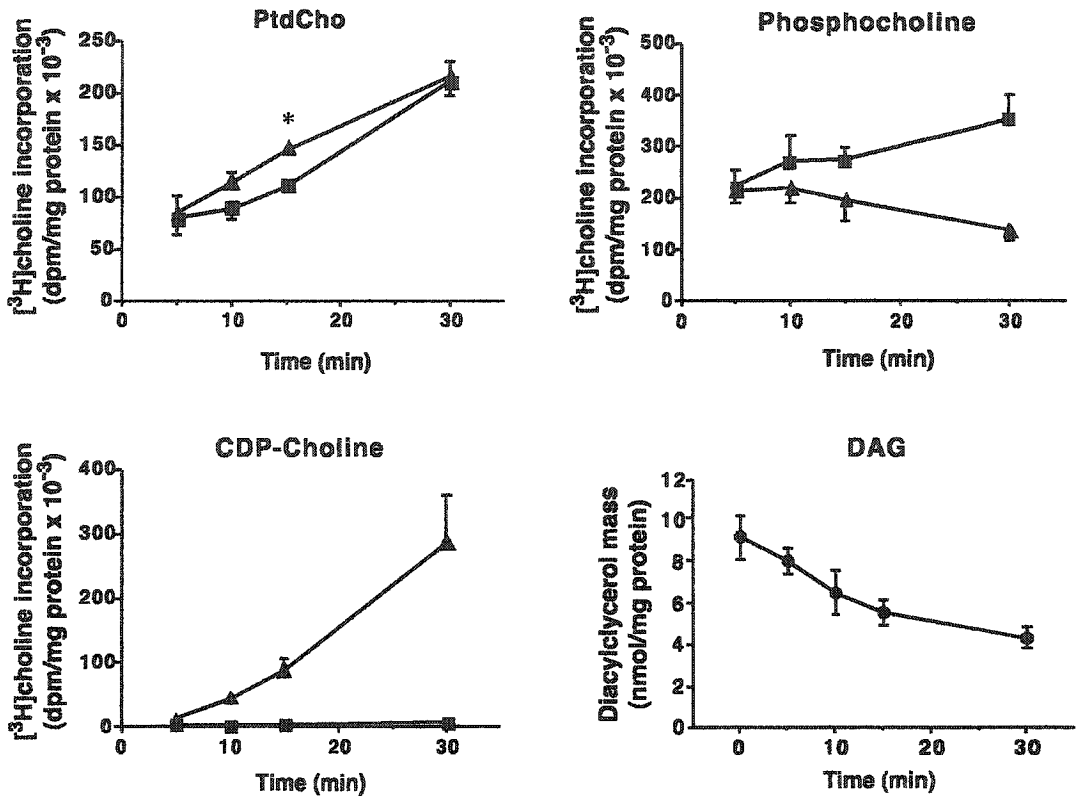

Figure 4.10 - Transient activation of PtdCho synthesis and decreased in DAG mass in FOH treated CHO cells. CHO cells were cultured as described in Figure 4.1 and placed in medium B for 24 h prior to start of experiments. Cells received choline-free medium containing [^{3}H]choline (2 μCi/ml) for 30 min prior to addition of 60 μM FOH (▲) or ethanol vehicle (■). Cells were harvested at the indicated times and [^{3}H]choline incorportion into PtdCho, phosphocholine, and CDP-choline was measured. DAG mass was measured from the same cell extracts as described in "Materials and Methods". Results are the mean and standard deviation of triplicate determinations from representative experiments repeated two other times with similar results, *p <0.05 compared to vehicle control.

4.1.6 DAG and Oleate prevent FOH-induced apoptosis

Previous studies implicated attenuation of DAG-dependent cell-survival signalling in the intiation of apoptosis by FOH and related isoprenoids (180, 280). The rapid decrease in cellular DAG mass concurrent with stimulation of CCTα activity and PtdCho synthesis in FOH-treated cells (Figures 4.10) suggested that over-consumption of DAG by the CDP-choline pathway could disrupt DAG homeostasis. If so, this would be alleviated under conditions where cells had an ample supply of DAG for PtdCho synthesis. Therefore, the effect of exogenous lipid on FOH-induced apoptosis was investigated. All studies conducted to this point were carried out in CHO cells that were cultured for 18-24 h under lipid-depleted conditions in medium containing LPDS. To investigate whether media conditions conferred protection against FOH-induced apoptosis, cells were maintained in medium containing either whole serum (FCS), or in LPDS medium supplemented with oleate or dioctanoyl-glycerol (diC8), which is a cell-permeable short-chain DAG previously shown to prevent apoptosis in response to the FOH-related isoprenoid geranylgeraniol (180). Both oleate and diC8 would be expected to provide substrate for the CPT-catalyzed terminal reaction in the CDP-choline pathway; DiC8 as a direct substrate molecule (91, 266) and oleate by stimulating *de novo* DAG synthesis (136).

CHO cells were treated with FOH (60 μM) for up to 4 h under the different culture conditions and FOH-induced apoptosis was monitored by SDS-PAGE and immunoblot analysis of the caspase substrates CCTα and PARP (Figure 4.11, A). As shown previously for cells cultured in LPDS, CCTα and PARP cleavage was evident by 1 h following addition of FOH. In contrast, cells cultured in FCS were resistant to FOH

for the 4 h time course. Pretreatment for 30 min with either oleate (500 μM) or diC8 (500 μM) also completely prevented FOH associated caspase-mediated cleavage of CCTα and PARP. We also tested the effect of the cell-permeable DAG analogues 1-oleoyl, 2-acetyl-glycerol (OAG - 500 μM) and 12-O-tetradecanoyl-phorbol 13-acetate (TPA - 100 nM) on FOH-mediated CCTα membrane translocation and caspase proteolysis. Cells pretreated with DAG analogues were exposed to 60 μM FOH for 1 h, separated into soluble and particulate fractions following digitonin-permeabilization and immunoblotted for CCTα (Figure 4.11, B). OAG treatment alone resulted in membrane translocation of CCTα, whereas DiC8 and TPA had no effect. Membrane translocation of CCTα in response to FOH occurred in the presence of the DAG analogues, and all three were protective against caspase cleavage of CCTα. However, there was a small amount of the CCTα cleavage product detected in TPA-treated cells (Figure 4.11, B see arrow). To rule out the possibility that the uptake of FOH was reduced in the presence of oleate (500 μM) or diC8 (500 μM), the uptake of [^{3}H]FOH for 1 h was measured in CHO cells. Supplementation with oleate did not decrease FOH uptake compared to control cells (No addition; 616 ± 13 *versus* oleate; 841 ± 82 dpm/mg protein/hr). The uptake of FOH in the presence of diC8 was increased by > 2 fold (616 ± 13 versus 1361 ± 12 dpm/mg protein/hr). Therefore the prevention of cleavage of CCTα and PARP by oleate or diC8 was not due to reduced uptake of FOH.

Incorporation of oleate into complex lipids such as DAG requires prior activation to its corresponding fatty acyl-CoA ester though the action of acyl-CoA synthase (128, 263). To test whether oleate conversion to its CoA ester or complex lipids was required for prevention of FOH-induced apoptosis, cells were treated with the fungal metabolite

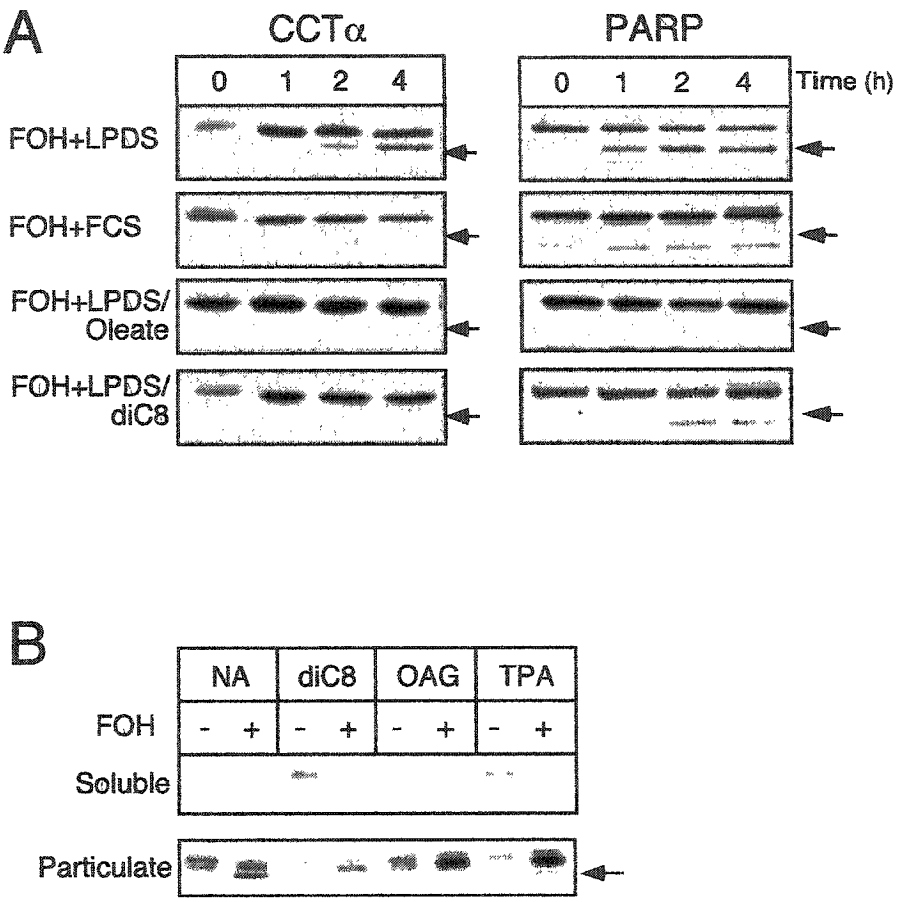

Figure 4.11 - FOH-induced PARP and CCTα cleavage is prevented by pretreatment with oleate or DAG. **(A)** CHO cells were cultured in 2 ml medium A (FCS) or in medium B (LPDS) and preincubated for 30 min with either oleate or diC8 (500 μM) 24 h prior to the addition of FOH (60 μM). Cells were harvested at the indicated times and total cell extracts (15 μg) were resolved by SDS-9%PAGE and immunoblotted for CCTα and PARP, as described in Figure 4.2. **(B)** Cells were preincubated for 30 min with DiC8 (500 μM), 1-octanoyl, 2-acetyl-DAG (OAG - 500 μM), or TPA (100 nM) prior to addition of FOH (60 μM) for 2 h. Soluble and particulate fractions were isolated from digitonin-permeabilized cells and resolved (7.5 μg) by SDS-10%PAGE and immunoblotted for CCTα.

triacsin C, an inhibitor of acyl-CoA synthase 1 and 4 (155). Triacsin C treatment in CHO cells caused an 83% decrease in the incorporation of [^{3}H]oleate into triacylglycerol, which is an end-product of *de novo* DAG synthesis (no addition; 5804 ± 223, triacsin C; 1009 ± 186 pmol/mg protein/hr). In contrast there was a 34% decrease in phospholipid labelling (no addition; 5905 ± 133, triacsin C 3912 ± 63 pmol/mg protein/hr). Oleate incorporation into phospholipids in the presence of triacsin C has previously been shown to be due to phospholipid remodeling pathways that involve triacsin C-insensitive acyl-CoA synthase activities (128, 155). Caspase activation in cells treated with FOH (60 μM) and oleate (500 μM) in the absence and presence of triacsin C was monitored by SDS-PAGE and immunoblot analysis of the caspase substrates CCTα and PARP (Figure 4.12, A). As shown previously (Figure 4.11, B), FOH treatment caused cleavage of both caspase substrates, and this was prevented by oleate supplementation. However, oleate was ineffective at preventing FOH-mediated cleavage of CCTα and PARP in the presence of triacsin C. Triacsin C treatment alone did not affect caspase activity or the ability of diC8 to prevent FOH-induced caspase cleavage of CCTα and PARP.

To provide a relative measure of apoptosis within cell populations under the different culture conditions, cells treated as described above were analyzed by Cell Death ELISA (Figure 4.12, B). In cells cultured in LPDS alone, FOH treatment for 2 h caused a >40-fold increase in the apoptotic index compared to vehicle controls. This increase in apoptosis was decreased to <10-fold in cells pretreated with oleate, and restored to >30-fold when oleate was added in the presence of triacsin C. The apoptotic index was largely unaffected by FOH in cells pretreated with diC8, and triacsin C had no effect on diC8-mediated rescue from FOH-induced apoptosis. These results indicate that oleate

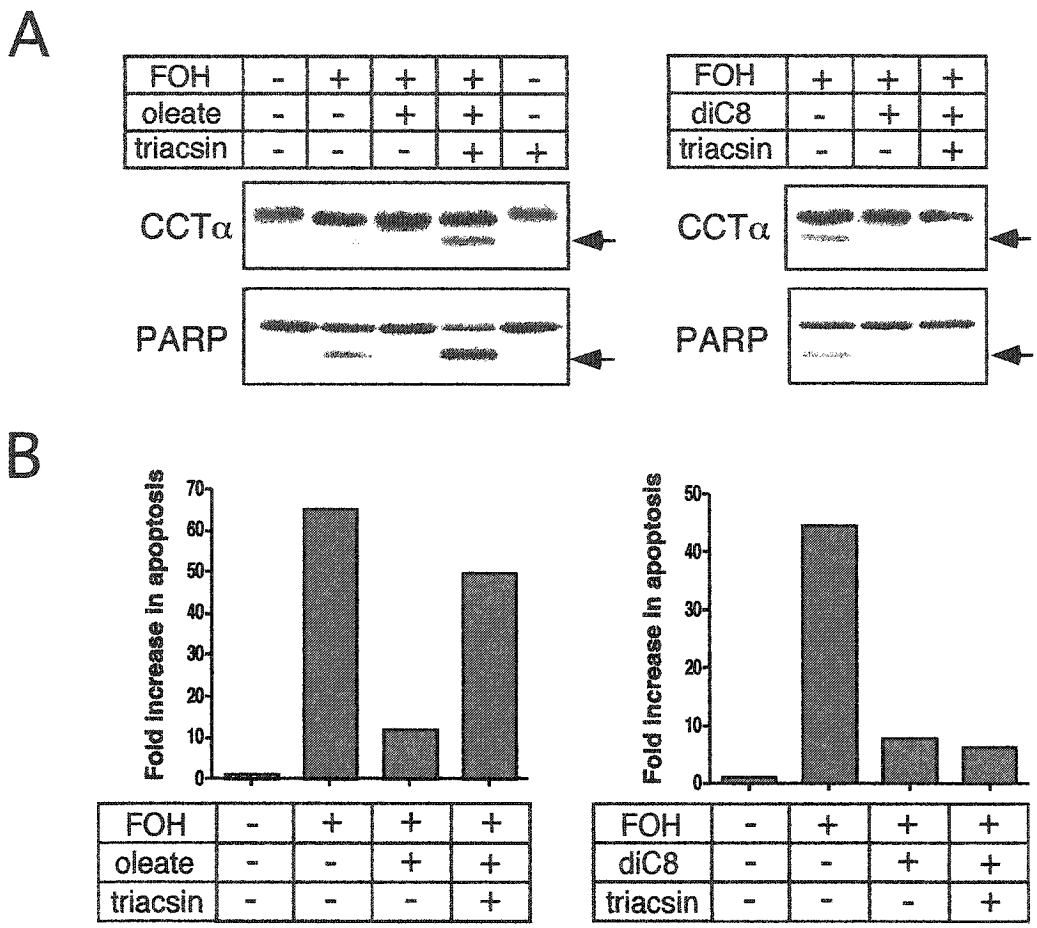

Figure 4.12 - Conversion of oleate to oleoyl-CoA is required for rescue of FOH-induced apoptosis. CHO cells were cultured in medium B for 24 h prior to the start of experiments. **(A)** Cells were preincubated for 30 min with oleate (500 μM) or diC8 (500 μM) in the absence or presence of triacsin C (9.6 μM) prior to 2 h treatment with FOH (60 μM). Proteins (15 μg) from total cell extracts were resolved immunoblotted for CCTα and PARP as described in Figure 4.3. This representative experiment was repeated one other time with similar results. **(B)** Relative levels of apoptosis in cells treated as described above was determined by Cell Death ELISA™ as described in "Material and Methods." Results are mean values from duplicate determinations of a representative experiment repeated once with similar results.

does not exert a direct protective effect against FOH, but must first be converted to its active acyl-CoA form and subsequently metabolized.

4.1.7 DAG and oleate prevent CCTα nuclear export

Prevention of CCTα cleavage by the caspase inhibitor z-VAD-fmk or mutation of the caspase-cleavage site did not prevent FOH-induced CCTα release from the nucleus (Figures 4.6 and 4.7), suggesting regulation by other FOH-mediated events. To test whether FOH depletion of DAG or inhibition of PtdCho synthesis caused CCTα relocalization, cells were cultured in medium containing FCS, LPDS, or LPDS supplemented with oleate (500 μM), diC8 (500 μM) or TPA (100 nM) prior to FOH addition for 2 h. Nuclear localization of CCTα was assessed by indirect immunofluorescence analysis, and Hoechst DNA-staining was used to visualize the nucleus and monitor changes in chromatin structure in response to FOH (Figure 4.13). As expected, CCTα was exported from the nucleus in 20-30% of cells cultured in LPDS and FOH for 2 h. In contrast, CCTα nuclear export was only detected in 5-10% of cells cultured in FCS. Most dramatically, CCTα remained completely sequestered within the nucleus in cells pretreated with oleate or diC8 prior to FOH addition. Nuclear morphology and chromatin structure was also unaffected by FOH in oleate- and diC8-pretreated cells. Interestingly, FOH-induced CCTα nuclear export was not prevented by pretreatment with the DAG analogue TPA, suggesting that supplementation of the CDP-choline pathway blocked CCTα export.

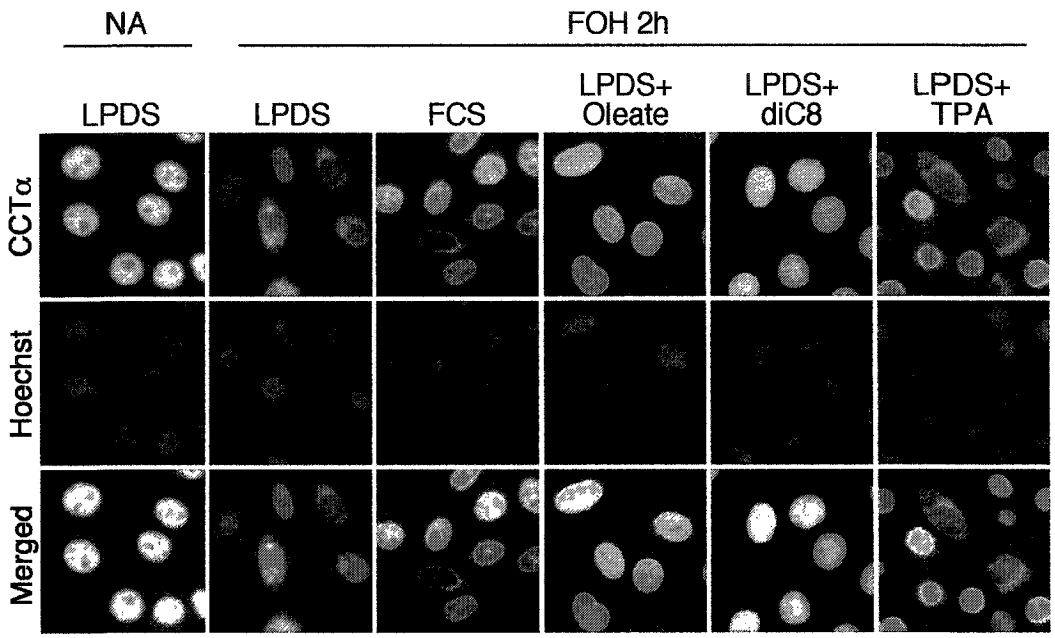

Figure 4.13 - Prevention of FOH-induced nuclear export of CCTα in CHO cells supplemented with oleate or DAG. CHO cells were cultured on glass coverslips as described in the legend to Figure 4.6. Cells were refed 2 ml medium A (FCS) or exchanged with 2 ml medium B (LPDS) 24 h prior to the addition of FOH (60 μM) or ethanol control (NA, no addition) for 2 h. Sets of cells incubated in medium B were treated with oleate (500 μM), diC8-DAG (500 μM) or TPA (100 nM) 30 min prior to addition of FOH. At the indicated times, cells were processed for immunofluorescence localization of CCTα and Hoescht 33258 as described in Figure 4.6. CCTα was visualized using an Alexa-488 conjugated secondary antibody. Images were obtained using an Axioplan 2 fluorescence microscope with a Planapo 100x oil immersion objective and equipped with a Spot CCD camera.

4.1.8 Oleyl alcohol, a non-substrate activator of CCTα, causes DAG depletion and CPT inhibition

Unlike known activators of CCTα such as fatty acids and DAG, FOH reduced DAG levels by activating CCTα without acting as a substrate for PtdCho synthesis, (54, 160, 293). We therefore tested if addition of other non-substrate activators of CCTα to CHO cells imitated FOH by inducing DAG-dependent apoptosis. Since it is a potent activator of CCT *in vitro* and *in vivo,* the poorly metabolized fatty alcohol oleyl alcohol (OLOH) was a good candidate for these studies (52). We initially characterized the effect of OLOH on PtdCho synthesis and DAG mass in CHO cells cultured in LPDS for 18-24 h. Cells were treated with OLOH (60 μM) for up to 2 h, pulse-labeled with [^{3}H]choline for the final 30 min of treatment, and radiolabel incorporation into PtdCho and the CDP-choline pathway intermediates phosphocholine and CDP-choline was measured (Figure 4.14). DAG mass was also quantified in the same cell extracts. PtdCho synthesis was stimulated (>3-fold) following OLOH treatment for 30 min. [^{3}H]phospocholine levels decreased in response to OLOH addition, indicating activation of CCTα. The initial burst of [^{3}H]PtdCho synthesis following OLOH addition was not sustained due to increasing inhibition of CPT, as indicated by accumulation of [^{3}H]CDP-choline. As in the case of FOH treatment (Figure 4.9), OLOH caused a time-dependent decrease in cellular DAG mass, which fell to 50% of control values by 2 h treatment time. Thus, OLOH mimicked the effects of FOH and induced CCTα activation, CPT inhibition and DAG depletion.

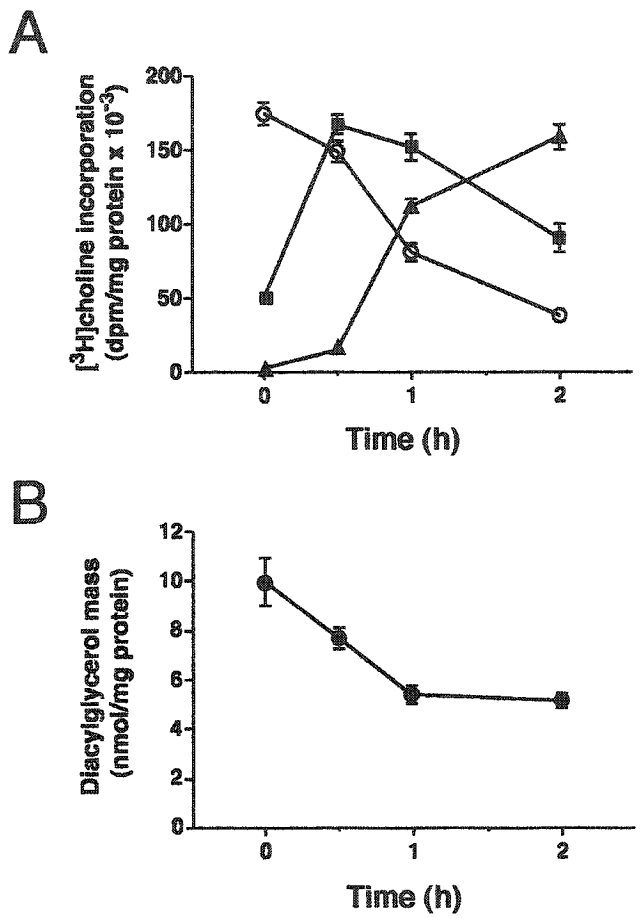

Figure 4.14 - Increased PtdCho synthesis and DAG depletion in response to the non-substrate CCTα activator oleyl alcohol. CHO were cultured in medium B for 24 h prior to the addition of oleyl alcohol (OLOH) (60 μM) for the indicated times. (**A**) Cells received choline-free medium containing [^{3}H]choline (2 μCi/ml) for the final 30 min of OLOH treatment. Cells were harvested and [^{3}H]choline incorportion into PtdCho (■) and its precursors phosphocholine (○) and CDP-choline (▲) was measured. (**B**) DAG mass was measured in the same cell lipid extracts as above. Results are the mean and standard deviation of triplicate determinations from a representative experiment repeated two other times with similar results.

4.1.9 Oleyl alcohol induces DAG-dependent apoptosis and CCTα nuclear export

To test if OLOH treatment of CHO cells resulted in caspase activation, cells cultured in LPDS were treated with increasing concentrations (10 - 80 μM) of OLOH for 2 h and caspase cleavage of CCTα and cell death was assessed (Figure 4.15). Similar to FOH, OLOH treatment caused the appearance of the caspase-cleavage product of CCTα at higher doses (60 and 80 μM) (Figure 4.15A). Supplementation of the medium containing LPDS with diC8 prevented caspase cleavage of CCTα in response to OLOH (60 μM). Cell Death ELISA analysis indicated a 30-fold increase in apoptosis in cells treated with 60 μM OLOH compared to untreated controls, whereas no increase in apoptosis was evident when cells were pretreated with diC8 prior to OLOH addition (Figure 4.15, B).

Since OLOH induced DAG-dependent cleavage of CCTα and apoptosis, we also examined the effect of OLOH on CCTα nuclear localization. Cells were cultured in LPDS and treated with OLOH (60 μM) for up to 4 h, in the absence or presence of diC8 (500 μM) (Figure 4.16). Nuclear localization of CCTα was assessed by indirect immunofluorescence analysis, and Hoechst DNA-staining was used to visualize the nucleus and monitor changes in chromatin structure. Similar to FOH, OLOH caused translocation of CCTα from the nucleoplasm to the NE. OLOH also caused nuclear export of CCTα, which was evident in 20-30% of the cell population 2 h after OLOH addition. After 4 h OLOH exposure, numerous cells in the population (30-40%) displayed chromatin condensation typical of apoptotic cells. The fluorescence intensity of CCTα immunostaining was typically weaker in these apoptotic cells, but was generally extranuclear or associated with discrete regions of the NE. In contrast, CCTα

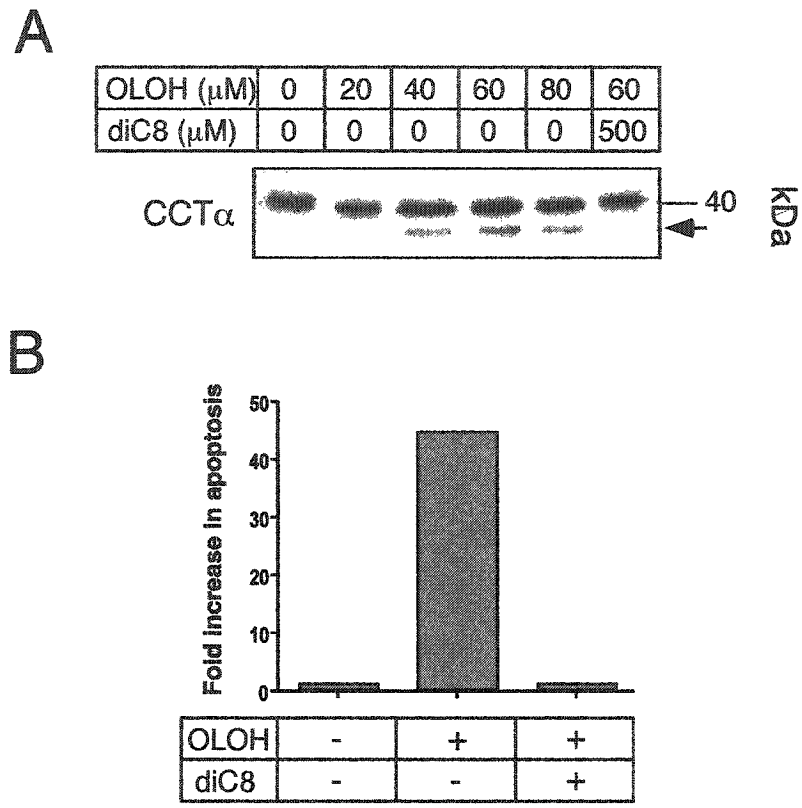

Figure 4.15 - Oleyl alcohol induces DAG-dependent apoptosis. CHO cells were cultured in medium B for 24 h prior to start of experiments. **(A)** Cells were incubated for 4 h with increasing concentrations of OLOH as indicated. One set of cells was preincubated for 30 min with diC8 (500 μM) prior to addition of OLOH (60 μM). Total cell extracts (15 μg) were resolved by SDS-9%PAGE and immunoblotted for CCTα. Shown is a representative experiment repeated one other time with similar results. **(B)** Apoptosis was measured by Cell Death ELISA™ in cells treated with OLOH (60 μM) for 4 h in the absence or presence of a 30 min preincubation with diC8 (500 μM). Results are expressed as fold increase in apoptosis over cells treated with vehicle control, and represent mean values from duplicate determinations of a representative experiment repeated once with similar results.

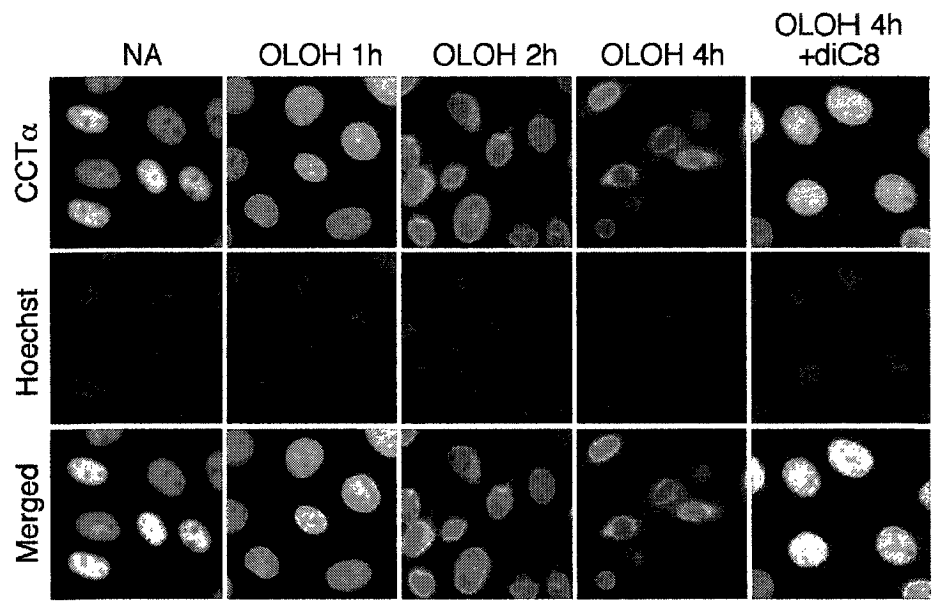

Figure 4.16 - DAG-dependent nuclear export of CCTα in oleyl alcohol-treated CHO cells. CHO cells were seeded on glass coverslips as described in the legend to Figure 4.6. On day 3, cells were cultured in 2 ml medium B for 24 h prior to the addition of OLOH (60 μM) for the indicated times. One set of cells was preincubated for 30 min with diC8 (500 μM) prior to addition of OLOH. Cells were processed for immunofluorescence localization of CCTα and Hoechst 33258 as described in Figure 4.6. CCTα was visualized using an Alexa-488 conjugated secondary antibody. Images were obtained using an Axioplan 2 fluorescence microscope with a Planapo 100x oil immersion objective and equipped with a Spot CCD camera.

remained completely sequestered within the nucleus of cells supplemented with diC8 prior to OLOH treatment. Nuclear morphology was also unaffected by OLOH in DiC8-pretreated cells. These experiments indicate that the non-substrate CCTα activator OLOH induces DAG-dependent CCTα nuclear export and apoptosis.

4.2 Discussion

The CDP-choline pathway for PtdCho synthesis is inhibited by numerous cytotoxic drugs, such as FOH, apparently at the terminal step in the pathway catalyzed by CPT (2, 304). In the current study, we demonstrate that FOH rapidly and potently stimulates the preceding reaction in the pathway catalyzed by the rate-limiting enzyme CCTα. FOH influenced CCTα at several levels, causing rapid activation and translocation of CCTα to the NE, export from the nucleus and activation of caspases that proteolyzed CCTα removing its nuclear localization signal (NLS). Nuclear export and caspase-mediated removal of the NLS would exclude CCTα from the nucleus and disrupt the compartmentalization of the CDP-choline pathway during FOH-induced apoptosis.

4.2.1 A metabolic basis for FOH-induced apoptosis

Several previous reports have shown FOH to be a potent inhibitor of the CDP-choline pathway, causing CDP-choline accumulation indicative of CPT inhibition (2, 186, 279). One study showed that FOH paradoxically activated the preceding reaction in the CDP-choline pathway catalyzed by CCT, causing an increase in membrane-associated CCT activity *in vitro* with a corresponding decrease in the inactive soluble fraction in lung A549 cells (186). The effect of FOH on CCTα regulation was investigated in detail in CHO cells using two separate radiolabelling methods. In the first, cells were treated with FOH prior to exposure to a brief pulse with [^{3}H]choline. This protocol has been used in numerous studies to demonstrate inhibition of the CDP-choline pathway by FOH (279). Both low-dose (20 μM) and high-dose (60 μM) FOH caused a reduction in [^{3}H]choline incorporation into phosphocholine, indicating activation of CCTα, while at the same time elevating [^{3}H]CDP-choline levels, indicative

of CPT inhibition. The net effect on radiolabel incorporation into PtdCho was complex and dependent on the balance between these two effects. Thus, low-dose FOH caused greater activation of CCTα relative to inhibition of the terminal step in the pathway, resulting in stimulation of PtdCho synthesis. On the other hand, high-dose FOH (60 μM) caused profound inhibition of CPT and PtdCho synthesis. FOH does not directly inhibit CPT activity *in vitro* (307), thus indicating that the metabolic block imposed by FOH at the CPT-catalyzed step in the CDP-choline pathway *in vivo* must occur by indirect means. Decreased availability of the substrate DAG has been implicated in CPT inhibition in several experimental systems (4, 136). Hypothesizing that initial activation of PtdCho synthesis could lead to DAG depletion and indirect CPT inhibition, we assessed the acute effects of high-dose FOH on the CDP-choline pathway and DAG mass using a second radiolabelling regime where CDP-choline pathway intermediates were labeled with [^{3}H]choline 30 min prior to and during FOH treatment. This revealed a significant and transient stimulation of PtdCho synthesis (>30%) following 15 min exposure to high-dose FOH that coincided with rapid cellular DAG depletion (>40%). These data are consistent with a model where the initial effect of FOH on the CDP-choline pathway is stimulation of PtdCho synthesis via activation of the rate-limiting enzyme CCTα, with eventual inhibition of the pathway caused by decreased availability of the CPT substrate DAG.

Disruption of DAG homeostasis and attenuation of PKC-signalling has been proposed as a mechanism by which apoptosis is induced by FOH and related isoprenoids. This is supported by studies in which apoptosis is prevented by addition of DAG analogues, or exacerbated by PKC inhibition (180, 323). FOH and geranylgeraniol

(GGOH) induce G_0/G_1 cell cycle arrest preceding the initiation of apoptosis in lung A549 cells (186). FOH also induced cell cycle arrest in the yeast *Saccharomyces cerevisae*, concurrent with rapid DAG depletion (175). The results in Figures 4.9 and 4.10 are the first to demonstrate a significant decrease in DAG mass in mammalian cells in response to FOH, providing further support for a DAG-dependent mode of action. Since the CDP-choline pathway is a major metabolic consumer of DAG (152), increased PtdCho synthesis could contribute to DAG depletion and attenuation of DAG-signalling in the initiation phase of FOH-induced apoptosis. Cellular DAG metabolism is complex, with numerous pathways consuming and creating DAG (282), therefore we can not exclude the possibility that FOH also affects DAG levels through mechanism(s) other than CCTα activation, such as *de novo* synthesis or conversion of PA to DAG by PA-phosphatase.

Although several reports have shown that PtdCho synthesis can be affected by exogenously added DAG molecules (91, 92, 266), the CDP-choline pathway is generally considered to have a minor role in attenuation of DAG signalling pathways (25, 117). This is in part due to DAG species selectivity of CPT, which favours *de novo* synthesized DAG enriched in saturated and monounsaturated fatty acyl chains (113, 114, 177) rather than highly unsaturated DAG signalling molecules produced from agonist-stimulated degradation of phosphoinositides and remodeled PtdCho (117, 282). However, the DAG species specificity of CPT has been shown to be reliant on CDP-choline concentration *in vitro* (177), raising the possibility that as CDP-choline levels rise during FOH treatment, DAG selection by CPT may be altered. Decreased substrate availability would also be expected to affect the DAG species utilized by CPT.

Perhaps the most important mechanism that prevents the CDP-choline pathway from negatively affecting other cellular DAG-dependent processes is coordination with agonist-stimulated PtdCho degradation through substrate-level activation of CCTα (58). FOH is unusual among CCTα-activating lipid metabolites in that it is not itself a substrate for PtdCho synthesis. This has important consequences with regards to its potential effect on the cellular PtdCho cycle. For instance, addition of exogenous oleate or treatment of cells with bacterial PtdCho-PLC potently stimulated CCTα and activated PtdCho synthesis. However, these treatments do not induce apoptosis because the lipid activators of CCTα in these cases, oleate and DAG, replenish substrates for PtdCho synthesis, resulting in maintenance of cellular DAG levels. Indeed, expression of a bacterial PtdCho-PLC in mouse NIH-3T3 fibroblasts resulted in the formation of a malignant phenotype (138), indicating that cell proliferation and survival signalling pathways were enhanced under these conditions. Stimulation of PtdCho synthesis by FOH may deplete cellular DAG levels in the absence of accompanying mechanisms to replenish cellular DAG supplies, such as *de novo* DAG synthesis, PtdCho degradation by PLD coupled with DAG generation by PA-phosphatase or PC-PLC (38, 181). A prediction of this hypothesis is that cells would be protected from FOH-induced apoptosis if plentiful substrate for the CDP-choline pathway were available. In support of this, CHO cells cultured under lipid-poor conditions were acutely sensitive to FOH-induced apoptosis, and supplementation of this medium with oleate or a cell-permeable short-chain DAG (diC8) rescued cells from the toxic effect of FOH (Figure 4.11). An alternative non-substrate activator of CCTα, oleyl alcohol (OLOH), mimicked FOH by

inducing cellular DAG depletion and apoptosis that was preventable by diC8 supplementation (Figures 4.14 and 4.15).

It is currently unclear whether oleate and diC8 conferred protection against FOH- or OLOH-induced apoptosis by acting as substrate for the CDP-choline pathway (38, 91, 189, 266) or by increasing PLD-mediated PtdCho turnover (38, 181). DiC8 is a known activator of PKC (64) which regulates PLD1 activity, and oleate has been reported to activate PLD activity *in vitro* (179) and in intact cells (148, 163, 164), although the mechanism is unknown. Inhibition of oleate conversion to its corresponding CoA ester by the acyl-CoA synthetase inhibitor triacsin C prevented its rescue of FOH-treated cells (Figure 4.12), suggesting that exogenous oleate prevented FOH-induced apoptosis by supplementing fatty acyl-CoA pools for glycerolipid synthesis.

The mechanism of oleate- and diC8-mediated resistance to FOH is under further investigation. Preliminary results indicate that these treatments reestablish PtdCho synthesis and partially restore endogenous DAG levels in FOH-treated cells (data not shown). If restoration of PtdCho synthesis is involved, this would support a theory first proposed by Voziyan *et al.* that FOH induces apoptosis by depletion of PtdCho required as a source for DAG and PKC activation (280). It is well-established that PtdCho is an important source of DAG that augments acute DAG-signalling events mediated by PLC-mediated degradation of PIP_2, and that this is essential for cell proliferation and survival (85, 117, 158). A previous study showed that restoration of PtdCho synthesis through over-expression of CPT did not prevent FOH-induced apoptosis in CHO cells, arguing that inhibition of PtdCho synthesis was not a causative factor (307). However, this mode of increasing PtdCho synthesis could have exacerbated metabolic insults related to DAG

availability in FOH-treated cells. It is unclear if PLD activity would be coordinated with a CPT-mediated increase in PtdCho synthesis since this would have bypassed CCTα, the rate-limiting and regulated enzyme in the CDP-choline pathway. If PtdCho turnover by PLD is a key determinant in resistance to FOH-induced apoptosis, then reestablishment of PtdCho synthesis by substrate level activation of CCTα could be a critical factor.

4.2.2 CCTα activation by FOH

CCTα is activated upon binding to membranes in response to activating lipids and/or alterations in membrane structure (58, 151). Lipids with a single hydroxyl groups, such as fatty alcohols and DAG, as well as anionic lipids such as fatty acids, promote membrane localization and activation of CCTα (51, 52). Isoprenoids are structurally related to these lipids and could promote CCTα membrane association by a similar mechanism. In support of this, *in vitro* activity of recombinant CCTα was stimulated by PtdCho vesicles containing FOH (Figure 4.4). The magnitude of activation was about 2-fold less than that afforded by PtdCho vesicles containing an equivalent amount of oleate, but was evident at low concentrations of FOH (2 to 10 mol%).

Similar to the effects of exogenous fatty acids on CHO cells (289), FOH appears to alter the membrane properties of the NE to favour the association of CCTα. Since FOH is a naturally occurring metabolite of the cholesterol biosynthetic pathway and its concentrations rise during increased flux through the cholesterol biosynthetic pathway (30, 183), it could also serve to coordinate cholesterol and PtdCho synthesis via activation of CCTα. Among several diverse apoptotic stimuli tested, activation and membrane association of CCTα was unique to FOH-induced apoptosis. Apoptotic programs induced by exposure to UV-irradiaton or the non-specific protein kinase

inhibitor chelerytherine, did not lead to CCTα translocation to the NE. Of several apoptotic drugs tested in a prior study (2), chelerythrine was the most potent inhibitor of PtdCho synthesis in HL-60 cells. This indicates that CCTα translocation and activation does not contribute to inhibition of PtdCho synthesis in that apoptotic program.

CCTα was rapidly dephosphorylated following FOH treatment in several cell types, as indicated by increased lower-molecular-mass isoforms on SDS-PAGE and immunoblots. CCTα dephosphorylation is correlated with, but is not necessary for membrane binding (120) and occurs in a cell cycle dependent manner (133). Therefore, dephosphorylation of CCTα in response to FOH treatment may interfere with the normal cellular regulation of CCTα by phosphorylation mechanisms.

4.2.3 FOH-induced CCTα nuclear export

Following FOH-induced translocation of CCTα to the NE, the enzyme was detected outside the nucleus by immunofluorescence analysis, indicating that it was actively exported from the nucleus or diffused out through a porous NE during FOH-induced apoptosis. Nuclear export of CCTα in FOH-treated cells was confirmed by demonstration that a soluble cytoplasmic marker (70 kDa dextran) did not enter the nucleus as CCTα was exiting, thereby ruling out loss of NE integrity as a mechanism of CCTα relocalization (Figure 4.8). Nuclear export of CCTα was especially evident in CHO MT58 cells overexpressing wild-type CCTα or a caspase-resistant mutant (CCT D28E). Nuclear export of CCT D28E also indicated that caspase cleavage of CCTα was not required for export and instead seemed to enhance this process. Nuclear export of CCTα may be dependent on activation and NE translocation, since it did not occur in response to chelerythrine or UV irradiation.

These results provide conclusive evidence of CCTα nuclear export in FOH-treated CHO cells. The subject of whether nuclear-localized CCTα could export from the nucleus under other conditions is controversial. A CCTα-GFP fusion protein was completely localized in the nucleus at all stages of the cell cycle and in different cell types, including CHO cells (67). In contrast, another study using indirect immunofluorescence methods showed evidence of CCTα export from the nucleus upon growth factor stimulation of quiescent IIC9 cells (196). While CCTα is endonuclear in many cultured cells (this study and 288, 290, 292), CCTα in pulmonary epithelial cells and lung tissue is localized in the cytoplasm or on the ER during all phases of the cell cycle (223, 269). In primary hepatocytes, CCTα was evenly distributed between the nucleus and the cytoplasm (119). A common feature of cells where cytoplasmic CCTα has been observed is a high demand for PtdCho synthesis. In growth factor-stimulated IIC9 cells, reentry into the cell cycle is accompanied by increased PtdCho synthesis to support cell growth and supply lipid signalling molecules, whereas in pulmonary epithelial cells, the synthesis of surfactant requires an abundant supply of PtdCho. In hepatocytes PtdCho is required for the synthesis of lipoproteins and bile (275). Therefore, CCTα localization could be altered when the cellular demand for PtdCho is high, in which case it would be advantageous for CDP-choline to be formed at the ER where the bulk of cellular CPT activity is located. By analogy, CCTα nuclear export in FOH-treated cells may represent a cell-stress response to the metabolic block at CPT, with CCTα relocalizing to the ER in an attempt to reestablish PtdCho synthesis. In support of this model, CCTα remained sequestered in the nucleus in FOH-treated cells supplemented with the CDP-choline pathway substrates oleate and DAG (Figure 4.13).

In contrast, the non-metabolizable DAG analogue TPA did not prevent FOH-induced CCTα nuclear export. This finding also rules out PKC-signalling as a mechanism for nuclear retention of CCTα. As further support for metabolic regulation of CCTα localization, FOH-induced CCTα nuclear export is mimicked by OLOH treatment, which also causes CCTα activation, DAG depletion and CDP-choline accumulation.

4.2.4 Caspase-mediated proteolysis of CCTα removes its nuclear localization signal

Following translocation to the NE and coincident with export to the cytoplasm, CCTα was cleaved by a caspase activity at TEED^{28}G. D28 is the final residue in the CCTα NLS (KVNSRKRRKEASSPNGATEED) (287), therefore cleavage at this site precisely removes this domain. Based on the recognition site TEED, it is likely that class III caspases are involved in CCTα proteolysis (262). Of these, only caspase-6 had preference for threonine in the P4 position and was capable of digesting CCTα to completion *in vitro* (159). Caspase-6 activity was detected in cell extracts from FOH-treated CHO cells and these extracts cleaved CCTα at D28. Caspase-8 also cleaved CCTα at the TEED site but is primarily involved in death receptor signalling (307) and seems unlikely to mediate FOH-induced apoptosis. Caspase-3 did not cleave CCTα, but its inhibition in intact cells by z-DEVD-fmk completely blocked both PARP and CCTα digestion. Thus, a likely sequence of events involves activation of caspase-3 by an unknown mechanism, and subsequent activation of caspase-6 and CCTα cleavage (243).

The caspase-6 substrates lamin A and C (198, 226) and several transcription factors (197) are found in the nucleus. Interestingly, lamins co-localized with CCTα at the NE in FOH-treated cells (data not shown), suggesting that both were cleaved in a concerted manner. Caspase proteolysis occurred simultaneously or following export of

CCTα from the nucleus in CHO cells, and was confined to the nucleus in other apoptotic programs. Thus, CCTα cleavage by caspase-6 substrates can take place in the nucleus, but it is unknown whether cleavage can take place in the cytoplasm. Since caspase inhibition and the D28E mutation did not effect CCTα translocation from the nucleus, it is clear that caspase cleavage was not required for nuclear export. However, the N-terminal CCTα NLS is required for its import into the nucleus (288), suggesting that nuclear export and removal of the CCTα NLS are coordinated events designed to permanently exclude CCTα from the nucleus.

The reasons for caspase targeting of CCTα nuclear localization are unknown and a subject for future investigation. Given the current data, several possibilities exist. Movement of soluble intermediates between enzymes in the CDP-choline pathway is a channeled process (26, 100, 101, 219) that presumably is dependent on a functional compartmentalization of enzymes. At first inspection, the nuclear localization of CCTα is enigmatic for a channeled process involving other enzymes in the cytoplasm. However, specific substructures in the nucleus, such as tubular invaginations of the NE (Chapter 5) could facilitate this process. Nuclear localization of CCTα may also serve to restrict the CDP-choline pathway to specific cellular pools of DAG, further preventing PtdCho synthesis from negatively impacting DAG-dependent processes in other cellular locations. If not a major site of PtdCho synthesis, the NE could represent a specialized site of PtdCho synthesis. One possibility is that it could be involved in the increase in nuclear volume that occurs during the cell cycle (99). Studies of disruption of lamina assembly during the cell cycle have indicated that a minimal nuclear volume is required for entry into S phase, and that prevention of nuclear assembly can result in cell cycle

arrest and apoptosis (278, 318). If PtdCho synthesis at the NE is coupled to maintenance of nuclear volume during the cell cycle, this could perhaps explain why nuclear localization of CCTα is targeted by caspases during apoptosis. It is reasonable that PtdCho synthesis would be coordinated with other events involved in expansion of the nuclear volume during the cell cycle, such as lamina assembly and DNA replication. PtdCho synthesis at the NE could provide an efficient means for the CDP-choline pathway to respond to an increased requirement of PtdCho to maintain nuclear volume during G1 and/or support the increase in nuclear volume that occurs during S phase. This may not be a requirement in all cell types since CCTα has been shown to be a cytosolic protein in lung alveolar type II cells independent of cell cycle changes in PtdCho synthesis (269).

The possibility that the N-terminal region affected by caspase cleavage contains other determinants of CCTα function in addition to the NLS cannot be discounted at this time. Recently, cysteine 37, adjacent to the caspase cleavage site, was identified as an important determinant in CCTα dimerization through participation in an inter-subunit disulfide bond (311). In future studies, it would be worthwhile to examine the functional aspects of caspase-cleaved CCTα, including enzyme activity, phosphorylation and dimerization properties. In addition, it would be important to identify the nuclear export signal (NES) sequence in CCTα and determine its role in FOH-mediated export.

Since CCTα and CPT catalyze concurrent and tightly coupled reactions in the CDP-choline pathway, the accumulation of CDP-choline and reduction in PtdCho synthesis in response to FOH may reflect not only decreased substrate availability, but also disruption of enzyme localization. Our results suggest that altered PtdCho synthesis

and CDP-choline levels are due in part to persistent activation and mis-localization of CCTα during FOH-induced apoptosis, effectively uncoupling it from the subsequent step in the pathway and disrupting PtdCho synthesis.

Based on the current data, a model of the temporal sequence of events leading to CCTα nuclear export and FOH-induced apoptosis emerges (Figure 4.17). At the onset of cell exposure to FOH or other non-substrate activators of CCTα, increased CCTα activity leads to an increase in PtdCho synthesis. This is accompanied by DAG depletion that eventually causes a profound inhibition of PtdCho synthesis as it drops to limiting levels. CCTα export from the nucleus ensues due to a combination of activating signals and export mechanisms responsive to increased CDP-choline and/or inhibited PtdCho synthesis. This event could further exacerbate attenuation of DAG-mediated cell survival mechanisms in the initiation phase of apoptosis. Trapping of cytidine nucleotide in CDP-choline pools could also potentially affect other CTP-dependent functions. Cleavage of caspase substrates occurs and as a result CCTα is unable to reenter the nucleus, thus permanently disrupting compartmentalization of PtdCho synthesis.

By virtue of direct control over PtdCho synthesis and indirect control over lipid signalling molecules derived from PtdCho, CCTα is uniquely positioned to sense or regulate levels of these important lipids and thus control apoptotic or proliferative signals. Our results show that activation and caspase cleavage of CCTα and disruption of the CDP-choline pathway are key components of isoprenoid-mediated apoptotic programs.

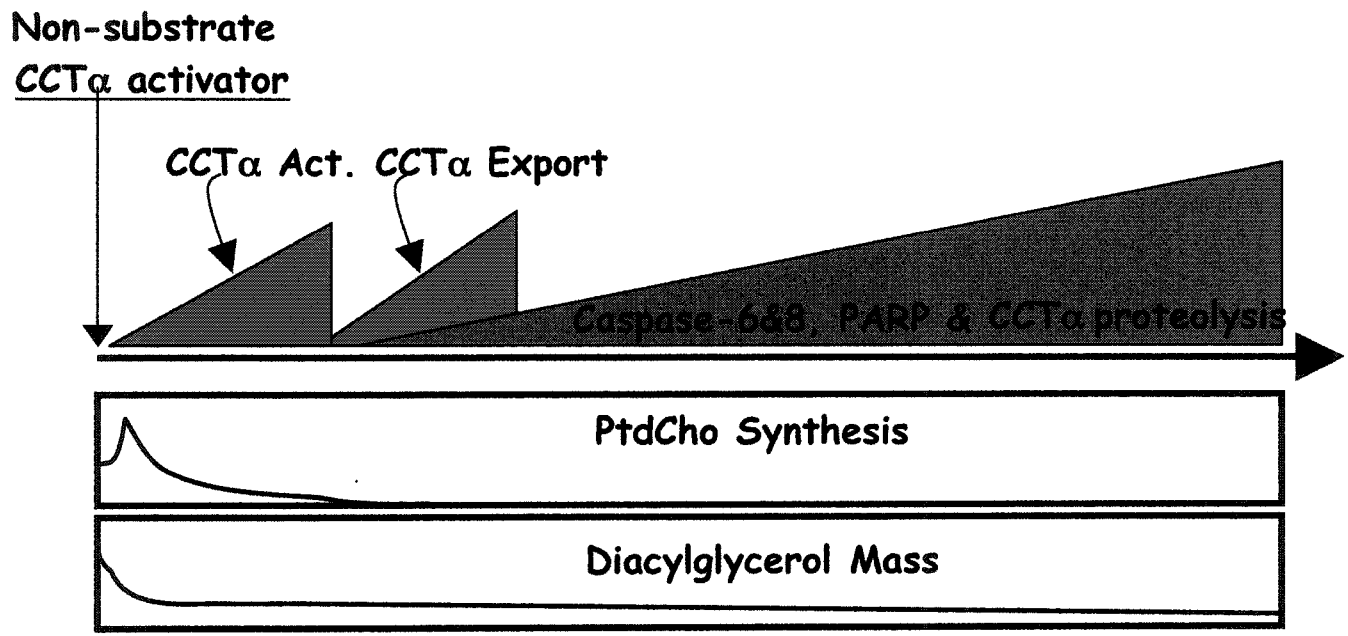

Figure 4.17 - Temporal events in FOH-induced apoptosis. Model of sequence of events following exposure of cells to non-substrate activators of CCTα (such as FOH). Abbreviations: PtdCho, phosphatidylcholine; Act., activation.

Chapter 5:

Effects of CCTα membrane association on the nucleoplasmic reticulum

5.1 Results

5.1.1 Fatty acid-activated CCTα associates with the nucleoplasmic reticulum

To gain insight into the role of CCTα in the nucleus, indirect immunofluorescence and confocal microscopy analysis was used to examine intranuclear sites of CCTα membrane association. For this purpose, CCTα translocation to the NE was induced in CHO cells by exposure to the fatty acid oleate, which has previously been shown to promote translocation of soluble CCT to membranes, with a concomitant increase in cellular PtdCho synthesis (52, 289). Cells were incubated in medium containing LPDS for 18-24 prior to oleate addition (500 μM) for 2 or 4 h. Relative to whole serum, LPDS treatment enhanced CCTα translocation in response to oleate. In untreated cells, immunostaining of CCTα revealed a soluble nucleoplasmic distribution that was entirely contained within the boundaries of the nuclear lamina, which was visualized by immunofluorescence analysis using an antibody detecting a common epitope in lamins A/C (Figure 5.1, A). Addition of oleate for 2 h resulted in CCTα translocation to the NE, as indicated by extensive overlap with lamin A/C immunostaining in merged images. CCTα and lamin A/C were also extensively co-localized in discreet intranuclear foci, as seen in single optical sections of oleate-treated cells (Figure 5.1, A and B). To morphologically characterize these structures, a series of images in the Z-axis (20 sections/nucleus) were acquired, followed by 3-D reconstruction (Figure 5.1, B). Serial projections of entire nuclei revealed intranuclear CCTα and lamin A/C containing structures that were filamentous extensions of the NE that in some cells (~2-5% of the population) formed an elaborate branched network.

Figure 5.1 - Association of CCTα with the NR in oleate-treated CHO cells. CHO cells were seeded onto coverslips and cultured in medium A. Cells were changed into medium B 24 h prior to start of experiments. Cells were treated for 2 h with oleate (500 μM) or no addition (NA), fixed and permeabilized in cold MeOH/acetone, and processed for immunofluoroscence detection of CCTα and lamin A/C using secondary antibodies conjugated to Alexa-555 and Alexa-488, respectively. (**A**) Single optical sections showing representative fields of cells under the different treatment conditions. (**B**) Projection of an entire nucleus of an oleate-treated cell constructed from a series of 20 consecutive optical sections (0.5 μm). (**C**) Oleate-treated cells were fixed and permeabilized as described in (A) and then labeled with Alexa-488 conjugated Con A to detect the NR and processed for immunofluorescence detection of CCTα and lamin A/C, which were visualized using Alexa-647 and Alexa-555 conjugated secondary antibodies, respectively. Consecutive optical sections spanning entire cells were obtained for 3D reconstruction analysis. The top view of the cells is depicted in the XY plane, while two side views (XZ and YZ) are shown on the narrow top and right-side panels. *Green line* shows the position of the XZ plane; *red line* shows the position of the YZ plane. Images were collected using a Zeiss LSM 510 confocal microscope equipped with a 100X objective and projections were performed using LSM 510 software. Bars, 10 μm.

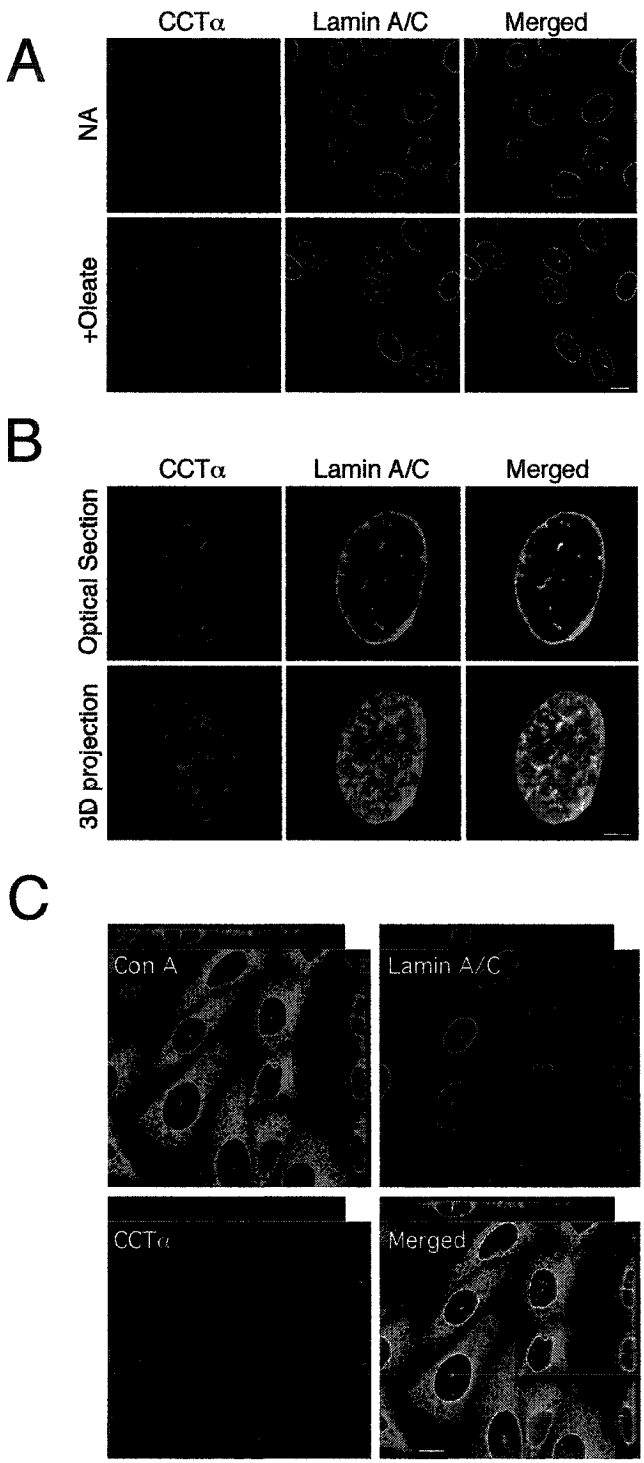
A
CCTα
Lamin A/C
Merged
NA
+Oleate
B
CCTα
Lamin A/C
Merged
Optical Section
3D projection
C
Con A
Lamin A/C
CCTα
Merged

Figure 5.1

Previous reports identified and characterized an intranuclear membrane system comprised of narrow tubular invaginations of the NE termed the nucleoplasmic reticulum (NR) (77, 95). A sensitive marker of ER components within narrow nuclear channels indicative of the NR is concanavalin (Con) A, a lectin that binds selectively to N-linked glycoproteins with high mannose content typically found in the ER and early secretory pathway (95, 111). Triple-labelling and 3-D confocal microscopy analysis of oleate-treated cells demonstrated labelling of filamentous intranuclear structures by fluorophore-conjugated Con A that precisely overlapped with intranuclear CCTα and lamin A/C immunostaining (Figure 5.1, C). Therefore we conclude the nuclear tubules associated with CCTα in oleate-treated cells correspond to the NR. In agreement with previous reports (95, 141), the NR was oriented vertically relative to the substrata and frequently seen to completely traverse the nuclei.

5.1.2 The nucleoplasmic reticulum consolidates the cellular loci of CDP-choline pathway enzymes

The CDP-choline pathway is comprised of three enzymes localized in separate cellular compartments in most cell types (top of Figure 5.2). Despite this physical separation, substrate channelling has been demonstrated to occur between pathway enzymes, indicating the compartmentalization of PtdCho synthesis (26, 101, 219). Results showing association of oleate-activated CCTα with the NR suggested that tubular invaginations of the double membrane NE containing cytoplasmic and ER components could represent potential sites for the consolidation of CDP-choline pathway enzymes.

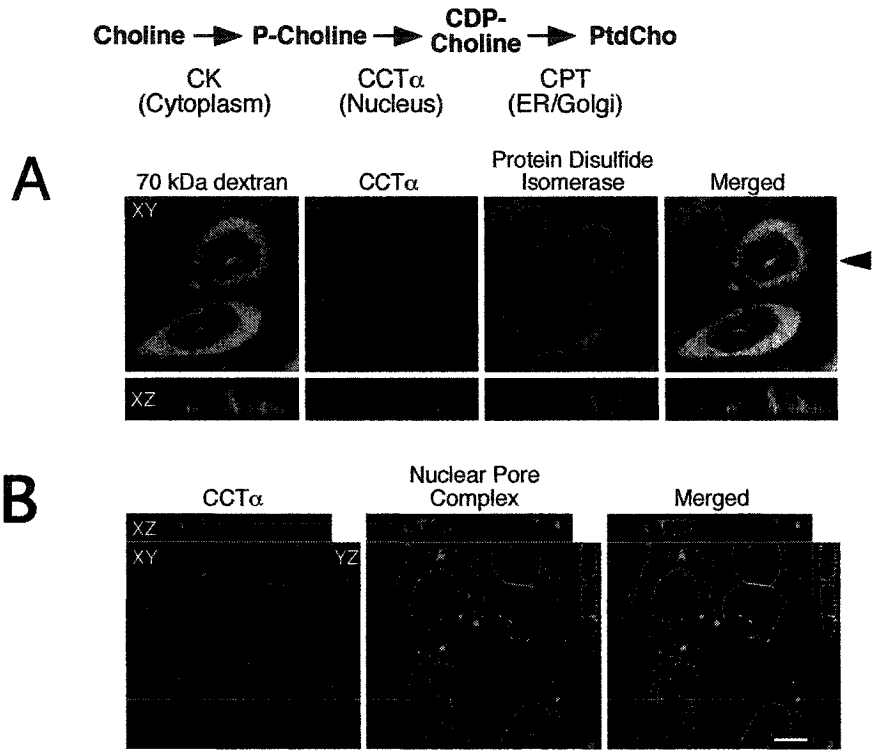

Figure 5.2 - The CDP-choline pathway within the NR in CHO cells. Schematic of the CDP-choline pathway is shown at the top indicating the enzymes involved and their known cellular localizations. **(A)** CHO cells were scrape-loaded with lysine-fixable Oregon green 488-labeled 70 kDa dextran as described in "Materials and Methods." After 8 h, culture medium was exchanged for medium B and cells were incubated for 18 h prior to 2 h treatment with oleate (500 μM). Cells were fixed and permeabilized in 3% formaldehyde/0.05% Trition X-100 and processed for immunofluorescence localization of CCTα and the luminal ER marker protein disulfide isomerase (PDI) using secondary antibodies conjugated to Alexa-647 and Alexa-555, respectively. The larger panel shows a top view of cells (XY-plane), while a side view (XZ-plane) is shown in the lower panels. The position of the XZ-plane is shown by an arrowhead. **(B)** CHO cells were cultured in medium A for 24 h prior to the addition of oleate (500 μM) for 2 h. Cells were fixed and permeabilized as in (A) and processed for immunofluorescence detection of CCTα and nuclear pore components (Nup62 and related epitopes), which were visualized using Alexa-555 and Alexa-488 conjugated secondary antibodies, respectively. Consecutive optical sections spanning entire cells were obtained for 3-D reconstruction. The top view of the cells is depicted in the XY plane, while two side views (XZ and YZ) are shown on the narrow top and right-side panels. *Green line* shows the position of the XZ plane; *red line* shows the position of the YZ plane. Bar, 10 μm. Images were obtained as described in Figure 5.1.

Fluorophore-conjugated Con A could potentially label single membrane invaginations derived from the inner nuclear membrane (INM) (23). To confirm that oleate-activated CCTα-associated with double membrane invaginations of the NE containing cytoplasm, CHO cells were scrape-loaded with the soluble cytoplasmic marker Oregon green 488-conjugated 70 kDa dextran in conjunction with immunofluorescence detection of protein disulfide isomerase (PDI), a luminal ER marker, and CCTα (Figure 5.2, A). In oleate-treated CHO cells, CCTα and PDI immunostaining was co-localized with soluble dextran within discreet intranuclear foci in single optical sections through the mid-nuclear region. These structures were revealed as narrow membrane channels traversing the nucleus when viewed in the XZ-plane.

To determine whether CCTα-associated NR contained nuclear pore complexes, co-localization of CCTα with a component of the nuclear pore complex (NPC) was examined in oleate-treated cells. Following 2 h oleate treatment, immunostaining of CCTα overlapped with that of the NPC in some, but not all, intranuclear foci in single optical Z-sections (Figure 5.2, B). These areas of co-localization corresponded to filamentous structures that traversed the nucleus in a vertical orientation, as visualized in XZ- and YZ-planes, analogous to the NR. This supports previous studies that showed the presence of NPCs in the NR (95, 141), and demonstrates their presence in the NR containing oleate-activated CCTα. Collectively, these experiments demonstrate that the NR consolidates the known cellular loci of the three CDP-choline pathway enzymes under conditions of stimulated PtdCho synthesis and that passage of small molecules across the NE can occur at this site. Therefore, the NR represents a potential cellular site for the compartmentalization of PtdCho synthesis.

5.1.3 Proliferation of the NR in fatty acid-treated cells

Membrane deformation leading to tubule formation at other organelle sites has been shown to occur as a result of alterations in membrane phospholipid environment (65, 72) or direct membrane-deforming abilities of some amphipathic proteins (88, 162). Thus, oleate-induced CCTα NE-association and/or resultant localized PtdCho synthesis could cause proliferation of the NR. To test this, the NR was examined by immunofluorescence analysis in untreated CHO cells and compared to cells exposed to oleate. Since the nuclear lamina is almost invariably associated with the NR (33), immunofluorescence analysis using an antibody to lamin A/C was performed to detect and quantify nuclear tubules of the NR in fixed cells. Lamin A was previously reported to associate with independent intranuclear foci in some cell-types (32, 134). Therefore, to unambiguously identify the NR, lamin A/C immunostaining was examined in 3-D reconstructions of consecutive optical Z-sections spanning the nucleus. Filamentous lamin A/C-positive structures continuous with the peripheral NE and spanning >50% of the nuclear volume (characteristic of nuclear tubules of the NR) were scored (Figure 5.3, A). Cells with >12 nuclear tubules, which are infrequently present in CHO cell populations, were excluded, as were multi-nucleated cells. For these and all subsequent experiments, nuclear tubule frequency was determined in three independent experiments (n>100 cells) using datasets collected from randomly selected fields. Results of the analysis showed that oleate treatment (500 μM) for 4 h caused a significant 80% increase in nuclear tubule frequency compared to untreated control cells. Immunostaining intensity of lamin A/C was unaffected by oleate using identical image acquisition parameters (top panel, Figure 5.3, A).

Figure 5.3 - Proliferation of the NR in fatty-acid treated cells. CHO cells grown on coverslips were cultured in medium B for 24 h prior to treatment with oleate (500 μM) or no addition (NA) for the indicated times. (**A**) The nuclear tubule marker protein lamin A/C was detected in cells fixed and permeabilized in cold MeOH/acetone using a monoclonal primary antibody followed by labeling with an Alexa-488 conjugated secondary antibody. Representative optical sections acquired using identical parameters are shown in the top panel. To identify filamentous intranuclear lamin A/C immunostaining patterns characteristic of the NR, serial Z-sections (20/cells) encompassing entire nuclei were obtained for analysis. (**B**) Cells were fixed and permeabilized in 3% formaldehyde/0.05% Triton X-100 and nuclear tubules were visualized by labeling with Alexa-488 conjugated Con A. Con A-positive intranuclear structures characteristic of NR were quantified in single optical sections through the mid-nuclear region of cells. (**C**) Distribution analysis of dataset represented in (B). (**D**) CHO cells seeded on coverslips were cultured in medium A and received fresh medium 24 h prior to addition of arachidonate (200 μM) for the indicated times. Nuclear tubule frequency was determined in fixed cells using Con A as a marker as described in (B). (**E**) F8 and NIH 3T3 fibroblasts were seeded on coverslips and cultured in DMEM +10% FCS. Cells were changed into DMEM + 10% LPDS for 24 h prior to the addition of oleate (500 μM) for 2 h. Con A-positive nuclear tubule frequency was determined in fixed cells as in (B). Results represent the mean and standard deviation from three separate determinations of >100 cells, t-test compared to NA, *$p<0.05$, ** $p<0.01$.

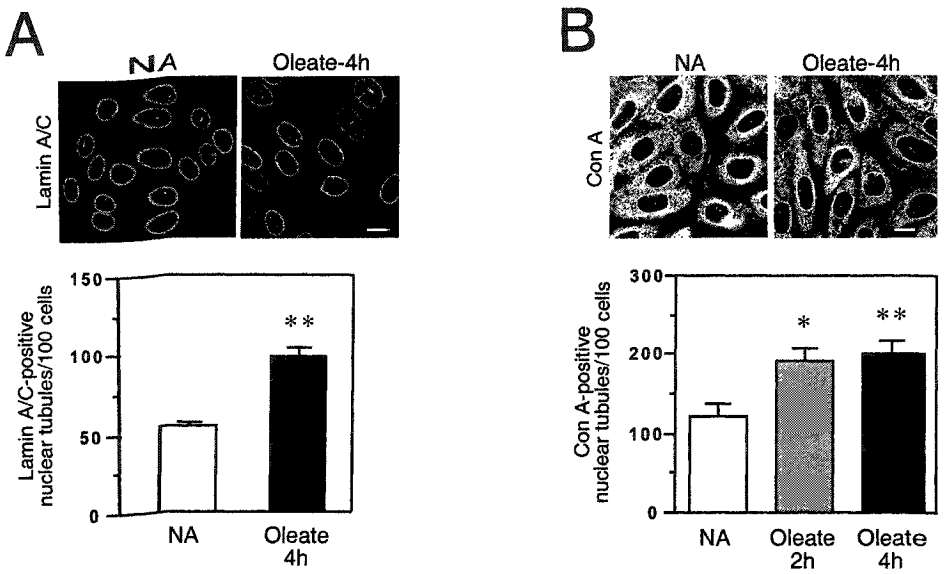

C

Condition	Total cells (n)	Tubules / nuclei (%)		
		0-1	2-4	>4
No addition	441	71.9	24.2	3.9
Oleate - 2h	461	51.4	38.9	9.7
Oleate - 4h	423	51.3	38.8	9.9

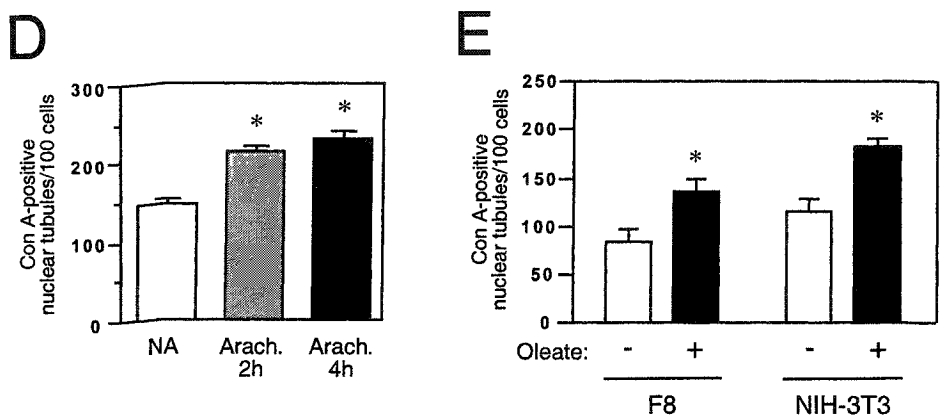

Figure 5.3

Bovine serum albumin (0.5%) was used as a carrier for oleate, and had no effect on nuclear tubule formation (data not shown).

To provide a second independent measure of proliferation of the NR in response to oleate, quantification studies were carried out using fluorophore-conjugated Con A as a marker of nuclear tubules. Single optical Z-sections (0.5 μm) of the mid-nuclear region of cells were collected for quantification of intranuclear Con A-positive structures (corresponding to nuclear tubules) in CHO cells cultured in the absence or presence of oleate. To exclude short indentations of the NE, intranuclear Con A-positive structures in contact with the peripheral NE that did not extend >1/3 into the nucleus were not scored, and cells were omitted that displayed hazy intranuclear Con A-staining indicative of close proximity of the optical Z-section to the basal or apical nuclear surface. Using these criteria, ~120 tubules/100 nuclei were detected in untreated cells (Figure 5.3, B). This value was >2-fold higher than that obtained by 3-D analysis of intranuclear lamin A/C immunostaining (Figure 5.3, A), perhaps indicating increased sensitivity of NR detection using fluorophore-conjugated Con A. Similar to results with the lamin A/C marker, there was a 60-70% increase in the frequency of Con A-positive nuclear tubules following oleate treatment for 2 or 4 h. Oleate treatment did not cause any gross alterations in nuclear shape, and the intensity of NR/ER-staining with fluorophore-conjugated Con A was similar between treatment groups using identical image acquisition parameters (top panel, Figure 5.3, B)

We also quantified the distribution of tubules in individual nuclei in the overall dataset for control and oleate-treated cells (n = 1325 cells) (Figure 5.3, C). The majority of nuclei in untreated cells (~70%) contained 0-1 detectable tubules, while only 4% of

nuclei had >4 tubules. Following 2 h or 4 h treatment with oleate, there was a 21% decrease in nuclei with 0-1 tubules with corresponding increases in nuclei with 2-4 and >4 tubules (15% and 6%, respectively). Within cells that had >4 tubules in individual nuclei, there was no significant difference in mean number of tubules under any experimental condition (average number of tubules/nuclei: untreated = 5.58±0.3, oleate 2h = 5.59±0.3, oleate 4 h = 5.86±0.2). These data indicate that the observed increase in nuclear tubule frequency was not due to a subpopulation of cells with a disproportionately large number of tubules, but rather to a general shift in the population distribution.

We next tested whether another fatty acid induced nuclear tubule formation, and occurrence in other cell lines. Similar to the effect of oleate, addition of the polyunsaturated fatty acid arachidonate (200 μM) for 2 or 4 h significantly increased the number of Con A-positive nuclear tubules in CHO cells by 45% and 55%, respectively (Figure 5.3, D). Nuclear tubule frequency was also increased significantly (~60%) in both F8 and NIH-3T3 cells following treatment with oleate (500 μM) for 2 h (Figure 5.3, E). Thus fatty acid-induced NR proliferation is common to several cultured cell lines.

5.1.4 CCTα expression level influences oleate-induced expansion of the NR

To investigate the link between oleate-induced nuclear tubule formation and CCTα membrane-binding and activity, the effect of CCTα expression on NR proliferation was examined in CHO MT58 cells stably overexpressing rat CCTα (CHO58-CCT) and vector-transfected control cells (CHO58-Vec) cultured in the absence or presence of oleate (500 μM) for 2 h. As noted previously, CHO MT58 cells have low levels of CCTα expression and activity due to a temperature-sensitive mutation in a

single functional CCTα allele (82). At the permissive temperature of 33°C, CHO58-Vec cells had sufficient CCTα activity and PtdCho synthesis to maintain cell viability (61). Therefore, to provide a valid comparison, both CHO58-Vec and CHO58-CCT cell lines were cultured at 33°C and then incubated at 37°C for the short duration of oleate treatment to allow optimal induction of CCTα membrane translocation and PtdCho synthesis, and to reduce endogenous CCT expression in vector control cells. SDS-PAGE and immunoblot analysis showed that CCTα expression in CHO58-CCT cells cultured at 37°C for 2 h was approximately 25-fold higher than that of CHO cells, whereas the low level of endogenous CCTα expression in CHO58-Vec cells appeared as a faint band upon overexposure of immunoblots (Figure 5.4, A). [^{3}H]Choline pulse-labelling analysis indicated basal PtdCho synthesis in CHO58-CCT cells was increased >4-fold relative to CHO58-Vec cells, which still maintained low levels of PtdCho synthesis at 37°C (Figure 5.4, B). PtdCho synthetic rates in both cell lines were stimulated ~2-fold by oleate treatment.

We next evaluated CCTα expression and NR proliferation in the two cell lines. Endogenous CCTα in CHO58-Vec cells treated with oleate was virtually undetectable by indirect immunofluorescence analysis, and intranuclear Con A-staining in these cells revealed a restricted NR represented as small foci in optical Z-sections (Figure 5.4, C). Immunofluorescence analysis of oleate-treated CHO58-CCT cells revealed partial localization of nucleoplasmic CCTα to the peripheral NE and intense immunostaining of intranuclear structures. The CCTα-associated intranuclear structures were extensively co-localized with fluorophore-conjugated Con A in optical Z-sections of the mid-nuclear region.

Figure 5.4 - Proliferation of the NR in response to oleate is CCTα-dependent. CHO58-Vec and CHO58-CCT cells cultured in medium A at the permissive-temperature of 33°C were changed into medium B for 24 h prior to the start of experiments. (**A**) CCTα expression levels were assessed by SDS-10%PAGE and immunoblot analysis in whole cell extracts from cells cultured at 37°C for 2 h prior to harvest. Parallel determination of endogenous CCTα levels in CHO cell extracts was performed for comparison purposes. Stripped blots were reprobed for actin to demonstrate equal loading. (**B**) CHO58-Vec and CHO58-CCT cells cultured as above were treated with oleate (500 μM) or no addition (NA) for 2 h at 37°C. Cells received choline-free medium containing [^{3}H]choline (2 μCi/ml) for the final 1 h of oleate treatment and [^{3}H]choline incorportion into PtdCho was determined. (**C**) CHO58-Vec and CHO58-CCT cells were seeded on coverslips and cultured as described above prior to treatment with oleate (500 μM) for 2 h at 37°C. Cells were processed as in Figure 5.3(B), stained with Alexa-488 conjugated Con A, and processed for immunofluorescence localization of CCTα using an Alexa-594 conjugated secondary antibody. (**D**) Frequency of Con A-positive nuclear tubules was determined as described in Figure 5.3, B. #$p<0.001$ compared to NA vector-transfected controls; *$p<0.05$ compared to NA. (**E**) Population distributions were determined from the overall dataset represented in (D).

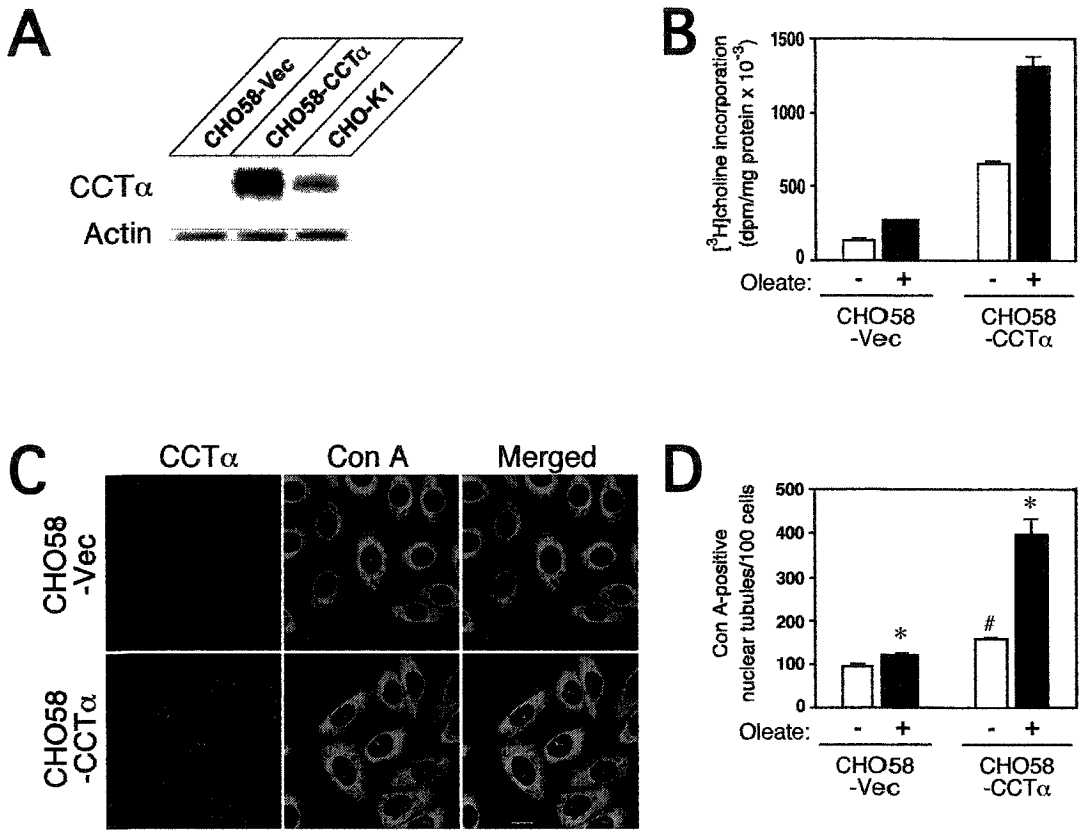

E

Cell Type	Condition	Total cells (n)	Tubules / nuclei (%)		
			0-1	2-4	>4
CHO58-Vec	No addition	429	77.4	20.1	2.5
	Oleate - 2h	379	70.0	27.4	2.6
CHO58-CCTα	No addition	406	60.1	33.5	6.4
	Oleate - 2h	423	20.6	42.3	37.1

Figure 5.4

Quantification of Con A-positive nuclear tubules under basal conditions showed a significant 65% increase in tubule frequency in CHO58-CCT cells compared to vector control cells (Figure 5.4, D). Oleate treatment resulted in a 250% increase in nuclear tubule frequency in CHO58-CCT cells, with a much smaller, but significant 26% increase in CHO58-Vec cells. Distribution analysis of complete datasets for each cell line indicated that the increase in nuclear tubule frequency following oleate treatment in CHO58-Vec cells (n = 808) was due to a 7% decrease in nuclei with 0-1 tubules, and a corresponding increase in nuclei with 2-4 tubules (Figure 5.4, E). There was no change in the number of nuclei with >4 nuclear tubules following oleate treatment. The distribution of nuclear tubule frequency in CHO58-CCT cells (n = 829) was considerably altered in response to oleate; nuclei with 0-1 nuclear tubules decreased by 40%, with a corresponding 9% increase in nuclei with 2-4 nuclear tubules and a 31% increase in nuclei with >4 tubules. This indicates that oleate-induced proliferation of the NR is strongly influenced by CCTα expression level and the rate of PtdCho synthesis.

5.1.5 Effect of lamin A expression on NR morphology in oleate-treated CHO cells overexpressing CCTα

Unlike the filamentous NR in oleate-treated CHO cells, NE invaginations in CHO58-CCT cells overexpressing CCTα were of inconsistent shape and size (Figure 5.4, C). Oval or slightly elongated CCTα and Con A-positive structures located in contact with the nuclear periphery were common. To further characterize the intranuclear structures formed in response to oleate treatment in CHO58-CCT cells, 3-D confocal microscopy analysis of CCTα, lamin A/C, and Con A immunostaining was performed to examine the orientation of these structures within the nucleoplasm and relationship to the

lamin nucleo-cytoskeleton. There was extensive co-localization of CCTα immunostaining and Con A-associated fluorescence within intranuclear structures following a 2 h treatment with oleate (500 μM), whereas overlap with the immunostaining pattern of lamin A/C was incomplete (Figure 5.5, A). When viewed in the XZ-plane, CCTα- and Con A-positive NE invaginations were oriented vertically relative to the substrata and often widened in diameter and terminated within the nucleoplasm. Lamin A/C immunostaining was typically more intense at the base of these structures and weak or undetectable in the broad terminal region.

Since analysis of oleate-treated CHO cells revealed the NR to consist of filamentous lamin-associated structures of consistent diameter (Figure 5.1, B and C), we questioned whether over-expression of CCTα in CHO58-CCT cells would cause lamins to become limiting in the formation of the NR in response to oleate. Therefore, we tested whether increased expression of lamin A, an isoform enriched in the nucleoplasmic cytoskeleton (123, 191), affected the morphology of NE invaginations in oleate-treated CHO58-CCT cells. CHO58-CCT cells were transiently transfected with a plasmid encoding a lamin A-GFP fusion protein previously shown to mimic properties of endogeous lamin A in CHO cells (131). Following ~24 h incubation to allow expression of lamin A-GFP, cells were treated with oleate (500 μM) for 2 h, and effects of lamin A-GFP expression on intranuclear CCTα immunostaining was assessed (Figure 5.5B). As shown in single optical Z-sections, expression of lamin A-GFP in oleate-treated CHO58-CCT cells resulted in the formation of an elaborate NR network that extensively overlapped with CCTα immunofluorescence. The filamentous CCTα immunostaining

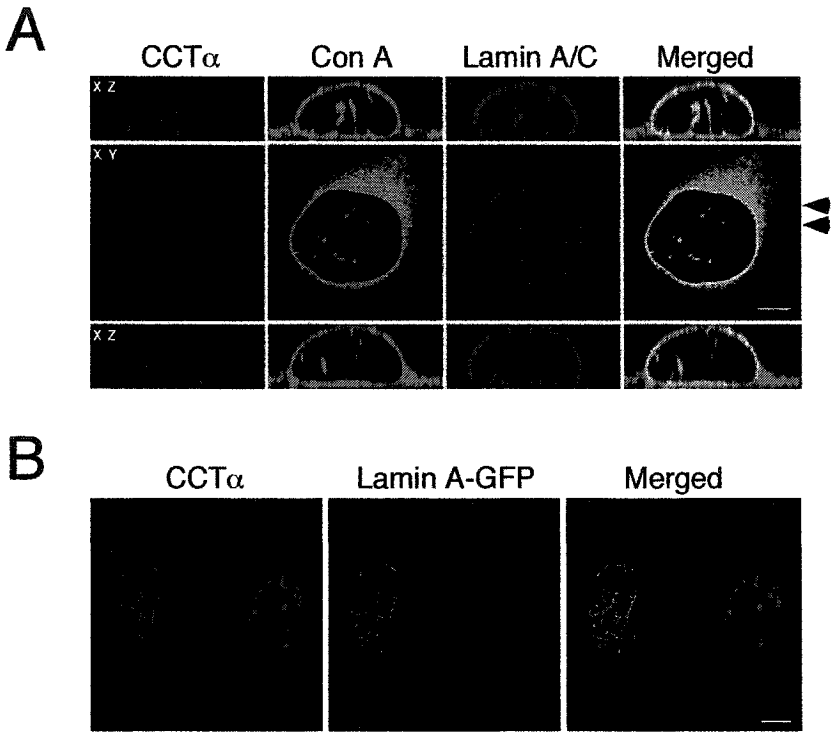

Figure 5.5 - Influence of lamin A expression on NR morphology in CCTα-overexpressing CHO cells. **(A)** CHO58-CCT cells were seeded on coverslips and cultured in medium A at 33°C. Cells were changed into medium B 24 h prior to 2 h treatment with oleate (500 μM). Coverslips were fixed and permeabilized in cold MeOH/acetone, labeled with Alexa-488 conjugated Con A, and processed for immunofluoescence detection of CCTα and lamin A/C using Alexa-647 and Alexa-555 conjugated secondary antibodies, respectively. Consecutive serial Z-sections spanning the entire cell were obtained using a Zeiss LSM 510 Meta confocal microscope equipped with a 100X objective and projections were performed using LSM 510 software. Two XZ views of the nucleus are shown in the top and bottom panels. Positions of reconstructed projections is indicated by black arrowheads. Bar, 5 μm. **(B)** Cells seeded onto coverslips and cultured as described in (A) were changed into medium B, and simultaneously transfected with cDNA encoding lamin A-GFP. Cells were incubated a further 24 h prior to addition of oleate (500 μM) for 2 h. Coverslips were fixed and permeabilized in 3% formaldehyde/0.05% Triton X-100, and processed for immunofluoescence detection of CCTα using an Alexa-594 conjugated secondary antibody. Images are from single optical sections (0.5 μm). Bar, 10 μm.

pattern in lamin A-GFP expressing cells was in clear contrast to broad fibrous CCTα-positive structures that were frequently seen in cells not expressing lamin A-GFP. The effect of lamin A-GFP on NR proliferation appeared to be dependent on its expression level, and was also evident in CHO MT58 cells transiently expressing high levels of lamin A-GFP (data not shown). Due to the extensive and heterogeneous nature of the NR network in cells expressing lamin A-GFP, quantification of the effect of oleate and/or CCTα expression on nuclear tubule formation within this context was not possible.

5.1.6 CCTα induces NR proliferation by two mechanisms in CHO cells

To probe the potential roles of catalytic and membrane-binding activity of CCTα in oleate-induced NR proliferation, the protein domains responsible for these activities were removed or disrupted by site-directed mutagenesis and resulting cDNAs were introduced into CHO MT58 cells cultured in the absence or presence of oleate (Figure 5.6). Mutations were introduced into a cDNA encoding rat CCTα fused to a C-terminal V5 epitope tag. Two point mutations were assessed for their ability to inhibit CCTα catalytic activity; (1) the first histidine residue of a conserved HXGH motif involved in CTP binding and catalysis in various cytidylyltransferases (277) was mutated to glycine (CCT H89G), and (2) a lysine residue previously shown to be required for catalysis by an unknown mechanism (112) was mutated to alanine (CCT K122A). Membrane-binding activity of CCTα was abolished by a C-terminal truncation at the end of the catalytic region following residue 236, which deletes the membrane-binding and phosphorylation domains (CCT Δ236). A previous study of the effect of this truncation on CCTα function showed that it relieved an inhibitory constraint imposed by the membrane binding domain, resulting in a soluble, constitutively-active enzyme (96).

A

CCT activity
(arbitrary units relative to wild-type)

	No addition	+PtdCho/ oleic acid
Wild-type	1	3.53
CCT H89G	0.01	0.03
CCT K122A	0.04	0.02
CCT Δ236	4.86	5.04

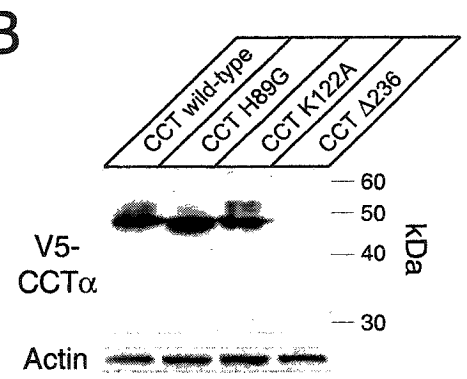

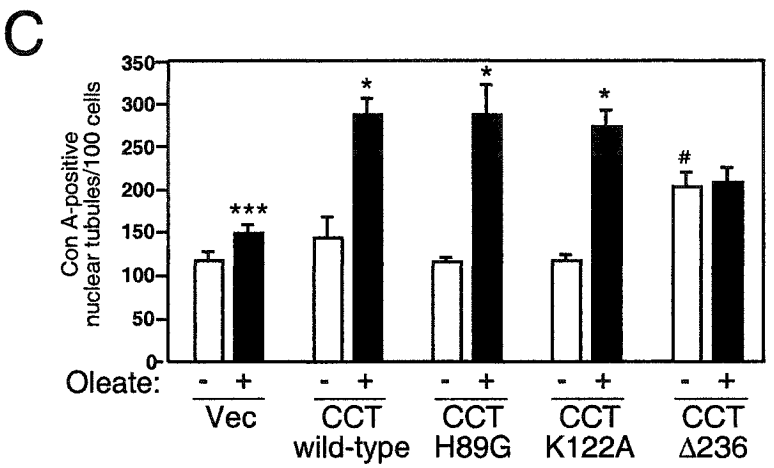

Figure 5.6 - Induction of NR proliferation by catalytic-dead and membrane binding-defective CCTα mutants. **(A)** CHO MT58 cells cultured as described in Figure 5.4 were transiently transfected with cDNAs encoding V5-tagged wild-type rat CCTα or the indicated mutant constructs 24 h prior to experiments. Whole cell extracts were assayed for CCTα activity as described in "Materials and Methods." Cells were incubated at the non-permissive temperature of 40°C for 1 h prior to harvest to reduce the influence of low level endogenous CCTα protein expression. Results were corrected for CCTα protein expression levels and expressed relative to wild-type controls. **(B)** Expression of V5-tagged CCTα protein in stably-transfected CHO MT58 cell pools was determined in whole cell extracts by SDS-10%PAGE and immunoblotting analysis. Stripped blots were reprobed for actin to demonstrate equal loading. **(C)** Pools of CHO MT58 cells stably expressing the indicated V5-tagged CCTα proteins were seeded onto coverslips and cultured in medium B for 24 h prior to treatment with oleate (500 μM) for 2 h or no addition. Cells were fixed and permeabilized, labeled with Alexa-488 conjugated Con A and frequency of Con A-positive nuclear tubules in cell populations was determined as described in "Materials and Methods." Cells expressing various CCTα proteins were identified for analysis by immunofluorescence detection using a monoclonal antibody to the V5 epitope tag and an Alexa-594 conjugated secondary antibody, #$p<0.05$ compared to vector-transfected controls; *$p<0.05$, **$p<0.02$, ***$p<0.005$ compared to no addition.

Preliminary transient transfection experiments in MT58 cells confirmed that these mutations had the predicted effects on CCTα function. The H89G and K122A mutations resulted in a catalytic-dead enzyme, as determined by *in vitro* CCT activity assays of whole cell extracts from transfected MT58 cells (Figure 5.6, A). *In vitro* activity of CCT Δ236 was increased ~5-fold compared to wild-type CCTα, and was not further stimulated by lipid addition in the form of PtdCho/oleic acid vesicles.

CHO MT58 cells were stably-transfected with the various CCTα cDNAs or empty vector control to quantify the effect of the introduced mutations on CCTα-dependent proliferation of the NR. To eliminate possible clonal variation effects, pools of cells were obtained (>100 clones/pool) in which approximately 20-30% of cells expressed the desired proteins as identified by immunofluorescence detection of V5-tagged CCTα constructs. SDS-PAGE and immunoblotting analysis showed that the CCT Δ236 mutant was expressed at much lower levels than wild-type CCTα and the catalytic-dead CCT H89G and CCT K122A proteins (Figure 5.6, B). As in previous experiments, confocal microscopy was employed to measure the frequency of Con A-positive nuclear tubules in cells expressing wild-type or mutants versions of CCTα, or vector-transfected control cells (Figure 5.6, C). Under basal conditions, expression of CCT H89G and CCT K122A had no effect on the frequency of nuclear tubules per nuclei compared to vector-transfected controls, while expression of wild-type CCTα caused a statistically insignificant 26% increase. In contrast, constitutively-active CCT Δ236 expression caused a significant 2-fold increase in nuclear tubules, suggesting that elevated CCTα enzyme activity increased tubule formation. Following treatment for 2 h with 500 μM oleate, there was a significant 26% increase in nuclear tubule frequency in vector-

transfected control cells. Ectopic expression of wild-type CCTα enhanced oleate-induced NR proliferation by 100% in relation to vector control cells. Catalytically-dead CCT H89G and CCT K122A both enhanced oleate-induced nuclear tubule formation to a greater degree than wild-type CCTα (150% and 130%, respectively), indicating that catalytic activity was not a strict requirement for CCTα-dependent NR proliferation in the presence of oleate. The elevated level of nuclear tubules in cells expressing soluble CCT Δ236 was maintained, but not enhanced further, in the presence of oleate.

The effect of the various V5-tagged CCTα proteins on NR morphology under basal and oleate-stimulated conditions can be seen in representative confocal images from the previous dataset (Figure 5.7). In untreated cells, immunostaining of ectopically-expressed wild-type and mutated CCTα was nucleoplasmic, and did not overlap with intranuclear Con A-positive foci corresponding to NE invaginations in single optical Z-sections (Figure 5.7, A). This was especially evident in CCT Δ236 expressing cells in which there were more numerous filamentous NE invaginations that were clearly distinct within the nucleoplasmic immunostaining pattern of CCT Δ236 in merged images.

In cells treated with oleate (500 μM) for 2 h, wild-type CCT, CCT H89G, and CCT K122A were extensively co-localized with proliferating intranuclear Con A-positive structures (Figure 5.7, B). Both catalytic-dead CCT H89G and CCT K122A were more robustly translocated to the NE and NR following oleate treatment compared to wild-type CCTα, suggesting that loss of catalytic function enhanced CCTα membrane binding and/or retention.

Figure 5.7 - Localization of catalytic-dead and membrane-binding defective CCTα mutants and relationship to the NR in CHO MT58 cells. Pools of CHO MT58 stably expressing the indicated V5-tagged CCTα proteins were seeded onto coverslips and cultured in the absence (A) or presence (B) of oleate (500 μM) for 2 h prior to fixation and permeabilization with 3% formaldehyde/0.05% Triton X-100. Coverslips were stained with Alexa-488 conjugated Con A and processed for immunofluorescence detection of V5-tagged CCTα proteins using an Alexa-594 conjugated secondary antibody. Images represent single optical sections obtained with a Zeiss LSM 510 Meta confocal microscope equipped with a 100X objective. Bar, 10 μm.

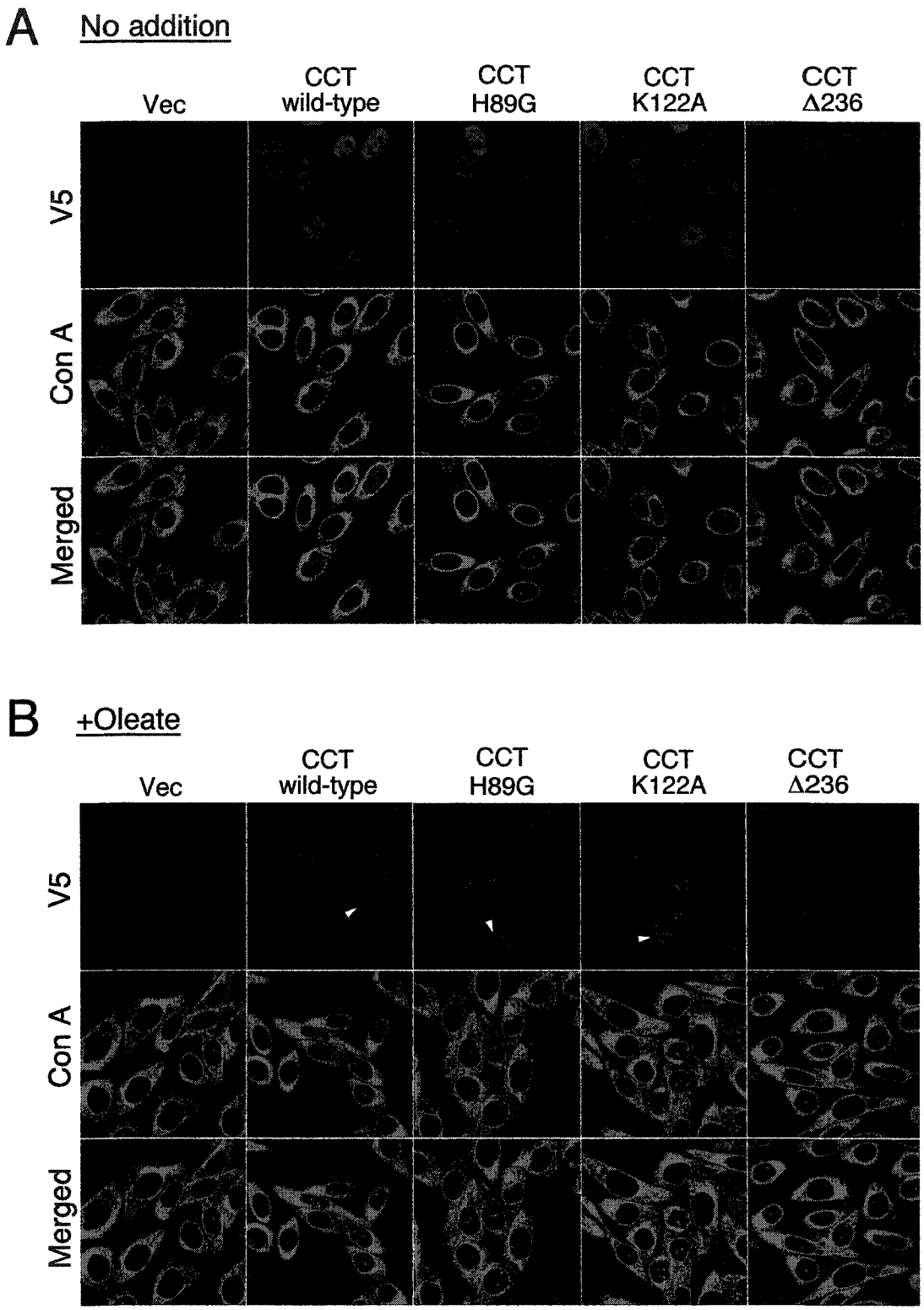
A
No addition
Vec
CCT wild-type
CCT H89G
CCT K122A
CCT Δ236
V5
Con A
Merged
B
+Oleate
Vec
CCT wild-type
CCT H89G
CCT K122A
CCT Δ236
V5
Con A
Merged

Figure 5.7

Nucleoplasmic localization of CCT Δ236 was unaffected by oleate addition. In a majority of cells, translocated CCTα proteins were preferentially associated with Con A-positive NR and discreet patches along the nuclear periphery, with little or no detectable immunostaining of the surrounding NE. Nucleoli were clearly visible as discontinuities in the CCTα nucleoplasmic immunostaining pattern and numerous CCTα- and Con A-positive tubules were closely juxtaposed to, or in apparent association with, nucleoli (arrowheads in Figure 5.7, B).

5.1.7 Membrane binding by CCTα causes liposome tubulation

The formation of tubular NE invaginations in MT58 cells expressing catalytic-dead CCTα prompted us to investigate whether CCTα could directly deform membranes. Several amphipathic proteins involved in membrane remodeling events in the cell, including dynamin, amphiphysin and endophilin, cause evagination of protein-free liposomes into thin tubules through direct interaction with the membrane bilayer (88). To test whether CCTα possessed a similar activity, purified recombinant rat CCTα (2.5 - 5 μM) was incubated at 37°C with liposomes (250 μM) prepared from total brain lipid extract or a synthetic formulation (50, 25, 17.5, 5, and 2.5 mol% of PtdCho, PtdEtn, PtdSer, oleic acid, and PtdIns-4-P, respectively), and liposome morphology was examined by negative-staining and transmission electron microscopy (TEM) (Figure 5.8). To ensure that observed alterations in liposome shape were not due to general effects of protein association or incubation condition, parallel incubations were carried out using the recombinant pleckstrin homology (PH) domain of oxysterol binding protein, a known PtdIns-polyphosphate binding domain (310).

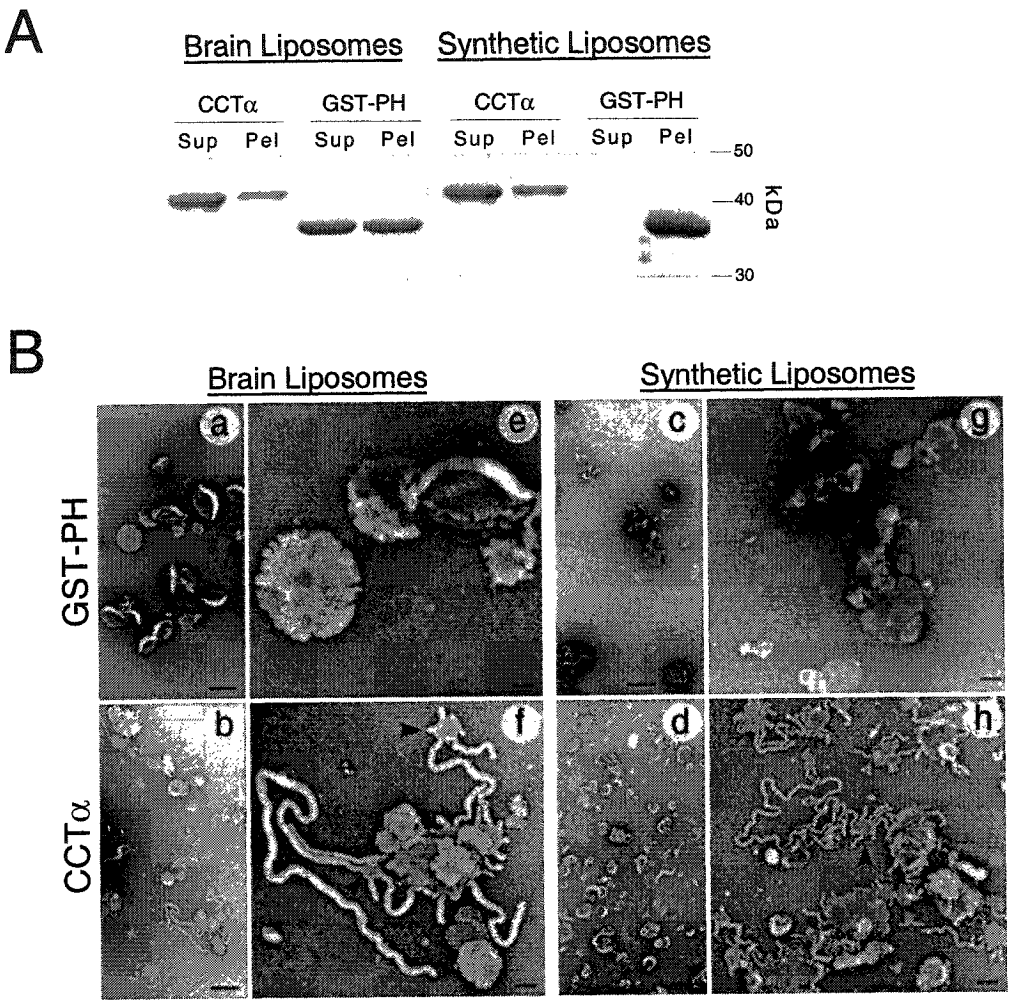

Figure 5.8 - Tubulation of protein-free liposomes by purified recombinant CCTα. Liposomes (250 μM) composed of total brain lipid extract or a synthetic formulation (50, 25, 17.5, 5, and 2.5 mol% of PtdCho, PtdEtn, PtdSer, oleic acid, and PtdIns-4-P, respectively) were incubated for 15 min at 37°C with purified recombinant CCTα or GST-PH (OSBP PH domain fused to GST) control protein (2.5 μM). **(A)** Following incubation with recombinant proteins, liposomes were sedimented by high-speed centrifugation. Protein associated with the supernatent (Sup) and pellet (Pel) fractions was subjected to SDS-10%PAGE and visualized by Coomassie stain. **(B)** Liposomes were incubated with recombinant proteins as above, and the resulting mixture was processed for TEM as described in "Materials and Methods." Samples were contrasted with lead citrate and uranyl acetate in order to visualize liposome morphology. Bars: (a-d) 500 nm; (e-h) 100 nm. Panels e, g, f and h represent magnified fields from a, c, b and d, respectively.

Initial liposome sedimentation assays indicated that both CCTα and the OSBP PH domain fused to GST (GST-PH) were partially bound to brain and synthetic liposomes following a 15 min incubation (Figure 5.8, A). GST-PH bound almost quantitatively to synthetic liposomes containing 2.5 mol% PtdIns-4-P. TEM revealed that CCTα binding robustly deformed spherical liposomes into long thin tubules (Figure 5.7, B). This activity was clearly distinguished from general protein binding, as the GST-PH protein had no appreciable effect on liposome morphology. The tubules formed by CCTα/bilayer interaction had a consistent diameter of ~50 nm for brain liposomes compared to ~20 nm for the synthetic liposomes. The majority of tubules extended in a non-branching manner from the main body of deformed liposomes. However, it was not uncommon to observe tethering from the main body to small spherical bodies from which further tubules emanated (arrowheads in Figure 5.8, B-f,h), suggesting that these were nucleation sites for the formation of branched structures. These *in vitro* studies indicate that CCTα can directly modulate membrane curvature, an activity that could play a role in the observed correlation between membrane-association of CCTα and NR proliferation *in vivo*.

5.1.8 The NR in oleate-treated CHO cells is continuous with the cytoplasm

To investigate in more detail the morphology of the NR formed as a result of oleate treatment, and in particular its relationship to the cytoplasm, the ultrastructure of the NR in oleate-treated and untreated CHO cells was examined in thin sections by TEM (Figure 5.9). Double membrane intranuclear structures were present within CHO cells cultured in the absence or presence of oleate, with no discernible morphological differences under the two conditions (Figure 5.9, A). In general, untreated cells had

Figure 5.9 - Cytoplasmic nuclear envelope invaginations in oleate-treated and untreated CHO cells. **(A)** CHO cells cultured as described in the legend to Figure 5.4 were incubated in the absence (a,b) or presence (c-e) of oleate (500 μM) for 2 h. Cells were fixed and embedded as described in "Materials and Methods," and thin sections (80 - 100 nm) were contrasted with lead citrate and uranyl acetate and viewed by TEM. (**a**) Low-power overview of untreated cell. (**b**) High-power magnification of framed region in (a) with an elongated view of a cytoplasmic NE invagination. (**c**) Low-power view of an oleate-treated cell demonstrating tubular-vesicular membranes within the cytoplasm characteristic of cross-sectional views the ER. (**d**) High-power magnification of a framed region in (c) showing ER-like single-membrane structures within both the cytoplasmic interior of the invagination and the greater cytoplasm (arrowheads). (**e**) High-power magnification of a framed region in (c) showing alternate views of NE invaginations. Bars: (a,c) 2 μm; (b) 500 nm; (d,e) 100 nm. **(B)** High-power views of representative NE invaginations in oleate-treated CHO cells demonstrating close association of some invaginations with nucleoli (a and b) and the variable diameters of the invaginations (arrowheads in c). Bars: (a-c) 500 nm; (inset of a) 100 nm. Abbreviations: Nu-nucleus; Cyt-cytoplasm; IV-invagination; No-nucleolus; NP-nuclear pore; INM-inner nuclear membrane; ONM-outer nuclear membrane.

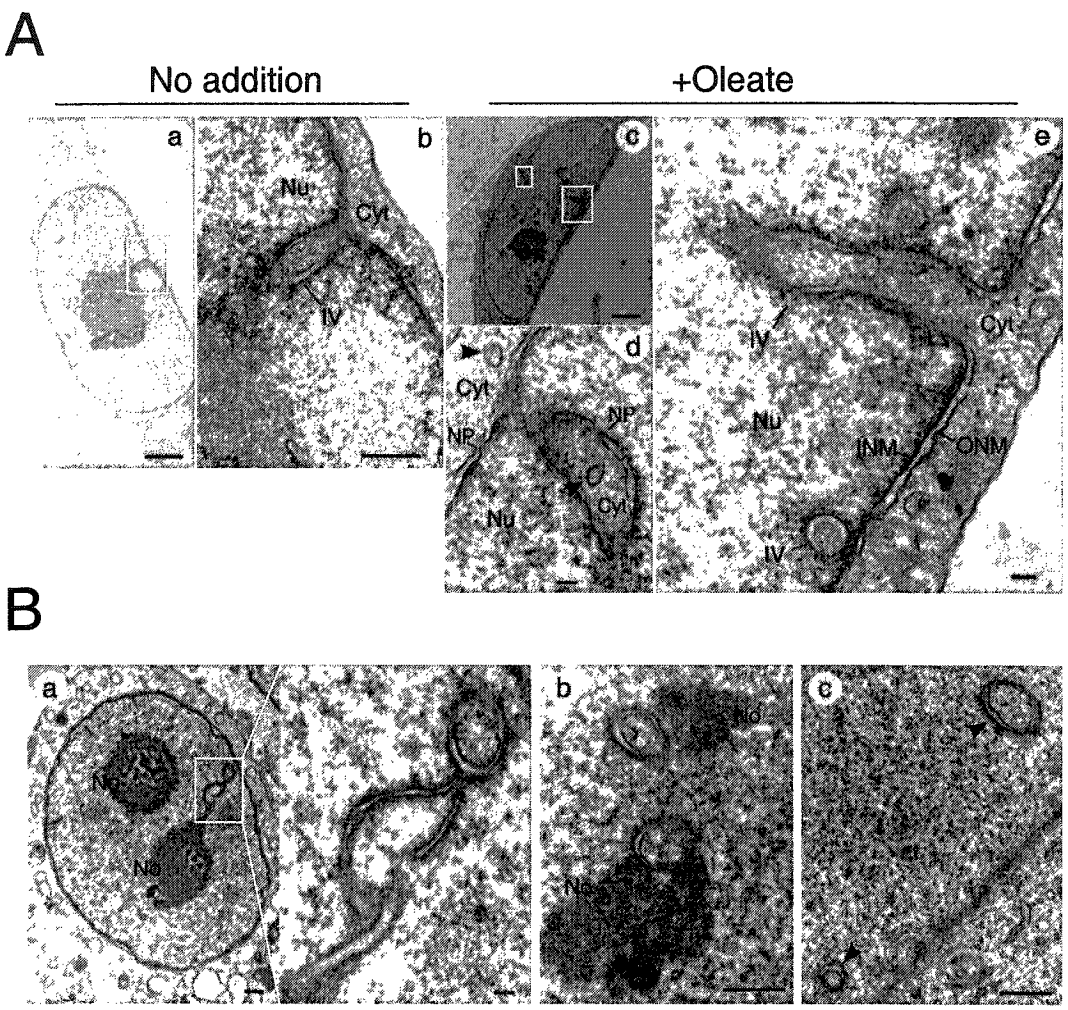

Figure 5.9

0-1 intranuclear membrane structures per nuclei, and it was not uncommon in oleate-treated cells to detect more than two such structures. The intranuclear membrane structures detected by TEM fell into two categories; (1) elongated structures unambiguously identifiable as cytoplasmic invaginations due to the continuance of their membranes and interior with the inner and outer NE and the cytoplasm, respectively (Figure 5.9, A-b and A-e), and (2) independent double membrane rings within the nucleoplasm (Figure 5.9, A-d, B-b and B-c). Several features present on the structures in the latter category appeared to represent horizontal cross-sections of cytoplasmic invaginations. Firstly, the distance between the two membrane layers was constant and similar to that between the inner and outer nuclear membranes (Figure 5.9, A-e). Secondly, occasional discontinuities along the double-layered membrane, analogous to nuclear pores, were identifiable on both the peripheral NE and the oval intranuclear membrane structures (Figure 5.9, A-d). Moreover, others have previously identified similar structures by EM in consecutive thin sections encompassing whole nuclei (95). Therefore, we conclude that the elongated and oval double membrane intranuclear structures detected by TEM analysis of CHO cells represent alternate views of cytoplasmic NR. Since no other intranuclear membrane structures were detected in oleate-treated cells ($n>50$), we can also conclude that the oleate-induced increase in nuclear tubules quantified by confocal microscopy analysis represents an increase in double membrane NE invaginations continuous with the cytoplasm.

The diameter of NE invaginations viewed in horizontal cross-section generally ranged from ~100 - 500 nm. The NR was often in contact with nucleoli in untreated cells (Figure 5.9, A-a) as well as in oleate-treated cells (Figure 5.9, B-a and B-b). This finding

is in agreement with previous reports of frequent association of the NR with nucleoli (95, 129). Small circular membranes were occasionally present within the cytoplasmic interior of invaginations, similar to membranes dispersed throughout the cytoplasm and characteristic of the tubulo-reticular ER (arrows in Figure 5.9, A-d).

5.1.9 Tubular membrane clusters associated with nuclear envelope invaginations in oleate-treated CHO cells overexpressing CCTα

Previous confocal microscopy results indicated that NE invaginations formed in oleate-treated CHO58-CCT cells overexpressing CCTα were broad structures with discontinuous association with lamin A/C (Figure 5.5, A). In order to further characterize these structures morphologically, CHO58-CCT cells were cultured in the absence or presence of oleate and thin-section TEM was performed. CHO MT58 cells transfected with empty vector (CHO58-Vec) were included in the analysis for comparison purposes. Double membrane invaginations of the NE in CHO58-Vec cells cultured in the absence or presence of oleate and in untreated CHO58-CCT cells were morphologically indistinguishable from those previously observed in TEM analysis of CHO cells (Figure 5.10, A and B). As expected, NE invaginations in oleate-treated CHO58-CCT cells were abundant, with many cells having multiple invaginations (Figure 5.10, A-i). Several unique features were associated with NE invaginations in oleate-treated *versus* untreated CHO58-CCT cells compared to NE invaginations observed by TEM in CHO cells with lower CCT expression levels. In particular, arrays of unorganized tubular membrane clusters (TMCs) were frequently observed in close association with the nucleoplasmic surface of double membrane cytoplasmic invaginations (Figure 5.10, A-j,k, and B-a).

Figure 5.10 - Association of nuclear envelope invaginations with tubular membrane clusters in oleate-treated CHO cells overexpressing CCTα. (A) CHO58-Vec (a-e) and CHO58-CCT cells (f-k) cultured as described in the legend to Figure 5.4 were incubated in the absence (a-c; f-h) or presence (d-e; i-k) of oleate (500 μM) for 2 h. Cells were processed for TEM as described in Figure 5.9. (**a**) Low-power overview of untreated CHO-Vec cell and high-power magnification of framed section containing NE invagination. (**b**) High-power view of an NE invagination in an alternative cell, showing the presence of ER-like membrane within the interior of the invagination (arrowhead). (**c**) Low-power overview of oleate-treated CHO-Vec cell. (**d and e**) High-power magnification of framed sections in (c) showing NE invaginations. (**f**) Low-power overview of untreated CHO58-CCT cell. (**g**) High-power magnification of a framed region in (f) depicting two NE invaginations, one close to a nucleolus (No). (**h**) High-power magnification of a framed region in (f) containing NE invagination of similar morphology to those seen in CHO-Vec cells (b and c). (**i**) Low-power overview of oleate-treated CHO58-CCT cell with numerous NE invaginations (arrowheads and contained in framed regions). (**j**) Medium-power magnification of a framed region in (i) containg three cytoplasmic NE invaginations and two small tubular single-membrane invaginations of the inner NE (arrowheads). Tubular membrane clusters (TMCs) are seen associated with both the nucleoplasmic and cytoplasmic faces of NE invaginations. (**k**) High-power magnification of a framed region in (i) containing three cytoplasmic NE invaginations. One is associated with a TMC, Bars: (a, c) 2 μm; (g, j) 500 nm; (all insets) 100 nm.

(**B**) High-power views of various representative NE invaginations in oleate-treated CHO58-CCT cells. (**a**) High magnification of NE invaginations depicted in (A-j), showing more detail of TMCs with arrowheads demonstrating ringed membrane structure with an electron-dense core within the cytoplasmic interior of one of the invaginations. (**b**) Crease-like inner NE invagination (arrowhead) contrasted with a cytoplasmic NE invagination depicted in the same image. (**c**) High-power magnification showing a membranous structure with an electron-dense core. (**d**) Crease-like invagination of the double membrane NE. An electron-dense structure within the cytoplasmic interior of the invagination is marked with an arrowhead. Bars: 100 nm.

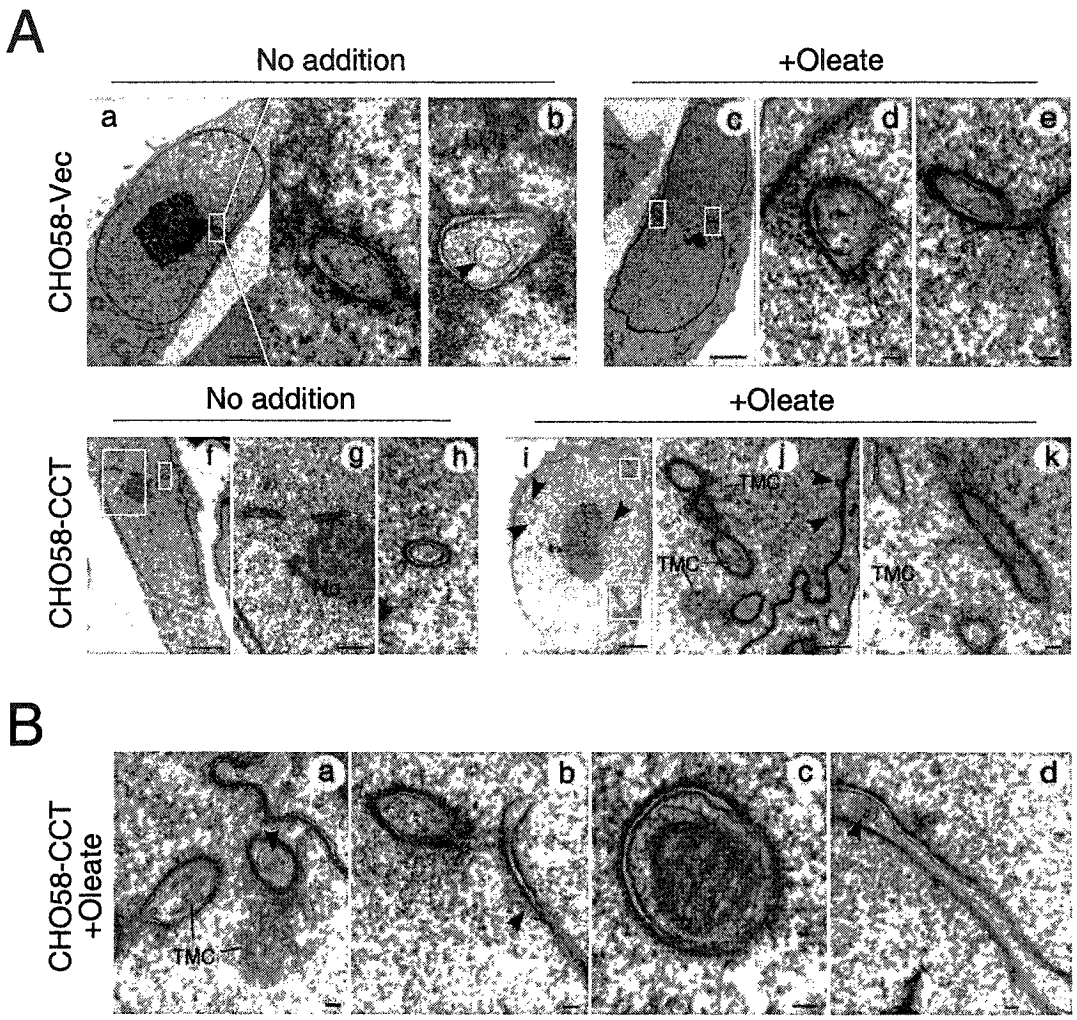
A
No addition
+Oleate
CHO58-Vec
a
b
c
d
e
No addition
+Oleate
CHO58-CCT
f
g
h
i
j
k
TMC
TMC
TMC
B
CHO58-CCT
+Oleate
a
b
c
d
TMC

Figure 5.10

TMCs were also identified within the cytoplasmic interior of some invaginations (Figure 5.10, A-j and B-a), suggesting these and the nucleoplasmic TMCs were of a similar origin.

Also present within the interior of some invaginations were oval structures with an electron-dense core and a visible surrounding membrane layer (Figure 5.10, B-c; arrowheads in Figure 5.10, B-a,d). While most invaginations viewed by TEM were tubular invaginations of the double membrane NE, elongated crease-like cytoplasmic NE invaginations (Figure 5.10, B-d) or single membrane invaginations of the INM were occasionally observed (arrowhead in Figure 5.10, B-b). Narrow tubular structures along the nuclear periphery were identifiable as INM invaginations due to an electron-dense outer surface identical to the nuclear lamina. It is unclear whether CCTα and/or oleate played a role in invagination of the INM since similar structures were occasionally seen in CHO58-Vec cells and untreated CHO58-CCT cells (data not shown). However, since the TMCs associated with nuclear envelope invaginations in oleate-treated CHO58-CCT cells were unique to this context, this strongly suggests that their formation is dependent on CCTα translocation and/or CDP-choline synthesis at this site.

5.2 Discussion

CCTα is predominantly a nuclear enzyme in many cell types and tissues, however the precise physiological role of this subcellular localization remains enigmatic (58, 151). In this study, we identify a previously unknown property of CCTα to deform membrane bilayers via its amphipathic membrane-binding domain, and provide morphological evidence that the manifestation of this activity within the nucleus is the formation of invaginations of the double membrane NE that extends the NR network.

5.2.1 CCTα associates with the nucleoplasmic reticulum

Our interest in examining nuclear CCTα stems from the identification of a caspase-6 cleavage site near the N-terminus of CCTα that results in removal of its NLS during apoptosis (Chapter 4). To gain insight into the role of nuclear localized CCTα in non-apoptotic cells, indirect immunofluorescence and confocal microscopy techniques were used to examine intranuclear sites of CCTα membrane association in CHO cells following stimulation of PtdCho synthesis by oleate. In its inactive form, CCTα primarily displays a soluble nucleoplasmic distribution in many cell types, including CHO cells (169, 288, 290). Following oleate addition, CCTα was extensively co-localized with the NE marker lamin A/C at both the peripheral NE, as previously reported (290), but also in filamentous intranuclear structures. At least one of these structures was present in most cells, with some having an extensive branched network. The presence of binding sites for Con A, a lectin that binds to ER-resident glycoproteins, unambiguously identified the intranuclear structures as the NR.

The NR has been characterized within nuclei of numerous mammalian cell-types and tissues (77, 95). It is comprised of tubular membrane structures that frequently 1)

traverse the entire nucleus in a vertical orientation relative to the substratum, 2) are continuous with the cytoplasm/ER and 3) contain nuclear pore complexes (95, 141). The precise function of the NR remains largely unknown, although it has been shown to be a site of localized Ca^{2+} release, suggestive of a role in intranuclear Ca^{2+} signalling. The NR has also been proposed to facilitate transport processes by extending the nuclear-cytoplasmic interface to specific intranuclear sites such as nucleoli (95), or by increasing the surface/volume ratio of the nucleus (141). Due to the presence of associated lamina, the NR could also provide structural support within the nucleus (33). The results presented in this chapter are the first to identify the association of a nuclear lipid biosynthetic enzyme (CCTα) and potentially other CDP-choline pathway enzymes with the NR.

5.2.2 The CDP-choline pathway in the nucleoplasmic reticulum

Immunofluorescence data demonstrated the presence of cytoplasmic and NE/ER components in CCTα-associated NE invaginations in oleate-treated CHO cells (Figure 5.2, A). Therefore, the NR consolidates the primary cellular loci of the CDP-choline pathway enzymes under conditions of stimulated PtdCho synthesis [choline kinase (cytoplasm)→CCTα (nucleus)→ CPT (ER)]. The reaction steps in the CDP-choline pathway involve both soluble and membrane-bound enzymes and substrates (154). There is considerable evidence that soluble intermediates in the CDP-choline pathway (choline, phosphocholine and CDP-choline) do not freely diffuse between sequential enzymes but are channeled from enzyme to enzyme along the pathway due to formation of a functional compartmentalization or complex of enzymes (26, 100, 101, 219). The NR is an attractive site for the compartmentalization of the CDP-choline pathway. It contains

NPCs (Figure 5.2, B and refs. 95, 139), thus allowing passage of small molecules between nuclear and cytoplasmic enzymes, and confinement of soluble CDP-choline pathway intermediates within a narrow space could facilitate their transfer to subsequent enzymes. Nuclear localization of CCTα also physically separates CCTα from the bulk of choline kinase and CPT activities in the cell, presumably precluding the formation of a multi-enzyme complex. Substrate channelling via this mechanism in cells in which CCTα is primarily nuclear-localized, such as CHO cells, could involve nuclear export of CCTα under activating conditions (58, 169, 196). However, we saw no evidence of CCTα export in oleate-treated CHO cells using a polyclonal antibody to detect endogenous CCTα, or a monoclonal antibody to detect overexpressed epitope-tagged CCTα in CHO MT58 cells. While we cannot rule out the possibility that nuclear export of CCTα occurred below the level of detection, it is unlikely that this would account for increased CCTα activity and PtdCho synthesis in oleate-treated CHO cells.

For the NR to be a major site of PtdCho synthesis, preferential association of CCTα with this structure would be required. Studies of CCT membrane binding *in vitro* have indicated that the presence of non-bilayer lipids, such as DAG and unsaturated PtdEtn, increase the ability of CCTα to associate with membranes by introducing membrane curvature stress (10, 11, 63). This is thought to result in uneven packing of polar head groups in the lipid bilayer, favouring insertion of the CCTα domain M amphipathic helix into the hydrophobic core of the bilayer. By analogy, a high degree of membrane curvature in membrane tubular structures could result in similar lateral packing defects that attract CCTα. Sterol carrier protein 2, which also binds to membranes via an amphipathic helical region, has been shown to preferentially bind to

highly curved membranes *in vitro* (125). While it remains an intriguing possibility that CCTα could similarly be a curvature-sensing protein, we did not observe unambiguous preferential binding of endogenous CCTα to NE invaginations over the peripheral NE in oleate-treated CHO cells by indirect immunofluorescence analysis (Figure 5.1). However, overexpressed wild-type CCTα as well as catalytic-dead CCTα mutants preferentially bound to the NR in oleate-treated CHO MT58 cells (Figure 5.7, B). Unlike endogenous CCTα, which displayed near complete translocation to the NE in response to oleate (500 μM), translocation of the overexpressed CCTα was incomplete, with considerable immunostaining detectable in a soluble nucleoplasmic distribution following oleate addition. This perhaps indicates that the ratio between CCTα expression and concentration of lipid activator could be a determinant for membrane binding site preference. It would be worthwhile in future experiments to assess membrane-binding sites of endogenous CCTα under conditions of minimal lipid activation. Testing the hypothesis that the NR is a major site of PtdCho synthesis would require measuring PtdCho synthesis under conditions whether the NR network is disrupted or enhanced, possibly by altering lamin A/C expression levels.

5.2.3 Effect of CCTα activation on the nucleoplasmic reticulum

NR proliferation in oleate-treated CHO cells was significantly increased as demonstrated using two independent markers; (1) filamentous intranuclear lamin A/C-positive structures continuous with the NE, and (2) intranuclear structures containing ER-resident glycoproteins labeled by the lectin Con A. Proliferation of the NE was associated with CCTα expression and activation in oleate-treated cells (Figure 5.1, C). Nuclear tubule frequency was also increased in CHO cells in response to the CCTα

activator arachidonic acid and in other cell lines treated with oleate (human F8 and mouse 3T3 fibroblasts), indicating that these effects are general in nature.

Overexpression studies in CHO MT58 cells provided compelling evidence that the effect of oleate on nuclear tubule formation was CCTα-dependent. Further analysis indicated that this mechanism may be co-dependent on CCTα membrane binding and catalytic activities. This was demonstrated by a 2.0-2.5-fold increase in NE invaginations in MT58 cells expressing two different catalytic-dead CCTα mutants in the presence of oleate, and a 2-fold increase in invaginations in cells expressing constitutively-active CCT Δ236 mutant in the absence of oleate. The ability of catalytic-dead CCTα mutants (CCT H89G and CCT K122A) to affect NR proliferation suggests that CCTα can directly alter membrane curvature due to a physical property of membrane binding. The fatty acid oleate was a necessary component indicating that cellular levels of CCTα membrane lipid activators would ultimately control the proliferation of the NR by this mechanism. The catalytic-dead CCTα proteins and wild-type CCTα preferentially associated with the NR, indicating that they facilitate the creation of their own preferred binding site. This could result in a feed-forward mechanism not only in NR formation, but also possibly for PtdCho synthesis.

Since the constitutively-active and membrane-binding defective mutant protein CCT Δ236 also induced NR proliferation, this suggests that nuclear CCTα enzymatic activity can act to increase NR proliferation by increasing PtdCho synthesis. A coordinated mechanism may expand the NR via CCTα membrane-binding coupled with PtdCho synthesis for tubule formation. Qualitatively, the NR in MT58 cells expressing CCT Δ236 was a fine reticular network that was distinguishable from oleate-induced NR

proliferation in MT58 cells overexpressing wild-type CCTα and CCT H89G and CCT K122A as viewed by immunofluorescence and confocal microscopy analysis. Future morphological studies will determine if the NR in these cells is altered compared to cells expressing CCTα with intact membrane-binding ability.

The mechanism of formation of the NR is currently unknown. One possibility is that stable membrane-bound intranuclear channels form in the vicinity of nucleoli during reformation of the nucleus following mitosis (95). However, this does not explain the dynamic nature of NR formation observed in interphase cell populations (141), nor does it explain the short-term effects (2 h) of oleate on nuclear tubule formation presented in this study. NE invaginations have also been shown to form in the vicinity of centrosomes at the start of mitosis, suggesting that cytoplasmic microtubules can drive their formation (22, 234). TEM has been used to characterize various types of NE invaginations formed by unknown mechanisms (21, 79, 129). For instance, overexpression of the integral INM protein lamin B receptor (LBR) resulted in numerous cytoplasmic NE invaginations (79). In the current study, TEM analysis showed that NE invaginations formed in oleate-treated CHO cells were of similar morphology (Figure 5.9), although not as abundant as invaginations formed by LBR overexpression. In both cases the invaginations extended the nuclear/cytoplasmic interface deep into the nucleus. Immunofluorescence analysis of oleate-treated CHO cells showed that NE invaginations contained NPCs, frequently traversed the entire nucleus, and were invariably associated with lamin A/C. Many of the invaginations observed in thin sections from untreated and oleate-treated CHO cells were in close or direct contact with nucleoli, in agreement with previous reports (95, 141). This was especially evident in fluorescence confocal microscopy images of nuclear

tubules formed in oleate-treated MT58 cells stably expressing wild-type CCTα and catalytic-dead CCTα mutants (Figure 5.7). Therefore formation of the NR in interphase cells could be oriented towards nucleoli, perhaps mediated by a nuclear cytoskeleton and/or nucleoli-associated proteins. This suggests a possible role for CCTα-induced NR proliferation in the transport of ribosomal intermediates from their site of synthesis in nucleoli to the cytoplasm.

Examination by thin section TEM of oleate-induced NE invaginations in CHO CHO58-CCT cells revealed their association with unorganized tubular membrane clusters (TMCs) that were devoid of lamina. There have been several previous reports of intranuclear membranes associated with NE invaginations. Overexpression of the nucleolar chaperone Nopp140 induced formation of nucleoli-associated invaginations comprised of organized membrane structures termed 'R-rings' (129). These structures appeared identical to an intranuclear tubular membrane array known as the nucleolar channel system identified in human endometrial tissue (259). NE invaginations associated with intranuclear membrane arrays were also shown to form in response to high expression levels of the ER-resident protein HMG-CoA reductase (HMGR) (23). Highly analogous membrane arrays form in the ER in both mammalian and yeast cells in response to overexpression of HMGR and other integral membrane proteins (214, 309, 315), and also by weak interactions between peripheral ER-associated proteins (246). These structures are alternatively termed crystalloid ER, karmellae or organized smooth ER (OSER). Interestingly, a recent report demonstrated the presence of onion-like membranes associated with the INM caused by high ER concentrations of a mis-targeted plasma membrane receptor (248). These structures were proposed to form through the

invagination into the nucleus of proliferating ER membranes. In oleate-treated CHO58-CCT cells, the appearance of TMCs was correlated with increased PtdCho synthesis following oleate addition, and was observed on both the cytoplasmic and nucleoplasmic sides of invaginations. This suggests that TMCs represent either independently proliferating membranes on both sides of the NE or membrane synthesis on the interior of the invagination that entered the interior of the nucleus through nuclear pores. Given the current data, we cannot rule out the possibility that the TMCs do not represent new membrane synthesis, but rather existing membrane that was pulled into the nucleus during the formation of an invagination (248). However, their presence in oleate-treated CHO58-CCT cells and absence in all other cellular conditions examined argue that this is not the case. It is possible that CCTα-induced NE invagination coupled with increased PtdCho synthesis may have played a role in the formation of intranuclear membrane arrays observed in previous studies. It is difficult to assess the relative contributions of membrane proliferation and membrane reorganization events in the formation of crystalloid ER structures due to the extensiveness of the existing ER membrane network (246). In an analogous fashion, formation of intranuclear membrane arrays could be considered a 'crystalloid NR' and provides a unique opportunity to assess the potential role of PtdCho synthesis in membrane proliferation events and the cellular response to protein accumulation in both nuclear (21, 23, 178) and ER membranes (214, 246, 309, 315). Since we observed oleate-induced TMC formation in CCTα overexpressing cells, experiments to assess TMC formation in the oleate-treated cells expressing catalytic-dead CCTα mutants are currently underway in our laboratory.

5.2.4 Lamin A expression affects nucleoplasmic reticulum morphology

Since the lamina makes contacts with chromatin (102, 226, 241), the CCTα dependent formation of lamin-associated NE invaginations in CHO cells (Chapter 5) could potentially affect chromatin organization and gene expression. Conversely, as the main cytoskeletal protein in the nucleus, lamin proteins could affect the morphology and extent of NR induced by CCTα membrane binding and PtdCho synthesis. Immunofluorescence analysis of oleate-induced NE invaginations in CHO58-CCT cells revealed that they were often associated with broad CCTα- and Con A-positive structures that did not label with antibody to lamin A/C. Cells transiently expressing a lamin A-GFP construct did not contain the broad CCTα-positive intranuclear structures (Figure 5.5, B). Instead, CCTα was present in an elaborate filamentous NR network that extensively overlapped with lamin A-GFP staining. Based on TEM results in oleate-treated CHO58-CCT cells, we can assume that the broad CCTα-positive structures observed by fluorescence confocal microscopy corresponded to TMCs, and that these unorganized membrane arrays did not form in cells with elevated levels of lamin A protein. In a previous live-cell study, an extensive NR network was characterized in CHO cells stably expressing lamin A-GFP (33). Evidence in that study indicated that the NR network was revealed, rather than created, by lamin A-GFP expression. This was clearly not the case in the current study, since the immunofluorescence pattern of an independent NR marker (CCTα) was drastically altered by lamin A-GFP expression. Since lamin A-GFP expression also resulted in apparent proliferation of the NR in untreated CHO58-CCT cells (results not shown), it is unclear if the filamentous NR network observed in oleate-treated cells was created by this treatment or already existed.

However, lamin A expression clearly affected the deposition of intranuclear membranes and altered NR morphology.

Our results uncover a previously unknown function of lamin A in affecting both the creation and the structure of the NR. In vertebrates, the A-type lamins, which include the A, AΔ10, and C splice variants of the lamin A gene, are highly expressed in terminally differentiated cells, whereas one or more of the B-type lamins, encoded from two separate genes, are expressed throughout development (reviewed in ref. 103). Lamin A is capable of directly binding to DNA, whereas lamin B interacts with chromatin through protein binding partners (226). In contrast to the B-type lamins, which predominantly assemble into the nuclear lamina underlying the NE, A-type lamins are also localized in intranuclear foci and filaments that appear to be intermediates for its assembly into the lamina (187). Lamin A involvement in the formation and/or stabilization of the NR could affect gene expression patterns through direct contacts with chromatin, or by affecting nuclear Ca^{2+} signalling (77). While our results implicate lamin A in the formation of the NR, future work will be needed to further define this role and assess possible functions of the other lamin isoforms in the stabilization and formation of this intranuclear membrane system.

5.2.5 CCTα tubulates membranes

The finding that catalytic-dead mutants of CCTα induced formation of nuclear tubules continuous with the NE indicates that CCTα can directly deform membranes independent of PtdCho synthesis. This theory was tested *in vitro* using a liposome-based assay system. TEM analysis of liposome morphology following incubation with purified CCTα revealed the formation of numerous long tubular evaginations from the previously

spherical liposomes (Figure 5.8, B). Numerous amphipathic proteins have been shown to possess the ability to directly affect membrane curvature, resulting in membrane tubule formation *in vitro* (reviewed in refs. 88, 329). For example amphiphysin (209), endophilan (209), and dynamin (324) are amphipathic proteins that can impose positive curvature on membrane bilayers. These proteins are involved in membrane-remodeling and vesicle formation in the endocytic and secretory pathways of the cell, and contain a universal membrane-deforming domain known as the (Bin/Amphiphysin/Rvs) BAR domain (209). The BAR domain has a characteristic concave surface formed by the intersection of homo-dimers into a bundle of six α-helices (209). BAR domain containing proteins are categorized as either 'weak', meaning they use the domain to sense and bind to curved membranes, and 'strong', meaning that they can impose membrane curvature. The 'strong' BAR domains contain an N-terminal amphipathic helix (209). Mutational analysis has indicated that membrane deformation is highly dependent on positively charged lysine residues at the interfacial region. Comparison of the amino acid sequence of the BAR domain and the CCTα demonstrates that CCTα does not contain the universal BAR domain. Similar to BAR domain containing proteins, CCTα forms a dimer (50), each domain M monomer has three α-helices (140, 317) and patches of positively charged lysine residues that are critical for membrane binding in response to anionic lipids (55). Therefore, CCTα may have structural similarity to the BAR domain and could induce membrane curvature by a similar mechanism.

Other proteins that bind to membranes via an amphipathic helix, such as epsin (93), can also tubulate membranes in the absence of a BAR domain. Tubulation of membranes by epsin has been proposed to be due to the amphipathic helical region

inserting into a bilayer thereby selectively increasing the lateral area of one monolayer (127). This results in a corresponding invagination of the opposing monolayer. This mechanism of membrane shape change was first proposed by the bilayer-couple hypothesis (239) and has been proposed for the *in vitro* membrane tubulation induced by lipid modifying enzymes (45) and transbilayer lipid movement (188). Since CCTα inserts its domain M region into the bilayer (139), it is possible that membrane tubulation results from an imposed increase in the surface area of one leaflet of the bilayer. The diameter of the tubules induced by CCTα varied depending on the composition of the liposomes. For instance, brain lipid extract had a relatively low content of the bilayer-forming lipid PtdCho relative to PtdEtn, which can promote non-bilayer phases (182), whereas the synthetic liposomes contained a relatively higher PtdCho content (Figure 5.8). This finding supports the proposal that the process of tubulation may be dependent on the lipid composition and elasticity of the membrane (10, 11).

It has also been proposed that certain membrane-binding proteins, such as the vesicle coat proteins clathrin or COPI and COPII, polymerize into a coat or a cage resulting in an oligomerization which physically shapes the membrane into an endocytic vesicle (127, 167). However, since the diameter of tubules induced by CCTα was variable, this suggests that CCTα does not form a rigid scaffold or lattice in order to deform membranes.

The finding that CCT membrane binding can directly deform membranes could have implications not only for the formation of the NR, but also suggests that cytoplasmic CCTα or the CCT β isoforms could be involved in membrane remodeling at the ER in other cell types. Interestingly, CCTβ2 affects neurite outgrowth in cultured

neuronal cells, presumably through its role in PtdCho synthesis (42). The results in Section 5 indicate that physical effects of CCT membrane binding also deserve consideration not only in mammalian cells, but also in other eukaryotic organisms such as yeast (98).

Our finding that CCTα affects the formation of the NR identifies a novel function of CCTα nuclear localization. As the role of the NR in various nuclear processes such as intranuclear Ca^{2+} signalling, gene expression, nuclear structural integrity and nuclear-cytoplasmic transport continues to be elucidated, we will gain a better understanding for the role of CCTα in the formation and function of this intranuclear membrane system. Ultimately this will illuminate the physiological significance of CCTα nuclear localization.

Chapter 6: Conclusion

This thesis research started out investigating the role of the SREBP pathway in the coordinate regulation of PtdCho synthesis with cholesterol and fatty acid metabolism through effects on CCTα activity. It ended examining a role of CCTα in the formation of tubular invaginations of the NE that are a component of the NR membrane system. Along the way we discovered that CCTα caspase cleavage and nuclear export are components of FOH-induced apoptosis. These projects are unified by the integration of CCTα regulatory mechanisms involving membrane binding and nuclear localization. Membrane binding allows CCTα to respond to cellular levels of CDP-choline pathway substrate, with the signal for CCTα activation dependent on fatty acid synthetic rates controlled by the SREBP pathway. This mode of activation also prevents inappropriate activation of CCTα and the CDP-choline pathway when cells are growing under conditions of low substrate availability, thus preventing attenuation of DAG-mediated cell proliferation and survival signalling by the CDP-choline pathway. CCTα nuclear localization could also be essential for the compartmentalization of the CDP-choline pathway, preventing its potential toxicity in rapidly growing cells. The NR could facilitate efficient PtdCho synthesis in the nuclear compartment by providing a structure that consolidates the CDP-choline pathway enzymes and facilitates the passage of soluble intermediates between enzymes. CCTα membrane binding and PtdCho synthesis in turn affects the formation of the NR, extending the nuclear-cytoplasmic interface to intranuclear sites. The ability of CCTα to directly deform membranes may represent a basic function conserved in other CCT enzymes. The dual abilities of CCTα to affect the deformation and synthesis of membranes make it an ideal candidate for involvement in

the formation of membrane tubular structures. This thesis provides evidence that CCTα affects numerous and diverse cellular processes including cellular membrane homeostasis, apoptosis and nuclear organization. These interrelated functions are co-dependent on CCTα membrane binding and nuclear localization.

Chapter 7: References

1. **Adany, I., E. M. Yazlovitskaya, J. S. Haug, P. A. Voziyan, and G. Melnykovych.** 1994. Differences in sensitivity to farnesol toxicity between neoplastically- and non-neoplastically-derived cells in culture. Cancer Lett **79:**175-9.
2. **Anthony, M. L., M. Zhao, and K. M. Brindle.** 1999. Inhibition of phosphatidylcholine biosynthesis following induction of apoptosis in HL-60 cells. J Biol Chem **274:**19686-92.
3. **Aoyama, C., A. Ohtani, and K. Ishidate.** 2002. Expression and characterization of the active molecular forms of choline/ethanolamine kinase-alpha and -beta in mouse tissues, including carbon tetrachloride-induced liver. Biochem J **363:**777-84.
4. **Araki, W., and R. J. Wurtman.** 1997. Control of membrane phosphatidylcholine biosynthesis by diacylglycerol levels in neuronal cells undergoing neurite outgrowth. Proc Natl Acad Sci U S A **94:**11946-50.
5. **Arnold, R. S., and R. B. Cornell.** 1996. Lipid regulation of CTP: phosphocholine cytidylyltransferase: electrostatic, hydrophobic, and synergistic interactions of anionic phospholipids and diacylglycerol. Biochemistry **35:**9917-24.
6. **Arnold, R. S., A. A. DePaoli-Roach, and R. B. Cornell.** 1997. Binding of CTP:phosphocholine cytidylyltransferase to lipid vesicles: diacylglycerol and enzyme dephosphorylation increase the affinity for negatively charged membranes. Biochemistry **36:**6149-56.
7. **Arthur, G., and R. Bittman.** 1998. The inhibition of cell signaling pathways by antitumor ether lipids. Biochim Biophys Acta **1390:**85-102.
8. **Atsumi, G., M. Murakami, K. Kojima, A. Hadano, M. Tajima, and I. Kudo.** 2000. Distinct roles of two intracellular phospholipase A2s in fatty acid release in the cell death pathway. Proteolytic fragment of type IVA cytosolic phospholipase A2alpha inhibits stimulus-induced arachidonate release, whereas that of type VI Ca2+-independent phospholipase A2 augments spontaneous fatty acid release. J Biol Chem **275:**18248-58.
9. **Atsumi, G., M. Tajima, A. Hadano, Y. Nakatani, M. Murakami, and I. Kudo.** 1998. Fas-induced arachidonic acid release is mediated by Ca2+-independent phospholipase A2 but not cytosolic phospholipase A2, which undergoes proteolytic inactivation. J Biol Chem **273:**13870-7.
10. **Attard, G. S., W. S. Smith, R. H. Templer, A. N. Hunt, and S. Jackowski.** 1998. Modulation of CTP:phosphocholine cytidylyltransferase by membrane torque tension. Biochem Soc Trans **26:**S230.
11. **Attard, G. S., R. H. Templer, W. S. Smith, A. N. Hunt, and S. Jackowski.** 2000. Modulation of CTP:phosphocholine cytidylyltransferase by membrane curvature elastic stress. Proc Natl Acad Sci U S A **97:**9032-6.
12. **Baburina, I., and S. Jackowski.** 1998. Apoptosis triggered by 1-O-octadecyl-2-O-methyl-rac-glycero-3- phosphocholine is prevented by increased expression of CTP:phosphocholine cytidylyltransferase. J Biol Chem **273:**2169-73.

13. **Baburina, I., and S. Jackowski.** 1999. Cellular responses to excess phospholipid. J Biol Chem **274:**9400-8.
14. **Bakovic, M., K. Waite, W. Tang, I. Tabas, and D. E. Vance.** 1999. Transcriptional activation of the murine CTP:phosphocholine cytidylyltransferase gene (Ctpct): combined action of upstream stimulatory and inhibitory cis-acting elements. Biochim Biophys Acta **1438:**147-65.
15. **Bakovic, M., K. Waite, and D. E. Vance.** 2003. Oncogenic Ha-Ras transformation modulates the transcription of the CTP:phosphocholine cytidylyltransferase alpha gene via p42/44MAPK and transcription factor Sp3. J Biol Chem **278:**14753-61.
16. **Bakovic, M., K. A. Waite, and D. E. Vance.** 2000. Functional significance of Sp1, Sp2, and Sp3 transcription factors in regulation of the murine CTP:phosphocholine cytidylyltransferase alpha promoter. J Lipid Res **41:**583-94.
17. **Balsinde, J., I. D. Bianco, E. J. Ackermann, K. Conde-Frieboes, and E. A. Dennis.** 1995. Inhibition of calcium-independent phospholipase A2 prevents arachidonic acid incorporation and phospholipid remodeling in P388D1 macrophages. Proc Natl Acad Sci U S A **92:**8527-31.
18. **Balsinde, J., and E. A. Dennis.** 1997. Function and inhibition of intracellular calcium-independent phospholipase A2. J Biol Chem **272:**16069-72.
19. **Banchio, C., L. M. Schang, and D. E. Vance.** 2003. Activation of CTP:phosphocholine cytidylyltransferase alpha expression during the S phase of the cell cycle is mediated by the transcription factor Sp1. J Biol Chem **278:**32457-64.
20. **Barbour, S. E., A. Kapur, and C. L. Deal.** 1999. Regulation of phosphatidylcholine homeostasis by calcium-independent phospholipase A2. Biochim Biophys Acta **1439:**77-88.
21. **Bastos, R., L. Ribas de Pouplana, M. Enarson, K. Bodoor, and B. Burke.** 1997. Nup84, a novel nucleoporin that is associated with CAN/Nup214 on the cytoplasmic face of the nuclear pore complex. J Cell Biol **137:**989-1000.
22. **Beaudouin, J., D. Gerlich, N. Daigle, R. Eils, and J. Ellenberg.** 2002. Nuclear envelope breakdown proceeds by microtubule-induced tearing of the lamina. Cell **108:**83-96.
23. **Berciano, M. T., R. Fernandez, E. Pena, E. Calle, N. T. Villagra, J. C. Rodriguez-Rey, and M. Lafarga.** 2000. Formation of intranuclear crystalloids and proliferation of the smooth endoplasmic reticulum in schwann cells induced by tellurium treatment: association with overexpression of HMG CoA reductase and HMG CoA synthase mRNA. Glia **29:**246-59.
24. **Bergmann, J., I. Junghahn, H. Brachwitz, and P. Langen.** 1994. Multiple effects of antitumor alkyl-lysophospholipid analogs on the cytosolic free Ca2+ concentration in a normal and a breast cancer cell line. Anticancer Res **14:**1549-56.
25. **Bishop, W. R., and R. M. Bell.** 1986. Attenuation of sn-1,2-diacylglycerol second messengers. Metabolism of exogenous diacylglycerols by human platelets. J Biol Chem **261:**12513-9.
26. **Bladergroen, B. A., M. J. Geelen, A. C. Reddy, P. E. Declercq, and L. M. Van Golde.** 1998. Channelling of intermediates in the biosynthesis of

phosphatidylcholine and phosphatidylethanolamine in mammalian cells. Biochem J **334 (Pt 3)**:511-7.

27. **Boggs, K., C. O. Rock, and S. Jackowski.** 1998. The antiproliferative effect of hexadecylphosphocholine toward HL60 cells is prevented by exogenous lysophosphatidylcholine. Biochim Biophys Acta **1389:**1-12.
28. **Boggs, K. P., C. O. Rock, and S. Jackowski.** 1995. Lysophosphatidylcholine and 1-O-octadecyl-2-O-methyl-rac-glycero-3- phosphocholine inhibit the CDP-choline pathway of phosphatidylcholine synthesis at the CTP:phosphocholine cytidylyltransferase step. J Biol Chem **270:**7757-64.
29. **Boggs, K. P., C. O. Rock, and S. Jackowski.** 1995. Lysophosphatidylcholine attenuates the cytotoxic effects of the antineoplastic phospholipid 1-O-octadecyl-2-O-methyl-rac-glycero-3- phosphocholine. J Biol Chem **270:**11612-8.
30. **Bradfute, D. L., C. J. Silva, and R. D. Simoni.** 1992. Squalene synthase-deficient mutant of Chinese hamster ovary cells. J Biol Chem **267:**18308-14.
31. **Bretscher, M. S.** 1973. Membrane structure: some general principles. Science **181:**622-9.
32. **Bridger, J. M., I. R. Kill, M. O'Farrell, and C. J. Hutchison.** 1993. Internal lamin structures within G1 nuclei of human dermal fibroblasts. J Cell Sci **104 (Pt 2):**297-306.
33. **Broers, J. L., B. M. Machiels, G. J. van Eys, H. J. Kuijpers, E. M. Manders, R. van Driel, and F. C. Ramaekers.** 1999. Dynamics of the nuclear lamina as monitored by GFP-tagged A-type lamins. J Cell Sci **112 (Pt 20):**3463-75.
34. **Brose, N., and C. Rosenmund.** 2002. Move over protein kinase C, you've got company: alternative cellular effectors of diacylglycerol and phorbol esters. J Cell Sci **115:**4399-411.
35. **Brown, A. J., L. Sun, J. D. Feramisco, M. S. Brown, and J. L. Goldstein.** 2002. Cholesterol addition to ER membranes alters conformation of SCAP, the SREBP escort protein that regulates cholesterol metabolism. Mol Cell **10:**237-45.
36. **Brown, M. S., and J. L. Goldstein.** 1997. The SREBP pathway: regulation of cholesterol metabolism by proteolysis of a membrane-bound transcription factor. Cell **89:**331-40.
37. **Brown, W. J., K. Chambers, and A. Doody.** 2003. Phospholipase A2 (PLA2) enzymes in membrane trafficking: mediators of membrane shape and function. Traffic **4:**214-21.
38. **Cabot, M. C., C. J. Welsh, H. T. Cao, and H. Chabbott.** 1988. The phosphatidylcholine pathway of diacylglycerol formation stimulated by phorbol diesters occurs via phospholipase D activation. FEBS Lett **233:**153-7.
39. **Campbell, H. A., and C. Kent.** 2001. The CTP:phosphocholine cytidylyltransferase encoded by the licC gene of Streptococcus pneumoniae: cloning, expression, purification, and characterization. Biochim Biophys Acta **1534:**85-95.
40. **Cao, Y., A. T. Pearman, G. A. Zimmerman, T. M. McIntyre, and S. M. Prescott.** 2000. Intracellular unesterified arachidonic acid signals apoptosis. Proc Natl Acad Sci U S A **97:**11280-5.
41. **Carman, G. M., and G. M. Zeimetz.** 1996. Regulation of phospholipid biosynthesis in the yeast Saccharomyces cerevisiae. J Biol Chem **271:**13293-6.

42. **Carter, J. M., K. A. Waite, R. B. Campenot, J. E. Vance, and D. E. Vance.** 2003. Enhanced expression and activation of CTP:phosphocholine cytidylyltransferase beta2 during neurite outgrowth. J Biol Chem **278:**44988-94.
43. **Chin, D. J., G. Gil, J. R. Faust, J. L. Goldstein, M. S. Brown, and K. L. Luskey.** 1985. Sterols accelerate degradation of hamster 3-hydroxy-3-methylglutaryl coenzyme A reductase encoded by a constitutively expressed cDNA. Mol Cell Biol **5:**634-41.
44. **Chomczynski, P., and N. Sacchi.** 1987. Single-step method of RNA isolation by acid guanidinium thiocyanate-phenol-chloroform extraction. Anal Biochem **162:**156-9.
45. **Christiansson, A., F. A. Kuypers, B. Roelofsen, J. A. Op den Kamp, and L. L. van Deenen.** 1985. Lipid molecular shape affects erythrocyte morphology: a study involving replacement of native phosphatidylcholine with different species followed by treatment of cells with sphingomyelinase C or phospholipase A2. J Cell Biol **101:**1455-62.
46. **Clarkson, T. B., R. W. Prichard, B. C. Bullock, R. W. St Clair, N. D. Lehner, D. C. Jones, W. D. Wagner, and L. L. Rudel.** 1976. Pathogenesis of artherosclerosis; some advances from using animal models. Exp Mol Pathol **24:**264-86.
47. **Cockcroft, S.** 1996. Phospholipase D: regulation by GTPases and protein kinase C and physiological relevance. Prog Lipid Res **35:**345-70.
48. **Colley, W. C., Y. M. Altshuller, C. K. Sue-Ling, N. G. Copeland, D. J. Gilbert, N. A. Jenkins, K. D. Branch, S. E. Tsirka, R. J. Bollag, W. B. Bollag, and M. A. Frohman.** 1997. Cloning and expression analysis of murine phospholipase D1. Biochem J **326 (Pt 3):**745-53.
49. **Colley, W. C., T. C. Sung, R. Roll, J. Jenco, S. M. Hammond, Y. Altshuller, D. Bar-Sagi, A. J. Morris, and M. A. Frohman.** 1997. Phospholipase D2, a distinct phospholipase D isoform with novel regulatory properties that provokes cytoskeletal reorganization. Curr Biol **7:**191-201.
50. **Cornell, R.** 1989. Chemical cross-linking reveals a dimeric structure for CTP:phosphocholine cytidylyltransferase. J Biol Chem **264:**9077-82.
51. **Cornell, R., and D. E. Vance.** 1987. Binding of CTP: phosphocholine cytidylyltransferase to large unilamellar vesicles. Biochim Biophys Acta **919:**37-48.
52. **Cornell, R., and D. E. Vance.** 1987. Translocation of CTP: phosphocholine cytidylyltransferase from cytosol to membranes in HeLa cells: stimulation by fatty acid, fatty alcohol, mono- and diacylglycerol. Biochim Biophys Acta **919:**26-36.
53. **Cornell, R. B.** 1992. Cholinephosphotransferase from mammalian sources. Methods Enzymol **209:**267-72.
54. **Cornell, R. B.** 1998. How cytidylyltransferase uses an amphipathic helix to sense membrane phospholipid composition. Biochem Soc Trans **26:**539-44.
55. **Cornell, R. B.** 1991. Regulation of CTP:phosphocholine cytidylyltransferase by lipids. 1. Negative surface charge dependence for activation. Biochemistry **30:**5873-80.

56. **Cornell, R. B.** 1991. Regulation of CTP:phosphocholine cytidylyltransferase by lipids. 2. Surface curvature, acyl chain length, and lipid-phase dependence for activation. Biochemistry **30:**5881-8.

57. **Cornell, R. B., G. B. Kalmar, R. J. Kay, M. A. Johnson, J. S. Sanghera, and S. L. Pelech.** 1995. Functions of the C-terminal domain of CTP: phosphocholine cytidylyltransferase. Effects of C-terminal deletions on enzyme activity, intracellular localization and phosphorylation potential. Biochem J **310:**699-708.

58. **Cornell, R. B., and I. C. Northwood.** 2000. Regulation of CTP:phosphocholine cytidylyltransferase by amphitropism and relocalization. Trends Biochem Sci **25:**441-7.

59. **Craig, L., J. E. Johnson, and R. B. Cornell.** 1994. Identification of the membrane-binding domain of rat liver CTP:phosphocholine cytidylyltransferase using chymotrypsin proteolysis. J Biol Chem **269:**3311-7.

60. **Cui, Z., and M. Houweling.** 2002. Phosphatidylcholine and cell death. Biochim Biophys Acta **1585:**87-96.

61. **Cui, Z., M. Houweling, M. H. Chen, M. Record, H. Chap, D. E. Vance, and F. Terce.** 1996. A genetic defect in phosphatidylcholine biosynthesis triggers apoptosis in Chinese hamster ovary cells. J Biol Chem **271:**14668-71.

62. **Cui, Z., M. Houweling, and D. E. Vance.** 1995. Expression of phosphatidylethanolamine N-methyltransferase-2 in McArdle-RH7777 hepatoma cells inhibits the CDP-choline pathway for phosphatidylcholine biosynthesis via decreased gene expression of CTP:phosphocholine cytidylyltransferase. Biochem J **312 (Pt 3):**939-45.

63. **Davies, S. M., R. M. Epand, R. Kraayenhof, and R. B. Cornell.** 2001. Regulation of CTP: phosphocholine cytidylyltransferase activity by the physical properties of lipid membranes: an important role for stored curvature strain energy. Biochemistry **40:**10522-31.

64. **Davis, R. J., B. R. Ganong, R. M. Bell, and M. P. Czech.** 1985. sn-1,2-Dioctanoylglycerol. A cell-permeable diacylglycerol that mimics phorbol diester action on the epidermal growth factor receptor and mitogenesis. J Biol Chem **260:**1562-6.

65. **de Figueiredo, P., A. Doody, R. S. Polizotto, D. Drecktrah, S. Wood, M. Banta, M. S. Strang, and W. J. Brown.** 2001. Inhibition of transferrin recycling and endosome tubulation by phospholipase A2 antagonists. J Biol Chem **276:**47361-70.

66. **DeBose-Boyd, R. A., J. Ou, J. L. Goldstein, and M. S. Brown.** 2001. Expression of sterol regulatory element-binding protein 1c (SREBP-1c) mRNA in rat hepatoma cells requires endogenous LXR ligands. Proc Natl Acad Sci U S A **98:**1477-82.

67. **DeLong, C. J., L. Qin, and Z. Cui.** 2000. Nuclear localization of enzymatically active green fluorescent protein- CTP:phosphocholine cytidylyltransferase alpha fusion protein is independent of cell cycle conditions and cell types. J Biol Chem **275:**32325-30.

68. **Dennis, E. A.** 1997. The growing phospholipase A2 superfamily of signal transduction enzymes. Trends Biochem Sci **22:**1-2.

69. **Dewey, R. E., R. F. Wilson, W. P. Novitzky, and J. H. Goode.** 1994. The AAPT1 gene of soybean complements a cholinephosphotransferase-deficient mutant of yeast. Plant Cell **6:**1495-507.
70. **Dobrosotskaya, I. Y., A. C. Seegmiller, M. S. Brown, J. L. Goldstein, and R. B. Rawson.** 2002. Regulation of SREBP processing and membrane lipid production by phospholipids in Drosophila. Science **296:**879-83.
71. **Dowd, S. R., M. E. Bier, and J. L. Patton-Vogt.** 2001. Turnover of phosphatidylcholine in Saccharomyces cerevisiae. The role of the CDP-choline pathway. J Biol Chem **276:**3756-63.
72. **Drecktrah, D., K. Chambers, E. L. Racoosin, E. B. Cluett, A. Gucwa, B. Jackson, and W. J. Brown.** 2003. Inhibition of a Golgi complex lysophospholipid acyltransferase induces membrane tubule formation and retrograde trafficking. Mol Biol Cell **14:**3459-69.
73. **Dunne, S. J., R. B. Cornell, J. E. Johnson, N. R. Glover, and A. S. Tracey.** 1996. Structure of the membrane binding domain of CTP:phosphocholine cytidylyltransferase. Biochemistry **35:**11975-84.
74. **Duplus, E., M. Glorian, and C. Forest.** 2000. Fatty acid regulation of gene transcription. J Biol Chem **275:**30749-52.
75. **Earnshaw, W. C., L. M. Martins, and S. H. Kaufmann.** 1999. Mammalian caspases: structure, activation, substrates, and functions during apoptosis. Annu Rev Biochem **68:**383-424.
76. **Ebinu, J. O., D. A. Bottorff, E. Y. Chan, S. L. Stang, R. J. Dunn, and J. C. Stone.** 1998. RasGRP, a Ras guanyl nucleotide- releasing protein with calcium- and diacylglycerol-binding motifs. Science **280:**1082-6.
77. **Echevarria, W., M. F. Leite, M. T. Guerra, W. R. Zipfel, and M. H. Nathanson.** 2003. Regulation of calcium signals in the nucleus by a nucleoplasmic reticulum. Nat Cell Biol **5:**440-6.
78. **Edwards, P. A., D. Tabor, H. R. Kast, and A. Venkateswaran.** 2000. Regulation of gene expression by SREBP and SCAP. Biochim Biophys Acta **1529:**103-13.
79. **Ellenberg, J., E. D. Siggia, J. E. Moreira, C. L. Smith, J. F. Presley, H. J. Worman, and J. Lippincott-Schwartz.** 1997. Nuclear membrane dynamics and reassembly in living cells: targeting of an inner nuclear membrane protein in interphase and mitosis. J Cell Biol **138:**1193-206.
80. **Endo, A.** 1992. The discovery and development of HMG-CoA reductase inhibitors. J Lipid Res **33:**1569-82.
81. **Esko, J. D., M. Nishijima, and C. R. Raetz.** 1982. Animal cells dependent on exogenous phosphatidylcholine for membrane biogenesis. Proc Natl Acad Sci U S A **79:**1698-702.
82. **Esko, J. D., M. M. Wermuth, and C. R. Raetz.** 1981. Thermolabile CDP-choline synthetase in an animal cell mutant defective in lecithin formation. J Biol Chem **256:**7388-93.
83. **Evan, G., and T. Littlewood.** 1998. A matter of life and cell death. Science **281:**1317-22.
84. **Evans, M. J., and J. E. Metherall.** 1993. Loss of transcriptional activation of three sterol-regulated genes in mutant hamster cells. Mol Cell Biol **13:**5175-85.

85. **Exton, J. H.** 1994. Phosphatidylcholine breakdown and signal transduction. Biochim Biophys Acta **1212:**26-42.
86. **Fadok, V. A., D. L. Bratton, D. M. Rose, A. Pearson, R. A. Ezekewitz, and P. M. Henson.** 2000. A receptor for phosphatidylserine-specific clearance of apoptotic cells. Nature **405:**85-90.
87. **Faleiro, L., and Y. Lazebnik.** 2000. Caspases disrupt the nuclear-cytoplasmic barrier. J Cell Biol **151:**951-9.
88. **Farsad, K., and P. De Camilli.** 2003. Mechanisms of membrane deformation. Curr Opin Cell Biol **15:**372-81.
89. **Feng, B., P. M. Yao, Y. Li, C. M. Devlin, D. Zhang, H. P. Harding, M. Sweeney, J. X. Rong, G. Kuriakose, E. A. Fisher, A. R. Marks, D. Ron, and I. Tabas.** 2003. The endoplasmic reticulum is the site of cholesterol-induced cytotoxicity in macrophages. Nat Cell Biol **5:**781-92.
90. **Fischer, U., R. U. Janicke, and K. Schulze-Osthoff.** 2003. Many cuts to ruin: a comprehensive update of caspase substrates. Cell Death Differ **10:**76-100.
91. **Florin-Christensen, J., M. Florin-Christensen, J. M. Delfino, and H. Rasmussen.** 1993. New patterns of diacylglycerol metabolism in intact cells. Biochem J **289 (Pt 3):**783-8.
92. **Florin-Christensen, J., M. Florin-Christensen, J. M. Delfino, T. Stegmann, and H. Rasmussen.** 1992. Metabolic fate of plasma membrane diacylglycerols in NIH 3T3 fibroblasts. J Biol Chem **267:**14783-9.
93. **Ford, M. G., I. G. Mills, B. J. Peter, Y. Vallis, G. J. Praefcke, P. R. Evans, and H. T. McMahon.** 2002. Curvature of clathrin-coated pits driven by epsin. Nature **419:**361-6.
94. **Freyberg, Z., A. Siddhanta, and D. Shields.** 2003. "Slip, sliding away": phospholipase D and the Golgi apparatus. Trends Cell Biol **13:**540-6.
95. **Fricker, M., M. Hollinshead, N. White, and D. Vaux.** 1997. Interphase nuclei of many mammalian cell types contain deep, dynamic, tubular membrane-bound invaginations of the nuclear envelope. J Cell Biol **136:**531-44.
96. **Friesen, J. A., H. A. Campbell, and C. Kent.** 1999. Enzymatic and cellular characterization of a catalytic fragment of CTP:phosphocholine cytidylyltransferase alpha. J Biol Chem **274:**13384-9.
97. **Friesen, J. A., M. F. Liu, and C. Kent.** 2001. Cloning and characterization of a lipid-activated CTP:phosphocholine cytidylyltransferase from Caenorhabditis elegans: identification of a 21-residue segment critical for lipid activation. Biochim Biophys Acta **1533:**86-98.
98. **Friesen, J. A., Y. S. Park, and C. Kent.** 2001. Purification and kinetic characterization of CTP:phosphocholine cytidylyltransferase from Saccharomyces cerevisiae. Protein Expr Purif **21:**141-8.
99. **Gant, T. M., and K. L. Wilson.** 1997. Nuclear assembly. Annu Rev Cell Dev Biol **13:**669-95.
100. **George, T. P., H. W. Cook, D. M. Byers, F. B. Palmer, and M. W. Spence.** 1991. Channeling of intermediates in the CDP-choline pathway of phosphatidylcholine biosynthesis in cultured glioma cells is dependent on intracellular Ca2+. J Biol Chem **266:**12419-23.

101. **George, T. P., S. C. Morash, H. W. Cook, D. M. Byers, F. B. Palmer, and M. W. Spence.** 1989. Phosphatidylcholine biosynthesis in cultured glioma cells: evidence for channeling of intermediates. Biochim Biophys Acta **1004:**283-91.
102. **Glass, J. R., and L. Gerace.** 1990. Lamins A and C bind and assemble at the surface of mitotic chromosomes. J Cell Biol **111:**1047-57.
103. **Goldman, R. D., Y. Gruenbaum, R. D. Moir, D. K. Shumaker, and T. P. Spann.** 2002. Nuclear lamins: building blocks of nuclear architecture. Genes Dev **16:**533-47.
104. **Goldstein, J. L., S. K. Basu, and M. S. Brown.** 1983. Receptor-mediated endocytosis of low-density lipoprotein in cultured cells. Methods Enzymol **98:**241-60.
105. **Goldstein, J. L., R. B. Rawson, and M. S. Brown.** 2002. Mutant mammalian cells as tools to delineate the sterol regulatory element-binding protein pathway for feedback regulation of lipid synthesis. Arch Biochem Biophys **397:**139-48.
106. **Golfman, L. S., M. Bakovic, and D. E. Vance.** 2001. Transcription of the CTP:phosphocholine cytidylyltransferase alpha gene is enhanced during the S phase of the cell cycle. J Biol Chem **276:**43688-92.
107. **Green, D. R.** 2000. Apoptotic pathways: paper wraps stone blunts scissors. Cell **102:**1-4.
108. **Green, D. R.** 1998. Apoptotic pathways: the roads to ruin. Cell **94:**695-8.
109. **Green, D. R., and G. I. Evan.** 2002. A matter of life and death. Cancer Cell **1:**19-30.
110. **Hannah, V. C., J. Ou, A. Luong, J. L. Goldstein, and M. S. Brown.** 2001. Unsaturated fatty acids down-regulate srebp isoforms 1a and 1c by two mechanisms in HEK-293 cells. J Biol Chem **276:**4365-72.
111. **Helenius, A., and M. Aebi.** 2001. Intracellular functions of N-linked glycans. Science **291:**2364-9.
112. **Helmink, B. A., J. D. Braker, C. Kent, and J. A. Friesen.** 2003. Identification of lysine 122 and arginine 196 as important functional residues of rat CTP:phosphocholine cytidylyltransferase alpha. Biochemistry **42:**5043-51.
113. **Henneberry, A. L., and C. R. McMaster.** 1999. Cloning and expression of a human choline/ethanolaminephosphotransferase: synthesis of phosphatidylcholine and phosphatidylethanolamine. Biochem J **339 (Pt 2):**291-8.
114. **Henneberry, A. L., G. Wistow, and C. R. McMaster.** 2000. Cloning, genomic organization, and characterization of a human cholinephosphotransferase. J Biol Chem **275:**29808-15.
115. **Henneberry, A. L., M. M. Wright, and C. R. McMaster.** 2002. The major sites of cellular phospholipid synthesis and molecular determinants of Fatty Acid and lipid head group specificity. Mol Biol Cell **13:**3148-61.
116. **Hennigar, R. A., M. Pochet, D. A. Hunt, A. E. Lukacher, V. J. Venema, E. Seal, and M. B. Marrero.** 1998. Characterization of fatty acid synthase in cell lines derived from experimental mammary tumors. Biochim Biophys Acta **1392:**85-100.
117. **Hodgkin, M. N., T. R. Pettitt, A. Martin, R. H. Michell, A. J. Pemberton, and M. J. Wakelam.** 1998. Diacylglycerols and phosphatidates: which molecular species are intracellular messengers? Trends Biochem Sci **23:**200-4.

118. **Horton, J. D., J. L. Goldstein, and M. S. Brown.** 2002. SREBPs: activators of the complete program of cholesterol and fatty acid synthesis in the liver. J Clin Invest **109:**1125-31.
119. **Houweling, M., Z. Cui, C. D. Anfuso, M. Bussiere, M. H. Chen, and D. E. Vance.** 1996. CTP: phosphocholine cytidylyltransferase is both a nuclear and cytoplasmic protein in primary hepatocytes. Eur J Cell Biol **69:**55-63.
120. **Houweling, M., H. Jamil, G. M. Hatch, and D. E. Vance.** 1994. Dephosphorylation of CTP-phosphocholine cytidylyltransferase is not required for binding to membranes. J Biol Chem **269:**7544-51.
121. **Houweling, M., L. B. Tijburg, W. J. Vaartjes, J. J. Batenburg, G. B. Kalmar, R. B. Cornell, and L. M. Van Golde.** 1993. Evidence that CTP:choline-phosphate cytidylyltransferase is regulated at a pretranslational level in rat liver after partial hepatectomy. Eur J Biochem **214:**927-33.
122. **Howe, A. G., and C. R. McMaster.** 2001. Regulation of vesicle trafficking, transcription, and meiosis: lessons learned from yeast regarding the disparate biologies of phosphatidylcholine. Biochim Biophys Acta **1534:**65-77.
123. **Hozak, P., A. M. Sasseville, Y. Raymond, and P. R. Cook.** 1995. Lamin proteins form an internal nucleoskeleton as well as a peripheral lamina in human cells. J Cell Sci **108 (Pt 2):**635-44.
124. **Hua, X., A. Nohturfft, J. L. Goldstein, and M. S. Brown.** 1996. Sterol resistance in CHO cells traced to point mutation in SREBP cleavage-activating protein. Cell **87:**415-26.
125. **Huang, H., J. M. Ball, J. T. Billheimer, and F. Schroeder.** 1999. Interaction of the N-terminus of sterol carrier protein 2 with membranes: role of membrane curvature. Biochem J **344 Pt 2:**593-603.
126. **Hunt, A. N., G. T. Clark, G. S. Attard, and A. D. Postle.** 2001. Highly saturated endonuclear phosphatidylcholine is synthesized in situ and colocated with CDP-choline pathway enzymes. J Biol Chem **276:**8492-9.
127. **Huttner, W. B., and J. Zimmerberg.** 2001. Implications of lipid microdomains for membrane curvature, budding and fission. Curr Opin Cell Biol **13:**478-84.
128. **Igal, R. A., P. Wang, and R. A. Coleman.** 1997. Triacsin C blocks de novo synthesis of glycerolipids and cholesterol esters but not recycling of fatty acid into phospholipid: evidence for functionally separate pools of acyl-CoA. Biochem J **324 (Pt 2):**529-34.
129. **Isaac, C., J. W. Pollard, and U. T. Meier.** 2001. Intranuclear endoplasmic reticulum induced by Nopp140 mimics the nucleolar channel system of human endometrium. J Cell Sci **114:**4253-64.
130. **Ishidate, K.** 1997. Choline/ethanolamine kinase from mammalian tissues. Biochim Biophys Acta **1348:**70-8.
131. **Izumi, M., O. A. Vaughan, C. J. Hutchison, and D. M. Gilbert.** 2000. Head and/or CaaX domain deletions of lamin proteins disrupt preformed lamin A and C but not lamin B structure in mammalian cells. Mol Biol Cell **11:**4323-37.
132. **Jackowski, S.** 1996. Cell cycle regulation of membrane phospholipid metabolism. J Biol Chem **271:**20219-22.
133. **Jackowski, S.** 1994. Coordination of membrane phospholipid synthesis with the cell cycle. J Biol Chem **269:**3858-67.

134. **Jagatheesan, G., S. Thanumalayan, B. Muralikrishna, N. Rangaraj, A. A. Karande, and V. K. Parnaik.** 1999. Colocalization of intranuclear lamin foci with RNA splicing factors. J Cell Sci **112 (Pt 24)**:4651-61.

135. **Jamil, H., G. M. Hatch, and D. E. Vance.** 1993. Evidence that binding of CTP:phosphocholine cytidylyltransferase to membranes in rat hepatocytes is modulated by the ratio of bilayer- to non-bilayer-forming lipids. Biochem J **291 (Pt 2)**:419-27.

136. **Jamil, H., A. K. Utal, and D. E. Vance.** 1992. Evidence that cyclic AMP-induced inhibition of phosphatidylcholine biosynthesis is caused by a decrease in cellular diacylglycerol levels in cultured rat hepatocytes. J Biol Chem **267**:1752-60.

137. **Jimenez-Lopez, J. M., M. P. Carrasco, J. L. Segovia, and C. Marco.** 2002. Hexadecylphosphocholine inhibits phosphatidylcholine biosynthesis and the proliferation of HepG2 cells. Eur J Biochem **269**:4649-55.

138. **Johansen, T., G. Bjorkoy, A. Overvatn, M. T. Diaz-Meco, T. Traavik, and J. Moscat.** 1994. NIH 3T3 cells stably transfected with the gene encoding phosphatidylcholine-hydrolyzing phospholipase C from Bacillus cereus acquire a transformed phenotype. Mol Cell Biol **14**:646-54.

139. **Johnson, J. E., R. Aebersold, and R. B. Cornell.** 1997. An amphipathic alpha-helix is the principle membrane-embedded region of CTP:phosphocholine cytidylyltransferase. Identification of the 3-(trifluoromethyl)-3-(m-[125I]iodophenyl) diazirine photolabeled domain. Biochim Biophys Acta **1324**:273-84.

140. **Johnson, J. E., N. M. Rao, S. W. Hui, and R. B. Cornell.** 1998. Conformation and lipid binding properties of four peptides derived from the membrane-binding domain of CTP:phosphocholine cytidylyltransferase. Biochemistry **37**:9509-19.

141. **Johnson, N., M. Krebs, R. Boudreau, G. Giorgi, M. LeGros, and C. Larabell.** 2003. Actin-filled nuclear invaginations indicate degree of cell de-differentiation. Differentiation **71**:414-24.

142. **Johnstone, R. W., A. A. Ruefli, and S. W. Lowe.** 2002. Apoptosis: a link between cancer genetics and chemotherapy. Cell **108**:153-64.

143. **Juin, P., A. O. Hueber, T. Littlewood, and G. Evan.** 1999. c-Myc-induced sensitization to apoptosis is mediated through cytochrome c release. Genes Dev **13**:1367-81.

144. **Jump, D. B.** 2004. Fatty acid regulation of gene transcription. Crit Rev Clin Lab Sci **41**:41-78.

145. **Kalmar, G. B., R. J. Kay, A. Lachance, R. Aebersold, and R. B. Cornell.** 1990. Cloning and expression of rat liver CTP: phosphocholine cytidylyltransferase: an amphipathic protein that controls phosphatidylcholine synthesis. Proc Natl Acad Sci U S A **87**:6029-33.

146. **Kalmar, G. B., R. J. Kay, A. C. LaChance, and R. B. Cornell.** 1994. Primary structure and expression of a human CTP:phosphocholine cytidylyltransferase. Biochim Biophys Acta **1219**:328-34.

147. **Karim, M., P. Jackson, and S. Jackowski.** 2003. Gene structure, expression and identification of a new CTP:phosphocholine cytidylyltransferase beta isoform. Biochim Biophys Acta **1633**:1-12.

148. **Kasai, T., K. Ohguchi, S. Nakashima, Y. Ito, T. Naganawa, N. Kondo, and Y. Nozawa.** 1998. Increased activity of oleate-dependent type phospholipase D during actinomycin D-induced apoptosis in Jurkat T cells. J Immunol **161:**6469-74.

149. **Kast, H. R., C. M. Nguyen, A. M. Anisfeld, J. Ericsson, and P. A. Edwards.** 2001. CTP:phosphocholine cytidylyltransferase, a new sterol- and SREBP-responsive gene. J Lipid Res **42:**1266-72.

150. **Kennedy, E. P., and S. B. Weiss.** 1956. The function of cytidine coenzymes in the biosynthesis of phospholipides. J Biol Chem **222:**193-214.

151. **Kent, C.** 1997. CTP:phosphocholine cytidylyltransferase. Biochim Biophys Acta **1348:**79-90.

152. **Kent, C.** 1990. Regulation of phosphatidylcholine biosynthesis. Prog Lipid Res **29:**87-105.

153. **Kent, C., and G. M. Carman.** 1999. Interactions among pathways for phosphatidylcholine metabolism, CTP synthesis and secretion through the Golgi apparatus. Trends Biochem Sci **24:**146-50.

154. **Kent, C., G. M. Carman, M. W. Spence, and W. Dowhan.** 1991. Regulation of eukaryotic phospholipid metabolism. Faseb J **5:**2258-66.

155. **Kim, J. H., T. M. Lewin, and R. A. Coleman.** 2001. Expression and characterization of recombinant rat Acyl-CoA synthetases 1, 4, and 5. Selective inhibition by triacsin C and thiazolidinediones. J Biol Chem **276:**24667-73.

156. **Kiss, Z.** 1999. Regulation of mitogenesis by water-soluble phospholipid intermediates. Cell Signal **11:**149-57.

157. **Kuhajda, F. P., E. S. Pizer, J. N. Li, N. S. Mani, G. L. Frehywot, and C. A. Townsend.** 2000. Synthesis and antitumor activity of an inhibitor of fatty acid synthase. Proc Natl Acad Sci U S A **97:**3450-4.

158. **Lacal, J. C., J. Moscat, and S. A. Aaronson.** 1987. Novel source of 1,2-diacylglycerol elevated in cells transformed by Ha-ras oncogene. Nature **330:**269-72.

159. **Lagace, T. A., J. R. Miller, and N. D. Ridgway.** 2002. Caspase processing and nuclear export of CTP:phosphocholine cytidylyltransferase alpha during farnesol-induced apoptosis. Mol Cell Biol **22:**4851-62.

160. **Lagace, T. A., M. K. Storey, and N. D. Ridgway.** 2000. Regulation of phosphatidylcholine metabolism in Chinese hamster ovary cells by the sterol regulatory element-binding protein (SREBP)/SREBP cleavage-activating protein pathway. J Biol Chem **275:**14367-74.

161. **Lauber, K., E. Bohn, S. M. Krober, Y. J. Xiao, S. G. Blumenthal, R. K. Lindemann, P. Marini, C. Wiedig, A. Zobywalski, S. Baksh, Y. Xu, I. B. Autenrieth, K. Schulze-Osthoff, C. Belka, G. Stuhler, and S. Wesselborg.** 2003. Apoptotic cells induce migration of phagocytes via caspase-3-mediated release of a lipid attraction signal. Cell **113:**717-30.

162. **Lee, E., M. Marcucci, L. Daniell, M. Pypaert, O. A. Weisz, G. C. Ochoa, K. Farsad, M. R. Wenk, and P. De Camilli.** 2002. Amphiphysin 2 (Bin1) and T-tubule biogenesis in muscle. Science **297:**1193-6.

163. **Lee, S. Y., E. J. Yeo, and M. U. Choi.** 1998. Phospholipase D activity in L1210 cells: a model for oleate-activated phospholipase D in intact mammalian cells. Biochem Biophys Res Commun **244:**825-31.
164. **Lee, Y., S. M. Song, H. S. Park, S. Kim, E. H. Koh, M. S. Choi, and M. U. Choi.** 2002. Elevation of oleate-activated phospholipase D activity during thymic atrophy. Immunology **107:**435-43.
165. **Leslie, C. C.** 2004. Regulation of arachidonic acid availability for eicosanoid production. Biochem Cell Biol **82:**1-17.
166. **Lim, P., R. Cornell, and D. E. Vance.** 1986. The supply of both CDP-choline and diacylglycerol can regulate the rate of phosphatidylcholine synthesis in HeLa cells. Biochem Cell Biol **64:**692-8.
167. **Lippincott-Schwartz, J., and W. Liu.** 2003. Membrane trafficking: coat control by curvature. Nature **426:**507-8.
168. **Lowry, O. H., N. J. Rosebrough, A. L. Farr, and R. J. Randall.** 1951. Protein measurement with the Folin phenol reagent. J Biol Chem **193:**265-75.
169. **Lykidis, A., I. Baburina, and S. Jackowski.** 1999. Distribution of CTP:phosphocholine cytidylyltransferase (CCT) isoforms. Identification of a new CCTbeta splice variant. J Biol Chem **274:**26992-7001.
170. **Lykidis, A., P. Jackson, and S. Jackowski.** 2001. Lipid activation of CTP: phosphocholine cytidylyltransferase alpha: characterization and identification of a second activation domain. Biochemistry **40:**494-503.
171. **Lykidis, A., K. G. Murti, and S. Jackowski.** 1998. Cloning and characterization of a second human CTP:phosphocholine cytidylyltransferase. J Biol Chem **273:**14022-9.
172. **Lykidis, A., J. Wang, M. A. Karim, and S. Jackowski.** 2001. Overexpression of a mammalian ethanolamine-specific kinase accelerates the CDP-ethanolamine pathway. J Biol Chem **276:**2174-9.
173. **MacDonald, J. I., and C. Kent.** 1993. Baculovirus-mediated expression of rat liver CTP:phosphocholine cytidylyltransferase. Protein Expr Purif **4:**1-7.
174. **MacDonald, J. I., and C. Kent.** 1994. Identification of phosphorylation sites in rat liver CTP: phosphocholine cytidylyltransferase. J Biol Chem **269:**10529-37.
175. **Machida, K., T. Tanaka, Y. Yano, S. Otani, and M. Taniguchi.** 1999. Farnesol-induced growth inhibition in Saccharomyces cerevisiae by a cell cycle mechanism. Microbiology **145:**293-9.
176. **Mallampalli, R. K., A. J. Ryan, J. L. Carroll, T. F. Osborne, and C. P. Thomas.** 2002. Lipid deprivation increases surfactant phosphatidylcholine synthesis via a sterol-sensitive regulatory element within the CTP:phosphocholine cytidylyltransferase promoter. Biochem J **362:**81-8.
177. **Mantel, C. R., A. R. Schulz, K. Miyazawa, and H. E. Broxmeyer.** 1993. Kinetic selectivity of cholinephosphotransferase in mouse liver: the Km for CDP-choline depends on diacylglycerol structure. Biochem J **289 (Pt 3):**815-20.
178. **Marelli, M., C. P. Lusk, H. Chan, J. D. Aitchison, and R. W. Wozniak.** 2001. A link between the synthesis of nucleoporins and the biogenesis of the nuclear envelope. J Cell Biol **153:**709-24.
179. **Massenburg, D., J. S. Han, M. Liyanage, W. A. Patton, S. G. Rhee, J. Moss, and M. Vaughan.** 1994. Activation of rat brain phospholipase D by ADP-

ribosylation factors 1,5, and 6: separation of ADP-ribosylation factor-dependent and oleate-dependent enzymes. Proc Natl Acad Sci U S A **91:**11718-22.

180. **Masuda, Y., M. Yoda, H. Ohizumi, T. Aiuchi, M. Watabe, S. Nakajo, and K. Nakaya.** 1997. Activation of protein kinase C prevents induction of apoptosis by geranylgeraniol in human leukemia HL60 cells. Int J Cancer **71:**691-7.
181. **McDermott, M., M. J. Wakelam, and A. J. Morris.** 2004. Phospholipase D. Biochem Cell Biol **82:**225-53.
182. **McIntosh, T. J.** 1996. Hydration properties of lamellar and non-lamellar phases of phosphatidylcholine and phosphatidylethanolamine. Chem Phys Lipids **81:**117-31.
183. **Meigs, T. E., and R. D. Simoni.** 1997. Farnesol as a regulator of HMG-CoA reductase degradation: characterization and role of farnesyl pyrophosphatase. Arch Biochem Biophys **345:**1-9.
184. **Meng, A., C. Luberto, P. Meier, A. Bai, X. Yang, Y. A. Hannun, and D. Zhou.** 2004. Sphingomyelin synthase as a potential target for D609-induced apoptosis in U937 human monocytic leukemia cells. Exp Cell Res **292:**385-92.
185. **Miles, E. W., S. Rhee, and D. R. Davies.** 1999. The molecular basis of substrate channeling. J Biol Chem **274:**12193-6.
186. **Miquel, K., A. Pradines, F. Terce, S. Selmi, and G. Favre.** 1998. Competitive inhibition of choline phosphotransferase by geranylgeraniol and farnesol inhibits phosphatidylcholine synthesis and induces apoptosis in human lung adenocarcinoma A549 cells. J Biol Chem **273:**26179-86.
187. **Moir, R. D., M. Yoon, S. Khuon, and R. D. Goldman.** 2000. Nuclear lamins A and B1: different pathways of assembly during nuclear envelope formation in living cells. J Cell Biol **151:**1155-68.
188. **Mui, B. L., H. G. Dobereiner, T. D. Madden, and P. R. Cullis.** 1995. Influence of transbilayer area asymmetry on the morphology of large unilamellar vesicles. Biophys J **69:**930-41.
189. **Muir, J. G., and A. W. Murray.** 1986. Mimicry of phorbol ester responses by diacylglycerols. Differential effects on phosphatidylcholine biosynthesis, cell-cell communication and epidermal growth factor binding. Biochim Biophys Acta **885:**176-84.
190. **Nakaya, M., Y. Masuda, S. Mihara, T. Aiuchi, T. Shibayama-Imazu, S. Nakajo, and K. Nakaya.** 1999. Analysis of caspases that are activated during apoptosis in leukemia U937 cells in response to geranylgeraniol. Anticancer Res **19:**5063-8.
191. **Neri, L. M., Y. Raymond, A. Giordano, S. Capitani, and A. M. Martelli.** 1999. Lamin A is part of the internal nucleoskeleton of human erythroleukemia cells. J Cell Physiol **178:**284-95.
192. **Newton, A. C.** 1997. Regulation of protein kinase C. Curr Opin Cell Biol **9:**161-7.
193. **Nohturfft, A., M. S. Brown, and J. L. Goldstein.** 1998. Sterols regulate processing of carbohydrate chains of wild-type SREBP cleavage-activating protein (SCAP), but not sterol-resistant mutants Y298C or D443N. Proc Natl Acad Sci U S A **95:**12848-53.

194. **Nohturfft, A., M. S. Brown, and J. L. Goldstein.** 1998. Topology of SREBP cleavage-activating protein, a polytopic membrane protein with a sterol-sensing domain. J Biol Chem **273:**17243-50.
195. **Nohturfft, A., R. A. DeBose-Boyd, S. Scheek, J. L. Goldstein, and M. S. Brown.** 1999. Sterols regulate cycling of SREBP cleavage-activating protein (SCAP) between endoplasmic reticulum and Golgi. Proc Natl Acad Sci U S A **96:**11235-40.
196. **Northwood, I. C., A. H. Tong, B. Crawford, A. E. Drobnies, and R. B. Cornell.** 1999. Shuttling of CTP:Phosphocholine cytidylyltransferase between the nucleus and endoplasmic reticulum accompanies the wave of phosphatidylcholine synthesis during the G(0) --> G(1) transition. J Biol Chem **274:**26240-8.
197. **Nyormoi, O., Z. Wang, D. Doan, M. Ruiz, D. McConkey, and M. Bar-Eli.** 2001. Transcription factor AP-2alpha is preferentially cleaved by caspase 6 and degraded by proteasome during tumor necrosis factor alpha-induced apoptosis in breast cancer cells. Mol Cell Biol **21:**4856-67.
198. **Orth, K., A. M. Chinnaiyan, M. Garg, C. J. Froelich, and V. M. Dixit.** 1996. The CED-3/ICE-like protease Mch2 is activated during apoptosis and cleaves the death substrate lamin A. J Biol Chem **271:**16443-6.
199. **Ou, J., H. Tu, B. Shan, A. Luk, R. A. DeBose-Boyd, Y. Bashmakov, J. L. Goldstein, and M. S. Brown.** 2001. Unsaturated fatty acids inhibit transcription of the sterol regulatory element-binding protein-1c (SREBP-1c) gene by antagonizing ligand-dependent activation of the LXR. Proc Natl Acad Sci U S A **98:**6027-32.
200. **Ovadi, J.** 1991. Physiological significance of metabolic channelling. J Theor Biol **152:**1-22.
201. **Parekh, D. B., W. Ziegler, and P. J. Parker.** 2000. Multiple pathways control protein kinase C phosphorylation. Embo J **19:**496-503.
202. **Park, Y. S., P. Gee, S. Sanker, E. J. Schurter, E. R. Zuiderweg, and C. Kent.** 1997. Identification of functional conserved residues of CTP:glycerol-3-phosphate cytidylyltransferase. Role of histidines in the conserved HXGH in catalysis. J Biol Chem **272:**15161-6.
203. **Pattridge, K. A., C. H. Weber, J. A. Friesen, S. Sanker, C. Kent, and M. L. Ludwig.** 2003. Glycerol-3-phosphate cytidylyltransferase. Structural changes induced by binding of CDP-glycerol and the role of lysine residues in catalysis. J Biol Chem **278:**51863-71.
204. **Pelech, S. L., H. B. Paddon, and D. E. Vance.** 1984. Phorbol esters stimulate phosphatidylcholine biosynthesis by translocation of CTP:phosphocholine cytidylyltransferase from cytosol to microsomes. Biochim Biophys Acta **795:**447-51.
205. **Pelech, S. L., P. H. Pritchard, D. N. Brindley, and D. E. Vance.** 1983. Fatty acids promote translocation of CTP:phosphocholine cytidylyltransferase to the endoplasmic reticulum and stimulate rat hepatic phosphatidylcholine synthesis. J Biol Chem **258:**6782-8.
206. **Perry, R. J., and N. D. Ridgway.** 2004. The role of de novo ceramide synthesis in the mechanism of action of the tricyclic xanthate D609. J Lipid Res **45:**164-73.

207. **Pessin, M. S., J. J. Baldassare, and D. M. Raben.** 1990. Molecular species analysis of mitogen-stimulated 1,2-diglycerides in fibroblasts. Comparison of alpha-thrombin, epidermal growth factor, and platelet-derived growth factor. J Biol Chem **265:**7959-66.

208. **Pessin, M. S., and D. M. Raben.** 1989. Molecular species analysis of 1,2-diglycerides stimulated by alpha-thrombin in cultured fibroblasts. J Biol Chem **264:**8729-38.

209. **Peter, B. J., H. M. Kent, I. G. Mills, Y. Vallis, P. J. Butler, P. R. Evans, and H. T. McMahon.** 2004. BAR domains as sensors of membrane curvature: the amphiphysin BAR structure. Science **303:**495-9.

210. **Pizer, E. S., F. J. Chrest, J. A. DiGiuseppe, and W. F. Han.** 1998. Pharmacological inhibitors of mammalian fatty acid synthase suppress DNA replication and induce apoptosis in tumor cell lines. Cancer Res **58:**4611-5.

211. **Preiss, J., C. R. Loomis, W. R. Bishop, R. Stein, J. E. Niedel, and R. M. Bell.** 1986. Quantitative measurement of sn-1,2-diacylglycerols present in platelets, hepatocytes, and ras- and sis-transformed normal rat kidney cells. J Biol Chem **261:**8597-600.

212. **Prescott, S. M., and R. L. White.** 1996. Self-promotion? Intimate connections between APC and prostaglandin H synthase-2. Cell **87:**783-6.

213. **Price, A. C., K. H. Choi, R. J. Heath, Z. Li, S. W. White, and C. O. Rock.** 2001. Inhibition of beta-ketoacyl-acyl carrier protein synthases by thiolactomycin and cerulenin. Structure and mechanism. J Biol Chem **276:**6551-9.

214. **Profant, D. A., C. J. Roberts, and R. L. Wright.** 2000. Mutational analysis of the karmellae-inducing signal in Hmg1p, a yeast HMG-CoA reductase isozyme. Yeast **16:**811-27.

215. **Raben, D. M., M. S. Pessin, L. A. Rangan, and T. M. Wright.** 1990. Kinetic and molecular species analyses of mitogen-induced increases in diglycerides: evidence for stimulated hydrolysis of phosphoinositides and phosphatidylcholine. J Cell Biochem **44:**117-25.

216. **Ramos, B., M. El Mouedden, E. Claro, and S. Jackowski.** 2002. Inhibition of CTP:phosphocholine cytidylyltransferase by C(2)-ceramide and its relationship to apoptosis. Mol Pharmacol **62:**1068-75.

217. **Ratnam, S., and C. Kent.** 1995. Early increase in choline kinase activity upon induction of the H-ras oncogene in mouse fibroblast cell lines. Arch Biochem Biophys **323:**313-22.

218. **Rawson, R. B., N. G. Zelenski, D. Nijhawan, J. Ye, J. Sakai, M. T. Hasan, T. Y. Chang, M. S. Brown, and J. L. Goldstein.** 1997. Complementation cloning of S2P, a gene encoding a putative metalloprotease required for intramembrane cleavage of SREBPs. Mol Cell **1:**47-57.

219. **Reo, N. V., M. Adinehzadeh, and B. D. Foy.** 2002. Kinetic analyses of liver phosphatidylcholine and phosphatidylethanolamine biosynthesis using (13)C NMR spectroscopy. Biochim Biophys Acta **1580:**171-88.

220. **Rhee, S. G., and Y. S. Bae.** 1997. Regulation of phosphoinositide-specific phospholipase C isozymes. J Biol Chem **272:**15045-8.

221. **Ridgway, N. D., D. M. Byers, H. W. Cook, and M. K. Storey.** 1999. Integration of phospholipid and sterol metabolism in mammalian cells. Prog Lipid Res **38:**337-60.
222. **Ridgway, N. D., and T. A. Lagace.** 2003. Regulation of the CDP-choline pathway by sterol regulatory element binding proteins involves transcriptional and post-transcriptional mechanisms. Biochem J **372:**811-9.
223. **Ridsdale, R., I. Tseu, J. Wang, and M. Post.** 2001. CTP:phosphocholine cytidylyltransferase alpha is a cytosolic protein in pulmonary epithelial cells and tissues. J Biol Chem **276:**49148-55.
224. **Rioja, A., A. R. Pizzey, C. M. Marson, and N. S. Thomas.** 2000. Preferential induction of apoptosis of leukaemic cells by farnesol. FEBS Lett **467:**291-5.
225. **Roche, E., J. Buteau, I. Aniento, J. A. Reig, B. Soria, and M. Prentki.** 1999. Palmitate and oleate induce the immediate-early response genes c-fos and nur-77 in the pancreatic beta-cell line INS-1. Diabetes **48:**2007-14.
226. **Ruchaud, S., N. Korfali, P. Villa, T. J. Kottke, C. Dingwall, S. H. Kaufmann, and W. C. Earnshaw.** 2002. Caspase-6 gene disruption reveals a requirement for lamin A cleavage in apoptotic chromatin condensation. Embo J **21:**1967-77.
227. **Rutherford, M. S., C. O. Rock, N. A. Jenkins, D. J. Gilbert, T. G. Tessner, N. G. Copeland, and S. Jackowski.** 1993. The gene for murine CTP:phosphocholine cytidylyltransferase (Ctpct) is located on mouse chromosome 16. Genomics **18:**698-701.
228. **Ryan, A. J., K. Fisher, C. P. Thomas, and R. K. Mallampalli.** 2004. Transcriptional repression of the CTP:phosphocholine cytidylyltransferase gene by sphingosine. Biochem J **Pt.**
229. **Ryan, A. J., D. M. McCoy, S. N. Mathur, F. J. Field, and R. K. Mallampalli.** 2000. Lipoprotein deprivation stimulates transcription of the CTP:phosphocholine cytidylyltransferase gene. J Lipid Res **41:**1268-77.
230. **Sakai, J., E. A. Duncan, R. B. Rawson, X. Hua, M. S. Brown, and J. L. Goldstein.** 1996. Sterol-regulated release of SREBP-2 from cell membranes requires two sequential cleavages, one within a transmembrane segment. Cell **85:**1037-46.
231. **Sakai, J., A. Nohturfft, D. Cheng, Y. K. Ho, M. S. Brown, and J. L. Goldstein.** 1997. Identification of complexes between the COOH-terminal domains of sterol regulatory element-binding proteins (SREBPs) and SREBP cleavage-activating protein. J Biol Chem **272:**20213-21.
232. **Sakai, J., R. B. Rawson, P. J. Espenshade, D. Cheng, A. C. Seegmiller, J. L. Goldstein, and M. S. Brown.** 1998. Molecular identification of the sterol-regulated luminal protease that cleaves SREBPs and controls lipid composition of animal cells. Mol Cell **2:**505-14.
233. **Sakamuro, D., V. Eviner, K. J. Elliott, L. Showe, E. White, and G. C. Prendergast.** 1995. c-Myc induces apoptosis in epithelial cells by both p53-dependent and p53-independent mechanisms. Oncogene **11:**2411-8.
234. **Salina, D., K. Bodoor, D. M. Eckley, T. A. Schroer, J. B. Rattner, and B. Burke.** 2002. Cytoplasmic dynein as a facilitator of nuclear envelope breakdown. Cell **108:**97-107.

235. **Samadder, P., C. Richards, R. Bittman, R. P. Bhullar, and G. Arthur.** 2003. The antitumor ether lipid 1-Q-octadecyl-2-O-methyl-rac-glycerophosphocholine (ET-18-OCH3) inhibits the association between Ras and Raf-1. Anticancer Res **23:**2291-5.
236. **Sanghera, J. S., and D. E. Vance.** 1989. Stimulation of CTP: phosphocholine cytidylyltransferase and phosphatidylcholine synthesis by calcium in rat hepatocytes. Biochim Biophys Acta **1003:**284-92.
237. **Savill, J., and V. Fadok.** 2000. Corpse clearance defines the meaning of cell death. Nature **407:**784-8.
238. **Schirmer, E. C., T. Guan, and L. Gerace.** 2001. Involvement of the lamin rod domain in heterotypic lamin interactions important for nuclear organization. J Cell Biol **153:**479-89.
239. **Sheetz, M. P., and S. J. Singer.** 1974. Biological membranes as bilayer couples. A molecular mechanism of drug-erythrocyte interactions. Proc Natl Acad Sci U S A **71:**4457-61.
240. **Shiratori, Y., M. Houweling, X. Zha, and I. Tabas.** 1995. Stimulation of CTP:phosphocholine cytidylyltransferase by free cholesterol loading of macrophages involves signaling through protein dephosphorylation. J Biol Chem **270:**29894-903.
241. **Shumaker, D. K., E. R. Kuczmarski, and R. D. Goldman.** 2003. The nucleoskeleton: lamins and actin are major players in essential nuclear functions. Curr Opin Cell Biol **15:**358-66.
242. **Simbulan-Rosenthal, C. M., D. S. Rosenthal, S. Iyer, H. Boulares, and M. E. Smulson.** 1999. Involvement of PARP and poly(ADP-ribosyl)ation in the early stages of apoptosis and DNA replication. Mol Cell Biochem **193:**137-48.
243. **Slee, E. A., C. Adrain, and S. J. Martin.** 2001. Executioner caspase-3, -6, and -7 perform distinct, non-redundant roles during the demolition phase of apoptosis. J Biol Chem **276:**7320-6.
244. **Sleight, R., and C. Kent.** 1983. Regulation of phosphatidylcholine biosynthesis in mammalian cells. II. Effects of phospholipase C treatment on the activity and subcellular distribution of CTP:phosphocholine cytidylyltransferase in Chinese hamster ovary and LM cell lines. J Biol Chem **258:**831-5.
245. **Smith, E. B.** 1974. The relationship between plasma and tissue lipids in human atherosclerosis. Adv Lipid Res **12:**1-49.
246. **Snapp, E. L., R. S. Hegde, M. Francolini, F. Lombardo, S. Colombo, E. Pedrazzini, N. Borgese, and J. Lippincott-Schwartz.** 2003. Formation of stacked ER cisternae by low affinity protein interactions. J Cell Biol **163:**257-69.
247. **Sohal, P. S., and R. B. Cornell.** 1990. Sphingosine inhibits the activity of rat liver CTP:phosphocholine cytidylyltransferase. J Biol Chem **265:**11746-50.
248. **Sorensen, V., A. Brech, D. Khnykin, E. Kolpakova, L. Citores, and S. Olsnes.** 2004. Deletion mutant of FGFR4 induces onion-like membrane structures in the nucleus. J Cell Sci **117:**1807-19.
249. **Srere, P. A.** 1987. Complexes of sequential metabolic enzymes. Annu Rev Biochem **56:**89-124.
250. **Storey, M. K., D. M. Byers, H. W. Cook, and N. D. Ridgway.** 1997. Decreased phosphatidylcholine biosynthesis and abnormal distribution of

CTP:phosphocholine cytidylyltransferase in cholesterol auxotrophic Chinese hamster ovary cells. J Lipid Res **38:**711-22.

251. **Storey, M. K., K. L. Clay, T. Kutateladze, R. C. Murphy, M. Overduin, and D. R. Voelker.** 2001. Phosphatidylethanolamine has an essential role in Saccharomyces cerevisiae that is independent of its ability to form hexagonal phase structures. J Biol Chem **276:**48539-48.
252. **Sugimoto, H., M. Bakovic, S. Yamashita, and D. E. Vance.** 2001. Identification of transcriptional enhancer factor-4 as a transcriptional modulator of CTP:phosphocholine cytidylyltransferase alpha. J Biol Chem **276:**12338-44.
253. **Sugimoto, H., S. Sugimoto, K. Tatei, H. Obinata, M. Bakovic, T. Izumi, and D. E. Vance.** 2003. Identification of Ets-1 as an important transcriptional activator of CTP:phosphocholine cytidylyltransferase alpha in COS-7 cells and co-activation with transcriptional enhancer factor-4. J Biol Chem **278:**19716-22.
254. **Sweitzer, T. D., and C. Kent.** 1994. Expression of wild-type and mutant rat liver CTP: phosphocholine cytidylyltransferase in a cytidylyltransferase-deficient Chinese hamster ovary cell line. Arch Biochem Biophys **311:**107-16.
255. **Tabas, I.** 2002. Consequences of cellular cholesterol accumulation: basic concepts and physiological implications. J Clin Invest **110:**905-11.
256. **Taneva, S., J. E. Johnson, and R. B. Cornell.** 2003. Lipid-induced conformational switch in the membrane binding domain of CTP:phosphocholine cytidylyltransferase: a circular dichroism study. Biochemistry **42:**11768-76.
257. **Tang, W., G. A. Keesler, and I. Tabas.** 1997. The structure of the gene for murine CTP:phosphocholine cytidylyltransferase, Ctpct. Relationship of exon structure to functional domains and identification of transcriptional start sites and potential upstream regulatory elements. J Biol Chem **272:**13146-51.
258. **Terce, F., H. Brun, and D. E. Vance.** 1994. Requirement of phosphatidylcholine for normal progression through the cell cycle in C3H/10T1/2 fibroblasts. J Lipid Res **35:**2130-42.
259. **Terzakis, J. A.** 1965. The nucleolar channel system of human endometrium. J Cell Biol **27:**293-304.
260. **Tessner, T. G., C. O. Rock, G. B. Kalmar, R. B. Cornell, and S. Jackowski.** 1991. Colony-stimulating factor 1 regulates CTP: phosphocholine cytidylyltransferase mRNA levels. J Biol Chem **266:**16261-4.
261. **Thornberry, N. A., and Y. Lazebnik.** 1998. Caspases: enemies within. Science **281:**1312-6.
262. **Thornberry, N. A., T. A. Rano, E. P. Peterson, D. M. Rasper, T. Timkey, M. Garcia-Calvo, V. M. Houtzager, P. A. Nordstrom, S. Roy, J. P. Vaillancourt, K. T. Chapman, and D. W. Nicholson.** 1997. A combinatorial approach defines specificities of members of the caspase family and granzyme B. Functional relationships established for key mediators of apoptosis. J Biol Chem **272:**17907-11.
263. **Tomoda, H., K. Igarashi, J. C. Cyong, and S. Omura.** 1991. Evidence for an essential role of long chain acyl-CoA synthetase in animal cell proliferation. Inhibition of long chain acyl-CoA synthetase by triacsins caused inhibition of Raji cell proliferation. J Biol Chem **266:**4214-9.

264. **Topham, M. K., M. Bunting, G. A. Zimmerman, T. M. McIntyre, P. J. Blackshear, and S. M. Prescott.** 1998. Protein kinase C regulates the nuclear localization of diacylglycerol kinase-zeta. Nature **394:**697-700.
265. **Topham, M. K., and S. M. Prescott.** 2002. Diacylglycerol kinases: regulation and signaling roles. Thromb Haemost **88:**912-8.
266. **Toth, M.** 1993. Attenuation of diacylglycerol signal in the primordial human placenta: role of phosphatidylcholine formation. Biochim Biophys Acta **1210:**105-12.
267. **Travers, K. J., C. K. Patil, L. Wodicka, D. J. Lockhart, J. S. Weissman, and P. Walter.** 2000. Functional and genomic analyses reveal an essential coordination between the unfolded protein response and ER-associated degradation. Cell **101:**249-58.
268. **Tronchere, H., M. Record, F. Terce, and H. Chap.** 1994. Phosphatidylcholine cycle and regulation of phosphatidylcholine biosynthesis by enzyme translocation. Biochim Biophys Acta **1212:**137-51.
269. **Tseu, I., R. Ridsdale, J. Liu, J. Wang, and M. Post.** 2002. Cell cycle regulation of pulmonary phosphatidylcholine synthesis. Am J Respir Cell Mol Biol **26:**506-15.
270. **Tso, J. Y., X. H. Sun, T. H. Kao, K. S. Reece, and R. Wu.** 1985. Isolation and characterization of rat and human glyceraldehyde-3-phosphate dehydrogenase cDNAs: genomic complexity and molecular evolution of the gene. Nucleic Acids Res **13:**2485-502.
271. **Tsujii, M., and R. N. DuBois.** 1995. Alterations in cellular adhesion and apoptosis in epithelial cells overexpressing prostaglandin endoperoxide synthase 2. Cell **83:**493-501.
272. **Utal, A. K., H. Jamil, and D. E. Vance.** 1991. Diacylglycerol signals the translocation of CTP:choline-phosphate cytidylyltransferase in HeLa cells treated with 12-O- tetradecanoylphorbol-13-acetate. J Biol Chem **266:**24084-91.
273. **van den Bosch, H.** 1974. Phosphoglyceride metabolism. Annu Rev Biochem **43:**243-77.
274. **van der Sanden, M. H., M. Houweling, L. M. van Golde, and A. B. Vaandrager.** 2003. Inhibition of phosphatidylcholine synthesis induces expression of the endoplasmic reticulum stress and apoptosis-related protein CCAAT/enhancer-binding protein-homologous protein (CHOP/GADD153). Biochem J **369:**643-50.
275. **Vance, D. E., and J. E. Vance (ed.).** 2002. Biochemistry of lipids, lipoproteins, and membranes, 4th ed. Elsevier Science, Amsterdam.
276. **Vance, D. E., C. J. Walkey, and Z. Cui.** 1997. Phosphatidylethanolamine N-methyltransferase from liver. Biochim Biophys Acta **1348:**142-50.
277. **Veitch, D. P., D. Gilham, and R. B. Cornell.** 1998. The role of histidine residues in the HXGH site of CTP:phosphocholine cytidylyltransferase in CTP binding and catalysis. Eur J Biochem **255:**227-34.
278. **Vlcek, S., B. Korbei, and R. Foisner.** 2002. Distinct functions of the unique C terminus of LAP2alpha in cell proliferation and nuclear assembly. J Biol Chem **277:**18898-907.

279. **Voziyan, P. A., C. M. Goldner, and G. Melnykovych.** 1993. Farnesol inhibits phosphatidylcholine biosynthesis in cultured cells by decreasing cholinephosphotransferase activity. Biochem J **295:**757-62.
280. **Voziyan, P. A., J. S. Haug, and G. Melnykovych.** 1995. Mechanism of farnesol cytotoxicity: further evidence for the role of PKC-dependent signal transduction in farnesol-induced apoptotic cell death. Biochem Biophys Res Commun **212:**479-86.
281. **Waite, K. A., and D. E. Vance.** 2000. Why expression of phosphatidylethanolamine N-methyltransferase does not rescue Chinese hamster ovary cells that have an impaired CDP-choline pathway. J Biol Chem **275:**21197-202.
282. **Wakelam, M. J.** 1998. Diacylglycerol--when is it an intracellular messenger? Biochim Biophys Acta **1436:**117-26.
283. **Wakelam, M. J., C. P. Briscoe, A. Stewart, T. R. Pettitt, M. J. Cross, A. Paul, J. M. Yule, S. D. Gardner, and M. Hodgkin.** 1993. Phosphatidylcholine hydrolysis: a source of multiple lipid messenger molecules. Biochem Soc Trans **21:**874-7.
284. **Walkey, C. J., G. B. Kalmar, and R. B. Cornell.** 1994. Overexpression of rat liver CTP:phosphocholine cytidylyltransferase accelerates phosphatidylcholine synthesis and degradation. J Biol Chem **269:**5742-9.
285. **Wang, A., and E. A. Dennis.** 1999. Mammalian lysophospholipases. Biochim Biophys Acta **1439:**1-16.
286. **Wang, Y., and C. Kent.** 1995. Effects of altered phosphorylation sites on the properties of CTP:phosphocholine cytidylyltransferase. J Biol Chem **270:**17843-9.
287. **Wang, Y., and C. Kent.** 1995. Identification of an inhibitory domain of CTP:phosphocholine cytidylyltransferase. J Biol Chem **270:**18948-52.
288. **Wang, Y., J. I. MacDonald, and C. Kent.** 1995. Identification of the nuclear localization signal of rat liver CTP:phosphocholine cytidylyltransferase. J Biol Chem **270:**354-60.
289. **Wang, Y., J. I. MacDonald, and C. Kent.** 1993. Regulation of CTP:phosphocholine cytidylyltransferase in HeLa cells. Effect of oleate on phosphorylation and intracellular localization. J Biol Chem **268:**5512-8.
290. **Wang, Y., T. D. Sweitzer, P. A. Weinhold, and C. Kent.** 1993. Nuclear localization of soluble CTP:phosphocholine cytidylyltransferase. J Biol Chem **268:**5899-904.
291. **Warden, C. H., and M. Friedkin.** 1985. Regulation of choline kinase activity and phosphatidylcholine biosynthesis by mitogenic growth factors in 3T3 fibroblasts. J Biol Chem **260:**6006-11.
292. **Watkins, J. D., and C. Kent.** 1992. Immunolocalization of membrane-associated CTP:phosphocholine cytidylyltransferase in phosphatidylcholine-deficient Chinese hamster ovary cells. J Biol Chem **267:**5686-92.
293. **Watkins, J. D., and C. Kent.** 1991. Regulation of CTP:phosphocholine cytidylyltransferase activity and subcellular location by phosphorylation in Chinese hamster ovary cells. The effect of phospholipase C treatment. J Biol Chem **266:**21113-7.

294. **Weber, C. H., Y. S. Park, S. Sanker, C. Kent, and M. L. Ludwig.** 1999. A prototypical cytidylyltransferase: CTP:glycerol-3-phosphate cytidylyltransferase from bacillus subtilis. Structure Fold Des **7:**1113-24.

295. **Weinhold, P. A., D. A. Feldman, M. M. Quade, J. C. Miller, and R. L. Brooks.** 1981. Evidence for a regulatory role of CTP : choline phosphate cytidylyltransferase in the synthesis of phosphatidylcholine in fetal lung following premature birth. Biochim Biophys Acta **665:**134-44.

296. **Weinhold, P. A., M. E. Rounsifer, L. Charles, and D. A. Feldman.** 1989. Characterization of cytosolic forms of CTP: choline-phosphate cytidylyltransferase in lung, isolated alveolar type II cells, A549 cell and Hep G2 cells. Biochim Biophys Acta **1006:**299-310.

297. **Weinhold, P. A., M. E. Rounsifer, and D. A. Feldman.** 1986. The purification and characterization of CTP:phosphorylcholine cytidylyltransferase from rat liver. J Biol Chem **261:**5104-10.

298. **Weiss, S. B., S. W. Smith, and E. P. Kennedy.** 1958. The enzymatic formation of lecithin from cytidine diphosphate choline and D-1,2-diglyceride. J Biol Chem **231:**53-64.

299. **Whatley, R. E., K. Satoh, G. A. Zimmerman, T. M. McIntyre, and S. M. Prescott.** 1994. Proliferation-dependent changes in release of arachidonic acid from endothelial cells. J Clin Invest **94:**1889-900.

300. **Whatley, R. E., E. D. Stroud, M. Bunting, G. A. Zimmerman, T. M. McIntyre, and S. M. Prescott.** 1993. Growth-dependent changes in arachidonic acid release from endothelial cells are mediated by protein kinase C and changes in diacylglycerol. J Biol Chem **268:**16130-8.

301. **Wieder, T., C. E. Orfanos, and C. C. Geilen.** 1998. Induction of ceramide-mediated apoptosis by the anticancer phospholipid analog, hexadecylphosphocholine. J Biol Chem **273:**11025-31.

302. **Wieprecht, M., T. Wieder, C. C. Geilen, and C. E. Orfanos.** 1994. Growth factors stimulate phosphorylation of CTP:phosphocholine cytidylyltransferase in HeLa cells. FEBS Lett **353:**221-4.

303. **Wieprecht, M., T. Wieder, C. Paul, C. C. Geilen, and C. E. Orfanos.** 1996. Evidence for phosphorylation of CTP:phosphocholine cytidylyltransferase by multiple proline-directed protein kinases. J Biol Chem **271:**9955-61.

304. **Williams, S. N., M. L. Anthony, and K. M. Brindle.** 1998. Induction of apoptosis in two mammalian cell lines results in increased levels of fructose-1,6-bisphosphate and CDP-choline as determined by 31P MRS. Magn Reson Med **40:**411-20.

305. **Winrow, C. J., M. L. Hemming, D. M. Allen, G. B. Quistad, J. E. Casida, and C. Barlow.** 2003. Loss of neuropathy target esterase in mice links organophosphate exposure to hyperactivity. Nat Genet **33:**477-85.

306. **Wolf, B. B., and D. R. Green.** 1999. Suicidal tendencies: apoptotic cell death by caspase family proteinases. J Biol Chem **274:**20049-52.

307. **Wright, M. M., A. L. Henneberry, T. A. Lagace, N. D. Ridgway, and C. R. McMaster.** 2001. Uncoupling farnesol-induced apoptosis from its inhibition of phosphatidylcholine synthesis. J Biol Chem **276:**25254-61.

308. **Wright, P. S., J. N. Morand, and C. Kent.** 1985. Regulation of phosphatidylcholine biosynthesis in Chinese hamster ovary cells by reversible membrane association of CTP: phosphocholine cytidylyltransferase. J Biol Chem **260:**7919-26.
309. **Wright, R., M. Basson, L. D'Ari, and J. Rine.** 1988. Increased amounts of HMG-CoA reductase induce "karmellae": a proliferation of stacked membrane pairs surrounding the yeast nucleus. J Cell Biol **107:**101-14.
310. **Wyles, J. P., C. R. McMaster, and N. D. Ridgway.** 2002. Vesicle-associated membrane protein-associated protein-A (VAP-A) interacts with the oxysterol-binding protein to modify export from the endoplasmic reticulum. J Biol Chem **277:**29908-18.
311. **Xie, M., J. L. Smith, Z. Ding, D. Zhang, and R. B. Cornell.** 2004. Membrane binding modulates the quaternary structure of CTP: Phosphocholine cytidylyltransferase. J Biol Chem.
312. **Yabe, D., M. S. Brown, and J. L. Goldstein.** 2002. Insig-2, a second endoplasmic reticulum protein that binds SCAP and blocks export of sterol regulatory element-binding proteins. Proc Natl Acad Sci U S A **99:**12753-8.
313. **Yabe, D., R. Komuro, G. Liang, J. L. Goldstein, and M. S. Brown.** 2003. Liver-specific mRNA for Insig-2 down-regulated by insulin: implications for fatty acid synthesis. Proc Natl Acad Sci U S A **100:**3155-60.
314. **Yabe, D., Z. P. Xia, C. M. Adams, and R. B. Rawson.** 2002. Three mutations in sterol-sensing domain of SCAP block interaction with insig and render SREBP cleavage insensitive to sterols. Proc Natl Acad Sci U S A **99:**16672-7.
315. **Yamamoto, A., R. Masaki, and Y. Tashiro.** 1996. Formation of crystalloid endoplasmic reticulum in COS cells upon overexpression of microsomal aldehyde dehydrogenase by cDNA transfection. J Cell Sci **109 (Pt 7):**1727-38.
316. **Yamashita, A., T. Sugiura, and K. Waku.** 1997. Acyltransferases and transacylases involved in fatty acid remodeling of phospholipids and metabolism of bioactive lipids in mammalian cells. J Biochem (Tokyo) **122:**1-16.
317. **Yang, J., J. Wang, I. Tseu, M. Kuliszewski, W. Lee, and M. Post.** 1997. Identification of an 11-residue portion of CTP-phosphocholine cytidylyltransferase that is required for enzyme-membrane interactions. Biochem J **325:**29-38.
318. **Yang, L., T. Guan, and L. Gerace.** 1997. Lamin-binding fragment of LAP2 inhibits increase in nuclear volume during the cell cycle and progression into S phase. J Cell Biol **139:**1077-87.
319. **Yang, T., P. J. Espenshade, M. E. Wright, D. Yabe, Y. Gong, R. Aebersold, J. L. Goldstein, and M. S. Brown.** 2002. Crucial step in cholesterol homeostasis: sterols promote binding of SCAP to INSIG-1, a membrane protein that facilitates retention of SREBPs in ER. Cell **110:**489-500.
320. **Yang, W., K. P. Boggs, and S. Jackowski.** 1995. The association of lipid activators with the amphipathic helical domain of CTP:phosphocholine cytidylyltransferase accelerates catalysis by increasing the affinity of the enzyme for CTP. J Biol Chem **270:**23951-7.
321. **Yang, Y. A., W. F. Han, P. J. Morin, F. J. Chrest, and E. S. Pizer.** 2002. Activation of fatty acid synthesis during neoplastic transformation: role of

mitogen-activated protein kinase and phosphatidylinositol 3-kinase. Exp Cell Res **279:**80-90.

322. **Yang, Y. A., P. J. Morin, W. F. Han, T. Chen, D. M. Bornman, E. W. Gabrielson, and E. S. Pizer.** 2003. Regulation of fatty acid synthase expression in breast cancer by sterol regulatory element binding protein-1c. Exp Cell Res **282:**132-7.
323. **Yazlovitskaya, E. M., and G. Melnykovych.** 1995. Selective farnesol toxicity and translocation of protein kinase C in neoplastic HeLa-S3K and non-neoplastic CF-3 cells. Cancer Lett **88:**179-83.
324. **Yoon, Y., K. R. Pitts, and M. A. McNiven.** 2001. Mammalian dynamin-like protein DLP1 tubulates membranes. Mol Biol Cell **12:**2894-905.
325. **Zaccheo, O., D. Dinsdale, P. A. Meacock, and P. Glynn.** 2004. Neuropathy target esterase and its yeast homologue degrade phosphatidylcholine to glycerophosphocholine in living cells. J Biol Chem.
326. **Zhang, D., W. Tang, P. M. Yao, C. Yang, B. Xie, S. Jackowski, and I. Tabas.** 2000. Macrophages deficient in CTP:Phosphocholine cytidylyltransferase-alpha are viable under normal culture conditions but are highly susceptible to free cholesterol-induced death. Molecular genetic evidence that the induction of phosphatidylcholine biosynthesis in free cholesterol-loaded macrophages is an adaptive response. J Biol Chem **275:**35368-76.
327. **Zhou, B. B., and S. J. Elledge.** 2000. The DNA damage response: putting checkpoints in perspective. Nature **408:**433-9.
328. **Zhou, W., P. J. Simpson, J. M. McFadden, C. A. Townsend, S. M. Medghalchi, A. Vadlamudi, M. L. Pinn, G. V. Ronnett, and F. P. Kuhajda.** 2003. Fatty acid synthase inhibition triggers apoptosis during S phase in human cancer cells. Cancer Res **63:**7330-7.
329. **Zimmerberg, J., and S. McLaughlin.** 2004. Membrane curvature: how BAR domains bend bilayers. Curr Biol **14:**R250-2.
330. **Zinser, E., C. D. Sperka-Gottlieb, E. V. Fasch, S. D. Kohlwein, F. Paltauf, and G. Daum.** 1991. Phospholipid synthesis and lipid composition of subcellular membranes in the unicellular eukaryote Saccharomyces cerevisiae. J Bacteriol **173:**2026-34.